Sparse Tableau Formulation for Power System Networks and Its Applications

By

BYUNGKWON PARK

A dissertation submitted in partial fulfillment of

the requirements for the degree of

Doctor of Philosophy

(Electrical Engineering)

at the

UNIVERSITY OF WISCONSIN-MADISON

2018

Date of final oral examination: 2018/06/22

The dissertation is approved by the following members of the Final Oral Committee:
Christopher L. DeMarco, Professor, Electrical and Computer Engineering
Bernard C. Lesieutre, Professor, Electrical and Computer Engineering
Thomas M. Jahns, Professor, Electrical and Computer Engineering
Michael C. Ferris, Professor, Computer Sciences
Stephen J. Wright, Professor, Computer Sciences

To me and my family..

ACKNOWLEDGMENTS

I would like to articulate my deep gratitude to the many people who have helped me complete my graduate educations. First and foremost, I would like to give special thanks to my advisor, Dr. Christopher DeMarco. I still remember the very first moment that I started working with him through the independent study. Since then, his patience, support and dedication have been the most important encouragement for me to reach where I am today. In addition, his professionalism about research and his attitude toward students have been an irreplaceable object of veneration that I can look up as a scholar. He will be one of the most important people in my lifetime.

I would like to acknowledge my doctoral committee members. Dr. Michael Ferris's knowledge of optimization theory/practice and guidance/assistance in numerous projects has been invaluable. Insight from his optimization knowledge has been essential to my dissertation research and topic. I was fortunate to take many interesting classes from Dr. Bernard Leiseutre and Dr. Thomas Jahns in electric power systems and electric machines. Their instruction has been a great inspiration for addressing interesting ideas to solve practical and challenging problems. For my advanced optimization class, Dr. Stephen Wright has been a valuable professor. I really appreciate their insightful comments and time for my dissertation.

I have been also very fortunate to have the Power Systems group at UW-Madison. I would like to thank current graduate students: Raja Timihiri, Jonathan Snodgrass, Perry Channegowda, Seunguy Min, Sowmya Acharya, Sogol Babaeinejadsarookolaee, Woongkul Lee as well as former graduate students: Dan Wu, Daniel Molzahn, Fatou Thiam, Honghao Zheng, Hilary Brown, Jongmin Lim, Juhyung Kim. Many thanks also go out to friends of optimization group:

Jayanth Netha, Jesse Holzer, Lisa Tang. Special appreication goes to Kyubin Lee, Soongyu Yi, Soovin Yoon for their friendship and pleasant times in Madison.

I am also thankful to Dr. Zhi Zhou and Dr. Audun Botterud for their help and advice during the internship at Argonne National Laboratory. This valuable experience has built my confidence in being an independent investigator and has expanded not only my knowledge to different energy-related research area, but also network of collaborators for future research.

I would like to express my deepest gratitude to my girlfriend, Masha Kobzeva for her unconditional love, friendship, patience and support over all these years. My success would not have been possible without her sacrifices and supports. I also have to thank my family for their love and blessings. My parents, Yeonsik Park and Soonja Moon have provided the ideal environment that I can pursue my study in USA. Especially, it is my mother who supports me with unconditional love and blessings. I am also very thankful to my sister, Jiyoon Park for all her cheer and encouragement. It is no exaggeration to say that their constant support and love during the graduate school has been the overriding factor for achieving my goals.

I gratefully acknowledge the support of the University of Wisconsin-Madison Department of Electrical and Computer Engineering, research assistantships funded by grants from the Federal Energy Regulatory Commission and the Department of Energy.

Finally, this thesis is dedicated to my family, my lovely mother Soonja Moon, father Yeonsik Park and sister Jiyoon Park.

Table of Contents

List of Tables

List of Figures

Abstract

Grid modeling for electric power systems optimization and control has long, well-studied history. Although many excellent texts and tutorials carefully describe such grid models, choices for mathematical power system representations are inevitably made in context of specific component technologies, operational objectives and computational tools. As the grid sees rapid changes in its network elements (e.g. FACT devices), operational objectives (e.g. integration of distributed energy resources) and computational tools (e.g. advanced optimization and control applications), approaches to grid modeling benefit from re-examination. To this end, this work focuses on developing grid models, which move from those classical concepts toward the most effective models and representations based on the multiport representations of components, and Sparse Tableau Formulation (STF) of network constraints. STF adopts a straightforward, algorithmic approach in network constraint formulation that clearly establishes the conceptual origin of each constraint (either KCL, KVL, or individual component behavior), and is well suited to facilitate research in grid optimization.

In this dissertation, we first discuss the standard AC optimal power flow (OPF) formulation in regard to computational time, robustness of convergence, and objective values, including such refinements as modeling of generator capability curves. These standard formulations widely use Nodal Analysis (and hence the Y_{bus} nodal admittance matrix) to describe the network constraints on the problem, which requires the restrictive assumption of admittance representation for elements (i.e., the current flow through each element must be expressible as a function of its terminal voltage(s)). This observation is one of the factors motivating this work. From the initial contribution of resolving limitations imposed by Y_{bus}, we adopt STF from standard circuit analysis in ways particularly suited to describe power system network

constraints in optimization. This dissertation documents the STF approach in the context of the power system, and discusses its relationship to other modeling approaches. We then apply STF to formulate the OPF problem. We argue that this approach improves conceptual clarity in formulating constraints and improves fidelity in capturing physical behavior and engineering limits. With numerical examples, we demonstrate that STF provides computational speed comparable or superior to standard modeling approaches, while increasing flexibility.

Next, we demonstrate the very important practical advantage that STF can simply and directly represent circuit breaker actions in the security-constrained OPF (SCOPF). SCOPF problem is an extension of OPF with added constraints that ensure continued safe operation in the vent of individual component failures termed "contingencies." One of the challenges in the SCOPF is to formulate and impose appropriate constraints for all relevant power component outages to form the "contingency cases." Realistic representation of substations, including the information regarding circuit breaker configurations, is crucial for contingencies. However, this often challenges standard modeling approach based on the Y_{bus}, which requires "topology processing." This imposes additional effort and time to represent contingency scenarios. In this thesis, we construct full nonlinear SCOPF problem with STF, showing its advantage of providing a uniform data structure for contingency analysis, and thus avoiding the need for topology processing.

In addition, motivated by recent advances in convex relaxations for the traditional Y_{bus}-based OPF problem, we derive new convex relaxations suited to the STF formulation of the OPF problem. Two approaches are proposed, relaxing either node current variables or node admittance variables, and several techniques are suggested to improve the quality of relaxed solution.

In the final portion of this thesis, we employ STF to model transmission networks with high penetration of distributed energy resources (DERs) and Flexible AC Transmission System (FACTS) devices. This advanced modeling includes the detailed representation of substations to capture distribution network information with high penetration of DERs. This section also discusses modeling of the Unified Power Flow Controller (UPFC), an example of a particularly

versatile FACTS device. It is shown that STF facilitates direct representation of physically relevant quantities as decision variables associated with these elements, thereby improving analysis of their impacts on transmission networks.

CHAPTER 1

Introduction

1.1 Motivation

Wide-spread electrification is viewed as one of the greatest engineering achievements of the 20^{th} century [1]. Since its first development, management of electric power system to schedule electricity generation resources to meet demand in real time has been an important task. Optimization algorithms play an ever-expanding role to achieve this continuous match between supply and demand, while meeting the many engineering and environmental constraints of grid operation. These problems involve asset owners, grid operators, electricity markets and other stakeholders and include tools for transmission/generation expansion planning [2], maintenance scheduling [3], unit commitment [4] and electricity dispatch with day ahead, hour ahead and real-time frameworks.

Under the banner of the Smart Grid [5], power systems today see growing integration of technologies from communications, advanced control, signal processing, power electronics, and data analytics, coupled with improving efficiency and cost effectiveness of distributed energy resources. These trends open the door to a much wider range of control actions and decision variables in grid planning and operation, and motivate new optimization approaches to exploit

these opportunities.

One of the central optimization problem underlying grid planning and operation is optimal power flow (OPF) [6]. OPF problem is to find the optimal operating point for power system network in terms of a specified objective function with network constraints and engineering constraints. Industry statistic shows electric industry revenues in the United States were $381 billion in 2016 [7] and recent studies have suggested that a five percent improvement to ACOPF solutions could be a credible goal, with such improvements estimated to yield twenty billion dollars annual savings in the U.S. [6].

The vast majority of OPF approaches formulate the network constraints based on the bus admittance matrix Y_{bus}, in which the bus voltage phasors serve as the key "state" variables, analogous to a "strict" nodal analysis in standard circuit theory [8], [9]. However, a strict nodal analysis disallows many standard circuit elements by its requirement that each element's current(s) should be expressible as a function of its current(s) [10]. In a power systems context, the Y_{bus} formulation imposes similar restrictions; e.g. a fixed Y_{bus} is unable to represent ideal circuit breakers in the network, because one cannot describe the current through the element as a function of voltage when the breaker is closed. These limitations spur growing recognition of the value of node-breaker representations [11], [12], that allow realistic representation of substation reconfiguration via circuit breakers in contingency analysis. However, much of the literature seeking to develop advanced OPF algorithms has remained focused on Y_{bus} formulations, and lacks the generality of node-breaker representations.

The work of this thesis will seek to gain the flexibility of general node-breaker formulations, while adopting a straightforward, algorithmic approach to network constraint formulation that is well suited to the OPF. To this end, it is worthwhile to briefly review comparable developments in the history of computer-aided analysis tools for electronic circuit design. While this is a vast literature, relevant early milestones applying optimization in automated network design include [13], [14] and in particular [15]. **"Sparse Tableau Formulation (STF)"** was particularly advocated by IBM for electronic design in the context of circuit optimization. While it failed to achieve the wide-spread adoption enjoyed by its contemporary and competitor SPICE

[16], the circuit analysis program ASTAP [17],[18] developed by IBM successfully utilized STF. The benefits of a STF-based formulation for power flow equations were explored in the late 1970's by [19], but have received little attention in subsequent decades.

Advances in optimization algorithms, and in particular with automated elimination techniques that reduce penalties associated with the retention of large numbers of variables, make a sparse formulation more attractive. This thesis introduces a new approach to modeling power networks using STF. It overcomes drawbacks of the Y_{bus} by expressing network components constraints more flexibly, while still yielding a challenging computation at scale, and allowing sufficient flexibility to address issues of practical interest (e.g., allowing both bus-branch and node-breaker models of the electrical network). With careful construction, STF is successfully employed for power system networks and this new technique affects the initial formulation of the problem. To the author's best knowledge, it is the first attempt since 1979 [19] to apply STF to power system analysis. STF is then applied to the power flow problems, optimal power flow problems (OPF), and convex relaxations of the OPF respectively.

The first application constructs the power flow equations using STF. The power flow equations are the backbone for power system analysis and are used in many tools to operate reliable, stable and economical power systems. Compared to standard power flow formulation using the nodal analysis via the Y_{bus}, STF retains all variables of interest.

The second application is to construct OPF problems, and in particular, the security-constrained OPF (SCOPF) problem. The SCOPF problems is typically hard due to nonconvexity of power flow equations and large dimension of practical problems when many contingencies are considered. To mitigate the difficulty, most of approaches for SCOPF problems uses the DC power flow model [20], which is linear approximation of the AC power flow model under some severe simplifying assumptions. However, this can be quite inaccurate when many contingency cases are considered. In highly loaded conditions, the DC power flow's lossless assumption is particularly problematic. Another main difficulty of the SCOPF problem is that the simulation of large numbers of contingencies which involves bus splits and bus mergers is not possible with existing power system planning software. This is because the standard network algorithms

for the SCOPF problem use the bus-branch model in which there is no direct representation of the circuit breaker configuration. This shortcoming motivates the node-breaker model, and highlights the limitations of traditional Y_{bus} modeling approach for contingency analysis.

This thesis formulates the full nonlinear SCOPF problem using STF and discusses its usefulness in both the bus-branch model and node-breaker model. Numerical experiments are conducted showing that 1) STF provides comparable computational efficiency, 2) the full nonlinear SCOPF problem presents behaviors that are no accurately captured in the linear DC power flow model. Our formulation is used as benchmark for an open OPF competition planned by ARPA-E. Then, we consider an alternative method to address security in the power system networks instead of exploring STF. To this end, we investigate zonal reserves scheduling.

The third application establishes convex relaxations based on STF of OPF problems (STF relaxation). Recent approaches using convex relaxation in OPF, especially semidefinite programming (SDP) [21], has drawn attention of the research community due to its ability to often obtain a global solution. Unfortunately, with additional variables in STF, its structure does not admit a natural SDP formulation and alternative approaches to allow convex relaxation problems are discussed. Majority of nonconvex equations appears with bilinear terms. The McCormick envelope, a well-known linear convex envelope technique [22] for bilinear constraints, is used to relax the problem. Several methods to strengthen the convex relaxation problem are proposed. The proposed methods are compared and tested on test cases provided in the MATPOWER distribution [23].

The last application seeks to develop advanced modeling of power system networks for the accurate representation of substations with high penetration of distributed energy resources (DERs) and the Unified Power Flow Controller (UPFC) which is an example of a particularly versatile FACTS devices. We employ STF to represent such substations with circuit breakers and UPFC that can be accurately represented as the series voltage source, together with the real power coupling to the sending-end generator.

Along with specific contributions in the topics above, we re-emphasize the basic idea: Sparse Tableau Formulation provides a very versatile means of modeling power system networks. This

allows us to have the general statement of various power system optimizations and design problems without abandoning the computational efficiency. Also, as electric power grid becomes more complicated with significant penetration of renewable generation, increased demand-side flexibility and control devices such as power electronics, Sparse Tableau Formulation will provide increased flexibility to modeling these components.

1.2 Background: The Power Flow Equations

Given a connected power system, Let **N** denote the set of all buses, **G** the set of all generators, and **L** set of all transmission lines. The power flow equations describe the power system network operating point in sinusoidal steady state and hence are based on complex phasor representation of voltage-current relationships at each bus. However, in power systems operations, active and reactive power values injected at each bus and/or complex bus voltage magnitudes at each bus are specified quantities, rather than current. Hence, the ultimate relation of interest is between complex powers and complex voltages.

AC Power Flow Model. Using polar coordinate for complex voltages and rectangular representation for complex power, the power flow balance equations at bus j are often formulated as [24]:

$$P_j = P_{g,j} - P_{d,j} = \sum_{k=1}^{n} \{|V_j||V_k|G_{jk}cos(\delta_j - \delta_k) + |V_j||V_k|B_{jk}sin(\delta_j - \delta_k)\} \qquad \forall j \in \mathbf{N} \qquad (1.1)$$

$$Q_j = Q_{g,j} - Q_{d,j} = \sum_{k=1}^{n} \{|V_j||V_k|G_{jk}sin(\delta_j - \delta_k) - |V_j||V_k|B_{jk}cos(\delta_j - \delta_k)\} \qquad \forall j \in \mathbf{N} \qquad (1.2)$$

where P_j and Q_j are the net active and reactive power injection with active/reactive power generation $P_{g,j}$/$Q_{g,j}$ and active/reactive power demand $P_{d,j}$/$Q_{d,j}$ at bus j, and V_j and δ_j are the bus voltage magnitude and phase angle at bus j, and Y_{bus} = G+jB is the network admittance matrix. Each bus is classified as PQ, PV or slack, with different constraints imposed at each class of bus, which represents behaviors appropriate to model different equipment at a given bus. PQ buses, which generally correspond to load locations, hold P_j and Q_j as specified values, and impose the active power (1.1) and reactive power (1.2) balance equations as constraints at that bus. PV buses, which typically correspond to buses at which generators having control

systems holding fixed voltage and active power, specify a voltage magnitude $|V_j|$ and active power injection P_j, and use active power (1.1) equations as constraints at those buses. One slack bus is selected, typically as a generator bus, with constant $|V_j|$ and δ_j to ensure overall network-wide conservation of power in light of power system losses. For the slack bus, typically $j = 1$, the active and the reactive power equations (1.1), (1.2) are not imposed as constraints; rather, at the slack bus the constraints imposed are simply:

$$|V_1| = |V_1^0| \tag{1.3}$$

$$\delta_1 = 0. \tag{1.4}$$

The power flow equations can also be written compactly in matrix/vector form in terms of Y_{bus}

$$I = Y_{bus} V \tag{1.5}$$

$$P = real(V \odot I^*) = real(V \odot (Y_{bus} V)^*) \tag{1.6}$$

$$Q = imag(V \odot I^*) = imag(V \odot (Y_{bus} V)^*) \tag{1.7}$$

where $I \in \mathbb{C}^N$ is the node complex current injection vector; $V \in \mathbb{C}^N$ is the node complex voltage vector; $\odot$ is the Hadamard product and $()^*$ is the conjugate operation. For readers interested in the derivation of the complex voltage phasors and the bus admittance matrix from the network transmission line, refer to [24] for details.

There are several methods, such as Gauss-Seidel or Newton-Raphson to solve the non-linear power flow equations above. The most commonly used technique is Newton-Raphson that is dependent on initial guess of the solution voltage magnitudes and angles. This method requires a matrix of derivatives of the power flow equations, known as power flow Jacobian matrix, with respect to voltage magnitudes and angles. The Jacobian matrix needs to be calculated with voltage values obtained previous iteration, and in simple Newton-Raphson, is updated at every iteration until convergence. The power flow formulation using Jacobian matrix can be constructed [25]

$$\begin{bmatrix} J11 & J12 \\ J21 & J22 \end{bmatrix} \begin{bmatrix} \Delta\delta \\ \Delta|V| \end{bmatrix} = \begin{bmatrix} \Delta P \\ \Delta Q \end{bmatrix} \tag{1.8}$$

where

$$J11 = \frac{\partial P}{\partial \delta}, \quad J12 = \frac{\partial P}{\partial |V|}, \quad J21 = \frac{\partial Q}{\partial \delta}, \quad J22 = \frac{\partial Q}{\partial |V|}$$

DC Power Flow Model. An approximate power flow model sometimes employed by the power industry is DC power flow model [20]. The DC power flow is a particular linear approximation to the AC power flow under four assumptions. First, for high voltage transmission systems, the branch resistance is typically much smaller than branch reactance, so that branch resistance may be neglected and susceptance can be approximated by $b_{jk} \approx \frac{-1}{x_{jk}}$. Second, power system is lightly loaded, which implies that the voltage angle difference between the two buses of a branch is small and therefore $sin\delta_{jk} \approx \delta_j - \delta_k$, $cos\delta_{jk} \approx 1$. Third, any shunt susceptance between a bus and the ground can be neglected $b_{j0} \approx 0$. Finally, each bus has enough reactive power to maintain the bus voltage magnitude near its rated value, which implies that the reactive power balance equations can be neglected, and all voltage magnitudes are assumed to be 1 p.u. With the above four assumptions, the real power flow in a branch can be calculated by

$$P_{jk} = \frac{\delta_j - \delta_k}{x_{jk}} \tag{1.9}$$

and, therefore, bus real power injections are calculated by

$$P_j = \sum_{k \in \mathbf{N}(j)} P_{jk} = \sum_{k \in \mathbf{N}(j)} b_{jk}(\delta_j - \delta_k) = \sum_{k=1}^{N} B_{jk}(\delta_j - \delta_k) \tag{1.10}$$

where $\mathbf{N}(j)$ is subset of neighboring buses connected to bus j; B is a susceptance matrix of Y_{bus}. Notice that only variables δ_j, the bus voltage angles, in (1.10) appear as a linear relation to the active powers P_j with coefficients set by network parameter B.

1.3 Background: The Optimal Power Flow Problem

The power flow equations enable engineers to determine the operating voltage magnitude and angles for a specified set of input values. i.e., generator active power injections and voltage magnitude at PV buses and load active and reactive power at PQ buses. The optimal power flow determines decision variable values that produce an optimal operation point for the power system network in terms of a specified objective function with both network constraints (i.e., the

power flow equations) and engineering constraints (e.g., limits on voltage magnitudes, active and reactive power generation, and flows through transmission lines and transformers).

The sum of individual generator cost functions (i.e. operating cost in $/hour) is typically chosen as the objective function, although other objective functions, such as network losses, are also possible. The OPF problem is non-convex due to the nature of the power flow equations [26] and it is in general hard to obtain a guaranteed global solution. Non-convexity of the OPF problem has made solution techniques an ongoing research topic since the problem was first introduced by Carpentier in 1962 [27].

A mathematical description of the OPF problem as it is classically formulated may be described as follows. Consider the n-bus power system with sets **N**, **G** and **L** as defined above. The number of rows for bus, branch and generator vectors are n_b, n_l and n_g respectively. Let $S_{g,j} = P_{g,j} + Q_{g,j}$ be the $n_g \times 1$ vector of generator injections $\forall j \in \mathbf{G}$, and $S_{d,j} = P_{d,j} + Q_{d,j}$ the $n_b \times 1$ vector of complex load at all buses $\forall j \in \mathbf{N}$. Here $V_j = V_j^m e^{j\delta_j}$ represents the voltage phasor, for all buses $\forall j \in \mathbf{N}$. For a transmission line or transformer connecting bus j to bus k, let S_{jk} represents the apparent power flowing into the transmission line at bus j. Define an individual generator cost function as follows:

$$\tilde{c}_j(P_{g,j}) = \alpha(P_{g,j})^2 + \beta P_{g,j} + \gamma \qquad \forall j \in \mathbf{G} \tag{1.11}$$

Here α, β and γ are the coefficients of the polynomial generator cost function with $P_{g,j}$ typically specified in units of MW, and $\tilde{c}_j$ in $/hour. Piecewise linear generator cost functions are also commonly employed. The sum of individual generator cost functions makes up overall system-wide cost, again with typical units of cost in $/hour. The decision variable vector x for the standard AC OPF problem consists of $2n_b \times 1$ vectors of voltage angles δ and voltage magnitudes V^m and the $2n_g \times 1$ vectors of generator active injections P_g and reactive power injections Q_g. The dimension of the decision variable x is $2(n_b + n_g) \times 1$.

$$x = \begin{bmatrix} \delta \\ V^m \\ P_g \\ Q_g \end{bmatrix}$$

The objective function is to minimize a summation of each generator quadratic or piecewise-linear cost function. In this work, we focus on quadratic cost function.

$$\textbf{min} \sum_{j \in \mathbf{G}} \tilde{c}_j(P_{g,j}) \tag{1.12a}$$

The set of contstraints are

$$\text{Active. Balance:} \quad real(V \odot (Y_{bus}V)^*)_j = P_{g,j} - P_{d,j}, \quad \forall j \in \mathbf{N} \tag{1.12b}$$

$$\text{Reactive. Balance:} \quad imag(V \odot (Y_{bus}V)^*)_j = Q_{g,j} - Q_{d,j}, \quad \forall j \in \mathbf{N} \tag{1.12c}$$

$$\text{Line and Transformer Limit:} \quad (S_{jk})^2 - (S_{jk}^{max})^2 \leq 0, \quad \forall jk \in \mathbf{L} \tag{1.12d}$$

(apparent power form)

$$\text{Gen. Limit:} \quad P_j^{min} \leq P_{g,j} \leq P_j^{max}, \quad \forall j \in \mathbf{G} \tag{1.12e}$$

$$Q_j^{min} \leq Q_{g,j} \leq Q_j^{max}, \quad \forall j \in \mathbf{G} \tag{1.12f}$$

$$\text{Vol. Limit:} \quad V_j^{min} \leq V_j^m \leq V_j^{max}, \quad \forall j \in \mathbf{N} \tag{1.12g}$$

The flows as characterized above employ apparent power, expressed in MVA. However, the engineering considerations that require limits on flows may dictate other choices, such as real powers or current flows, yielding the following three possible forms for the line flow constraints.

$$\begin{cases} S_{jk}, & \text{apparent power} \\ P_{jk}, & \text{real power} \\ I_{jk}, & \text{current} \end{cases} \tag{1.12h}$$

This classical formulation is sufficient for modeling most small test systems. Chapter 2 contains a more detailed formulation of the OPF problem suitable for realistic system models that include realistic refinements such as parallel lines and the multiple generators at the same bus.

1.4 Background: Sparse Tableau Analysis

In circuit analysis, perhaps the most widely used approach in basic texts is that of nodal analysis, that seeks to solve for node-to-reference voltages. Once these node voltages have

been calculated, one may solve for the branch currents provided all elements in the circuit are "voltage controlled," i.e. they allow for this solution of circuit in terms of voltage [10], [28].

A major shortcoming of nodal analysis is that it forbids many standard circuit elements from the class of allowable circuits; disallowed elements include the voltage source, ideal transformer, ideal op amp, etc. [10]. These shortcomings can be viewed as arising from the fact that nodal analysis is a special case of a more general analysis method. General analysis consists of linearly independent KVL equations, linearly independent KCL equations, and the constitutive relations of each circuit element. Analysis using this list of equations is called Tableau Analysis and conceptually, it is simpler than node analysis.

Since we define all variables, three vectors (v, e, i: node voltages, port voltages and port currents), no variables are eliminated in the tableau equations. Because we should have as many equations as there are variables, it is clear that the tableau analysis involves many more equations than nodal analysis as the price of increased generality. However, this misfortune turns out to be a blessing in disguise due to the fact that the matrix associated with tableau analysis is substantially sparse, which is why it is often called **Sparse Tableau Anlaysis**. Therefore, highly efficient numerical algorithms [29], [30] can be brought to bear. To formulate the circuit constraints via sparse tableau analysis, consider the following simple algorithm [10]:
Step 1. Draw the digraph of the circuit and connect it if necessary so that the resulting circuit is connected. Pick an arbitrary reference node and formulate the corresponding incidence matrix A.
Step 2. Write a complete set of linearly independent KCL equations:

$$Ai(t) = 0 \tag{1.13}$$

Step 3. Write a complete set of linearly independent KVL equations:

$$e(t) - A^T v(t) = 0 \tag{1.14}$$

Step 4. Write the constitutive relations of each circuit component. If the circuit is linear and time invariant, these equations can always be recast into the form

$$Me(t) + Ni(t) = u_s(t) \tag{1.15}$$

(1.13), (1.14), and (1.15) construct the tableau equations. In addition, this analysis can be generalized to nonlinear equations when branch equations (1.15) are nonlinear. Simple example is provided in Chapter 3. This thesis employs this formulation for power system networks, and most specifically for SCOPF.

1.5 Background: Power System Security

An overriding factor for power system operation is to maintain system security [31]. Secure operation involves selection of operational decision variables such that the system keeps operating with credible component failures. For example, transmission line may be damaged by a storm or taken off-line because of maintenance requirement. With proper operational decisions, the remaining transmission lines can accommodate the increased loading and still remain within limit. Since events that cause components to fail are usually unpredictable, the system must be operated at all times such that the system will not have any dangerous situation when credible events happen. To this end, power system equipment is designed to be operated within certain limits and protected by automatic relays that switch equipment off from the system if these limits are violated. If events that cause the system limit violations, and relay action then causes further overloads, it is usually referred to as a cascading failure. Then, entire system or some major part of system may be completely de-energized, which leads it to a **system blackout** [32].

Thus, most large power systems install equipment that operations personnel monitors and operates the system in a reliable manner. The techniques and equipment for these issues are commonly titled **system security enhancement**. System security can be split into three main activities; 1) system monitoring, 2) contingency analysis, and 3) security-constrained optimal power flow; these are implemented in an operations control center.

Simply speaking, system monitoring provides the system operators with appropriate up-to-date information on the condition of the power system. Using telemetry systems, critical quantities such as voltages, currents, power flows, and the status of circuit breakers, and switches in every substation can be monitored/measured and the values of measurements can

be transmitted to a central location. State estimation plays a role in this system to produce the best estimate of the current power system conditions or “state” from telemetered system data. Such system is usually combined with supervisory control and data acquisition (SCADA) system allowing operators to control circuit breakers, switches and transformer taps remotely.

The second crucial security function is that of contingency analysis. This performs “what if” analysis examining possible power system disturbances. It evaluates and prioritizes the impacts on the power system when disturbances occur. These analyses are based on a computer simulation to evaluate the effects and calculate any overloads resulting from each outage event. As the simplest form of contingency analysis, a standard power flow program can be used combined with procedures to set up the system configuration for each outage.

Lastly, the third major security function, on which this thesis mostly focuses, is that of security-constrained optimal power flow. In this function, an optimal power flow is combined with a contingency analysis to adjust a system operating point on the optimal dispatch of the power system network so that no violations occur when contingencies are considered. To describe how this can be done, we divide the power system into four operating status.

- **Optimal dispatch:** this is the state the power system is operating before any contingency. It is optimal with respect to economic operation, but it may not be secure.

- **Post contingency:** this is the state the power system is operating after a contingency happened. This condition might violate security conditions (line or transformer beyond its flow limit, or a bus voltage outside the limit)

- **Secure dispatch:** this is the state the power system is operating with no contingency outages, but with corrections to the operating points to avoid security violations.

- **Secure post-contingency:** this is the state the power system is operating after a contingency happened with corrections.

These four operating points are described in Figure 1.1-1.2, in which trivial lossless power system are present with two generators, a load and a double circuit line.

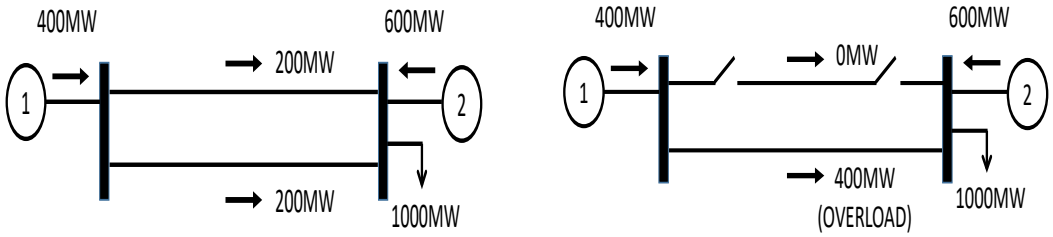

(a) Optimal Dispatch, pre-contingency (b) Post Contingency State

Figure 1.1: Optimal operating point without security constratins

We assume that the system is operating at the minimum cost with the 400MW from generator 1 and the 600MW from generator 2. This implies that generator 1 is cheaper than generator 2 and we further suppose that each line of the double circuit line can carry a maximum of 300MW. Thus, there is no line load violation in the base-operating condition in Figure 1.1a. However, if one of the double circuit line becomes open due to a failure, as in Figure 1.1b, then remaining line has an overload. This system now is not secure and we do not want this condition.

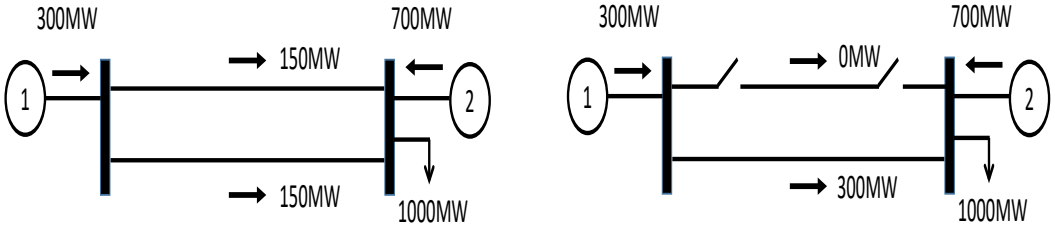

(a) Secure Dispatch (b) Secure Post Contingency State

Figure 1.2: Optimal operating point with security constratins

To have secure operation, we will correct the condition by reducing the generation on generator 1 to 300MW in Figure 1.2a. Now, if the same contingency condition is considered, the post-contingency condition is secure in Figure 1.2b. With the adjustment on generation on unit 1 and unit 2, this system might be more expensive, but we have prevented the post-contingency operating state from producing an overload that may lead to system blackout. This is the essence of security corrections and security-constrained optimal power flow (SCOPF). It seeks

to find a operating point as described in Figure 1.2. Much of this thesis concentrates on SCOPF problem.

1.6 Dissertation Organization

This thesis is organized with three major themes: comprehensive examination of the existing ACOPF problems, the application of STF for power system networks and convex relaxation for STF of OPF problems. Chapter 2 introduces and reviews the existing OPF problems, by providing a structured, empirical comparison of three different ACOPF formulations, and evaluating the numerical solution properties of the formulations in terms of computational time, robustness of convergence and optimal solution using different nonlinear solvers. Also, we construct the ACOPF problems with PV buses enhanced with representation of generator capability curves, the so-called "D-curves," that provide more realistic modeling of constraints on output. The D-curve constraints improve on simplistic rectangular PQ limits, and their impact on the OPF is examined in terms of solution speed and value of the optimal solution.

Chapter 3 provides the construction of STF for power system networks. Algorithm of STF for power system networks including construction of incidence matrix, network element equations is discussed in detail and applied for power flow analysis. The specific network elements in which the standard formulation Y_{bus} fails or proves hard to model are presented with examples; ideal transformer, circuit breaker and three-winding transformer. Useful by-product of STF applied for power flow is discussed in terms of contingency analysis since the Jacobian matrix associated with these equations corresponds to the sensitivity matrix relating injection power and current flow on line. Then, computational efficiency of STF is demonstrated for OPF problems.

The thesis next details investigation into the application of STF for security-constrained OPF problems (SCOPF). Chapter 4 begins with the definition of "preventive" SCOPF (PSCOPF) and discusses necessary enhancements for the PSCOPF problem; 1) introducing the speed droop-characteristic for each generator as governor power flow equations in contingency cases to formulate the PSCOPF problem. 2) the node-breaker model, for which STF can be also useful. Then, STF is employed to formulate the nonlinear PSCOPF problem under the node-breaker

model with three different coordinate systems. Chapter 4 continues to conduct a comprehensive numerical experiment with different level of contingency showing that STF shows comparable or better computational efficiency with greatly improved generality.

The approach employed in Chapter 4 can be viewed more generally as a stochastic programming problem over a set of contingency scenarios. These would be an ideal approach since it explicitly represents the events of uncertainties with the network constraints in the model. However, such approach is still computationally hard to get a solution within desired time for large-scale problems. Therefore, Chapter 5 investigates a traditional method to address security in the power system, which schedules additional generation capacity as operating reserve. It develops a tool to dynamically schedule zonal reserves to enhance the deliverability of energy with wind power forecasts.

Chapter 6 then investigates the convex relaxation technique for STF of OPF problem. The limitation of existing convex relaxation techniques for STF is discussed, and then alternative approaches (STF relaxation) are presented using the McCormick envelope. Heuristic methods to strengthen the convex relaxation problem are proposed, and Chapter 6 concludes with numerical case studies. Numerical experiments are conducted with proposed relaxation techniques and demonstrates the important condition when STF relaxation can be strength as well as scalability.

Finally, Chapter 7 develops advanced modeling of DERs and UPFCs with STF for OPF problem. It is shown that STF can accurately represents network elements such as circuit breakers (important for representation of substations with DERs) and series connected ideal voltage sources (important for representation of UPFCs). Then, it is applied to formulate ACOPF with DERs and UPFCs, and their impacts (and the new decision variables they introduce) are analyzed in case studies.

The remainder of the thesis discusses relationships between these developments and addresses future work. Proposed directions for future work include the appropriate linear approximation of STF for power system network, application to represent three-phase unbalanced distribution networks, the extension of STF to more sophisticated FACTS network elements, bound tightening technique for convex relaxation problem, additional investigation into the

constructing tighter McCormick envelope to reduce the relaxation gap.

1.7 Contributions

The contributions of this report can be organized in two major areas: 1) theoretical, practical, and modeling advances in STF for power system networks, and 2) techniques for constructing the convex relaxation problem for STF.

1. Theoretical, practical and modeling advances for STF

Theoretically, we show (constructively) that the power system networks can always be casted in STF and apply it to different topics in power system networks. Specifically, we rigorously illustrate how to construct STF, prove that the standard Y_{bus} and modified nodal analysis (MNA) modeling approach is one of the special modeling method from STF, which shows that STF is a more general modeling approach.

Practically, STF is used to formulate the power flow and optimal power flow problem. To the author's knowledge, it is the first attempt to use STF to solve OPF problems, and that efficiently represents the node-breaker model for contingency analysis in SCOPF. We propose the sensitivity matrix that can be directly used to evaluate the change in power injections with respect to the change in line loads. We also show that the computational efficiency of STF by comparing with standard ACOPF problems.

In modeling advances, we provide straightforward treatment of three atypical network elements; ideal transformer, circuit breaker, three-winding transformer, that all challenge the Y_{bus} approach. An anticipated future modeling contribution would be the incorporation of power electronics devices as multiport network elements.

2. Theoretical, practical and modeling advances for the PSCOPF problem

Theoretically, we provide the example that there are no inactive contingency constraints for the PSCOPF problem in the nonlinear model. This example shows that every single outage possibly changes the feasible region of optimization problem.

Practically, we propose the governor power flow equation necessary to accurately model the physical behavior of power system network in contingency scenarios and to find a feasible point

in a contingency scenario. We show that the computational efficiency of STF in comparison with standard ACOPF problems.

In modeling advances, STF is employed to formulate the PSCOPF problem for the node-breaker model. It is shown that STF can successfully model and solve the PSCOPF under the node-breaker model with circuit breaker actions between buses.

We also consider an alternative approach to address computational issues of PSCOPF with additional generation capacity as operating reserves. We co-optimize energy and reserves simultaneously and propose a tool to dynamically schedule zonal reserves with wind power forecasts.

3. Techniques for constructing the convex relaxation of STF for OPF problem

The report next contributes to techniques for constructing the convex relaxation of STF for OPF problem. We first study the limitation of existing approach for STF and present two alternative approaches. We then propose the algorithm to construct convex relaxation of STF for OPF problems (STF relaxations). Heuristic methods to strengthen STF relaxation are discussed and specific conditions where STF relaxation provides a tighter lower bound are illustrated.

4. Advanced modeling of DERs and UPFC device modeling

Theoretically, we derive linear and nonlinear element equations of STF to represent behavior of UPFC for OPF problem. It is shown that STF avoids the introduction of low impedance branch to represent ideal voltage sources and complex manipulation to describe the real power energy coupling.

Practically, we combine the recommended power flow model for the scenario of high penetration of DER, which expands the substation to contain distribution network information with the node breaker model. We then analyze the impact of modeling of DERs and UPFC on power system networks.

1.8 Publication

Several publications have resulted from the research detailed in this thesis. Works from Chapter 2 and 4 are published as

1. Byungkwon Park, Lisa Tang, Michael C. Ferris and Christopher L. DeMarco, "Examination of three different ACOPF formulations with generator capability curves," *IEEE Transaction on Power Systems*, vol. 32, no. 4, 2017

2. Byungkwon Park and Christopher L. DeMarco, "Transmission Matrix Representation of Network constraints in Security-Constrained Optimal Power Flow," *North American Power Symposium (NAPS)*, 18-20 September 2016

Works from Chapters 3 and 4 are submitted for publication as

3. Byungkwon Park, Jesse Holzer and Christopher L. DeMarco, "A Sparse Tableau Formulation for Node-Breaker Representations in Security-Constrained Optimal Power Flow," Submitted to *IEEE Transaction on Power Systems*, 2018

4. Byungkwon Park, Jayanth Netha, Michael C. Ferris and Christopher L. DeMarco, "Sparse Tableau Analysis for Power System Analysis and Design," submitted to *North American Power Symposium (NAPS)*, September 2018

Works from Chapters 5 are submitted for publication as

5. Byungkwon Park, Audun Botterud, Prakash Thimmapuram and Zhi Zhou, "Dynamic Scheduling of Zonal Reserve for Grid Deliverability Improvement with Wind Power," submitted to *IEEE Transaction on Power Systems*, 2018

Works from Chapters 6 are published as

6, Byungkwon Park and Christopher L. DeMarco, "Sparse Tableau Relaxation for the Optimal Power Flow Problem," *55th Annual Allerton Conference on Communication, Control, and Computing*, 3-6 October 2017

Works from Chapters 7 are submitted for publication as

7. Byungkwon Park and Christopher L. DeMarco, "Advanced Modelling of DERs and UPFC devices with Sparse Tableau Formulation for ACOPF," submitted to *IEEE Transaction on Power*

Systems, 2018

Other publications, unrelated to sparse tableau formulation for power system networks investigated in this report, include work on optimal control and decomposition of optimal power flow of power system networks.

8. Byungkwon Park and Christopher L. DeMarco, "Optimal Control with The Waveform Relaxation and Its Applications for The Power System," *IEEE Power & Energy Society General Meeting (GM)*, 17-21 July 2016

9. Byungkwon Park and Christopher L. DeMarco, "Active/reactive power decomposition approaches to the AC optimal power flow problem," *North American Power Symposium (NAPS)*, 7-9 September 2014

CHAPTER 2

Standard ACOPF formulation

The optimal power flow seeks to minimize a grid-related objective function subject to network equality constraints and operational inequality constraints (active and reactive power generation output limits, voltage constraints, and flow limits on transmission lines and transformers). The challenge of these problems is well recognized, due to the nonconvexity of power flow equations and the large dimension of practical problems. Approximation techniques are often used in practice, at the risk that the operational decisions produced may be sub-optimal, with greater operational cost and possible environmental impacts of unnecessary emissions and energy use. Therefore, efficient techniques for solving ACOPF with realistic, engineering-based representation of operational limits are important. Recent studies have suggested that a five percent improvement to ACOPF solutions could be a credible goal, with such improvements estimated to yield twenty billion dollars annual savings in the U.S.[6]

In the ACOPF literature, the majority of authors have long used the polar-voltage formulations introduced in the early 1960's by Carpentier. However, a number of researchers have advocated a rectangular power-voltage and current injection formulation for power flow or optimal power flow. Other variants include a power flow formulation with current injections and a mix of polar and rectangular coordinates, as is mentioned in [33]. A current injection

algorithm based on the use of a constant nodal admittance matrix was described in [34], but acknowledged that the constant nodal admittance matrix imposed significant shortcomings because PV buses could not be represented.

More recent works employing current injection variables to construct the ACOPF problems include [35], wherein it is argued that the resulting structure of the Hessian matrix for the constraint equations will ensure a convex constraint set. However, that work requires all buses in the power flow formulation to be PQ buses, which may provide a poor representation of the operational characteristic of generator buses. Other results in [36] developed a rectangular voltage OPF, but the power flow equations still require all PQ buses, and that paper did not use current quantities to impose the conservation constraints at nodes. A recent FERC report [37] suggests the rectangular current-voltage ACOPF formulation, and its linear approximation, could be easier to solve than traditional quadratic power flow formulations. Computational performance of solution techniques for the ACOPF is studied [38] and a comparative analysis for different power flow formulations is presented in [39], but this paper did not address the ACOPF problem.

This chapter seeks to contribute to the existing optimal power flow literature by providing a structured, empirical comparison of three different ACOPF formulations, and evaluating the numerical solution properties of the formulations. Broadly speaking, these formulations differ through nonlinear change of coordinates on key decision variables. They are compared in terms of computational time, robustness of convergence and optimal solution using different nonlinear solvers. Also, we construct the ACOPF problems with PV buses enhanced with representation of generator capability curves, the so-called “D-curves," that constrain generator active and reactive output. The D-curve constraints provide more accurate generator output constraints than simplistic rectangular PQ limits, and their impact on the OPF is examined in terms of solution speed and value of the optimal solution.

This chapter is organized as follows. Section 2.1 provides three different formulations for the ACOPF. Instead of using the nodal admittance matrix, we introduce variables for line power flows and use the summation of those quantities to calculate network-wide constraints. With

this slight change, we obtain linear equations for node balance equations, which leads us to have constant Hessian matrices. Problems are formulated in GAMS and three solvers (KNITRO, CONOPT, IPOPTH) are examined based on empirical experience indicating that those are best suited for solving ACOPF problems. Section 2.2 proposes additional enhancements: six choices of initial conditions, and D-curve constraint modeling. Section 2.3 discusses results from each formulation and examines properties in terms of computational time, robust convergence and optimal objective value. Observations regarding formulation, solver and initial condition are provided. Note that while this chapter begins our process of examing alternate OPF formulations, treatment of the Sparse Tableau Formulation will await Chapter 3.

2.1 ACOPF Formulation

2.1.1 Notation and Nomenclature

In this section, we provide three different decision variable coordinate frames for the ACOPF, those of Polar Power-Voltage, Rectangular Power-Voltage, and Rectangular Current-Voltage. Compared to the standard OPF formulation described in Section 2.2, this formulation contains a more generalized formulation of OPF problems suitable for realistic system models that include parallel lines and the possibility of multiple generators at the same bus. Tables 2.1 and 2.2 provide the notation of set and parameters used in these different OPF formulations. Note that the convention used in our models is that a positive flow on a line represents a withdrawal at its source end (j) and an injection at its terminating end (k). Sets $\mathbf{C}$ and $\mathbf{G}_j$ are used to account for multiple lines and generators respectively.

Set	Description
$\mathbf{N}$	Set of buses in the transmission network
$\mathbf{G}$	Set of generators in the transmission network
$c \in \mathbf{C}$	Index number for multi-circuit line
$\mathbf{L} \subseteq \mathbf{N} \times \mathbf{N} \times \mathbf{C}$	Set of lines in the transmission network
$\mathbf{G}_j \in \mathbf{G}$	Subset of generators $\mathbf{G}$ at bus $j \in \mathbf{N}$

Table 2.1: Description of Sets

Parameters	Description
$\tilde{c}_j(\cdot)$	Cost function for generation at bus $j \in \mathbf{N}$
$P_{d,j}, Q_{d,j}$	Real and reactive power demand at bus $j \in \mathbf{N}$
g^s_j, b^s_j	Shunt conductance and susceptance at bus $j \in \mathbf{N}$
P^{max}_{jkc}	Real power limit on line $jkc \in \mathbf{L}$
I^{max}_{jkc}	Current limit on line $jkc \in \mathbf{L}$
P^{min}_j, P^{max}_j	Lower/upper active power injection limits $j \in \mathbf{G}$
Q^{min}_j, Q^{max}_j	Lower/upper reactive power injection limits $j \in \mathbf{G}$
V^{min}_j, V^{max}_j	Voltage magnitude lower and upper limits at bus $j \in \mathbf{N}$

Table 2.2: Description of Parameters

Note that the OPF literature contains several common choices for the physical quantity monitored in setting transmission line flow limits; the typical choices are apparent power, current magnitude, or active power. It has for many years been most common in OPF to represent thermal line limits in terms of a maximum allowable apparent power [6]. However, it is important to recognize that while this choice may be convenient (in that it uses quantities that normally appear in power flow equations), and may represent a reasonable approximation to the actual engineering limit, the most accurate representation of thermal limits on overhead transmission lines should be expressed in terms of current magnitude. Indeed, any review of both conductor vendor's material and engineering literature affirms that thermal line limits are expressed in terms of ampacity; a widely-cited paper [40] states the engineering goal and the associated limit very succinctly: "Because adequate clearances must be maintained, even under emergency conditions, the conductor temperature at the end of a short-time overload period must be restricted to its maximum design value. It is then necessary to determine how much current a conductor can carry for a short period of time without exceeding this temperature" Hence, the premise of this thesis is that current magnitude is the inherently superior choice as the monitored quantity for ACOPF, as it more realistically relates to the primary engineering concerns motivating imposition of thermal line limits [41]. We will also consider the use of active power as the monitored quantity for line limits, on the premise that while inferior to current magnitude, its use is worthwhile to allow comparison to results based on DCOPF

approximations. However, contrary to common practice, apparent power will not be used as a monitored limit in this chapter.

2.1.2 Polar Power-Voltage Formulation

The Polar Power-Voltage formulation represents complex quantities in polar form and explicitly uses sines and cosines in the power flow constraints. $P_{g,j}$, $Q_{g,j}$, V_j and θ_j denote the active/reactive power support provided by generators and bus voltage magnitudes/angles at bus $j \in \mathbf{N}$ respectively, while active and reactive power on a line are denoted by P_{jkc} and Q_{jkc} respectively. The advantage of adding these flow variables will be discussed later. Polar Power-Voltage formulation for the ACOPF problem can be written with the following form:

$$\min_{P,Q,P_{jkc},Q_{jkc},\theta,V} \quad \sum_j \tilde{c}_j(P_{g,j}) \tag{2.1a}$$

The set of contstraints are

$$\text{Power Flow on jk:} \quad P_{jkc} = f^1(\theta,V), \quad Q_{jkc} = f^2(\theta,V), \quad \forall jkc \in \mathbf{L} \tag{2.1b}$$

$$\text{Power Flow on kj:} \quad P_{kjc} = g^1(\theta,V), \quad Q_{kjc} = g^2(\theta,V), \quad \forall jkc \in \mathbf{L} \tag{2.1c}$$

$$\text{Active. Balance:} \quad \sum_{k\in\mathbf{G}_j} P_{g,k} - \sum_{\substack{jkc \\ (kc\in\mathbf{L})}} P_{jkc} - P_{d,j} - (V_j)^2 g_j^s = 0, \quad \forall j \in \mathbf{N} \tag{2.1d}$$

$$\text{Reactive. Balance:} \quad \sum_{k\in\mathbf{G}_j} Q_{g,k} - \sum_{\substack{jkc \\ (kc\in\mathbf{L})}} Q_{jkc} - Q_{d,j} + (V_j)^2 b_j^s = 0, \quad \forall j \in \mathbf{N} \tag{2.1e}$$

$$\text{Gen. Limit:} \quad P_j^{min} \le P_{g,j} \le P_j^{max}, \quad Q_j^{min} \le Q_{g,j} \le Q_j^{max}, \quad \forall j \in \mathbf{G} \tag{2.1f}$$

$$\text{Volt. Limit:} \quad V_j^{min} \le V_j \le V_j^{max}, \quad \frac{-\pi}{3} \le \theta_j - \theta_k \le \frac{\pi}{3}, \quad \forall jk \in \mathbf{L} \tag{2.1g}$$

$$\text{Line Limit:} \quad -P_{jkc}^{max} \le P_{jkc} \le P_{jkc}^{max}, \quad \forall jkc \in \mathbf{L} \tag{2.1h}$$

Notice that f^1, f^2, g^1, g^2 are nonlinear nonconvex functions of variables, voltage angles and magnitudes. Variables for real and reactive power flow on lines $jkc \in \mathbf{L}$ are defined in (2.1b), (2.1c), and node balance equations represented via variables P_{jkc} and Q_{jkc}. As a rough surrogate for stability constraints (and to pragmatically limit the search space in solution algorithms), limits on bus angle differences across transmission lines are imposed. As discussed

above, inequality constraints on the monitored line flow quantity are included to represent the thermal limits on the transmission lines. Here, inequality constraints on active power flow on lines are imposed.

2.1.3 Rectangular Power-Voltage Formulation

The second ACOPF formulation uses the rectangular form of complex quantities, resulting in quadratic power flow constraints with respect to these quantities. Unlike the polar formulation, bus voltage quantities V_j and θ_j are separated into real and imaginary parts, with $V_j = \sqrt{(V_j^d)^2 + (V_j^q)^2}$ and $\theta_j = tan^{-1}(\frac{V_j^q}{V_j^d})$ $\forall j \in \mathbf{N}$. Rectangular Power-Voltage formulation for the ACOPF problem can then be written in the following form:

$$\min_{P,Q,P_{jkc},Q_{jkc},V^d,V^q} \quad \sum_j \tilde{c}_j\left(P_{g,j}\right) \tag{2.2a}$$

The set of contstraints are

$$\text{Power Flow on jk:} \quad P_{jkc} = f^3(V^d,V^q), \quad Q_{jkc} = f^4(V^d,V^q), \quad \forall jkc \in \mathbf{L} \tag{2.2b}$$

$$\text{Power Flow on kj:} \quad P_{kjc} = g^3(V^d,V^q), \quad Q_{kjc} = g^4(V^d,V^q), \quad \forall jkc \in \mathbf{L} \tag{2.2c}$$

$$\text{Active. Balance:} \quad \sum_{k\in\mathbf{G}_j} P_{g,k} - \sum_{\substack{kc \\ (jkc\in\mathbf{L})}} P_{jkc} - P_{d,j} - \left((V_j^d)^2 + (V_j^q)^2\right) g_j^s = 0, \quad \forall j \in \mathbf{N} \tag{2.2d}$$

$$\text{Reactive. Balance:} \quad \sum_{k\in\mathbf{G}_j} Q_{g,k} - \sum_{\substack{kc \\ (jkc\in\mathbf{L})}} Q_{jkc} - Q_{d,j} + \left((V_j^P)^2 + (V_j^Q)^2\right) b_j^s = 0, \quad \forall j \in \mathbf{N} \tag{2.2e}$$

$$\text{Volt. Limit:} \quad (V_j^{max})^2 \le (V_j^d)^2 + (V_j^q)^2 \le (V_j^{max})^2, \quad \forall j \in \mathbf{N} \tag{2.2f}$$

$$\text{Gen. Limit:} \quad P_j^{min} \le P_{g,j} \le P_j^{max}, \quad Q_j^{min} \le Q_{g,j} \le Q_j^{max}, \quad \forall j \in \mathbf{G} \tag{2.2g}$$

$$\text{Line Limit:} \quad -P_{jkc}^{max} \le P_{jkc} \le P_{jkc}^{max}, \quad \forall jkc \in \mathbf{L} \tag{2.2h}$$

Equations (2.1b), (2.1c) from the polar model which define real and reactive power on lines and node balance equations are rewritten in the rectangular formulation as (2.2b), (2.2c). Notice that f^3, f^4, g^3, g^4 are quadratic nonconvex functions of variables, real and imaginary part of the bus voltage. Additionally, the voltage magnitude limit is no longer a simple bound constraint but is enforced by the quadratic inequality. Bus angle difference limits are no longer imposed; this sacrifices the (albeit approximate) treatment of stability concerns in the constraints, but in

rectangular coordinates, the previous motivation of limiting the size of the search space is no longer relevant.

2.1.4 Rectangular Current-Voltage Formulation

The third ACOPF model is the rectangular current-voltage formulation which considers the flow of current instead of power on a line. Therefore, the model computes real and reactive current on a line, $\{i^d_{jkc}, i^q_{jkc}\}\ \forall jkc \in \mathbf{L}$, instead of $\{P_{jkc}, Q_{jkc}\}\ \forall jkc \in \mathbf{L}$, the real and reactive power on a line. Similar to the rectangular power-voltage model, the I-V formulation uses the rectangular form of complex quantities. Therefore, line flow constraints are once again quadratic in nature. The Rectangular Current-Voltage formulation for the ACOPF problem can be written in the following form:

$$\min_{P,Q,i^d,i^q,V^P,V^Q} \quad \sum_j \tilde{c}_j\left(P_{g,j}\right)$$

The set of contstraints are

$$\text{Curr. Flow on jk:} \quad i^d_{jkc} = f^5(V^d, V^q), \quad i^q_{jkc} = f^6(V^d, V^q), \quad \forall jkc \in \mathbf{L} \tag{2.3a}$$

$$\text{Curr. Flow on jk:} \quad i^d_{kjc} = g^5(V^d, V^q), \quad i^q_{kjc} = g^6(V^d, V^q), \quad \forall jkc \in \mathbf{L} \tag{2.3b}$$

$$\text{Active. Balance:} \quad \sum_{k \in \mathbf{G}_j} P_{g,k} - P_{d,j} - V^d_j \sum_{\substack{kc \\ (jkc \in \mathbf{L})}} i^d_{jkc} - V^q_j \sum_{\substack{kc \\ (jkc \in \mathbf{L})}} I^q_{jkc} - \left((V^d_j)^2 + (V^q_j)^2\right) g^s_j = 0, \quad \forall j \in \mathbf{N} \tag{2.3c}$$

$$\text{Reactive. Balance:} \quad \sum_{k \in \mathbf{G}_j} Q_{g,k} - Q_{d,j} + V^P_j \sum_{\substack{kc \\ (jkc \in \mathbf{L})}} i^q_{jkc} - V^q_j \sum_{\substack{kc \\ (jkc \in \mathbf{L})}} i^d_{jkc} + \left((V^d_j)^2 + (V^q_j)^2\right) b^s_j = 0, \quad \forall j \in \mathbf{N} \tag{2.3d}$$

$$\text{Volt. Limit:} \quad (V^{min}_j)^2 \le (V^d_j)^2 + (V^q_j)^2 \le (V^{max}_j)^2, \quad \forall j \in \mathbf{N} \tag{2.3e}$$

$$\text{Gen. Limit:} \quad P^{min}_j \le P_{g,j} \le P^{max}_j, \quad Q^{min}_j \le Q_{g,j} \le Q^{max}_j, \quad \forall j \in \mathbf{G} \tag{2.3f}$$

$$\text{Curr. Limit:} \quad (i^d_{jkc})^2 + (i^q_{jkc})^2 - (I^{max}_{jkc})^2 \le 0, \quad \forall jkc \in \mathbf{L} \tag{2.3g}$$

Notice that f^5, f^6, g^5, g^6 are the linear function of variables, real and imaginary part of the bus voltage. Inequality constraints for the magnitude of current flow on lines are imposed. Note

that the current flow equations (2.3a), (2.3b) are linear. This leads to a Hessian of the current-voltage constraints that is constant, with possible benefit in solution time. Three different ACOPF formulations are summarized in the Table 2.3 below.

	Polar PV	**Rec PV**	**Rec IV**
Variables	$\|V\|$,θ,P,Q,P_{jkc},Q_{jkc}	V^d,V^q,P,Q,P_{jkc},Q_{jkc}	V^d,V^q,P,Q,i^d,i^q
Nonlinear equations (no condsidering shunt elements for power balance)	- Line power flow	- Line power flow - Voltage magnitude	- Power balance - Current magnitude - Voltage magnitude
# of variables	2**N**+2**E**+2**G**	2**N**+2**E**+2**G**	2**N**+2**E**+2**G**
# of equations	2**N**+4**L** (eq) 2**N**+4**E**+4**G** (ineq)	2**N**+4**L** (eq) 2**N**+2**E**+4**G** (ineq)	2**N**+2**L** (eq) 2**N**+1**E**+4**G** (ineq)

Table 2.3: Summary of three different ACOPF formulations

2.2 Enhancements to the ACOPF problems

2.2.1 Initial Conditions

Because ACOPF problems are often non-convex, may have disconnected feasible regions, and are in general difficult to solve in large cases, providing good starting points is an important step in any solution approach. With different selection of initial conditions, problems vary in their computational time, convergence properties, and convergence to possibly different local optimal solutions. Table 2.4 describes in detail six different choices of initial conditions for ACOPF problems that were studied here. With the exception of `ic=2` (**Flat starting point**), voltage magnitudes, angles, real power and reactive power variables are initialized according to methodologies described in Table 2.4, and line flow variables are calculated from these values.

The use of decoupled ACOPF [42], (initial condition `ic=4`), exploits the long-recognized property of the power flow Jacobian matrix: that under light-to-moderate loading conditions, the off-diagonal submatrix blocks are “small," reflecting the fact that network flow of active power is relatively weakly dependent on bus voltage magnitudes, while reactive power flow is relatively weakly dependent on bus voltage phase angles. Thus, the ACOPF problem approximately decouples into two lower dimensional nonlinear subproblems (active and reactive). By solving

the two subproblems (possibly with multiple iterations alternating between the two), one obtains one choice of initial condition for ACOPF problems. To solve the decoupled ACOPF to yield this initial condition, the same solver used by the fully coupled ACOPF problem is applied for consistency. For example, if KNITRO is used to examine ACOPF problem solutions, then the decoupled ACOPF problem which will be provided as an initial condition also uses KNITRO.

Option	Description
`ic=0`	**[Midpoint]** Begin with all voltage magnitudes, voltage angles, real power, and reactive power variables at the midpoint of their bounds
`ic=1`	**[Random]** All variables initialized using random draws between variable bounds except for voltage angles set to zero
`ic=2`	**[Flat]** Flat start, where all initial guesses for voltage magnitude and voltage angle are set to 1.0 and zero, respectively, and power flow initial guesses are set to zero
`ic=3`	**[DC/AC]** Real power and voltage angle values are initialized using a DCOPF model. Voltage magnitudes are initialized at 1.0. Reactive power is initialized using relevant equations from the AC transmission line model (applied to each line separately) and the initialized voltage magnitude and voltage angle values
`ic=4`	**[Decoupled]** Voltage magnitude, voltage angle, real power and reactive power variables are initialized using a decoupled ACOPF model.
`ic=5`	**[DCLoss]** Real power and voltage angle values are initialized using a DCOPF model with line loss approximation (5% increaed demand). Voltage magnitudes are initialized at 1.0. Reactive power is initialized using relevant equations from the AC transmission line model (applied to each line separately) and the initialized voltage magnitude and voltage angle values.

Table 2.4: Six initial conditions for ACOPF problems.

Notice that the system is lossless in DCOPF problems, which is not true in the ACOPF. Therefore, line losses are (very) approximately represented in the DCOPF (used for `ic=5`) by means of increasing demands at each end of each transmission line, with half of a base-case loss value assigned to each side of the line. This was found to avoid overly “tight” initial conditions that resulted if the DCOPF completely neglected losses. This simple change proved to be effective, providing better starting points for the active power generation variable.

2.2.2 Generator Capability Curve

In many ACOPF formulations, generator limits are represented by “rectangle constraints" on active and reactive power output. That is, independent maximum and minimum limits on active and reactive power output are used to model generators’ capabilities. However, more accurate, physically based limits yield generator capability curves in the P-Q plane that are more similar to a roman letter capital $\mathscr{D}$, rather than the rectangle shape. Hence these are often termed "D-curves." Methods to represent generator’s capabilities accurately in OPF can be found in [43, 44]. The impact of reactive power limits is investigated for maximum loading and active/reactive OPF market model in [43]. The work in [44] employs detailed generator modeling including automatic voltage regulator and speed governor with generator capability curves in OPF, and establishes that the most accurate capability curves require dependence on generator voltage magnitude. Here, we first derive the voltage-independent D-curves, that can be identified from only typical power flow information. For cases where more detailed generator parameters are available, we demonstrate use of the more accurate voltage-dependent D-curve constraints.

The D-curve consists of three limits, namely the armature current limit, field current limit and end region heating limit. Each of these limits are represented by a circle and the D-curve is constructed by intersection region of these three circles. This section defines equations to model D-curves from given values, P^{max}/P^{min} and Q^{max}/Q^{min}. More detail regarding the construction of equations, and contents of this section can be found in [45]. An example of the capability curve for typical generators resulting from the procedure in this document is displayed in Figure 2.1.

2.2.2.1 Armature Current Limit

This limit is defined using the rated MVA of the generator. The armature current limit is described by a circle with center at the origin and radius equal to the rated MVA of the generator. Lacking more detailed information, we define

$$R^{max} = \max\left(P^{max}, Q^{max}\right) \tag{2.4}$$

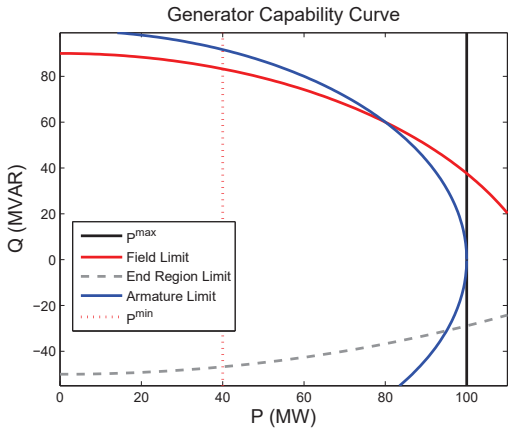

Figure 2.1: Generator Capability Curve

as the R^{max}, maximum radius of the circle. The constraint for the armature current limit is

$$P^2 + Q^2 \leq \left(R^{max}\right)^2 \tag{2.5}$$

where P and Q denote the active and reactive power outputs of the generator.

2.2.2.2 Field Current Limit

An equation for this limit in terms of generator parameters is derived in [46]. However, standard machine ratings are used to approximate this limit, with the goal of using only information available in a standard power flow data set. A circle has three degrees of freedom, two representing the location of the center $\left(P_0^{field}, Q_0^{field}\right)$ and one the radius $\left(r^{field}\right)$. Therefore, specifying a circle requires three pieces of information. By using the fact that the field current limit is a circle on the Q-axis [46], $P_0^{field} = 0$ is obtained. We then suppose that maximum output of reactive power is located at zero active power output. This implies that the circle contains the point $(0, Q^{max})$. Lastly, we use the knowledge that the standard machine specifications use operation at rated power factor, which is an intersection point between the field current limit and the armature current limit. With assumption that a rated power factor is 0.80 lagging, a second point$(0.8R^{max}, 0.6R^{max})$ on the circle is obtained. The parameters for the field current

limit circle are then given by a solution to

$$\left(0.8R^{max}\right)^2 + \left(0.6R^{max} - Q_0^{field}\right)^2 = \left(r^{field}\right)^2 \tag{2.6a}$$

$$\left(Q^{max} - Q_0^{field}\right)^2 = \left(r^{field}\right)^2 \tag{2.6b}$$

Solving (28) yields values of Q_0^{field} and r^{field}

$$Q_0^{field} = \frac{(Q^{max})^2 - (R^{max})^2}{2(Q^{max} - 0.6R^{max})} \tag{2.7a}$$

$$r^{field} = Q^{max} - Q_0^{field} \tag{2.7b}$$

the resulting field current limit is

$$P^2 + \left(Q - Q_0^{field}\right)^2 \leq \left(r^{field}\right)^2 \tag{2.8}$$

2.2.2.3 End Region Heating Limit

The lower portion of the D-curve is ascribed to heating of the end regions of the synchronous generator. Unlike the case of the field current limits, there is not a detailed derivation for these limits from the generator parameters [46]. Therefore, we use several assumptions to approximate these limits in similar manner as to the field current limits. Specifically, we assume 1) a circle with center $\left(P_0^{end}, Q_0^{end}\right)$ and radius r^{end} on the Q-axis (i.e., $P_0^{end} = 0$) describes the end region heating limit, 2) minimum output of reactives power is located at zero active power output, which indicates that the point $\left(0, Q^{min}\right)$ is on this circle, and 3) this limit and the armature current limit intersect at 0.95 power factor leading. With these assumptions, we develop a similar argument to that used in the end region heating limit:

$$\left(0.95R^{max}\right)^2 + \left(Q_0^{end} - 0.31R^{max}\right)^2 = \left(r^{end}\right)^2 \tag{2.9a}$$

$$\left(Q_0^{end} - Q^{min}\right)^2 = \left(r^{end}\right)^2 \tag{2.9b}$$

Solving (31) yields values of Q_0^{end} and r^{end}

$$Q_0^{end} = \frac{\left(Q^{min}\right)^2 - (R^{max})^2}{2\left(Q^{min} + 0.31R^{max}\right)} \tag{2.10a}$$

$$r^{end} = Q_0^{end} - Q^{min} \tag{2.10b}$$

The resulting end region heating limit is

$$P^2 + \left(Q - Q_0^{end}\right)^2 \leq \left(r^{end}\right)^2 \tag{2.11}$$

In the ACOPF problem, equations (2.5), (2.8), and (2.11) replace (2.1f), (2.2g) and (2.3f) according to the formulation when D-curve constraints are used. Notice that shape of D-curve constraints varies depending on the values of Q_0^{field} and Q_0^{end} and only negative values of Q_0^{field} and positive values of Q_0^{end} are physically meaningful. Accordingly, 1) if $Q_0^{field} \geq 0$, we will choose to represent the upper portion of the capability curve as a horizontal line (i.e., $Q \leq Q^{max}$) and disregard the value of Q_0^{field}, 2) if $Q_0^{end} \leq 0$, we will choose to represent the upper portion of the capability curve as a horizontal line (i.e., $Q \geq Q^{min}$) and disregard the value of Q_0^{end}. 3) if numerical issue $Q_0^{field} \approx -inf$ with $Q^{max} \approx 0.6R^{max}$ in the equation (2.7a) occurs, we will fix parameter $Q_0^{field} = \max(Q_0^{field}, 10^{-5})$.

- *Voltage-dependent D-curve (when additional generator parameters available)*

In the previous section, the approximated D-curve constraints are derived in the P-Q plane with the assumption that only power flow data is available. However, more accurately, the D-curve constraints will depend also on performance thresholds from generator auxiliary equipment (such as step-up transformer). In this case, generator output is affected also by terminal voltage, and this terminal voltage is heavily influenced by step-up transformer [40]. A simple equivalent circuit of a synchronous generator that considers these effects is shown in Figure 2.2a.

Let I denote stator current, E the constant emf behind a synchronous reactance X, and V the generator terminal voltage. The armature current limit and field current limit may then be expressed as

$$P^2 + Q^2 \leq (VI^{max})^2 \tag{2.12}$$

$$P^2 + \left(Q + \frac{V^2}{X}\right) \leq \left(\frac{E^{max}V}{X}\right)^2 \tag{2.13}$$

In practice, the generator voltage may typically vary within +5% of rated value, but may rise to 10% above rated value with step-up transformer due to voltage drop across the step-up

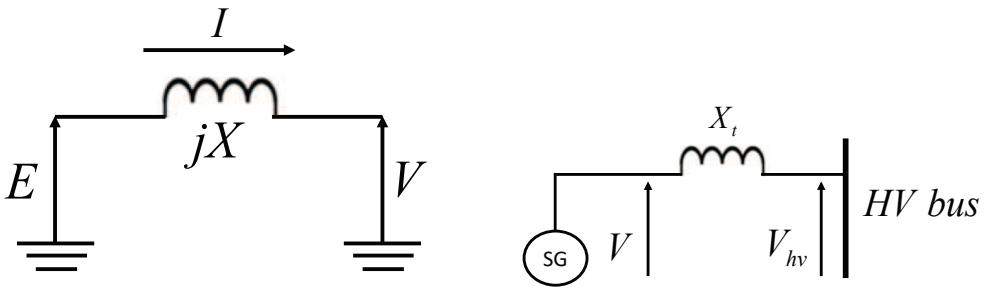

(a) SG simplified circuit

(b) The generator connection via step-up transformer to HV bus

Figure 2.2: Examples of synchronous generator and step-up transformer

transformer reactance described in Figure 2.2b. This voltage drop has to be considered, and is represented by

$$\frac{Q}{V_{hv}} = \frac{V - V_{hv}}{X_t} \tag{2.14}$$

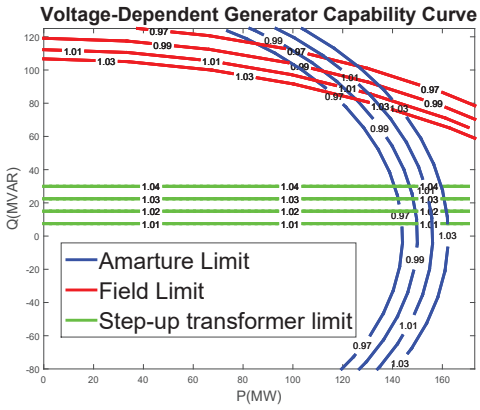

Figure 2.3: Voltage-dependent Generator Capability Curve (different curves for the same limit represent different terminal voltages, e.g. 1.03 is at the terminal voltage V=1.03 pu)

An example of a voltage-dependent generator capability curve including step-up transformer is given in Figure 2.3. For this illustration, HV bus voltage is fixed with 1 pu and the step-up transformer ratio is constant during operation (no tap changer). Thus, when additional information (I^{max}, E^{max}, X, and step-up transformer) about generator is given, equations 2.12, 2.13, and 2.14 can be replaced with 2.5 and 2.8 to represent the voltage-dependent D-curve.

2.2.3 Limitations on adoption of the D-curve model

Ideally, one might seek to impose nonlinear generator D-curve constraints in ACOPF models at all generator buses. However, if one seeks to use the limited data typically available with power flow cases to estimate the D-curve limits, unrealistically small feasible regions will sometimes result. In particular, if the original data is such that the ratio of $\frac{P^{max}}{P^{min}}$ or $\frac{Q^{max}-Q^{min}}{Q^{max}}$ is too small, the estimated area within the D-curve is very small, and use of these constraints is not advised at generator locations where these problems occur. In these cases, the size of an initial rectangle constraint for active and reactive output limits is insufficient to characterize a realistic D-curve constraint. To identify generators whose given data is not suitable for imposing the D-curve constraint, work here used a heuristic test as follows. The ratios $\frac{P^{max}}{P^{min}}$ and $\frac{Q^{max}-Q^{min}}{Q^{max}}$ are formed, and the D-curve constraint is not applied for generators that have $\frac{P^{max}}{P^{min}} \leq 1.1$ or $\frac{Q^{max}-Q^{min}}{Q^{max}} \leq 0.1$. Figure 2.4 below summarizes when the D-curve constraint was imposed in the studies here. Figure 2.4a shows the example of generator that is constrained to produce a fixed

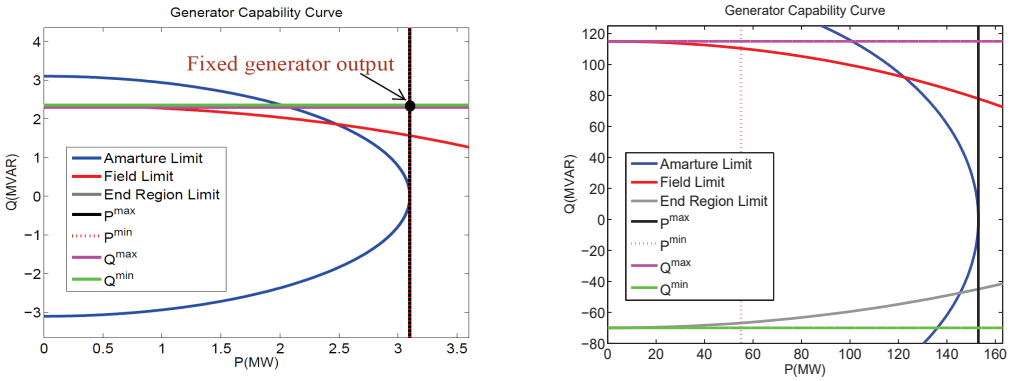

(a) Generator not suitable

(b) Generator suitable

Figure 2.4: Example of when to impose the D-curve constraints

output. The end region heating limit is eliminated because of the nonphysical Q_0^{end} value. In Figure 2.4a , since $P^{max} = P^{min}$ and $Q^{max} = Q^{min}$, the rectangle constraint for this generator output limit is a fixed single point which locates outside of the D-curve constraint. If this case does occur, we use the original rectangle constraint instead of the D-curve constraint. On the other hand, Figure 2.4b describes the generator that has reasonable ratio of $\frac{P_{max}}{P_{min}}$ and $\frac{Q_{max}-Q_{min}}{Q_{max}}$

so that the D-curve constraint lies inside of its rectangle constraint. The D-curve constraint is implemented for this case which is typical for synchronous generators.

2.3 Examination of the ACOPF

ACOPF problems are formulated and calculated in GAMS. Default values for each solver's option are used. In this chapter, the 118 and 2736sp bus test systems from the MATPOWER library are employed as representative examples of our results with three solvers (IPOPTH, KINTRO, CONOPT).

2.3.1 Advantage of adding flow variables

This section investigates the advantage of employing flow quantities as explicit decision variables, as opposed to computing flows from bus voltage variables and line parameters. In brief, the question is that of a tradeoff between larger number of variables that facilitate simpler computations in constraint equations, versus fewer variables but more complex computations in each constraint equation. Results are benchmarked against computational time in a standard ACOPF in the publicly available MATPOWER package [23]. The standard ACOPF, that uses voltage phasors as the key network variables, formulates the OPF problem with polar coordinates using the admittance matrix (Y_{bus}) to calculate the node power balance equations. For the test, since standard ACOPF uses polar coordinate, Polar Power-Voltage is used, and results are depicted in Figure 2.5.

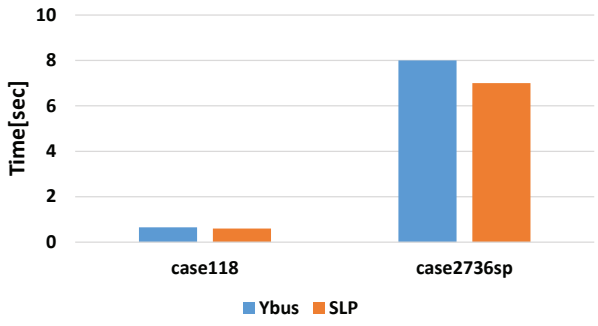

Figure 2.5: Computational time on “Ybus" version versus “SLP" version

There, the label "Y_{bus}" denotes the standard ACOPF using the admittance matrix, while the label "SLP" denotes our formulation using the summation of line power (SLP) flows in the node balance equations. In these tests, the computational time for the large system (case2736sp) was reduced using the SLP formulation. This is consistent with the general rule of thumb in sparse computation techniques, that while elimination of variables may reduce the size of problem, it does not necessarily improve performance. We also have observed this phenomenon in other test cases with our other formulations (Rectangular Power-Voltage and Rectangular Current-Voltage)

2.3.2 Computational Time

Analysis of ACOPF formulations in terms of their computational time is displayed here for the 118-bus and 2736sp-bus cases only. While space limitation prohibits their display here, other test cases of similar size have been examined, and yielded quite similar outcomes in regard to computation time.

Computational (CPU) time for each formulation is shown in Figure 2.6-2.11. In brief, "time" as displayed in the Figures refers to the measured CPU time, from generating initial conditions to production of an optimal solution, and is calculated as the average value. However, initial conditions (`ic=3`, `ic=4`, `ic=5`) require nontrivial computation time in their generation, so a black line used to show CPU time from initial conditions to an optimal solution (i.e. upper part above black line is the time to generate initial conditions).

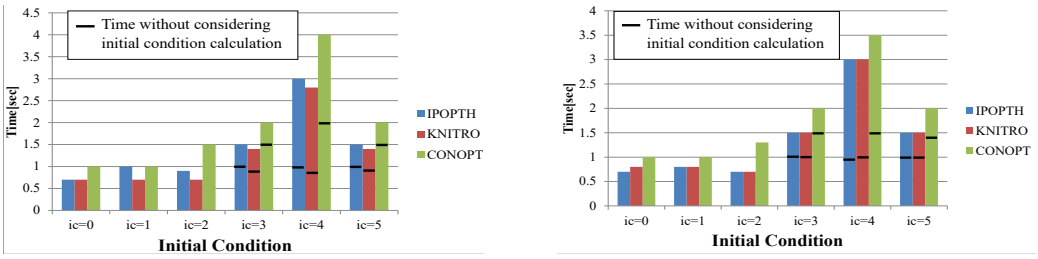

(a) Without D-curve constraints

(b) With D-curve constraints

Figure 2.6: Computational time for Polar Power-Voltage formulation with the 118-bus case

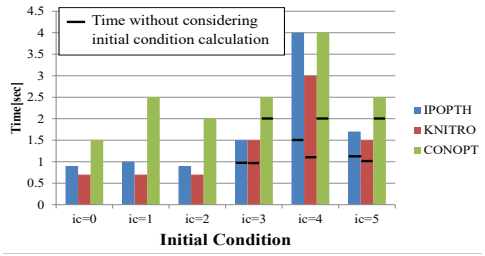

(a) Without D-curve constraints

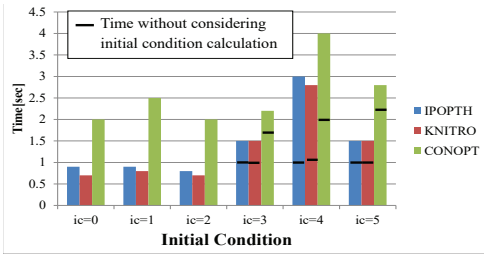

(b) With D-curve constraints

Figure 2.7: Computational time for Rectangular Power-Voltage formulation with the 118-bus case

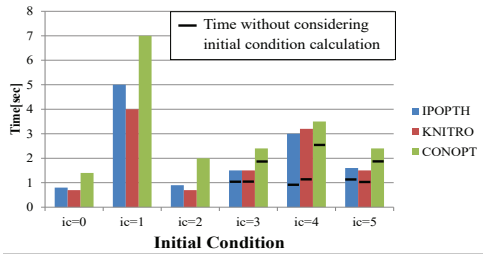

(a) Without D-curve constraints

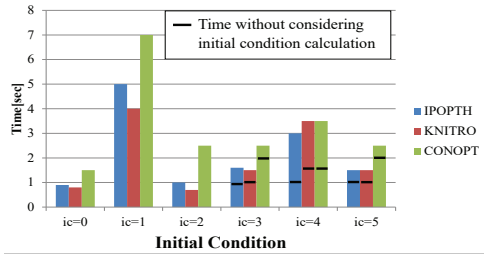

(b) With D-curve constraints

Figure 2.8: Computational time for Rectangular Current-Voltage formulation with the 118-bus case

For instance, `ic=3` with solver IPOPTH in Figure 2.6a requires roughly 0.5 second to obtain an initial condition. Notice that the CPU time for each of initial conditions is displayed with a truncated maximum of 60 seconds in Figure 2.9-2.11. Initial conditions among (`ic=3`, `ic=4`, `ic=5`) which contain no black line in bars indicate it takes greater than 60 seconds even without considering the time to generate its initial condition.

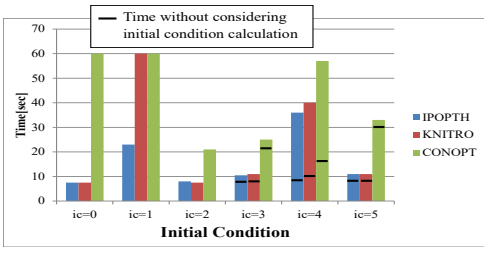

(a) Without D-curve constraints

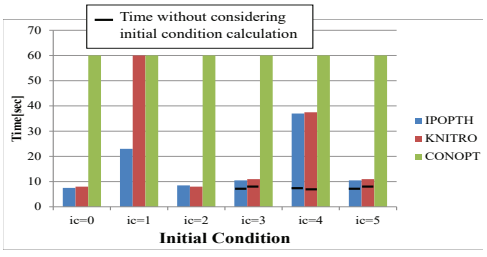

(b) With D-curve constraints

Figure 2.9: Computational time for Polar Power-Voltage formulation with the 2736sp-bus case

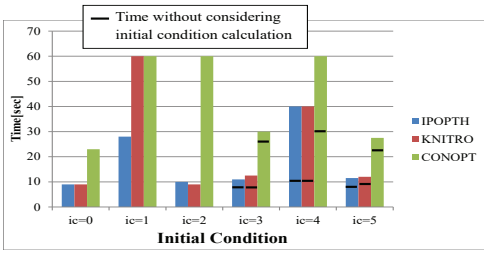

(a) Without D-curve constraints

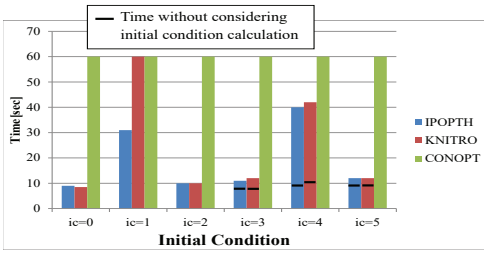

(b) With D-curve constraints

Figure 2.10: Computational time for Rectangular Power-Voltage formulation with the 2736sp-bus case

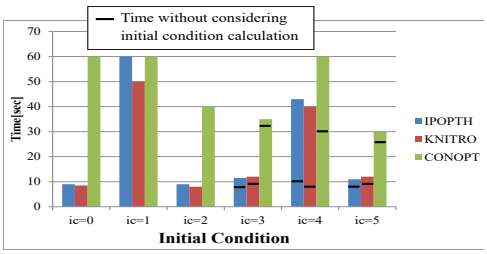

(a) Without D-curve constraints

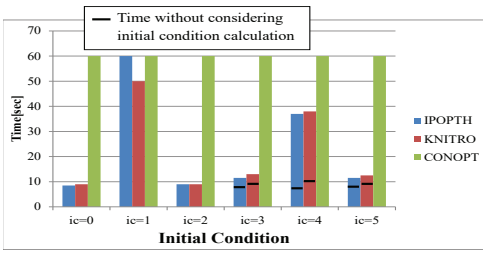

(b) With D-curve constraints

Figure 2.11: Computational time for Rectangular Current-Voltage formulation with the 2736sp-bus case

Figures 2.6-2.8 and 2.9-2.11 show CPU run time for the 118-bus case and 2736sp-bus case respectively. As expected, CPU time in (b) is slightly longer in almost all cases when modeling D-curve constraints. 1) In terms of formulation, cost of time to obtain an optimal solution for Rectangular Power-Voltage is slightly higher than any other ACOPF formulations. 2) With regard to solver, IPOPTH and KNITRO solvers show better performance for ACOPF problems than CONOPT in most cases. For these problems, we have found IPOPTH and KNITRO to be faster and more robust, especially compared to CONOPT, which takes quite a bit longer to converge. D-curve constraints make CONOPT struggle in finding an optimal solution for all initial conditions for the 2736sp-bus case. 3) On the aspect of initial conditions, without considering the time to generate initial conditions, most initial conditions are attractive except for the random, `ic=1`. However, `ic=0,2` provide the fastest convergence for the ACOPF with/without the D-curve constraint irrespective of consideration of generating time for initial conditions.

2.3.3 Robustness of Convergence

This section compares feasibility of ACOPF problems for each formulation with different initial conditions. The ability of a given solver to locate a feasible point from given initial conditions is summarized in Table 2.5.

		POLAR		REC-PV		REC-IV	
		without D-C	with D-C	without D-C	with D-C	without D-C	with D-C
case118	ic=0	O (ALL)	O (ALL)	O (ALL)	O (ALL)	O (ALL)	O (ALL)
	ic=1	O (ALL)	O (ALL)	O (ALL)	O (ALL)	O (ALL)	O (ALL)
	ic=2	O (ALL)	O (ALL)	O (ALL)	O (ALL)	O (ALL)	O (ALL)
	ic=3	O (ALL)	O (ALL)	O (ALL)	O (ALL)	O (ALL)	O (ALL)
	ic=4	O (ALL)	O (ALL)	O (ALL)	O (ALL)	O (ALL)	O (ALL)
	ic=5	O (ALL)	O (ALL)	O (ALL)	O (ALL)	O (ALL)	O (ALL)
case2736sp	ic=0	O (ALL)	O (ALL)	O (ALL)	O (ALL)	O (ALL)	O (ALL)
	ic=1	O (ALL)	O (ALL)	O (ALL)	O (ALL)	O (ALL)	O (ALL)
	ic=2	O (ALL)	O (ALL)	O (ALL)	O (ALL)	O (ALL)	O (ALL)
	ic=3	O (ALL)	O (ALL)	O (ALL)	O (ALL)	O (ALL)	O (ALL)
	ic=4	O (ALL)	O (ALL)	O (ALL)	O (ALL)	O (ALL)	O (ALL)
	ic=5	O (ALL)	O (ALL)	O (ALL)	O (ALL)	O (ALL)	O (ALL)

Table 2.5: Feasibility of ACOPF problems

In the table, $\mathbf{D-C}$ indicates D-curve constraints, with the entries of **O** or **X** indicating feasible or infeasible, respectively. The solver employed is indicated in parentheses to the right of **O** or **X** entry. For example, **O**(ALL) means that it is feasible for all solvers, while **O**(IPOPTH) would indicate that it is only feasible when IPOPTH solver is used. All solvers are able to find a feasible point for all test cases when D-curve constraints are applied. Based on these results, none of ACOPF formulations are superior in their ability to yield feasible points, and all solvers display the ability to handle D-curve constraints.

2.3.4 Objective Value

In order to determine the impact of D-curve constraints on the final solution, we also examine the final objective value, as shown in Table 2.6. These values are provided by all solvers as they produce the same solution. As Table 2.6 indicates, the optimal objective for the 2736sp-bus case is slightly higher.

		POLAR-PV		REC-PV		REC-IV	
		without D-C	with D-C	without D-C	with D-C	without D-C	with D-C
case118	ic=0	129.66K $	129.66K $	129.66K $	129.66K $	129.66K $	129.66K $
	ic=1	129.66K $	129.66K $	129.66K $	129.66K $	129.66K $	129.66K $
	ic=2	129.66K $	129.66K $	129.66K $	129.66K $	129.66K $	129.66K $
	ic=3	129.66K $	129.66K $	129.66K $	129.66K $	129.66K $	129.66K $
	ic=4	129.66K $	129.66K $	129.66K $	129.66K $	129.66K $	129.66K $
	ic=5	129.66K $	129.66K $	129.66K $	129.66K $	129.66K $	129.66K $
case2736sp	ic=0	1307.83K $	1309.03K $	1307.83K $	1309.03K $	1307.83K $	1309.03K $
	ic=1	1307.83K $	1309.03K $	1307.83K $	1309.03K $	1307.83K $	1309.03K $
	ic=2	1307.83K $	1309.03K $	1307.83K $	1309.03K $	1307.83K $	1309.03K $
	ic=3	1307.83K $	1309.03K $	1307.83K $	1309.03K $	1307.83K $	1309.03K $
	ic=4	1307.83K $	1309.03K $	1307.83K $	1309.03K $	1307.83K $	1309.03K $
	ic=5	1307.83K $	1309.03K $	1307.83K $	1309.03K $	1307.83K $	1309.03K $

Table 2.6: Objective value for ACOPF problems

This can be explained as the imposition of the D-curve constraint reduces the feasible region as shown in Figure 2.1, meaning that the standard solution using rectangular bound constraints does not lie within the more restricted D-curve area. In the 118-bus case however, the similar objective value indicate that the inclusion of D-curve constraints make no difference. This implies that the standard solution with rectangle generator output limits stays within the more restricted D-curve area, so that it obtains the essentially identical objective value. While the increase in objective values is modest, use of D-curve constraints as generator capability curves within ACOPF problems is shown to have some impact.

2.3.5 Observation

Summary observations about preferred formulation, solver and initial condition are made in Table 2.7. Polar Power-Voltage and Rectangular Current-Voltage formulation are preferred since they both provide fast convergence. The hope that one might see attractive behavior in solution time with Rectangular Current-Voltage, since equations of apparent current flow are linear has not been proven true in general. Solvers IPOPTH and KNITRO are preferred since they provide a good performance for ACOPF problems in terms of solution time. Decoupled ACOPF solution `ic=4` serves as a good initial condition when the time for generating an initial condition is ignored, though it has disadvantages: possibility of creating infeasibility and cost of the time

to obtain a solution. Overall, simple initial conditions, `ic=0,2`, show better performance than other initial conditions developed.

	Priority of Selection
Formulation	Polar Power-Voltage, Rectangular Current-Voltage
Solver	IPOPTH, KNITRO
Initial Condition	`ic=0`, `ic=2`

Table 2.7: Selection for formulation, solver and initial condition

2.4 Conclusion

This chapter has presented three different ACOPF formulations: Polar Power-Voltage, Rectangular Power-Voltage and Rectangular Current-Voltage. All formulation employ line flow quantities as explicit decision variables, and use summations of those variables to construct node balance equality constraints. With this construction, the familiar Y_{bus} bus admittance matrix is not employed.

Six different methods of generating starting points to initialize ACOPF problems are described and studied. The generator capability curve ("D-curve constraints") are treated, including voltage dependent D-curves, to accurately characterize generator output limits. The resulting families of ACOPF problems are examined in three aspects: robustness of convergence, computational time, and achieved objective function value. Based on results, the Polar-PV and Rectangular-CV show the best performance in terms of computational time. For solution algorithms, IPOPTH and KNITRO proved the most attractive solvers, since these were typically faster and more robust in comparison to CONOPT. In regard to choice of initial conditions, `ic=0,2` showed the faster convergence for the ACOPF with or without the D-curve constraints, relative to other (seemingly more "innovative") initial condition choices. Moreover, experience here suggests that D-curve constraints have modest impact, with only small increases in computation time and optimal objective value. Techniques to construct D-curve constraints contain several assumptions on available data regarding generator parameters, and their impact on the problem is demonstrated. Therefore, if one has more detailed generator descriptions available,

these could yield more accurate D-curve constraints that could yield results slightly different from those here. The reader will also note that Rectangular Current-Voltage formulation, with its advantage of linear equations in many of its limit inequalities, yields computational speed comparable to those of Polar Power-Voltage.

CHAPTER 3

Sparse Tableau Formulation for Power System Networks

3.1 Overview

The classical modeling approach for power networks is based on the bus admittance matrix Y_{bus}, which the bus voltage phasors serve as the key "state" variables for the network, analogous to nodal analysis in standard circuit theory [8], [9]. The Y_{bus} formulation is widely used in many power system analyses because it simply and efficiently summarizes in matrix form the parameters of a transmission system.

However, shortcoming of nodal analysis is that it disallows many standard circuit elements from the class of allowable components such as the voltage source, ideal transformer, ideal op amp, etc. [10]. In circuit analysis, a completely general analysis method, so-called Sparse Tableau Analysis, is introduced to resolve this drawback. Similarly, Y_{bus} formulation restricts many power system network elements. This chapter presents a method to overcome these shortcomings by appropriately adapting Sparse Tableau Formulation (STF) used in circuit analysis.

The organization of this chapter is as follow. Section 3.2 reviews the general Sparse Tableau Formulation from a standard circuit analysis perspective. Section 3.3 then examines the characteristics of the power system application that allow simplification of general Sparse Tableau Formulation. Section 3.4 discusses the relationship between STF and other modeling approaches (the Y_{bus} and Modified Nodal Analysis) in those cases for which both may be applied, examines atypical network elements, modelling of which Sparse Tableau Formulation proves particular advantageous. The application to representative OPF examples in a general purpose optimization tool [47], along with comparisons of computational speed between STF and Y_{bus} formulations, is described in Section 3.5.

3.2 Background

Here, we review the key steps to construct STF circuit constraint equations in 1.4. As a case of interest in power systems, we give special attention to two-port circuit elements. Treatment of two-terminal elements is an easy, simpler case. We assume that the circuit analysis is conducted with respect to complex phasor branch or port currents, denoted i, complex phasor branch or port voltages, denoted v, and complex node voltages/current, denoted V/I. Note that all equality constraints below are complex.

Step 1. Write a complete set of linearly independent Kirchhoff's current law (KCL) equations:

$$Ai = 0 \tag{3.1}$$

Step 2. Write a complete set of linearly independent KVL equations:

$$v - A^T V = 0 \tag{3.2}$$

Step 3. Write the element constitutive equations. If the circuit elements are all affine linear, these may be written as:

$$F_v v + F_i i = u_s \tag{3.3}$$

where A is the node-to-element incident matrix; F_v, F_i are network element matrices; and u_s represents a possible exogenous forcing term, typically representing an independent current or voltage source.

Equations (3.1), (3.2), and (3.3) are the tableau equations. For an element represented as two-port, v and i quantities appear in "port-pairs," as illustrated in the Figure 3.1.

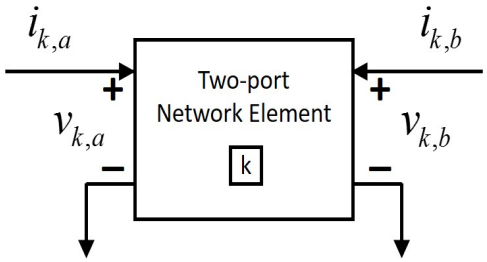

Figure 3.1: Two port representation for network element k

A transmission line is the two-port element perhaps appearing most commonly in the power systems model. In this context, port a quantities are typically termed "sending end" positive sequence voltage and current, and port b quantities termed "receiving end." A two-port element's constitutive relations place two independent algebraic constraints on the four variables (v_a, i_a, v_b, i_b) to specify the element's behavior. For each network element k, in the case of complex, phasor-based analysis, these constraints take the general implicit form

$$f_k : \mathbb{C}^4 \longrightarrow \mathbb{C}^2$$

$$f_k(v_{k,a}, i_{k,a}, v_{k,b}, i_{k,b}) = \begin{bmatrix} 0 \\ 0 \end{bmatrix} \tag{3.4}$$

With all element equations composed together as $f(v,i) = \mathbf{0}$, observe that the element constitutive equation (3.3) in the linear tableau equation is a special affine case of $f(v,i) = \mathbf{0}$; in particular:

$$f(v,i) = \mathbf{0} \triangleq F_v v + F_i i - u_s = 0 \tag{3.5}$$

To illustrate, consider the simple circuit shown in Figure 3.2. It consists of three elements: a voltage source, an ideal transformer described by $v_1 = \frac{n_1}{n_2} v_2$, $i_2 = -\frac{n_1}{n_2} i_1$, and a linear element described by $v_3 = Z i_3$. Applying the preceding steps, we can construct KCL, KVL and element

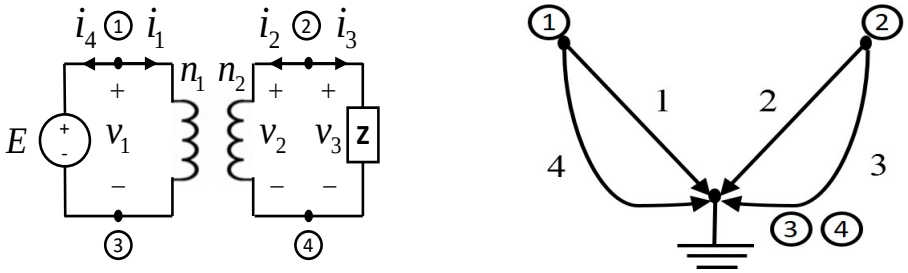

(a) Linear resistive circuit (b) Associated digraph

Figure 3.2: The linear resistive circuit and associated digraph

constitutive equations as following

KCL:
$$AI = 0 \Leftrightarrow \underbrace{\begin{bmatrix} 1 & 0 & 0 & 1 \\ 0 & 1 & 1 & 0 \end{bmatrix}}_{\mathbf{A}} \underbrace{\begin{bmatrix} i_1 \\ i_2 \\ i_3 \\ i_4 \end{bmatrix}}_{\mathbf{i}} = \underbrace{\begin{bmatrix} 0 \\ 0 \end{bmatrix}}_{\mathbf{0}} \tag{3.6}$$

KVL:
$$v - A^T V = \Leftrightarrow \underbrace{\begin{bmatrix} v_1 \\ v_2 \\ v_3 \\ v_4 \end{bmatrix}}_{\mathbf{v}} - \underbrace{\begin{bmatrix} 1 & 0 \\ 0 & 1 \\ 0 & 1 \\ 1 & 0 \end{bmatrix}}_{\mathbf{A}^T} \underbrace{\begin{bmatrix} V_1 \\ V_2 \end{bmatrix}}_{\mathbf{V}} = \underbrace{\begin{bmatrix} 0 \\ 0 \\ 0 \\ 0 \end{bmatrix}}_{\mathbf{0}} \tag{3.7}$$

Branch Equations: (3.8)

$$\left.\begin{array}{l} n_2 v_1 - n_1 v_2 = 0 \\ n_1 i_1 + n_2 i_2 = 0 \\ v_3 - Z i_3 = 0 \\ v_4 = E \end{array}\right\} \Leftrightarrow \underbrace{\begin{bmatrix} n_2 & -n_1 & 0 & 0 \\ 0 & 0 & 0 & 0 \\ 0 & 0 & 1 & 0 \\ 0 & 0 & 0 & 1 \end{bmatrix}}_{\mathbf{F}_v} \underbrace{\begin{bmatrix} v_1 \\ v_2 \\ v_3 \\ v_4 \end{bmatrix}}_{\mathbf{v}} + \underbrace{\begin{bmatrix} 0 & 0 & 0 & 0 \\ n_1 & n_2 & 0 & 0 \\ 0 & 0 & -Z & 0 \\ 0 & 0 & 0 & 0 \end{bmatrix}}_{\mathbf{F}_i} \underbrace{\begin{bmatrix} i_1 \\ i_2 \\ i_3 \\ i_4 \end{bmatrix}}_{\mathbf{i}} = \underbrace{\begin{bmatrix} 0 \\ 0 \\ 0 \\ E \end{bmatrix}}_{\mathbf{u}_s}$$

As described above, incidence matrix A and corresponding two constant matrices F_v, F_i are immediately identifiable in the construction. Therefore, we observe that the circuit is linear iff its branch equations can be written in the form of F_v, F_i, and time-invariant iff both

F_v, F_i are constant with respect to time. As we will see in the next section, standard power system elements within the transmission network are linear and time-invariant; however, we will argue that for models common used in OPF, generators and loads may be represented as nonlinear current sources/sinks.

DEFINITION 3.1. (The Tableau Matrix) Since (3.6), (3.7) and (3.8) which constitute the tableau equation consist of a system of linear equations, it is convenient and more illuminating to rewrite them as a single matrix equation

$$\underbrace{\left[\begin{array}{cc|cccc|cccc} 0 & 0 & 0 & 0 & 0 & 0 & 1 & 0 & 0 & 1 \\ 0 & 0 & 0 & 0 & 0 & 0 & 0 & 1 & 1 & 0 \\ \hline -1 & 0 & 1 & 0 & 0 & 0 & 0 & 0 & 0 & 0 \\ 0 & -1 & 0 & 1 & 0 & 0 & 0 & 0 & 0 & 0 \\ 0 & -1 & 0 & 0 & 1 & 0 & 0 & 0 & 0 & 0 \\ -1 & 0 & 0 & 0 & 0 & 1 & 0 & 0 & 0 & 0 \\ \hline 0 & 0 & n_2 & -n_1 & 0 & 0 & 0 & 0 & 0 & 0 \\ 0 & 0 & 0 & 0 & 0 & 0 & n_1 & n_2 & 0 & 0 \\ 0 & 0 & 0 & 0 & 0 & 1 & 0 & 0 & -Z & 0 \\ 0 & 0 & 0 & 0 & 0 & 0 & 0 & 0 & 0 & 0 \end{array}\right]}_{\mathbf{T}} \underbrace{\left[\begin{array}{c} V_1 \\ V_2 \\ \hline v_1 \\ v_2 \\ v_3 \\ v_4 \\ \hline i_1 \\ i_2 \\ i_3 \\ i_4 \end{array}\right]}_{\mathbf{x}} = \underbrace{\left[\begin{array}{c} 0 \\ 0 \\ \hline 0 \\ 0 \\ 0 \\ 0 \\ \hline 0 \\ 0 \\ 0 \\ E \end{array}\right]}_{\mathbf{u}} \tag{3.9}$$

The tableau matrix T is as it is shown in (3.9) often very sparse, thereby allowing highly efficient numerical algorithms. In general, it can be recast into the compact matrix form with $\mathbf{0}$ and $\mathbf{I}$ denoting a zero and an identity matrix of appropriate dimension.

Linear Tableau Equation :

$$\underbrace{\begin{bmatrix} \mathbf{0} & \mathbf{0} & A \\ -A^T & \mathbf{I} & \mathbf{0} \\ \mathbf{0} & F_v & F_i \end{bmatrix}}_{\mathbf{T}} \underbrace{\begin{bmatrix} V \\ v \\ i \end{bmatrix}}_{\mathbf{x}} = \underbrace{\begin{bmatrix} 0 \\ 0 \\ u_s \end{bmatrix}}_{\mathbf{u}} \tag{3.10}$$

3.3 Sparse Tableau Formulation for Power System Networks

This section applies STF described in the previous section for power system networks. Standard power system network elements are represented as a two-port element and the transmission matrix representation is employed to build branch equations for each network element. With all variables (port voltages v, port currents i, node voltages V and node current I) defined, the corresponding incidence matrix A is constructed to impose linear KCL and KVL equations.

PROPOSITION 3.1. (Sparse Tableau Formulation for power system networks) Standard power system networks can be cast into the compact matrix form using the sparse tableau matrix (3.10) with time-invariant circuit elements implying constant F_v, F_i matrices, with each network element being a non-independent source and with each bus having an exogenous current source, yielding $u_s = I$. The STF is summarized as:

$$\text{STF for power system networks:} \qquad \underbrace{\begin{bmatrix} \mathbf{0} & \mathbf{0} & A \\ -A^T & \mathbf{I} & \mathbf{0} \\ \mathbf{0} & F_v & F_i \end{bmatrix}}_{\mathbf{T}} \underbrace{\begin{bmatrix} V \\ v \\ i \end{bmatrix}}_{\mathbf{x}} = \underbrace{\begin{bmatrix} I \\ 0 \\ 0 \end{bmatrix}}_{\mathbf{u}} \tag{3.11}$$

where I represents externally injected current source from generators or loads. Reasoning for the proof of this theroem is discussed systematically from the next section.

3.3.1 Network Elements Modeling

Proof. First step to prove the **PROPOSITION 3.1** is to consider the standard power system network circuit elements, which are a two-port element as depicted in Figure 3.1 to construct branch equations. Typical examples of two-port network elements would be transmission lines and transformers. In OPF applications, transmission lines are often considered in terms of their π-equivalent circuit, rather than in the two-port [ABCD]-transmission matrix. Hence, their data is typically provided as the three real-value parameters R, X and B, with associated complex series impedance for line given by $Z = R + jX$ and shunt $Y = jB$. At the sending end

and receiving end ports, terminal behavior equivalent to the two-port may be captured in a circuit composed only of simpler two-terminal elements [48], as shown in Figure 3.3.

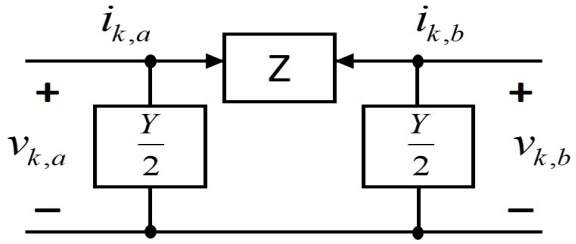

Figure 3.3: π-equivalent circuit for transmission line

However, in standard power systems textbook presentations, one then recovers a two-port constitutive relation consistent with (3.4) by constructing the "Transmission Matrix."

$$\begin{bmatrix} v_{k,a} \\ i_{k,a} \end{bmatrix} = \underbrace{\begin{bmatrix} 1+\frac{ZY}{2} & Z \\ Y(1+\frac{ZY}{4}) & 1+\frac{ZY}{2} \end{bmatrix}}_{\textbf{Transmission Matrix}} \begin{bmatrix} v_{k,b} \\ -i_{k,b} \end{bmatrix} \Longrightarrow \underbrace{\left[\begin{array}{cc|cc} 1 & 0 & -(1+\frac{ZY}{2}) & Z \\ 0 & 1 & -Y(1+\frac{ZY}{4}) & (1+\frac{ZY}{2}) \end{array}\right]}_{\textbf{Representative circuit element } F_k \in \mathbb{C}^{2\times 4}} \begin{bmatrix} v_{k,a} \\ i_{k,a} \\ v_{k,b} \\ i_{k,b} \end{bmatrix} = \begin{bmatrix} 0 \\ 0 \end{bmatrix} \tag{3.12}$$

To adapt the equations (3.12) to STF (3.11), we can re-write the branch equation as

$$\left[\begin{array}{cc|cc} 1 & -(1+\frac{ZY}{2}) & 0 & Z \\ 0 & -Y(1+\frac{ZY}{4}) & 1 & (1+\frac{ZY}{2}) \end{array}\right] \begin{bmatrix} v_{k,a} \\ v_{k,b} \\ i_{k,a} \\ i_{k,b} \end{bmatrix} = \begin{bmatrix} 0 \\ 0 \end{bmatrix}$$

Thus, Linear Element Equations for transmission line:

$$\underbrace{\begin{bmatrix} 1 & -(1+\frac{ZY}{2}) \\ 0 & -Y(1+\frac{ZY}{4}) \end{bmatrix}}_{\mathbf{F}_{k,v}} \begin{bmatrix} v_{k,a} \\ v_{k,b} \end{bmatrix} + \underbrace{\begin{bmatrix} 0 & Z \\ 1 & (1+\frac{ZY}{2}) \end{bmatrix}}_{\mathbf{F}_{k,i}} \begin{bmatrix} i_{k,a} \\ i_{k,b} \end{bmatrix} = \begin{bmatrix} 0 \\ 0 \end{bmatrix} \tag{3.13}$$

Thereby, we obtain the corresponding constant F_v and F_i matrices for the network element of transmission line. The other typical network element is a transformer. Here, voltage gain of

transformer is expressed as complex scalar n to account for phase shifting transformers (real-value voltage gain is for an ideal step up/down transformer allowing only voltage magnitude to change). Then, the corresponding transmission matrix representation is

$$\begin{bmatrix} v_{k,a} \\ i_{k,a} \end{bmatrix} = \begin{bmatrix} n & 0 \\ 0 & \frac{1}{n^*} \end{bmatrix} \begin{bmatrix} v_{k,b} \\ -i_{k,b} \end{bmatrix} \Longrightarrow \left[\begin{array}{cc|cc} 1 & 0 & -n & 0 \\ 0 & 1 & 0 & \frac{1}{n^*} \end{array}\right] \begin{bmatrix} v_{k,a} \\ i_{k,a} \\ v_{k,b} \\ i_{k,b} \end{bmatrix} = \begin{bmatrix} 0 \\ 0 \end{bmatrix} \tag{3.14}$$

This can be equivalently re-written as

$$\text{Linear Element Equation for transformer: } \underbrace{\begin{bmatrix} 1 & -n \\ 0 & 0 \end{bmatrix}}_{\mathbf{F}_{k,v}} \begin{bmatrix} v_{k,a} \\ v_{k,b} \end{bmatrix} + \underbrace{\begin{bmatrix} 0 & 0 \\ 1 & \frac{1}{n^*} \end{bmatrix}}_{\mathbf{F}_{k,i}} \begin{bmatrix} i_{k,a} \\ i_{k,b} \end{bmatrix} = \begin{bmatrix} 0 \\ 0 \end{bmatrix} \tag{3.15}$$

For each of these cases, it is straightforward to identify the corresponding constant F_v and F_i matrices. Note that for these very typical network elements, (3.13) and (3.15) contain only constant coefficients, have no independent sources, and therefore are simple linear functions.

3.3.2 Construction of the incidence matrix A

Remaining constraints are simple linear expressions imposing KVL and KCL interconnection constraints. Since a node-to-element incident matrix A is defined over all network elements, we need to organize all network element variables (port voltages and port currents):

$$v \triangleq \left[\begin{array}{c} v_{1,a} \\ v_{1,b} \\ \hline v_{2,a} \\ v_{2,b} \\ \hline \vdots \\ \vdots \\ \hline v_{l,a} \\ v_{l,b} \end{array}\right], \quad i \triangleq \left[\begin{array}{c} i_{1,a} \\ i_{1,b} \\ \hline i_{2,a} \\ i_{2,b} \\ \hline \vdots \\ \vdots \\ \hline i_{l,a} \\ i_{l,b} \end{array}\right]$$

Thus, $v, i \in \mathbb{C}^{2l}$ where l is number of network elements. Goal in representing KCL is to efficiently to assemble the right hand side of the general current balance equations. To this end, the incidence matrix is then composed entirely of values of 1 or 0 by the following rule:

$$A(j,r) \in \mathbb{R}^{N\times 2l} \triangleq \begin{cases} 1, & \text{if } r\text{th component of } i \text{ corresponds to an elements'} \\ & \text{sending or receiving terminal leaving node } j \\ \hline -1, & \text{if } r\text{th component of } i \text{ corresponds to an elements'} \\ & \text{sending or receiving terminal entering node } j \\ \hline 0, & \text{otherwise} \end{cases} \tag{3.16}$$

Therefore, the current conservation law of KCL is written simply as

$$I - Ai = 0 \ \in \mathbb{C}^N \tag{3.17}$$

where $I \in \mathbb{C}^N$ is the complex current injection from generators or loads at each node; $i \in \mathbb{C}^{2l}$ is the complex branch current carried away from node by network elements. We can also use A to relate port voltages to bus voltages in a manner that guarantees KVL is automatically satisfied. Similarly, linear voltage law of KVL is written as

$$v - A^T V = 0 \ \in \mathbb{C}^{2l} \tag{3.18}$$

where $V \in \mathbb{C}^N$ is the vector of bus voltages. The equation (3.18) is to assign the correct bus voltage to any port voltage of a port connected to that bus. Now, to construct the sparse tableau matrix (3.11), F_v and F_i can be defined as

$$F_v = \begin{bmatrix} F_{1,v} & 0 & \cdots & 0 \\ 0 & F_{2,v} & 0 & \vdots \\ \vdots & \vdots & \ddots & 0 \\ 0 & \cdots & \cdots & F_{l,v} \end{bmatrix} \in \mathbb{C}^{2l\times 2l} \quad F_i = \begin{bmatrix} F_{1,i} & 0 & \cdots & 0 \\ 0 & F_{2,i} & 0 & \vdots \\ \vdots & \vdots & \ddots & 0 \\ 0 & \cdots & \cdots & F_{l,i} \end{bmatrix} \in \mathbb{C}^{2l\times 2l} \tag{3.19}$$

where F_v and F_i are block diagonal matrix composed of previously described $F_{k,v}$, $F_{k,i}$ matrices. Finally, with matrices F_v, F_i, A and variables v, i, V, I as defined above, we can describe power system networks using STF as (3.11). ■

Notice that here we define current source elements I, and this motivates introduction of a special class of nonlinear one-port element as illustrated in Figure 3.4, that facilitates power flow analysis.

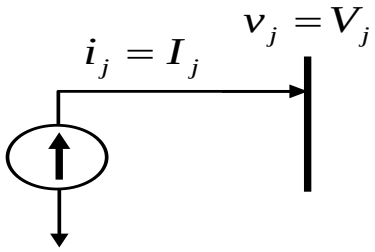

Figure 3.4: Nonlinear current source element as one port element

Then, nonlinear element equation as a equation (3.4) for current source I_j for bus j can be defined by

$$\text{Nonlinear Element Equations}: \quad f_j(v_j, i_j) = 0 \triangleq i_j = \frac{(S_{g,j} - S_{d,j})^*}{v_j^*} \tag{3.20}$$

For simplicity, note that here the element index, j, is assumed to be the same as the index of the bus to which it connects. With this indexing choice, note that $S_j = S_{g,j} - S_{d,j}$, $i_j = I_j$, and $v_j = V_j$ implying

$$\Longrightarrow I_j - \frac{S_j^*}{V_j^*} = 0 \tag{3.21}$$

where $S_{g,j}$ and $S_{d,j}$ are specified apparent power generation and load at bus j. Notice that equation (7.5) is similar to approach in traditional Gauss-Seidel formulation of power flow [24] and, provided v_j identically zero is excluded from the solution set of interest, is equivalent to $S_j = V_j I_j^*$, which is the typical "power balance equation." Notice that standard power flow equations are coupled nonlinear functions, whereas STF power flow equations put all nonlinearity in one bus at a time. Thus, only corresponding bus voltage and bus current are present in these nonlinear functions, indicating there is no coupling between variables associated with different buses in these equations. This property allows STF to have less number of nonzero elements in the Hessian matrix of optimization solving algorithm, which could provide computational efficiency.

3.4 Property of Sparse Tableau Formulation

3.4.1 Relationship to Nodal Analysis and $\mathbf{Y}_{bus}$

As noted previously, textbook power flow analyses typically employ the admittance matrix Y_{bus} to model the transmission network. $Y_{bus} \in \mathbb{C}^{N \times N}$ represents the nodal admittance of the buses in power system networks, and results from writing KCL equations at nodes/buses in terms of node voltages, which is referred to "nodal analysis". A more general procedure for constructing Y_{bus} can be found [8], [9]. Here, we illustrate that Y_{bus} may be obtained from STF, when rank conditions permit, through elimination of intermediate variables. As will become apparent, the required rank conditions place restrictions on allowable circuit element behavior; the greater generality of STF lies in relaxing these restrictions.

LEMMA 3.1. (Y_{bus} and Sparse Tableau Formulation) Standard modeling approach Y_{bus} used in most power system networks represents algebraic elimination of variables from STF with a restrictive assumption.

Proof. Observe that Y_{bus} is a network parameter relating bus voltage and bus current in a way:

$$I = Y_{bus} V \tag{3.22}$$

To relate Y_{bus} to STF, all we need to do is to obtain (3.22) from STF. Consider STF:

$$\begin{cases} Ai = I \\ v = A^T V \\ F_v v + F_i i = 0 \end{cases} \tag{3.23}$$

With these equations under the assumption of F_i full rank, we can solve for i such that

$$i = -(F_i)^{-1} \cdot F_v \cdot v \tag{3.24}$$

Then, substitute the KVL equation $v = A^T V$, yielding

$$i = -(F_i)^{-1} \cdot F_v \cdot A^T V \quad \text{by KCL } I = Ai \tag{3.25}$$

$$I = \underbrace{-A \cdot (F_i)^{-1} \cdot F_v \cdot A^T}_{\mathbf{Y}_{bus}} V \tag{3.26}$$

This demonstrates that the Y_{bus} formulation may be viewed as a simple algebraic elimination of variables from STF and this elimination requires a restrictive assumption that F_i is a full rank matrix, which also requires a full rank condition of each $F_{k,i}$ matrix. ■

This lemma shows that STF is more general modeling approach, in the sense that Y_{bus} is obtained from STF only with the restrictive assumption that F_i is invertible. Important network elements such as ideal transformers and circuit breakers fail this requirement.

3.4.2 Relationship to Modified Nodal Analysis

One approach to overcome the limitations of Y_{bus} that has been employed in power literature is that of MNA [49]. MNA retains select branch currents as explicit variables, in addition to node voltages of a "pure" NA formulation. In the power context, MNA has been employed in transient and fault analysis [50], [51]. Other works [52], [53] use MNA for power flow analysis in distribution systems. In state estimation, MNA has been used to overcome ill-conditioning of Y_{bus} in the presence of very low impedance branches [54], [55]. This section demonstrates that STF serves to generalize MNA/NA.

LEMMA 3.2. (MNA and STF) MNA can be viewed as appropriate algebraic elimination of variables from STF.

Proof. MNA extends nodal analysis by maintaining constraints and variables associated with network elements that nodal analysis cannot handle. Typically, MNA has more variables than NA but less variables than STF. In compact form, MNA can be described as

$$\begin{bmatrix} Ybus & D^1 \\ D^2 & H \end{bmatrix} \begin{bmatrix} V \\ i \end{bmatrix} = \begin{bmatrix} I \\ 0 \end{bmatrix} \tag{3.27}$$

To relate MNA to STF, we partition linear element equations from (3.10) with superscript 2 indicating network element variables that have F_i^2 invertible as

$$\begin{bmatrix} F_v^1 & 0 \\ 0 & F_v^2 \end{bmatrix} \begin{bmatrix} v^1 \\ v^2 \end{bmatrix} + \begin{bmatrix} F_i^1 & 0 \\ 0 & F_i^2 \end{bmatrix} \begin{bmatrix} i^1 \\ i^2 \end{bmatrix} = \begin{bmatrix} 0 \\ 0 \end{bmatrix} \tag{3.28}$$

KCL and KVL equations can then be partitioned as

$$\begin{bmatrix} A^1 & A^2 \end{bmatrix} \begin{bmatrix} i^1 \\ i^2 \end{bmatrix} = I, \begin{bmatrix} v^1 \\ v^2 \end{bmatrix} = \begin{bmatrix} (A^1)^T \\ (A^2)^T \end{bmatrix} V \tag{3.29}$$

Eliminating v^1, v^2 and i^2 from equations above yields MNA:

$$\begin{bmatrix} -A^2(F_i^2)^{-1}F_v^2(A^2)^T & A^1 \\ F_v^1(A^1)^T & F_i^1 \end{bmatrix} \begin{bmatrix} V \\ i^1 \end{bmatrix} = \begin{bmatrix} I \\ 0 \end{bmatrix} \tag{3.30}$$

where $Y_{bus} = -A^2(F_i^2)^{-1}F_v^2(A^2)^T$, $D^1 = A^1$, $D^2 = F_v^1(A^1)^T$, $H = F_i^1$ and $i = i^1$. This demonstrates that MNA formulation may be viewed as an appropriate algebraic elimination of variables from STF. Therefore, the relationship with Y_{bus} and MNA shows that STF is a complete general modeling approach, in the sense that Y_{bus} is obtained from STF only with the restrictive assumption that F_i is invertible and MNA is obtained from STF by appropriately eliminating intermediate variables. ■

3.4.3 Atypical Network Elements using Sparse Tableau Formulation

Part of the argument for STF lies in the convenience with which atypical network elements may be treated, in contrast to the Y_{bus} formulation, that often requires "tricks" in handling such elements. In this section, we provide three examples for atypical network elements: 1) Ideal Transformer, 2) Circuit Breaker, and 3) Three-winding Transformer.

Atypical Element 3.1. (Ideal Transformer) Consider an ideal transformer (3.15). It is apparent that F_i is not invertible, which implies Y_{bus} fails to model the ideal transformer as a stand-alone element. Power system specialists will recognize that in the Y_{bus} formulations, ideal transformers are never treated "stand-alone." Rather, series or shunt impedances representing leakage and/or magnetizing reactances are always lumped in as part of the transformer model.

Atypical Element 3.2. (Circuit Breaker) More importantly, consider the circuit representation of a circuit breaker with binary integer parameter γ indicating switch position.

$$\text{Circuit breaker closed, } \gamma = 1: \quad \begin{cases} v_a - v_b = 0 \\ i_a + i_b = 0 \end{cases} \implies \underbrace{\begin{bmatrix} 1 & -1 \\ 0 & 0 \end{bmatrix}}_{\mathbf{F}_v} \begin{bmatrix} v_a \\ v_b \end{bmatrix} + \underbrace{\begin{bmatrix} 0 & 0 \\ 1 & 1 \end{bmatrix}}_{\mathbf{F}_i} \begin{bmatrix} i_a \\ i_b \end{bmatrix} = \begin{bmatrix} 0 \\ 0 \end{bmatrix} \tag{3.31}$$

$$\text{Circuit breaker open, } \gamma = 0: \quad \begin{cases} i_a = 0 \\ i_b = 0 \end{cases} \implies \underbrace{\begin{bmatrix} 0 & 0 \\ 0 & 0 \end{bmatrix}}_{\mathbf{F}_v} \begin{bmatrix} v_a \\ v_b \end{bmatrix} + \underbrace{\begin{bmatrix} 1 & 0 \\ 0 & 1 \end{bmatrix}}_{\mathbf{F}_i} \begin{bmatrix} i_a \\ i_b \end{bmatrix} = \begin{bmatrix} 0 \\ 0 \end{bmatrix} \tag{3.32}$$

$$\text{Circuit breaker: } \underbrace{\begin{bmatrix} \gamma & -\gamma \\ 0 & 0 \end{bmatrix}}_{\mathbf{F}_v} \begin{bmatrix} v_a \\ v_b \end{bmatrix} + \underbrace{\begin{bmatrix} (1-\gamma) & 0 \\ \gamma & 1 \end{bmatrix}}_{\mathbf{F}_i} \begin{bmatrix} i_a \\ i_b \end{bmatrix} = \begin{bmatrix} 0 \\ 0 \end{bmatrix} \tag{3.33}$$

Similarly, F_i is not guaranteed invertible for both breaker positions, which implies that modeling approach with a fixed Y_{bus} fails to model the circuit breaker. Instead, the Y_{bus} based analysis must rely on "topology processing," which may be viewed as a means to compute and switch between different Y_{bus} matrices, with differing dimensions depending on breaker settings.

Atypical Element 3.3. (Three-winding Transformer) Power system networks often contain three-winding transformers shown in Figure 3.5. Traditional Y_{bus} based modelling approaches

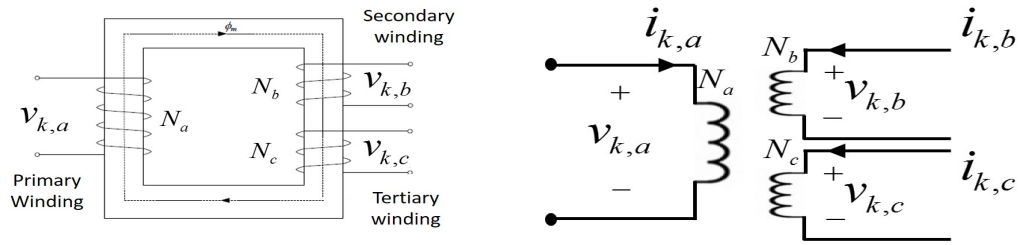

(a) Structure of a three-winding transformer (b) Three-port representation

Figure 3.5: Schematic diagram of a transformer with three windings

introduce equivalent impedances Z_p, Z_s and Z_t in the "star node" configuration [56], [57], [58],

with the magnetizing current and core losses modelled in a magnetizing branch. Arbitrary location of the magnetizing branch is one of the drawbacks of this approach. In addition, this modeling approach with Y_{bus} can create numeric difficulties, because in most large transformers the value of Z_s is very small or even negative. The use of non-physical negative impedances, while common practice, is arguably undesirable, and may challenge automated model data verification methods. We argue that a three-winding transformer is much more appropriately modelled as a three-port; indeed, an arbitrary ideal n-winding transformer may easily be represented as an n-port.

The modeling of a three-winding transformer becomes straightforward with STF. Consider the ideal behavior of a three-winding transformer (which are similar to those of two-winding ideal transformer):

$$\text{Three-winding transformer:} \quad \begin{cases} \frac{1}{N_a} v_a - \frac{1}{N_b} v_b = 0 \\ \frac{1}{N_b} v_b - \frac{1}{N_c} v_c = 0 \\ N_a i_a + N_b i_b + N_c i_c = 0 \end{cases}$$

$$\Longrightarrow \text{Linear Element Equation:} \quad \underbrace{\begin{bmatrix} \frac{1}{N_a} & -\frac{1}{N_b} & 0 \\ 0 & \frac{1}{N_b} & -\frac{1}{N_c} \\ 0 & 0 & 0 \end{bmatrix}}_{\mathbf{F}_v} \begin{bmatrix} v_a \\ v_b \\ v_c \end{bmatrix} + \underbrace{\begin{bmatrix} 0 & 0 & 0 \\ 0 & 0 & 0 \\ N_a & N_b & N_c \end{bmatrix}}_{\mathbf{F}_i} \begin{bmatrix} i_a \\ i_b \\ i_c \end{bmatrix} = \begin{bmatrix} 0 \\ 0 \end{bmatrix}$$

Hence, we can easily model an ideal three-winding transformer as a three-port network element with STF.

3.4.4 Illustrative example with three bus system

This section details STF for power system networks by providing an illustrative example with four-bus system depicted in Figure 3.6.

This system consists of four buses as ①, ②, ③, ④, and four network elements, two transmission lines as 1, 2, one three-winding transformer 3 and one circuit breaker 4. Notice that the Y_{bus} approach cannot model this example directly due to three winding transformer

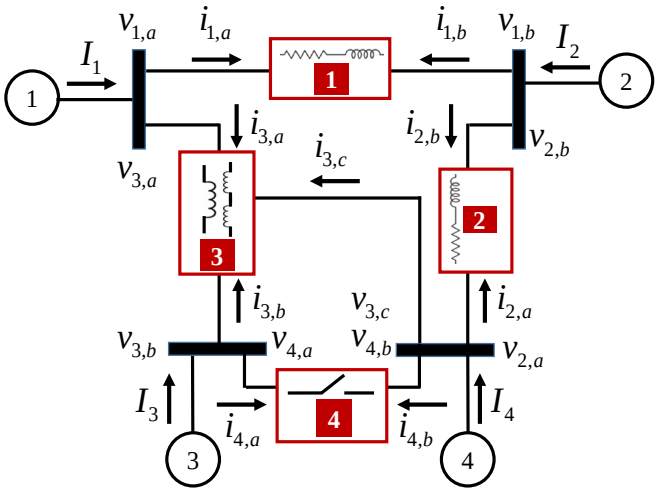

Figure 3.6: Four-bus system for STF

and circuit breaker. Based on the rule (7.2), we can construct the incident matrix A as

$$A = \begin{array}{c} \begin{array}{cccccccccc} \boxed{1},a & \boxed{1},b & \boxed{2},a & \boxed{2},b & \boxed{3},a & \boxed{3},b & \boxed{3},c & \boxed{4},a & \boxed{4},b & \end{array} \\ \left(\begin{array}{cccc|cccc|cc} 1 & 0 & 0 & 0 & 1 & 0 & 0 & 0 & 0 \\ 0 & 1 & 0 & 1 & 0 & 0 & 0 & 0 & 0 \\ 0 & 0 & 0 & 0 & 0 & 1 & 0 & 1 & 0 \\ 0 & 0 & 1 & 0 & 0 & 0 & 1 & 0 & 1 \end{array}\right) \begin{array}{c} ① \\ ② \\ ③ \\ ④ \end{array} \end{array}$$

Each row corresponds to the node and each two-column corresponds to port a or b of the network element. Then, branch equations for each network element can be constructed with $F_{\boxed{k},v}$ for $k \in (1,2)$, $F_{\boxed{3},v}$, and $F_{\boxed{4},v}$

$$F_{\boxed{k},v} = \begin{bmatrix} 1 & -(1+\frac{Z_{\boxed{k}}Y_{\boxed{k}}}{2}) \\ 0 & -Y_{\boxed{k}}(1+\frac{Z_{\boxed{k}}Y_{\boxed{k}}}{4}) \end{bmatrix}, F_{\boxed{3},v} = \begin{bmatrix} \frac{1}{n_a} & -\frac{1}{n_b} & 0 \\ 0 & \frac{1}{n_b} & -\frac{1}{n_c} \\ 0 & 0 & 0 \end{bmatrix}, F_{\boxed{4},v} = \begin{bmatrix} \gamma & -\gamma \\ 0 & 0 \end{bmatrix}$$

Similarly, $F_{\boxed{k},i}$ for $k \in (1,2)$, $F_{\boxed{3},i}$ and $F_{\boxed{4},i}$ can be constructed as

$$F_{\boxed{k},i} = \begin{bmatrix} 0 & Z_{\boxed{k}} \\ 1 & (1+\frac{Z_{\boxed{k}}Y_{\boxed{k}}}{2}) \end{bmatrix}, F_{\boxed{3},i} = \begin{bmatrix} 0 & 0 & 0 \\ 0 & 0 & 0 \\ n_a & n_b & n_c \end{bmatrix}, F_{\boxed{3},i} = \begin{bmatrix} (1-\gamma) & 0 \\ \gamma & 1 \end{bmatrix}$$

where $Z_{\boxed{k}}$, $Y_{\boxed{k}}$ are parameters for the transmission lines $\boxed{1}$ and $\boxed{2}$; n_a, n_b, n_c are turns ratio for the three-winding transformer $\boxed{3}$; γ is binary switch position for the circuit breaker $\boxed{4}$.

Next, we can define all corresponding variables as $v \triangleq [v_{1,a}, v_{1,b}, v_{2,a}, v_{2,b}, v_{3,a}, v_{3,b}, v_{3,c}, v_{4,a}, v_{4,b}]^T$, $i \triangleq [i_{1,a}, i_{1,b}, i_{2,a}, i_{2,b}, i_{3,a}, i_{3,b}, i_{3,c}, i_{4,a}, i_{4,b}]^T$, $V \triangleq [V_1, V_2, V_3, V_4]^T$, $I \triangleq [I_1, I_2, I_3, I_4]^T$. Then, STF for this four-bus system network can be expressed in (3.10) and in detail

$$
\underbrace{\left[\begin{array}{cccc|ccccccccc|cccccccc|c}
0 & 0 & 0 & 0 & 0 & 0 & 0 & 0 & 0 & 0 & 0 & 0 & 0 & 1 & 0 & 0 & 0 & 1 & 0 & 0 & 0 & 0 & V_1 \\
0 & 0 & 0 & 0 & 0 & 0 & 0 & 0 & 0 & 0 & 0 & 0 & 0 & 0 & 1 & 0 & 1 & 0 & 0 & 0 & 0 & 0 & V_2 \\
0 & 0 & 0 & 0 & 0 & 0 & 0 & 0 & 0 & 0 & 0 & 0 & 0 & 0 & 0 & 0 & 0 & 0 & 1 & 0 & 1 & 0 & V_3 \\
0 & 0 & 0 & 0 & 0 & 0 & 0 & 0 & 0 & 0 & 0 & 0 & 0 & 0 & 0 & 1 & 0 & 0 & 0 & 1 & 0 & 1 & V_4 \\
\hline
-1 & 0 & 0 & 0 & 1 & 0 & 0 & 0 & 0 & 0 & 0 & 0 & 0 & 0 & 0 & 0 & 0 & 0 & 0 & 0 & 0 & 0 & v_{1,a} \\
0 & -1 & 0 & 0 & 0 & 1 & 0 & 0 & 0 & 0 & 0 & 0 & 0 & 0 & 0 & 0 & 0 & 0 & 0 & 0 & 0 & 0 & v_{1,b} \\
0 & 0 & 0 & -1 & 0 & 0 & 1 & 0 & 0 & 0 & 0 & 0 & 0 & 0 & 0 & 0 & 0 & 0 & 0 & 0 & 0 & 0 & v_{2,a} \\
0 & -1 & 0 & 0 & 0 & 0 & 0 & 1 & 0 & 0 & 0 & 0 & 0 & 0 & 0 & 0 & 0 & 0 & 0 & 0 & 0 & 0 & v_{2,b} \\
-1 & 0 & 0 & 0 & 0 & 0 & 0 & 0 & 1 & 0 & 0 & 0 & 0 & 0 & 0 & 0 & 0 & 0 & 0 & 0 & 0 & 0 & v_{3,a} \\
0 & 0 & -1 & 0 & 0 & 0 & 0 & 0 & 0 & 1 & 0 & 0 & 0 & 0 & 0 & 0 & 0 & 0 & 0 & 0 & 0 & 0 & v_{3,b} \\
0 & 0 & 0 & -1 & 0 & 0 & 0 & 0 & 0 & 0 & 1 & 0 & 0 & 0 & 0 & 0 & 0 & 0 & 0 & 0 & 0 & 0 & v_{3,c} \\
0 & 0 & -1 & 0 & 0 & 0 & 0 & 0 & 0 & 0 & 0 & 1 & 0 & 0 & 0 & 0 & 0 & 0 & 0 & 0 & 0 & 0 & v_{4,a} \\
0 & 0 & 0 & -1 & 0 & 0 & 0 & 0 & 0 & 0 & 0 & 0 & 1 & 0 & 0 & 0 & 0 & 0 & 0 & 0 & 0 & 0 & v_{4,b} \\
\hline
0 & 0 & 0 & 0 & \multicolumn{4}{c}{\multirow{2}{*}{$F_{\boxed{1},v}$}} & 0 & 0 & 0 & 0 & 0 & 0 & \multicolumn{4}{c}{\multirow{2}{*}{$F_{\boxed{1},i}$}} & 0 & 0 & 0 & 0 & 0 & 0 & i_{1,a} \\
0 & 0 & 0 & 0 & \multicolumn{4}{c}{} & 0 & 0 & 0 & 0 & 0 & 0 & \multicolumn{4}{c}{} & 0 & 0 & 0 & 0 & 0 & 0 & i_{1,b} \\
0 & 0 & 0 & 0 & 0 & 0 & \multicolumn{3}{c}{\multirow{2}{*}{$F_{\boxed{2},v}$}} & 0 & 0 & 0 & 0 & 0 & 0 & 0 & \multicolumn{3}{c}{\multirow{2}{*}{$F_{\boxed{2},i}$}} & 0 & 0 & 0 & 0 & 0 & i_{2,a} \\
0 & 0 & 0 & 0 & 0 & 0 & \multicolumn{3}{c}{} & 0 & 0 & 0 & 0 & 0 & 0 & 0 & \multicolumn{3}{c}{} & 0 & 0 & 0 & 0 & 0 & i_{2,b} \\
0 & 0 & 0 & 0 & 0 & 0 & 0 & 0 & \multicolumn{2}{c}{\multirow{2}{*}{}} & 0 & 0 & 0 & 0 & 0 & 0 & 0 & 0 & \multicolumn{2}{c}{\multirow{2}{*}{}} & 0 & 0 & i_{3,a} \\
0 & 0 & 0 & 0 & 0 & 0 & 0 & 0 & \multicolumn{2}{c}{$F_{\boxed{3},v}$} & 0 & 0 & 0 & 0 & 0 & 0 & 0 & 0 & \multicolumn{2}{c}{$F_{\boxed{3},i}$} & 0 & 0 & i_{3,b} \\
0 & 0 & 0 & 0 & 0 & 0 & 0 & 0 & \multicolumn{2}{c}{\multirow{2}{*}{}} & 0 & 0 & 0 & 0 & 0 & 0 & 0 & 0 & \multicolumn{2}{c}{\multirow{2}{*}{}} & 0 & 0 & i_{3,c} \\
0 & 0 & 0 & 0 & 0 & 0 & 0 & 0 & 0 & 0 & 0 & \multicolumn{2}{c}{\multirow{2}{*}{$F_{\boxed{4},v}$}} & 0 & 0 & 0 & 0 & 0 & 0 & 0 & \multicolumn{2}{c}{\multirow{2}{*}{$F_{\boxed{4},i}$}} & i_{4,a} \\
0 & 0 & 0 & 0 & 0 & 0 & 0 & 0 & 0 & 0 & 0 & \multicolumn{2}{c}{} & 0 & 0 & 0 & 0 & 0 & 0 & 0 & \multicolumn{2}{c}{} & i_{4,b}
\end{array}\right]}_{\mathbf{T}}
\underbrace{\left[\begin{array}{c} V_1 \\ V_2 \\ V_3 \\ V_4 \\ \hline v_{1,a} \\ v_{1,b} \\ v_{2,a} \\ v_{2,b} \\ v_{3,a} \\ v_{3,b} \\ v_{3,c} \\ v_{4,a} \\ v_{4,b} \\ \hline i_{1,a} \\ i_{1,b} \\ i_{2,a} \\ i_{2,b} \\ i_{3,a} \\ i_{3,b} \\ i_{3,c} \\ i_{4,a} \\ i_{4,b} \end{array}\right]}_{\mathbf{x}}
=
\underbrace{\left[\begin{array}{c} I_1 \\ I_2 \\ I_3 \\ I_4 \\ \hline 0 \\ 0 \\ 0 \\ 0 \\ 0 \\ 0 \\ 0 \\ 0 \\ 0 \\ \hline 0 \\ 0 \\ 0 \\ 0 \\ 0 \\ 0 \\ 0 \\ 0 \\ 0 \end{array}\right]}_{\mathbf{u}}
\tag{3.34}
$$

3.5 Application of Sparse Tableau Formulation

We have derived STF for power system networks and STF can be applied for many different power system analyses such as power flow, optimal power flow, fault analysis, contingency analysis and dynamic analysis. This section applies STF for two important power system

analyses, power flow and optimal power flow problem. They are very similar in terms of the system of equations, but the purpose of each problem is bit different. Roughly speaking, we use the OPF problem when we want to determine the generator dispatch. That is, we use the OPF if we know generator cost information, line flow limits, etc. and want to know what the cheapest operating point is (assuming objective function is cost function of generators). We use the power flow problem when we already have a dispatch that we are interested in studying and want to know the consequences of using that dispatch such as bus voltages and line flows.

3.5.1 Power Flow Analysis with Sparse Tableau Formulation

Consider STF:

$$\begin{bmatrix} \mathbf{0} & \mathbf{0} & A \\ -A^T & \mathbf{1} & \mathbf{0} \\ \mathbf{0} & F_v & F_i \end{bmatrix} \begin{bmatrix} V \\ v \\ i \end{bmatrix} = \begin{bmatrix} I \\ 0 \\ 0 \end{bmatrix}, \quad \text{or equivalently} \quad \begin{cases} Ai = I \\ v = A^T V \\ F_v v + F_i i = 0 \end{cases} \tag{3.35}$$

As it is typical in power flow formulations, suppose that generators and loads connected to the network are specified by the active and reactive power they inject and withdraw at node j respectively. So associated with each bus j, net complex power injection is $S_j = P_j + jQ_j$ where $P_j = P^0_{g,j} - P_{d,j}$ and $Q_j = Q_{g,j} - Q_{d,j}$ with ^{0} indicating that $P_{g,j}$ is known, but $Q_{g,j}$ is unknown. Then, net complex power injection S_j for each bus j is related to complex bus voltage V_j and net complex current injection I_j via

$$S_j - V_j \odot (I_j)^* = 0 \tag{3.36}$$

Considering STF and the purpose of power flow analysis that the variable of interest would be bus voltage phasor and line flow, we might implement the elimination of port voltage variable v, resulting in "Reduced Sparse Tableau Formulation (RSTF)" as

$$\begin{bmatrix} \mathbf{0} & A \\ F_v A^T & F_i \end{bmatrix} \begin{bmatrix} V \\ i \end{bmatrix} = \begin{bmatrix} I \\ 0 \end{bmatrix} \quad \text{or equivalently} \quad \begin{cases} Ai - I = 0 \\ F_v A^T V + F_i i = 0 \end{cases} \tag{3.37}$$

With equation 3.36, power flow problem then may be written as

$$\text{Active. Balance:} \quad real(V \odot (Ai)^*)_j = P^0_{g,j} - P_{d,j}, \quad j \in PV, PQ\, bus \tag{3.38a}$$

$$\text{Reactive. Balance:} \quad imag(V \odot (Ai)^*)_j = -Q_{d,j}, \quad j \in PQ\, bus \tag{3.38b}$$

$$\text{Linear Element Equation:} \quad real(F_v A^T V + F_i i) = 0 \tag{3.38c}$$

$$imag(F_v A^T V + F_i i) = 0 \tag{3.38d}$$

Solving (3.38) provides the operating point of bus voltage and current flow on branch which is an additional information compared to the standard PF problem (1.5).

REMARK 3.1. (Sensitivity analysis) The problem of contingency analysis is that of considering the power system network with security requirements. Secure operation requires that the system can withstand (selected) N-1 contingencies [59]. Most of the methods currently in use involve either cumbersome topology changes considering actual line removal, and resolve the net set of equations [60] or using simplified model such as DC power flow [61], [62]. Using Sparse Tableau Formulation allows resulting equations in which line currents, bus voltages all appear explicitly. Thus, a change in line loads and bus voltage can be easily related to changes in the net power injection.

Using vector notation, the power flow equations (3.38) can be conveniently expressed as follows:

$$N(x) = 0, \quad \text{where } x = [V, i]^T \tag{3.39}$$

The typical iterative method using Netwon-Raphson can be used to solve by

$$x^{n+1} = x^n + \Delta x^n, \quad \text{with } N(x^n) + J^n \Delta x^n = 0 \tag{3.40}$$

More specifically, with polar coordinate system as $V = |V|e^{j\delta}$ and $i = |i|e^{j\theta}$ in order to obtain

directly the information of variables of interest; bus voltage magnitude/angle and line loads.

$$
\begin{aligned}
N(x^n) + J^n \Delta x^n = 0 \Longrightarrow & \underbrace{\begin{bmatrix} \Delta P \\ \Delta Q \\ 0 \\ 0 \end{bmatrix}}_{\mathbf{N(x^n)}} + \underbrace{\frac{\partial N}{\partial x}}_{\mathbf{J}^n} \underbrace{\begin{bmatrix} \Delta |V| \\ \Delta \delta \\ \Delta |i| \\ \Delta \theta \end{bmatrix}}_{\Delta\, \mathbf{x}^n} = \underbrace{\begin{bmatrix} 0 \\ 0 \\ 0 \\ 0 \end{bmatrix}}_{\mathbf{0}} \\
\Longrightarrow & \underbrace{\begin{bmatrix} \Delta P \\ \Delta Q \\ 0 \\ 0 \end{bmatrix}}_{\mathbf{N(x^n)}} + \underbrace{\begin{bmatrix} J_{\Delta P, \Delta |V|} & J_{\Delta P, \Delta \delta} & J_{\Delta P, \Delta |i|} & J_{\Delta P, \Delta \theta} \\ J_{\Delta Q, \Delta |V|} & J_{\Delta Q, \Delta \delta} & J_{\Delta Q, \Delta |i|} & J_{\Delta Q, \Delta \theta} \\ J_{\Delta 0^d, \Delta |V|} & J_{\Delta 0^d, \Delta \delta} & J_{\Delta 0^d, \Delta |i|} & J_{\Delta 0^d, \Delta \theta} \\ J_{\Delta 0^q, \Delta |V|} & J_{\Delta 0^q, \Delta \delta} & J_{\Delta 0^q, \Delta |i|} & J_{\Delta 0^q, \Delta \theta} \end{bmatrix}}_{\mathbf{J}^n} \underbrace{\begin{bmatrix} \Delta |V| \\ \Delta \delta \\ \Delta |i| \\ \Delta \theta \end{bmatrix}}_{\Delta\, \mathbf{x}^n} = \underbrace{\begin{bmatrix} 0 \\ 0 \\ 0 \\ 0 \end{bmatrix}}_{\mathbf{0}}
\end{aligned}
\tag{3.41}
$$

Inspection of the Jacobian matrix in (3.41) reveals the sensitivity matrix of current magnitude and complex power injection $J_{\Delta P, \Delta |i|}$, $J_{\Delta Q, \Delta |i|}$ as well as bus voltage magnitude/angle and complex power injection. Observe that components of J^n change depending on an operating point. Thus, direct obtaining of this sensitivity matrix from the Jacobian matrix would be the potential benefit of using Sparse Tableau Formulation. The general form of the Jacobian matrix J is shown

$$
\begin{array}{c}
\begin{matrix} \quad PQ\ bus \quad & \quad PV+PQ\ bus \quad & \quad 2l \quad & \quad 2l \quad \end{matrix} \\
J = \left(\begin{array}{c|c|c|c}
real\left(\frac{\partial V \odot (Ai)^*}{\partial |V|}\right) & real\left(\frac{\partial V \odot (Ai)^*}{\partial \delta}\right) & real\left(\frac{\partial V \odot (Ai)^*}{\partial |i|}\right) & real\left(\frac{\partial V \odot (Ai)^*}{\partial \theta}\right) \\
imag\left(\frac{\partial V \odot (Ai)^*}{\partial |V|}\right) & imag\left(\frac{\partial V \odot (Ai)^*}{\partial \delta}\right) & imag\left(\frac{\partial V \odot (Ai)^*}{\partial |i|}\right) & imag\left(\frac{\partial V \odot (Ai)^*}{\partial \theta}\right) \\
real\left(\frac{\partial (F_v A^T V + F_i i)}{\partial |V|}\right) & real\left(\frac{\partial (F_v A^T V + F_i i)}{\partial \delta}\right) & real\left(\frac{\partial (F_v A^T V + F_i i)}{\partial |i|}\right) & real\left(\frac{\partial (F_v A^T V + F_i i)}{\partial \theta}\right) \\
imag\left(\frac{\partial (F_v A^T V + F_i i)}{\partial |V|}\right) & imag\left(\frac{\partial (F_v A^T V + F_i i)}{\partial \delta}\right) & imag\left(\frac{\partial (F_v A^T V + F_i i)}{\partial |i|}\right) & imag\left(\frac{\partial (F_v A^T V + F_i i)}{\partial \theta}\right)
\end{array}\right)
\begin{matrix} PQ\ bus \\ PV+PQ\ bus \\ 2l \\ 2l \end{matrix}
\end{array}
\tag{3.42}
$$

$$\frac{\partial(V \odot (Ai)^*)}{\partial |V|} = diag(\delta \odot (Ai)^*), \quad \in \mathbb{C}^{N \times N} \tag{3.43}$$

$$\frac{\partial(V \odot (Ai)^*)}{\partial \delta} = \mathbf{j} \cdot diag(V \odot (Ai)^*), \quad \in \mathbb{C}^{N \times N} \tag{3.44}$$

$$\frac{\partial(V \odot (Ai)^*)}{\partial |i|} = diag(V) \cdot (A \cdot diag(\theta))^*, \quad \in \mathbb{C}^{N \times l} \tag{3.45}$$

$$\frac{\partial(V \odot (Ai)^*)}{\partial \theta} = diag(V) \cdot (A \cdot \mathbf{j} \cdot diag(i))^*, \quad \in \mathbb{C}^{N \times l} \tag{3.46}$$

$$\frac{\partial(F_v A^T V + F_i i)}{\partial |V|} = F_v A^T \cdot diag(\delta), \quad \in \mathbb{C}^{2l \times N} \tag{3.47}$$

$$\frac{\partial(F_v A^T V + F_i i)}{\partial \delta} = \mathbf{j} \cdot F_v A^T \cdot diag(V), \quad \in \mathbb{C}^{2l \times N} \tag{3.48}$$

$$\frac{\partial(F_v A^T V + F_i i)}{\partial |i|} = F_i \cdot diag(\theta), \quad \in \mathbb{C}^{2l \times l} \tag{3.49}$$

$$\frac{\partial(F_v A^T V + F_i i)}{\partial \theta} = \mathbf{j} \cdot F_i \cdot diag(i), \quad \in \mathbb{C}^{2l \times l} \tag{3.50}$$

where $diag$ follows the MATLAB operator convention, representing operator to create diagonal matrix, and $\mathbf{j}$ is the square root of -1.

3.5.2 Optimal Power Flow with Sparse Tableau Formulation

This section applies STF to OPF problem. Suppose that generators and loads connected to the network are specified by the active and reactive power they inject and withdraw at node respectively. So associated with each bus j, net complex power injection is $S_j = P_j + jQ_j$ where $P_j = P_{g,j} - P_{d,j}$ and $Q_j = Q_{g,j} - Q_{d,j}$. In the OPF, P_j and Q_j will be a decision variables for bus j corresponding to a generator, and net complex power injection S_j is given as nonlinear element equations with the equation (3.21). The sum of individual quadratic generator cost functions is typically chosen as the objective function. Then, a representative OPF problem might take the following form:

$$\min_{P,Q,v,i,V,I} \quad \sum_{j \in \mathbf{G}} \tilde{c}_j \left(P_{g,j}\right) \quad \text{subject to} \tag{3.51a}$$

$$\text{Linear Element:} \quad F_v v + F_i i = 0 \tag{3.51b}$$

$$\text{KCL:} \quad I - A i = 0 \tag{3.51c}$$

$$\text{KVL:} \quad v - A^T V = 0 \tag{3.51d}$$

$$\text{Nonlinear Element:} \quad S - V \odot (I)^* = 0 \tag{3.51e}$$

$$\text{Gen. Limit:} \quad P_j^{min} \le P_{g,j} \le P_j^{max} \tag{3.51f}$$

$$Q_j^{min} \le Q_{g,j} \le Q_j^{max}, \forall j \in \mathbf{G} \tag{3.51g}$$

$$\text{Vol. Limit:} \quad V_j^{min} \le |V_j| \le V_j^{max}, \forall j \in \mathbf{N} \tag{3.51h}$$

$$\text{Line Limit:} \quad |i_{k,a/b}| \le i_k^{max}, \forall k \in \mathbf{L} \tag{3.51i}$$

One of the benefit to use STF for OPF problem is an explicit appearance of variable i, current flow on branch, so that thermal line limits with current magnitude as a superior choice [41] can be easily incorporated without an additional effort to express the equation of current flows. If these values are not kept in the variables set, they must be computed anyway, which corresponds to Y_{bus} and MNA approach.

3.5.3 Sparsity of MNA and STF in OPF

This section compares the sparsity of MNA and STF matrices in OPF problem. Typically, MNA has more compact form than STF. However, since current flow on lines must be computed to impose thermal line limits in OPF problems, additional constraints for current flow on lines should be included in MNA. For the purpose of comparison, we consider standard network elements for MNA and STF, and the Reduced STF (RSTF) with the trivial elimination of KVL equation ($v = A^T V$), in particular, is used. This trivial elimination has almost no impact on the computation of optimization solving algorithms, so use of full STF for OPF, as per (3.51), is recommended for its clarity. The resulting linear matrices for MNA and STF are:

$$MNA = \begin{bmatrix} Y_{bus} & D^1 \\ D^2 & H \end{bmatrix} \begin{bmatrix} V \\ i_{MNA} \end{bmatrix} = \begin{bmatrix} I \\ 0 \end{bmatrix}, \quad STF = \begin{bmatrix} 0 & A \\ F_v A^T & F_i \end{bmatrix} \begin{bmatrix} V \\ i \end{bmatrix} = \begin{bmatrix} I \\ 0 \end{bmatrix}$$

where $D^1 = \mathbf{0}$, $H = -\mathbf{I}$ with appropriate dimension of zero and identity matrices, and $D^2 = [Y_f, Y_t]^T$ with system branch admittance matrices Y_f and Y_t [23], relating the bus voltages to

the $i_{MNA} = [i_f, i_t]^T$ of branch currents at the *from* and *to* ends of all branches. Notice that the quantities of i_{MNA} and i are same, but order is different. The sparsity structure of resulting matrices for MNA and STF is shown in Figure 3.7.

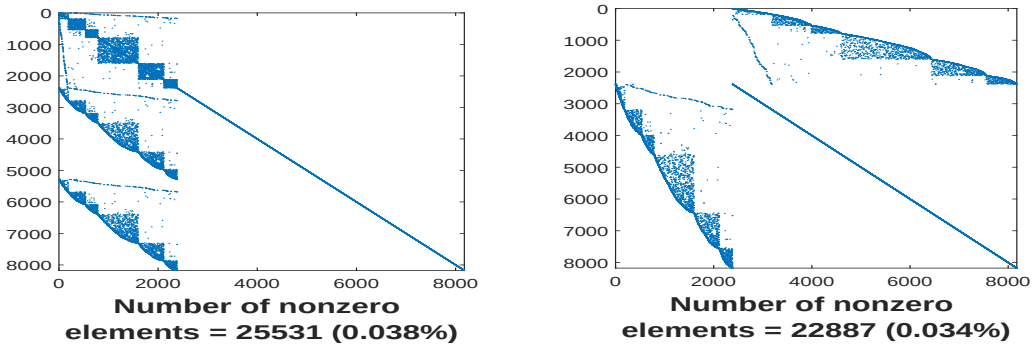

(a) The sparsity of MNA matrix

(b) The sparsity structure of STF matrix

Figure 3.7: The sparse matrix for MNA and STF with case2383wp test system

MATPOWER test cases [23] are used for the comparison and only one test system, case2383wp, is displayed here due to space limitation. However, other test cases have been examined and yielded quite similar outcomes. It is depicted that both matrices are very sparse. However, STF is sparser than MNA since the number of nonzero elements in STF is less than MNA, i.e., 22887 elements in STF compared to 25531 elements in MNA. This is due to keeping Y_{bus} in MNA and the disadvantage of keeping Y_{bus} is also discussed in [63].

3.5.4 Empirically Observed Computation Times

STF for OPF problem in rectangular coordinates (REC-STF) is compared with two standard OPF problems; the polar power-voltage (POLAR-Y_{bus}) and rectangular current-voltage (REC-IV-Y_{bus}) formulation selected as preferred formulations in terms of computational time [63]. Problems are formulated in GAMS [47] and solver KNITRO is selected based on the experience that there are a couple of advantages that KNITRO has over other solvers [64]. Computational time is evaluated on standard IEEE instances available from MATPOWER. The test cases range from 118 buses to as many as 3000 buses.

Notice that because REC-IV-Y_{bus} and REC-STF limit current magnitudes rather than ap-

	POLAR-Y_{bus}		REC-IV-Y_{bus}		REC-STF	
	Obj($/hr)	Time	Obj($/hr)	Time	Obj($/hr)	Time
case118	129660.68	0.3sec	129660.68	0.3sec	129660.68	0.3sec
case300	719725.07	0.6sec	719725.07	2sec	719725.07	0.6sec
case2383wp	1868511.82	5.6sec	1862367.02	5.2sec	1862367.02	6.3sec
case3012wp	2591706.57	5.8sec	2582670.47	5.9sec	2582670.47	6sec
case3120sp	2142703.76	5.8sec	2141532.10	6.3sec	2141532.10	6.5sec
case3375wp	7412030.67	54sec	7404635.99	11.7sec	7404635.99	11.4sec

Table 3.1: Comparison of ACOPF problems

parent power on lines, the solutions will be slightly different than the POLAR-Y_{bus} formulation that limits apparent power on lines. Three formulations show that a similar computational time is required to solve the problem for most test cases, and POLAR-Y_{bus} or REC-IV-Y_{bus} or REC-STF is more superior than others for some cases, which demonstrates that STF of OPF preserves the computational efficiency. This can be viewed that automatic intermediate variable eliminations of advanced optimization solving techniques [65] take advantage of the structure of STF for OPF problem.

3.6 Conclusion

In this chapter, we have detailed the modeling of power system networks, employing two-port representations of network component behavior, and STF for network interconnections. Definition and concepts of STF used in circuit analysis is appropriately manipulated and applied to power system networks. An illustrative example with four-bus system is given for developing of a concrete understanding. Two categories of practical issues associated with STF are discussed: modeling issues and the application to power flow and optimal power flow problem.

Relationship with Y_{bus} and MNA formulation is studied, and it has shown that Y_{bus} formulation is a special case obtained by elimination of variables with the restrictive assumption that F_i matrix needs to be invertible, and MNA is obtained by appropriate algebraic elimination of variables. Specific network elements in which STF becomes useful include atypical network ele-

ments where Y_{bus} formulation might lose a well-conditioned representation or fail all together. Example of three atypical network elements are given: ideal transformer, circuit breaker and three-winding transformer.

This chapter has provided two applications. First, power flow problem is constructed with STF. Since the typical iterative method using Netwon-Rapshon requires the Jacobian matrix that represents the sensitivity between variables, potential benefits of sensitivity information between power injections and line loads as a by-product with additional variables i, current flow on branch, are discussed for contingency analysis.

Next, optimal power flow problem is constructed with STF. It shows the benefit of having current flow i as explicit variables to impose lines' thermal limit, and is compared with standard ACOPF formulation. Two preferred formulations, polar power-voltage and rectangular current-voltage, are selected, and the experiment demonstrates that the equivalent computational efficiency of STF for OPF problem.

CHAPTER 4

A Sparse Tableau Formulation for Node-Breaker Representations in Security-Constrained Optimal Power Flow

Realistic representations of contingencies in AC optimal power flow (OPF) often challenge traditional "bus-branch" network models, which represent network constraints in terms of the familiar bus admittance matrix, Y_{bus}. Work-arounds for Y_{bus}-based analysis typically rely on "topology processing," switching between different Y_{bus} matrices depending on breaker settings. Instead of treating breaker action as altering network topology, this chapter represents a breaker's position as impacting only constraints associated with a single component, thereby maintaining fixed structure in network constraints.

4.1 Introduction

Maintaining secure grid operation continues to grow in importance as the power system sees a wider variety of participants, with new technologies, new operational objectives, and (unfortunately) new security threats. The effort to make grid "smarter" through improved

communication, control, and computation helps address these challenges, but also introduces new, more complex components that may be exposed to new mechanisms of outage [66]. Hence, it is more challenging than ever for the system operators to ensure that the system is operationally secure, able to withstand contingencies representing credible disturbance and component failure scenarios, while satisfying physical and operational constraints. To this end, the Security-Constrained Optimal Power Flow (SCOPF) is an extension of optimal power flow (OPF) that seeks to optimize a system objective (typically variable operating cost), while enforcing constraints of the normal operating state, as well as constraints that ensure acceptable operation under contingencies. The general title of SCOPF can encompass a wide range of modeling considerations depending upon the time scale of interest, the range of decision variables and control actions considered, and the contingency scenarios represented. In this chapter, we focus on the "preventive" SCOPF (PSCOPF) [67], and focus on a short time scale in which the main post-event remedial action is that of primary frequency response.

Practical SCOPF problems can present extremely large dimension when many contingencies are considered [68]. However, empirical evidence in the literature suggests that in many cases, large numbers of contingency constraints may be inactive, with only a subset of constraints determining the feasible region [69]. Techniques to exploit this characteristic are introduced [67], [70], and more recent approaches to finding and eliminating inactive constraints are presented in [69], [71], [72]. Other work [73] has proposed contingency filtering through an iterative PSCOPF approach.

However, for computational tractability, most of approaches above use DC power flow approximations. Such linear approximations potentially compromise accuracy under stressed system conditions likely to be encountered in many contingency cases. In part due to these concerns, other authors has advocated treatment of the full nonlinear PSCOPF problem [74]. In [75], the authors use interior point methods with contingency filtering and network compression method seeking to make PSCOPF tractable for large-scale systems. A recent European project (GARPUR) [76] also discusses the computational challenge of nonlinear SCOPF in large-scale systems, and the value of breaker switching as corrective action.

PSCOPF studies that treat contingencies in which breaker action yields bus splits or bus mergers present additional computational challenges to many existing formulations. This is because many standard PSCOPF use the so-called "bus-branch model." Over-simplifying slightly, bus-branch models may be characterized as being based purely on nodal analysis, in which buses play the role of circuit nodes, and bus (node) voltages are the only electrical variable explicitly maintained. The nodal analysis formulation gives rise to the familiar bus admittance matrix, Y_{bus}, on which standard power flow formulations are based. Such Y_{bus}-based models require work-arounds to represent circuit breaker action that splits or merges buses, which then changes the number of buses represented. One widely adopted work-around for this is that of "topology processing;" oversimplifying slightly, topology processing constructs a distinct (and possibly differently dimensioned) Y_{bus} for each possible breaker configuration. Therefore, comprehensive study of such contingencies using topology processing involves creating the equivalent of a large number of bus-branch models to describe the many possible post contingency topologies [77].

More complete approaches are often termed "node-breaker" models, replacing the simplified bus models by fully described substation (e.g., circuit breakers, switches, etc.) [78], [12], [11], [79] for contingency analysis. Node-breaker model often employ more general circuit analysis techniques, such as Modified Nodal Analysis, to overcome the limitation of nodal analysis that every element's current is describable as a function of its voltage. In particular, consider representation of an ideal circuit breaker between sections of a bus bar. In the admittance representation (Y_{bus}), the breaker is troublesome because it constitutes an infinite admittance when closed, and a zero admittance when open. This suggests value in new approaches to describe the node-break model for the PSCOPF problem.

To this end, this chapter builds Sparse Tableau Formulation (STF) for power system network to formulate the nonlinear PSCOPF problem under the node-breaker model. Benefits of STF-based formulation specific to power flow equations were explored in the late 1970's and early 1980's by [80] and [81]. STF is in many ways the most versatile formulation of circuit equations, and may be viewed as a natural generalization beyond Modified Nodal Analysis.

This chapter is organized as follows. Section 4.2 describes enhancements necessary for the

PSCOPF; the governor power flow equations in contingency cases and node-breaker model. Section 4.3 discusses STF in the node-breaker model for PSCOPF problem and constructs three different PSCOPF formulations. Section 4.4 investigates the different behavior between the linear and nonlinear model in terms of inactive contingency constraints, and computational performance of proposed STF. Conclusions are presented in Section 4.5.

4.2 Enhancements to Yield Preventive SCOPF

4.2.1 Problem Statement

A General formulation for the PSCOPF is expressed as follow:

$$\min_{x^c, u^0} \quad f^0(x^0, u^0) \tag{4.1}$$

subject to

$$g^c(x^c, u^0) = 0, \quad c \in C$$

$$h^c(x^c, u^0) \leq 0, \quad c \in C$$

Notice that a finite set of contingency cases are indexed as c with $c = 0$ denoting the base case configuration. In each contingency case, the additional constraints, equality and inequality, associated with outage contingencies are introduced as security constraints, in which new set of power balance equations and line flow equations are added for each outage contingency. These new sets of equations are represented by the indexed g^c and h^c, where the network is allowed to take a different operating point for each contingency scenario, with the indexed variable set.

In the PSCOPF, the term “preventive” indicates that the generator control settings must be selected such that all base case and contingency constraints are satisfied; adjustment of control set points is not allowed to re-establish feasibility in the face of a contingency. Control variables u^0 correspond to active power generation and voltage magnitude at generator buses. This subset of decision variables is uniform across the base case and all contingencies. State variables x^c correspond to voltage angle at all buses, voltage magnitude at load buses and reactive power generation, and can vary across each contingency case.

4.2.2 Governor Power Flow Equation

Usually, the OPF problem does not include frequency variables, and power balance model is expressed with only bus voltage variables. However, to allow generators' active power outputs to vary (modestly) away from their setpoint values in post-contingency, here we assume that the actual active power generation is composed of the setpoint value plus a term proportional to a system-wide frequency error. Even for line outage contingencies, system loss may change from the base case, requiring generation shift to maintain system-wide power balance. System-wide power imbalance causes the interconnection frequency to move away from nominal value. The formulation here utilizes system frequency error as a type of slack variable, allowing it to take on a distinct non-zero value for each contingency case.

The approach seeks to approximate the first control action to maintain frequency, that of governor response or primary regulation [46]. The power system network normally sees the speed droop control operate within a few seconds and reaches its maximum within a few tens of seconds after a disturbance. Then, full recovery is provided by longer time scale adjustments through automatic generation control (AGC), contingency reserve activation, and other controls. While STF formulation is easily extended, for simplicity only the short time scale governor control action is represented here. These constraints with frequency-based adjustment of generators' active power output are often described as "governor power flow equations" [82], [83]. The active power balance constraints at generator buses will take the following forms.

$$\text{Power Flow for base case:} \qquad real(V \odot (I)^*)_j = P_{g,j} - P_{d,j}$$

$$\text{Governor Power Flow for contingency case:} \qquad real(V \odot (I)^*)_j = (P_{g,j} - \eta_j \Delta\omega^c) - P_{d,j}$$

where $\Delta P_{g,j} = -\eta_j \Delta\omega^c$ with η_j droop coefficients for generator j, and $\Delta\omega^c$ is a slack variable representing a frequency change. Hence, to account for the imbalance due to one component failure, generators will adjust output by the amount $-\eta_j \Delta\omega^c$ in each contingency case. In fact, the introduction of slack variable is necessary 1) to accurately model the physical behavior of power system networks for contingency cases and 2) to find a feasible point in optimization problem.

A minor variation on this approach is also discussed in [84], with system-wide imbalance of real power in contingency case and generator participation factors. In that approach, system-wide imbalance of active power serves as the slack variable, and generator participation factors reflect governor action re-normalized with respect to power imbalance. Notice that this approach is very similar to the governor power flow approach of this section. The authors have performed computational experiments confirming that two approaches yield the same solution (as expected), but find the governor power flow formulation preferable due to its conceptual clarity. Introduction of a frequency slack variable also is advocated in [85].

4.2.3 Sparse Tableau Formulation of a Node-Breaker Model

Textbook power flow formulations and transmission planning studies often use the bus-branch models to represent power system networks. These models typically use a single bus to represent each substation, thus do not seek to represent details of circuit breakers within a substation.

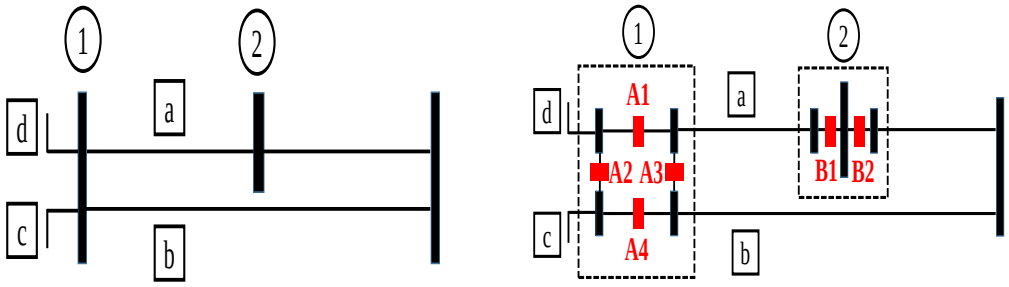

(a) The bus-branch model (b) The node-breaker model

Figure 4.1: The bus-branch VS node-breaker model

Figure 4.1 illustrates a bus-branch model on the left in which details of circuit breakers and nodes are aggregated into buses, while, as its name indicates, the node-breaker model on the right maintains these details [86]. In particular, note that in the greater detail on the right, bus 1 is composed of four nodes connected in a ring configuration. With all lines in service, the same bus-branch model results from a node-breaker model in which all four breakers $A1$ to $A4$ are closed, or from the case for which only $A1$ to $A3$ are closed, $A4$ open. That is, with all lines in

service, we get the same bus-branch model whether $A4$ is open or closed. However, consider a contingency in which line $\boxed{a}$ is removed from service. In the node-breaker model, this requires opening circuit breakers $B1$, $A1$ and $A3$. The outcome of line $\boxed{a}$ being removed from service is very different depending on whether breaker $A4$ is open or closed.

This simple example demonstrates the ways in which realistic representation of contingencies can challenge bus-branch models based on Y_{bus}. A Y_{bus}-based analysis must rely on "topology processing," which may be viewed as a means to switch between differently structured, and often differently dimensioned, Y_{bus} matrices depending on breaker settings [77]. In STF formulation developed here, the KVL and KCL circuit constraints are formulated for the "maximal" set of all possible nodes, with each circuit breaker (or line, transformer, etc.) treated as an individual component. For example, the illustration of Figure 4.1 has seven nodes, and eleven circuit components (though note that lines $\boxed{c}$ and $\boxed{d}$ must terminate to additional nodes not shown the diagram). The opening or closing of a breaker changes the voltage-to-current relation of that one component, but does not change the network topology.

On the other hand, STF can contribute to the node-breaker model. Consider three important network elements (transmission line, transformer and circuit breaker) for contingency analysis as described in Chapter 3, the linear (with respect to voltage and current) element equations for each individual network element k can be simply expressed as i) linear element equation for transmission line k:

$$\underbrace{\begin{bmatrix} 1 & -(1+\frac{ZY}{2}) \\ 0 & -Y(1+\frac{ZY}{4}) \end{bmatrix}}_{\mathbf{F}_{k,v}} \begin{bmatrix} v_{k,a} \\ v_{k,b} \end{bmatrix} + \underbrace{\begin{bmatrix} 0 & Z \\ 1 & (1+\frac{ZY}{2}) \end{bmatrix}}_{\mathbf{F}_{k,i}} \begin{bmatrix} i_{k,a} \\ i_{k,b} \end{bmatrix} = \begin{bmatrix} 0 \\ 0 \end{bmatrix} \tag{4.2}$$

where Z, Y are impedance and shunt parameters for line k; or ii) linear element equation for ideal transformer k:

$$\underbrace{\begin{bmatrix} 1 & -n \\ 0 & 0 \end{bmatrix}}_{\mathbf{F}_{k,v}} \begin{bmatrix} v_{k,a} \\ v_{k,b} \end{bmatrix} + \underbrace{\begin{bmatrix} 0 & 0 \\ 1 & \frac{1}{n^*} \end{bmatrix}}_{\mathbf{F}_{k,i}} \begin{bmatrix} i_{k,a} \\ i_{k,b} \end{bmatrix} = \begin{bmatrix} 0 \\ 0 \end{bmatrix} \tag{4.3}$$

where n is complex turns ratio for transformer k; or iii) linear element equation for circuit

breaker k:

$$\underbrace{\begin{bmatrix} \gamma & -\gamma \\ 0 & 0 \end{bmatrix}}_{\mathbf{F}_{k,v}} \begin{bmatrix} v_{k,a} \\ v_{k,b} \end{bmatrix} + \underbrace{\begin{bmatrix} (1-\gamma) & 0 \\ \gamma & 1 \end{bmatrix}}_{\mathbf{F}_{k,i}} \begin{bmatrix} i_{k,a} \\ i_{k,b} \end{bmatrix} = \begin{bmatrix} 0 \\ 0 \end{bmatrix} \tag{4.4}$$

with $\gamma = 1$ for circuit breaker closed and $\gamma = 0$ for circuit breaker open. For the work to follow, note that γ will be treated as a parameter, not a decision variable. Hence, we need not be concerned with the bilinear relation between γ and v or i.

Next, we define F_v and F_i by

$$F_v = \begin{bmatrix} F_{1,v} & 0 & \cdots & 0 \\ 0 & F_{2,v} & 0 & \vdots \\ \vdots & \vdots & \ddots & 0 \\ 0 & \cdots & \cdots & F_{l,v} \end{bmatrix} \in \mathbb{C}^{2l \times 2l} \quad F_i = \begin{bmatrix} F_{1,i} & 0 & \cdots & 0 \\ 0 & F_{2,i} & 0 & \vdots \\ \vdots & \vdots & \ddots & 0 \\ 0 & \cdots & \cdots & F_{l,i} \end{bmatrix} \in \mathbb{C}^{2l \times 2l} \tag{4.5}$$

where l is number of network elements. Then, by imposing the linear KCL and KVL constraints with a corresponding incidence matrix A, STF for power system network including all network elements can be expressed as

$$\underbrace{\begin{bmatrix} \mathbf{0} & \mathbf{0} & A \\ -A^T & \mathbf{I} & \mathbf{0} \\ \mathbf{0} & F_v & F_i \end{bmatrix}}_{\mathbf{T}} \underbrace{\begin{bmatrix} V \\ v \\ i \end{bmatrix}}_{\mathbf{x}} = \underbrace{\begin{bmatrix} I \\ 0 \\ 0 \end{bmatrix}}_{\mathbf{u}} \tag{4.6}$$

As described in Chapter 3, the equation (4.6) is a more general modeling approach than Y_{bus}-based methods. In particular, STF for contingency analysis proves valuable since the impact of circuit breaker status is simply captured by changing the parameter γ in element equation for circuit breakers. Hence, use of the equation (4.6) allows one to have circuit breakers changing position in a contingency.

Current source elements I plays special role in the power system and this motivates introduction of a special class of nonlinear one-port element to describe generation and load

behavior. The nonlinear element equation for current source I_j at bus j is defined as:

Nonlinear Element Equation for current source:

$$f_j(v_j, i_j) = 0 \triangleq i_j = \frac{(S_{g,j} - S_{d,j})^*}{v_j^*} \tag{4.7}$$

For simplicity, the element index, j, is assumed to be the same as the index of the bus to which it connects. With this indexing choice, note that $S_j = S_{g,j} - S_{d,j}$, $i_j = I_j$, and $v_j = V_j$ implying

$$\Longrightarrow I_j - \frac{S_j^*}{V_j^*} = 0 \tag{4.8}$$

where $S_{g,j}$ and $S_{d,j}$ are specified apparent power generation and load at bus j. Notice that equation (7.5) is similar to approach in traditional Gauss-Seidel formulation of power flow [24] and for non-zero v_j is equivalent to $S_j = V_j I_j^*$, which is the typical "power balance equation."

4.3 Formulation of the Optimization Problem using Sparse Tableau Formulation

This section first describes the way of representing contingencies with Sparse Tableau Formulation. Then, it constructs three different representations of the PSCOPF-DR problem, based on the selection of coordinate system for decision variables.

4.3.1 Sparse Tableau Formulation for contingency analysis

This section discusses the method to implement contingency constraints, especially focusing on circuit breaker actions of bus splits and bus mergers. The representation of breaker action in contingencies implies that the parameter γ^c may take unique values in each contingency. STF simply "concentrates" the effect of changing γ^c to equation (4.4). Use of STF allows us to just change the component behavior, and have a consistent structure for KVL and KCL equations for any breaker position.

Consider the modeling of transmission line with transformer which is usually done by combining these two. Using transmission matrix representation (TR), parameters for the line

that has a transformer (TR_{total}) can be expressed as

$$TR_{total} = \underbrace{\begin{bmatrix} 1+\frac{ZY}{2} & Z \\ Y(1+\frac{ZY}{4}) & 1+\frac{ZY}{2} \end{bmatrix}}_{TR_{line}} \underbrace{\begin{bmatrix} n & 0 \\ 0 & \frac{1}{n^*} \end{bmatrix}}_{TR_{transformer}} = \begin{bmatrix} \alpha & \beta \\ \zeta & \tau \end{bmatrix}$$

Then, consider binary contingency parameter to indicate switch position of network element k for each contingency case c such that

$$\text{Contingency Parameter:} \qquad \gamma_k^c = \begin{cases} 0, & \textbf{Element } k \textbf{ Open} \\ 1, & \textbf{Element } k \textbf{ Close} \end{cases}$$

With this pre-defined contingency parameter, the status of line outage can be conveniently switched over without changes on the data structure by linear element equation for transmission line status (TLS):

$$\begin{bmatrix} \gamma_k^c & -\alpha_k\gamma_k^c \\ 0 & -\zeta_k\gamma_k^c \end{bmatrix} \begin{bmatrix} v_{k,a} \\ v_{k,b} \end{bmatrix} + \begin{bmatrix} (1-\gamma_k^c) & \beta_k\gamma_k^c \\ \gamma_k^c & \tau_k\gamma_k^c-(\gamma_k^c-1) \end{bmatrix} \begin{bmatrix} i_{k,a} \\ i_{k,b} \end{bmatrix} = \begin{bmatrix} 0 \\ 0 \end{bmatrix} \tag{4.9}$$

Similarly, the status of circuit breaker for bus splits and bus mergers can be expressed by linear element equation for circuit breaker status (CBS):

$$\begin{bmatrix} \gamma_k^c & -\gamma_k^c \\ 0 & 0 \end{bmatrix} \begin{bmatrix} v_{k,a} \\ v_{k,b} \end{bmatrix} + \begin{bmatrix} (1-\gamma_k^c) & 0 \\ \gamma_k^c & 1 \end{bmatrix} \begin{bmatrix} i_{k,a} \\ i_{k,b} \end{bmatrix} = \begin{bmatrix} 0 \\ 0 \end{bmatrix} \tag{4.10}$$

These two equations implement the status (on/off) of transmission line k and circuit breaker k for bus splits and bus mergers with pre-defined parameters $\gamma_{k,c}$. This provides the non-dynamic data structure for each contingency c.

REMARK 4.1. (Application to Optimal Transmission Switching): A natural extension of the formulation here in (4.9) is that of Optimal Transmission Switching [87], that allows γ^c to be decision variables, and hence yields a mixed integer program.

4.3.2 Nomenclature

In this section, we provide the notation used in describing the PSCOPF formulations. The

Set	Description
$\mathbf{N}$	Set of buses in the transmission network
$\mathbf{G}$	Set of generators in the transmission network
$\mathbf{G}_j \in \mathbf{G}$	Subset of generators $\mathbf{G}$ at bus $j \in \mathbf{N}$
$\mathbf{L}$	Set of lines in the transmission network
$\mathbf{CB}$	Set of circuit breakers in the transmission network
$\mathbf{C}$	Set of contingency cases ($c = 0$ refering to the base case)

Table 4.1: Description of Sets

set $\mathbf{G}_j$ is used to account for multiple generators and set $\mathbf{C}$ is used to describe contingency level. Typically, one does not account for all possible contingencies, but rather focuses on the so-called $N-1$ contingencies that correspond to each single component outage. Note that any single component (transmission line, transformer, circuit breaker and generator) can be considered for the contingency case, but transmission line and circuit breaker are only considered for this work.

Parameter	Description
$\tilde{c}_j(\cdot)$	Cost function for generation at bus $j \in \mathbf{N}$
$P_{d,j}, Q_{d,j}$	Real and reactive power demand at bus $j \in \mathbf{N}$
g^s_j, b^s_j	Shunt conductance and susceptance at bus $j \in \mathbf{N}$
I^{max}_k	Current limit on line $k \in \mathbf{L}$
P^{min}_j, P^{max}_j	Lower/upper active power generation limits $j \in \mathbf{G}$
Q^{min}_j, Q^{max}_j	Lower/upper reactive power generation limits $j \in \mathbf{G}$
V^{min}_j, V^{max}_j	Voltage magnitude lower and upper limits at bus $j \in \mathbf{N}$
η_j	Droop coefficient for generator $j \in \mathbf{G}$

Table 4.2: Description of Parameters

The most common objective function, dollar-per-hour operating cost, is dependent only on generator set points (we assume that the compensation paid to a generator is based on only its set point power, and any additional power from governor response does not contribute to the objective function). In this work, we assume a 4% of droop percentage value for every generator implying $\eta_j = \frac{1}{0.04} P^{max}_j$.

Variables are defined in Table 4.3; port voltage and current ($v^c = v^{dc} + \mathbf{j} v^{qc}$ and $i^c = i^{dc} + \mathbf{j} i^{qc}$)

Variable	Description
v^c, i^c	Port voltage/current for contingency case $c \in \mathbf{C}$
V^c, I^c	Bus voltage/current for contingency case $c \in \mathbf{C}$
P_g	Active power generation
Q_g^c	Reactive power generation for $c \in \mathbf{C}$
$\Delta\omega^c$	Frequency error for $c \in \mathbf{C}$

Table 4.3: Description of Variables

are always expressed with rectangular coordinate system, yielding a linear voltage/current relationship in branch equations. Bus voltage and current ($V^c = V^{dc} + \mathbf{j}V^{qc}$ or $V^{mc}cos\delta^c + \mathbf{j}V^{mc}sin\delta^c$ and $I^c = I^{dc} + \mathbf{j}I^{qc}$ or $I^{mc}cos\theta^c + \mathbf{j}I^{mc}sin\theta^c$) are expressed in either rectangular or polar coordinate systems. For this problem, primary control variables are two real-value variables: the generator active power set point P_g and generator terminal voltage magnitude V^m. Since we assume 4% droop percentage value for each generator, allowable frequency error is limited to 2% (0.02), bounding $\Delta\omega^c$.

4.3.3 Rectangular Voltage-Current Formulation

Rectangular Sparse Tableau Formulation (REC-STF) uses the rectangular form of complex variables for bus voltage and current value as $V^c = V^{dc} + \mathbf{j}V^{qc}$ and $I^c = I^{dc} + \mathbf{j}I^{qc}$. The nonlinear element equations for power balance constraints are $S_j = V_j(I_j)^*$. In rectangular coordinate, it is equivalent to $S_j = V_j(I_j)^* = V_j^d I_j^d - \mathbf{j}V_j^d I_j^q + \mathbf{j}V_j^q I_j^d + V_j^q I_j^q$. Thus, REC-STF formulation for the PSCOPF-DR problem can be written:

$$\min_{P_g, Q_g^c, v^c, i^c, V^c, I^c, \Delta\omega} \quad \sum_{j \in \mathbf{G}} \tilde{c}_j(P_{g,j}) \qquad \text{subject to}$$

Transmission line status (TLS):

$$\begin{bmatrix} \gamma_k^c & -\alpha_k\gamma_k^c \\ 0 & -\zeta_k\gamma_k^c \end{bmatrix} \begin{bmatrix} v_{k,a}^c \\ v_{k,b}^c \end{bmatrix} + \begin{bmatrix} (1-\gamma_k^c) & \beta_k\gamma_k^c \\ \gamma_k^c & \tau_k\gamma_k^c - (\gamma_k^c - 1) \end{bmatrix} \begin{bmatrix} i_{k,a}^c \\ i_{k,b}^c \end{bmatrix} = \begin{bmatrix} 0 \\ 0 \end{bmatrix}, \quad k \in \mathbf{L}, c \in \mathbf{C} \tag{4.11a}$$

Circuit breaker status (CBS):

$$\begin{bmatrix} \gamma_k^c & -\gamma_k^c \\ 0 & 0 \end{bmatrix} \begin{bmatrix} v_{k,a}^c \\ v_{k,b}^c \end{bmatrix} + \begin{bmatrix} (1-\gamma_k^c) & 0 \\ \gamma_k^c & 1 \end{bmatrix} \begin{bmatrix} i_{k,a}^c \\ i_{k,b}^c \end{bmatrix} = \begin{bmatrix} 0 \\ 0 \end{bmatrix}, \quad k \in \mathbf{CB}, c \in \mathbf{C} \tag{4.11b}$$

Kirchhoff's current law (KCL):

$$\begin{aligned} real(Ai^c) &= I^{dc}, \quad c \in \mathbf{C} \\ imag(Ai^c) &= I^{qc}, \quad c \in \mathbf{C} \end{aligned} \tag{4.11c}$$

Kirchhoff's voltage law (KVL):

$$\begin{aligned} real(v^c) &= A^T V^{dc}, \quad c \in \mathbf{C} \\ imag(v^c) &= A^T V^{qc}, \quad c \in \mathbf{C} \end{aligned} \tag{4.11d}$$

Active power balance:

$$V_j^{dc} I_j^{dc} + V_j^{qc} I_j^{qc} + g_j^s \left((V_j^{dc})^2 + (V_j^{qc})^2 \right) = \left(\sum_{r \in \mathbf{G}_j} P_{g,r} - \eta_r \Delta\omega^c \right) - P_{d,j}, \quad j \in \mathbf{N}, c \in \mathbf{C} \tag{4.11e}$$

Reactive power balance:

$$-V_j^{dc} I_j^{qc} + V_j^{qc} I_j^{dc} - b_j^s \left((V_j^{dc})^2 + (V_j^{qc})^2 \right) = \sum_{r \in \mathbf{G}_j} Q_{g,r}^c - Q_{d,j}, \quad j \in \mathbf{N}, c \in \mathbf{C} \tag{4.11f}$$

Generator output limit:

$$P_r^{min} \le P_{g,r} - \eta_r \Delta\omega^c \le P_r^{max}, \quad r \in \mathbf{G}_j, j \in \mathbf{G}, c \in \mathbf{C} \tag{4.11g}$$

$$Q_r^{min} \le Q_{g,r}^c \le Q_r^{max}, \quad r \in \mathbf{G}_j, j \in \mathbf{G}, c \in \mathbf{C} \tag{4.11h}$$

Voltage magnitude limit:

$$V_j^{min} \le \sqrt{(V_j^{dc})^2 + (V_j^{qc})^2} \le V_j^{max}, \quad j \in \mathbf{N}, c \in \mathbf{C} \tag{4.11i}$$

Voltage magnitude fix:

$$\sqrt{(V_j^{d0})^2 + (V_j^{q0})^2} = \sqrt{(V_j^{dc})^2 + (V_j^{qc})^2}, \quad j \in \mathbf{G}, c \in C/\{0\} \tag{4.11j}$$

Line thermal limit:

$$(i_{k,a/b}^{dc})^2 + (i_{k,a/b}^{qc})^2 \le (I_k^{max})^2, \quad k \in \mathbf{L}, c \in \mathbf{C} \tag{4.11k}$$

Frequency error limit:

$$-0.02 \leq \Delta\omega^c \leq 0.02, \quad c \in C/\{0\} \tag{4.11l}$$

Slack bus condition:

$$V_{slack}^{qc} = 0, \quad c \in \mathbf{C} \tag{4.11m}$$

Base case condition:

$$\Delta\omega^0 = 0 \tag{4.11n}$$

Two set of equations, base case and contingency case, are described in detail. The base case represents the typical OPF formulation with the equation (4.11n) for $c = 0$. The contingency case represents the OPF formulation in quasi steady-state operating with $\Delta\omega^c \neq 0$ for $c \in C/\{0\}$. In a contingency case, equality constraints associated with voltage magnitude control is expressed in equation (4.11j), which indicates that the voltage magnitude at generator buses should remain unchanged from the base case value over contingency cases.

4.3.4 Polar Voltage-Current Formulation

Polar Sparse Tableau Formulation (POL-STF) uses the polar form of complex variables for bus voltage and current, representing these as $V^c = V^{mc}cos\delta^c + \mathbf{j}V^{mc}sin\delta^c$ and $I^c = I^{mc}cos\theta^c + \mathbf{j}I^{mc}sin\theta^c$. The nonlinear element equations for power balance constraints are equivalent to $S_j = V_j(I_j)^* = V_j^m I_j^m cos(\delta_j - \theta_j) + V_j^m I_j^m sin(\delta_j - \theta_j)$. POL-STF formulation for the PSCOPF-DR problem uses the same objective function as used in REC-STF. It can be written:

$$\min_{P_g, Q_g^c, v^c, i^c, V^c, I^c, \Delta\omega} \quad \sum_{j \in \mathbf{G}} \tilde{c}_j(P_{g,j}) \quad \text{subject to}$$

Kirchhoff's current law (KCL):

$$real(Ai^c) = I^{mc}cos\theta^c, \quad c \in \mathbf{C} \tag{4.12a}$$

$$imag(Ai^c) = I^{mc}sin\theta^c, \quad c \in \mathbf{C} \tag{4.12b}$$

Kirchhoff's voltage law (KVL):

$$real(v^c) = A^T(V^{mc} cos\delta^c), \quad c \in \mathbf{C} \tag{4.12c}$$

$$imag(v^c) = A^T(V^{mc} sin\delta^c), \quad c \in \mathbf{C} \tag{4.12d}$$

Active power balance:

$$V_j^{mc} I_j^{mc} cos(\delta_j^c - \theta_j^c) + g_j^s (V^{mc})^2 = (\sum_{r \in \mathbf{G}_j} P_{g,r} - \eta_r \Delta\omega^c) - P_{d,j}, \quad j \in \mathbf{N}, c \in \mathbf{C} \tag{4.12e}$$

Reactive power balance:

$$V_j^{mc} I_j^{mc} sin(\delta_j^c - \theta_j^c) - b_j^s (V^{mc})^2 = \sum_{r \in \mathbf{G}_j} Q_{g,r}^c - Q_{d,j}, \quad j \in \mathbf{N}, c \in \mathbf{C} \tag{4.12f}$$

Voltage magnitude limit:

$$V_j^{min} \leq V_j^{mc} \leq V_j^{max}, \quad j \in \mathbf{N}, c \in \mathbf{C} \tag{4.12g}$$

Voltage magnitude fix:

$$V_j^{m0} = V_j^{mc}, \quad j \in \mathbf{G}, c \in C/\{0\} \tag{4.12h}$$

subject to (4.11a), (4.11b), (4.11g), (4.11k), (4.11l), (4.11m), (4.11n)

Similarly, two set of equations, base case and contingency case, are described in detail. Since voltage magnitude appears explicitly as a variable, equations (4.12g), (4.12h) become linear, but as a trade-off, one has nonlinear relationships for KCL and KVL equations. Remaining network element equations (4.11a), (4.11b), generator limits (4.11g), current flow limits (4.11k), frequency error limits (4.11l), slack bus angle reference (4.11m) and base case condition (4.11n), stay the same.

4.3.5 Hybrid Voltage-Current Formulation

Hybrid Sparse Tableau Formulation (HYB-STF) chooses the hybrid form of complex variables for bus voltage and current value as $V^c = V^{mc} cos\delta^c + \mathbf{j} V^{mc} sin\delta^c$ (where V^m and δ are bus voltage magnitude and angle respectively) and $I^c = I^{dc} + \mathbf{j} I^{qc}$. The nonlinear element equations

for power balance constraints are equivalent to $S_j = V_j(I_j)^* = (V_j^m cos\delta_j)I_j^d - \mathbf{j}(V^m cos\delta_j)I_j^q + \mathbf{j}(V_j^m sin\delta_j)I_j^d + (V^m sin\delta_j)I_j^q$. Empirical evidence favoring polar coordinates only for bus voltage variables is our observation that the voltage magnitude constraints in rectangular coordinates tend to encounter significant problems in power flow convergence [88]. The HYB-STF formulation of the PSCOPF-DR problem can be written as:

$$\min_{P_g,Q_g^c,v^c,i^c,V^c,I^c,\Delta\omega} \quad \sum_{j\in\mathbf{G}} \tilde{c}_j(P_{g,j}) \quad \text{subject to}$$

Kirchhoff's current law (KCL):

$$real(Ai^c) = I^{dc}, \quad c \in \mathbf{C} \tag{4.13a}$$

$$imag(Ai^c) = I^{qc}, \quad c \in \mathbf{C} \tag{4.13b}$$

Kirchhoff's voltage law (KVL):

$$real(v^c) = A^T(V^{mc}cos\delta^c), \quad c \in \mathbf{C} \tag{4.13c}$$

$$imag(v^c) = A^T(V^{mc}sin\delta^c), \quad c \in \mathbf{C} \tag{4.13d}$$

Active power balance:

$$(V_j^{mc}cos\delta_j^c)I_j^{dc} + (V^{mc}sin\delta_j^c)I_j^{qc} + g_j^s(V^{mc})^2 = (\sum_{k\in\mathbf{G}_j} P_{g,r} - \eta_r\Delta\omega^c) - P_{d,j}, \quad j \in \mathbf{N}, c \in \mathbf{C} \tag{4.13e}$$

Reactive power balance:

$$(-V^{mc}cos\delta_j^c)I_j^{qc} + (V_j^{mc}sin\delta_j^c)I_j^{dc} - b_j^s(V^{mc})^2 = \sum_{k\in\mathbf{G}_j} Q_{g,r}^c - Q_{d,j}, \quad j \in \mathbf{N}, c \in \mathbf{C} \tag{4.13f}$$

subject to (4.11a), (4.11b), (4.11c), (4.11g), (4.11k), (4.12g), (4.12h), (4.11l), (4.11m), (4.11n)

In HYB-STF, voltage limits and fixed voltage equations become linear functions, and bus current is still expressed in rectangular form, yielding linear KCL but nonlinear KVL. The three different STF formulations for the PSCOPF-DR problem are summarized in Table 4.4.

4.4 Numerical Case Studies

This section presents case studies to illustrate the effectiveness of the proposed PSCOPF-DR formulation using STF and difference between the different choices of coordinate systems.

	REC-STF	**POL-STF**	**HYB-STF**
Nonconvex equations	- Power balance - Voltage magnitude - Voltage fix	- KCL - KVL - Power balance	- KVL - Power balance
# of nonconvex equations	$(2\mathbf{N}+\mathbf{N})\mathbf{C}+\mathbf{G}(\mathbf{C}-1)$	$(2\mathbf{N}+2\mathbf{L}+2\mathbf{N})\mathbf{C}$	$(2\mathbf{L}+2\mathbf{N})\mathbf{C}$

Table 4.4: Summary of three different PSCOPF-DR formulations

Problems are formulated in GAMS and solver KNITRO and IPOPTH [89] are selected based on the extensive empirical experience with standard ACOPF problems in [63]. During testing, we found that the nonlinear model for security analysis fails to find a feasible point for most of contingency cases if one does not introduce the slack frequency variables to account for changes in system losses. However, in the lossless DC power flow model a feasible point is found without need for frequency slack variables. Hence frequency slack variables are used only for the nonlinear model.

(a) Original substation for the bus-branch model of the RTS-96

(b) Modified substation for the node-breaker model of the RTS-96

Figure 4.2: The bus-branch vs node-breaker model for the RTS-96 network

In this work, two network systems, the RTS-96 network [90] is employed as a test case on the scale of one hundred buses, and a synthetic system produced under the ARPA-E GRID DATA project, the EPIGRIDS 1600-bus system [91] is employed as a somewhat larger test case. Each test system has two representations, one in the bus-branch model (BBM) and one in the node-breaker model (NBM). Modifications made to each system to incorporate bus-breaker detail are shown in Figures 4.2 and 4.3. For the RTS-96 network, three substations are expanded

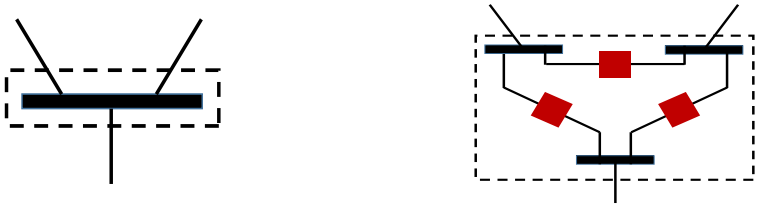

(a) Original substation for the bus-branch model of the EPIGRIDS

(b) Modified substation for the node-breaker model of the EPIGRIDS

Figure 4.3: The bus-branch vs node-breaker model for the EPIGRIDS 1600-bus network

to include a circuit breaker between buses. For the EPIGRIDS network, ten substations are expanded to include circuit breakers in a triangular shape among buses. Resulting network characteristics are summarized in the Table 4.5 with the number of buses, transmission lines and circuit breakers (CBs). Notice that the number of buses and CBs in the NBM is slightly larger than the BBM due to its detailed representation of substations with CBs. Other network elements such as generators, transformers and shunt elements are same for both networks. For the contingency case, only line outage is considered for the BBM and line and CB actions are considered for the NBM. Notice that CB action describes bus splits and bus mergers. As an example with the RTS-96 network, full N-1 contingency case implies that 120 sets of equality and inequality constraints corresponding to each line removal are included in the problem for the BBM, and 123 sets of equality and inequality constraints corresponding to each line and CB action are included in the problem for the NBM.

Table 4.5: Test networks characteristics

	Bus-breanch			Node-breaker		
	Buses	Lines	CBs	Buses	Lines	CBs
RTS-96	73	120	0	76	120	3
EPIGRIDS	1644	2432	0	1664	2432	30

Load demand at buses is not allowed to change over contingency cases and spring weekday at 4AM hour is used for the load data. While major physical and technical constraints should be met at all times, minor violation on line flow constraints are permitted for a short period of time.

For instance, line limits can be expressed with several different values such as normal and emergency rating, where emergency rating are used for a contingency case and higher than the normal rating. These limits are function of the contingency time frame and the pre-contingency operating point, and are obtained based on the fact that the current magnitude and the period of which the current has flowed on the line contribute the heat on the line [92], [93]. In other words, the limits on each network component in the network during a contingency are often less restrictive than those imposed on the component for the pre-contingency case. Thus, in this work, line limit values are increased by 150% from specified data, as emergency ratings for contingency cases.

4.4.1 DC-PSCOPF vs The nonlinear PSCOPF-DR

Perhaps the most significant differences between the linear and nonlinear models in the studies here are the lossless of the DCOPF, and its neglect of voltage variation. The lossless assumption could be crucial in terms of inactive constraints, since no re-dispatch of generator active power output would be required with line removal contingency cases, so long as none of lines hit their limit. This implies that generator active power set points stay same, and power flow on lines are adjusted to satisfy power balance equations (generation = demand) resulting in no change for the objective value.

In this situation, equality and inequality constraints induced by those removed lines are inactive constraints in DCOPF, in which no change in the feasible region of the problem is incurred, so that the problem obtains the same objective value. However, this is typically not true in the ACOPF problem since single line removal will likely change total power loss in the system from the base-case as well as the power balance. Then, re-dispatch of generator active power output is necessary to serve increased system loss (typically, but not always true) and demand. Voltage magnitude limit also could play a role that generator active power set point is needed to be changed. Mathematically, consider the simplified power balance equation:

$$\sum_{j \in \mathbf{N}} \sum_{r \in \mathbf{G_j}} P_{g,r} = \sum_{j \in \mathbf{N}} P_{d,j} + P_{loss} \tag{4.14}$$

Suppose demand $P_{d,j}$ is fixed. In the linear model, system is lossless, $P_{loss} = 0$, implying there is the possibility that $P_{g,r}$ stays same as long as none of post-contingency transmission line flows become binding due to the line outage. On the contrary, the nonlinear model has loss, $P_{loss} \neq 0$, and loss is function of contingency case c such that $P_{loss} = f(*, c)$. It is hard to obtain an analytic representation of contingency-dependent loss function, but we can claim that this loss would change with the line outage. This implies that system must adjust $P_{g,r}$ to compensate a changed system loss. Figure 4.4a and 4.4b describe objective values for the different level of contingency cases between the linear and nonlinear model for the security analysis. The x-axis indicates contingency level (number of removed line) from 0 to 120 (since RTS-96 system has 120 transmission lines), with 0 meaning the base case or pre-contingency case. The y-axis indicates objective values and is scaled by base case solution as $f^*_{scaled,c} = \frac{f^*_c}{f^*_0}$, for $c \in C$ where f^*_c is objective value from the contingency level c.

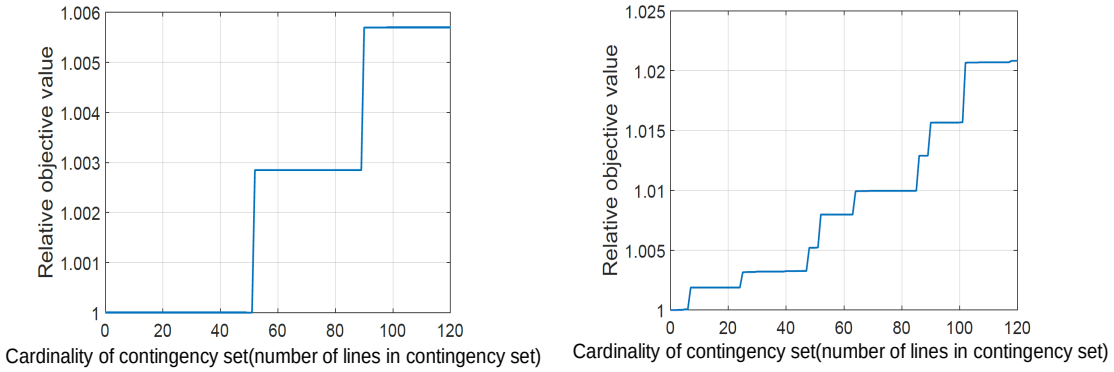

(a) Linear Model

(b) Nonlinear Model

Figure 4.4: Difference between the linear and nonlinear model for the security analysis

In Figure 4.4a, there are two points at line 52 and line 90, in which objective value has a big jump, whereas other values stay same value from the previous value. These are the critical lines that cut off the original feasible region of the problem so that it obtains a different objective value from previous values. Rest of the lines are inactive constraints, which has no contribution to the shape of the original feasible region. Thus, full contingency level solution produces the same objective value with contingency level including only line 52 and 90 for the linear model. Contingency filtering technique or constraints screening method would find these two lines as

non-inactive constraints and remaining lines will be abandoned in the PSCOPF problem.

On the other hand, Figure 4.4b describes different results for the nonlinear model, which shows multiple jumps as the contingency level increases with larger increase in objective value than that of the linear model at the full contingency level ($2\% \gg 0.6\%$). Considering the usage of frequency variable, this test describes that all lines are subject to change the objective value so there are no inactive constraints, which implies every line removal could change the objective value, although there are some lines with small amount of change in the objective value for the nonlinear model.

4.4.2 Computational Results

4.4.2.1 Results for the RTS-96 Network

In order to evaluate the performance of proposed three different formulations, this section conducted comprehensive comparison on the RTS-96 network with the purpose of finding a feasible point within a reasonable time. For each experiment, different contingency "levels" were examined: from 15 component outages through full component outages (full N-1 contingency) are considered for the comparison. The modest size of RTS-96 allows us to treat all N-1 contingency cases for the PSCOPF-DR problem. Computational time and objective values for the BBM with standard ACOPF formulation using NA [63] are compared with the node-breaker model (NBM) with STF, which corresponds to our models (4.11), (4.12), (4.13).

Since the quantity of thermal line limits becomes important when many contingency constraints are considered, for fair comparison, the REC-IV-NA that represents the standard rectangular ACOPF formulation enforcing current magnitude limits on lines is used. Notice that this computational comparison is approximate, because the standard ACOPF formulation is not able to represent the breaker action without topology processing, that was not undertaken here.

The results are encapsulated in Table 4.6. The "–" means finding no solution in 10 min. Number in the first column indicates the contingency level. That is, for the BBM, RTS-96(full) is the RTS-96 test system with the removal of 120 lines. For the NBM, RTS-96(full) is RTS-96 test

	REC-IV-NA (BBM)		REC-STF (NBM)		POL-STF (NBM)		HYB-STF (NBM)	
	Obj ($/h)	Time (sec)	Obj ($/h)	Time (sec)	Obj ($/h)	Time (sec)	Obj ($/h)	Time (sec)
KNITRO								
RTS-96(0)	242975.19	0.06	242975.19	0.06	242975.19	0.6	242975.19	0.1
RTS-96(15)	243027.83	2	243027.83	2	243027.83	167	243027.83	3
RTS-96(30)	243033.70	3.5	243033.70	4	–	NA	243033.70	5
RTS-96(45)	243035.84	7.5	243035.84	8	–	NA	243035.84	8
RTS-96(60)	245262.31	18	245262.31	16	–	NA	245262.31	25
RTS-96(85)	245282.89	27	245282.89	47	–	NA	245282.89	42
RTS-96(100)	247503.79	34	247503.79	45	–	NA	247503.79	44
RTS-96(full)	247507.76	55	247507.83	85	–	NA	247507.83	65
IPOPTH								
RTS-96(0)	242975.19	0.1	242975.19	0.1	242975.19	0.6	242975.19	0.1
RTS-96(15)	243027.83	3	243027.83	3.5	243027.83	170	243027.83	3.5
RTS-96(30)	243033.70	5	243033.70	7	–	NA	243033.70	8
RTS-96(45)	243035.84	12	243035.84	9	–	NA	243035.84	15
RTS-96(60)	245262.31	25	245262.31	23	–	NA	245262.31	19
RTS-96(85)	245282.89	40	245282.89	45	–	NA	245282.89	64
RTS-96(100)	247503.79	45	247503.79	50	–	NA	247503.79	65
RTS-96(full)	247507.76	70	247507.83	65	–	NA	247507.83	100

Table 4.6: Computational time for the PSCOPF-DR problem

system with the removal of 120 lines and 3 circuit breakers. Objective values at RTS-96(full) are different since the NBM has three more circuit breakers contingencies. It has been observed that POL-STF formulation is very unstable and the computational time is noticeably longer to obtain the optimal solution. It is shown that as we increase the contingency level, not only objective value increases but also typically computational time increases. In general, REC-STF and HYB-STF are comparable to REC-IV-NA in computational speed. In KNITRO, HYB-STF tends to be faster than REC-STF, but the reverse is true when employing the IPOPTH solver. In some instances, REC-STF and HYB-STF are faster than REC-IV-NA.

4.4.3 Results for the EPIGRIDS 1600-Bus Network

4.4.3.1 Corrective approach

For the EPIGRIDS 1600-bus network, The POL-STF is not considered due to observed unstable behavior. Notice that generator terminal voltage magnitude is assumed to be held within narrow bounds about its setpoint value in contingency cases [94]. In particular, for the EPIGRIDS network studies, the following limits are imposed:

$$|V_j^{m0} - V_j^{mc}| \leq V_j^{m0}\varepsilon, j \in N_g, c \in C/\{0\} \tag{4.15}$$

where ε is the alloable deviation of generator voltage magnitude from the base case condition after contingency. Note that $\varepsilon = 0$ indicates a strictly "preventive" approach. For this test, 2% (0.02) is used for ε and fixed voltage constraints (4.11j), (4.12h) are replaced with (4.15).

Consideration of the full set of N-1 contingency cases for the EPIGRIDS network proved unmanageable within the memory limitation of computational tools employed in this study. Therefore, the study here considered up to a set of 200 contingencies, which leads to the total of around 500 violations (line limit and voltage magnitude limit) from an initial starting point generated by a conventional (non-OPF) power flow computation. Table 4.7 summarizes results for PSCOPF-DR problem in this system. An entry of "No Memory" indicates the optimization routine was unable to reach solution due to memory limitations. For the EPIGRIDS network, it may be observed that REC-STF and HYB-STF outperform REC-IV-NA as more than 100 contingency cases are considered. The authors hypothesize that these results are because REC-STF and HYB-STF yield significantly fewer nonzero entries in the Hessian matrix, with significant impact on computational time as the problem size becomes large.

Notice that the BBM formulation treated here only considers line outages for contingency cases, but the NBM can treat line and circuit breaker switching for contingency cases. Thus, we consider contingency cases of circuit breaker actions between buses under the NBM along with 100 line contingencies. Since the BBM must use topology processing to represent these contingencies, it is not considered in this comparison. In addition, even though it would be difficult to accurately estimate the computational time of topology processing and compare with

Table 4.7: Computational time for the PSCOPF-DR problem with the EPIGRIDS network

	REC-IV-NA (BBM)		REC-STF (NBM)		HYB-STF (NBM)	
	Obj ($/h)	Time (sec)	Obj ($/h)	Time (sec)	Obj ($/h)	Time (sec)
KNITRO						
EPIGRIDS(0)	212827.88	10	212827.88	10	212827.88	10
EPIGRIDS(60)	212869.86	246	212869.86	250	212869.86	260
EPIGRIDS(100)	212869.86	2427	212869.86	370	212869.86	390
EPIGRIDS(160)	212869.87	4100	212869.87	3000	212869.87	3300
EPIGRIDS(200)	–	No Memory	–	No Memory	–	No Memory
IPOPTH						
EPIGRIDS(0)	239094.21	10	175229.72	10	239103.36	10
EPIGRIDS(60)	212869.86	400	212869.86	420	212869.86	300
EPIGRIDS(100)	212869.86	840	212869.86	550	212869.86	520
EPIGRIDS(160)	212869.87	1400	212869.87	1114	212869.87	1240
EPIGRIDS(200)	–	No Memory	–	No Memory	–	No Memory

the NBM, it is evident that total computational time of the BBM with these contingencies would be greater than the NBM. This is because topology processing would add time to REC-IV-NA, which already requires 2427 sec with 100 contingencies without the added burden of topology processing. Table 4.8 shows results of circuit breaker outages with the NBM. The total of 30 circuit breakers are included with previously defined 100 line contingencies. For example, EPIGRIDS(100+10) means the EPIGRIDS network with the removal of 100 lines and with the action fo 10 circuit breakers.

Table 4.8: The EPIGRIDS network with circuit breaker outages

	REC-STF (NBM)		HYB-STF (NBM)	
	Obj ($/h)	Time (sec)	Obj ($/h)	Time (sec)
KNITRO				
EPIGRIDS(100+10)	212869.87	400	212869.87	550
EPIGRIDS(100+20)	212869.87	650	212869.87	670
EPIGRIDS(100+30)	212869.87	850	212869.87	880

Based on empirical results from the RTS-96 and EPIGRIDS test networks, the studies display the following characteristics:

- **Overall Summary:**

  1) As expected, if one increases the number of contingencies considered, the system operating cost and computational time increase which might represent the system security cost.

  2) STF is comparable in computation time to REC-IV-NA, and REC-STF and HYB-STF are faster than REC-IV-NA as problem size becomes large.

  3) In general, REC-STF and HYB-STF appear to be the preferred formulations for the PSCOPF-DR problem.

  4) Importantly, STF can successfully model/solve the PSCOPF-DR problem with the NBM; in contrast, REC-IV-NA requires additional topology processing.

4.4.3.2 Topological corrective action

In this section, we consider topological corrective actions (TCA) for contingency scenarios. TCA via transmission line switching can be adequately handled in the BBM, whereas circuit breaker switching that merges or splits buses requires the NBM. Therefore, here we focus on circuit breaker switching that merges or splits buses. These types of circuit breaker actions can be easily incorporated using STF, simply by allowing the parameter γ_k^c to be a binary variable. However, the inclusion of topological corrections in the PSCOPF-DR increase the computation time significantly, and the overall problem becomes a nonconvex MINLP due to the introduction of binary decision variables. While of great practical interest, computational tractability in such MINLP-type SCOPF problems remains a significant challenge [76].

Therefore, we consider pre-defined binary contingency parameters for TCA with circuit breaker switching, instead of treating these as binary decision variables. To illustrate, we consider three circuit breakers (CB_1, CB_2, CB_3) in the substation (bus 9) with 100 contingencies, which has 8 possible positions in total. For example, (CB_1 = 1, CB_2 = 1, CB_3 = 1) means all CBs are closed. The results are illustrated in Table 4.9, which shows the impact of changing post-contingency breaker settings on objective value and computational time in the PSCOPF-DR problem. Different breaker settings yield different solution and solving time. For this particular

Table 4.9: Topological corrective action for the EPIGRIDS network

	CB Position			REC-STF (NBM)		HYB-STF (NBM)	
	CB_1	CB_2	CB_3	Obj ($/h)	Time (sec)	Obj ($/h)	Time (sec)
KNITRO							
EPIGRIDS(100)	1	1	1	212869.84	370	212869.84	390
EPIGRIDS(100)	1	1	0	212869.84	350	212869.84	400
EPIGRIDS(100)	1	0	1	212869.86	595	212869.86	420
EPIGRIDS(100)	1	0	0	212904.66	440	212904.66	490
EPIGRIDS(100)	0	1	1	212869.84	480	212869.84	460
EPIGRIDS(100)	0	1	0	212885.81	440	212885.81	480
EPIGRIDS(100)	0	0	1	213024.11	470	213024.11	500
EPIGRIDS(100)	0	0	0	213023.81	400	213023.81	450

test, the network topology with ($CB_1 = 1$, $CB_2 = 1$, $CB_3 = 0$) would appear to be good (if not truly optimal) choice, because since it yields the lowest objective value and is faster than other breaker position selections.

4.5 Conclusion

This chapter has described a Sparse Tableau Formulation (STF) suitable for the PSCOPF problem, and argued for its efficacy when treating breaker actions that re-configure buses in contingencies. Enhancements necessary for the PSCOPF problem are discussed; governor power flow equations and the node-breaker model. STF proves particularly advantages for the node-breaker model that challenges the traditional modeling approach (nodal analysis). STF approach allows treatment of the PSCOPF-DR problem with full node-breaker detail. It is demonstrated that this approach allows use of uniform structure of KVL and KCL constraints as breakers change, "localizing the impact of any breaker action within a component equation for that one breakers." Computational comparison made with the standard Y_{bus}-based ACOPF formulation shows the proposed STF formulation provides comparable computational speed in modest sized problems, and superior computational speed in the larger problems studied here.

STF allows users to formulate and implement the problem in a manner that is well-suited

for the security analysis. Taking the advantage of STF to model network components including circuit breakers, we believe that formulation and implementation for the security analysis becomes simple and straightforward. An important future research direction will be to develop an efficient method to incorporate integer decision variables, allowing the choice of breaker configurations in each contingency part of the optimization. Another future research direction related to this work is to consider more than N-1 contingency cases such as N-2 contingency scenarios with “corrective” SCOPF (CSCOPF) using STF. On the computational issue for large-scale systems, we also want to consider a contingency filtering scheme to pre-select critical contingencies, thus reduce the number of contingencies.

CHAPTER 5

Probabilistic Zonal Reserve Requirements for Grid Deliverability Improvement with Wind Power

5.1 Overview

5.1.1 Motivation

The approach to ensure a secure system employed in Chapter 4 can be viewed more generally as a "worst-case" stochastic programming problem over a set of contingency scenarios because the system is required to guarantee all constraints are met for every contingency. An ideal approach would explicitly represent contingency events probabilistically with the network constraints in the model. However, such approach is still computationally hard for large-scale problems. In this chapter, we focus on an alternative method to address security in the power system networks, without explicit need for STF. Instead we include renewable energy resources as additional sources of uncertainty in the system with network component failures.

Traditionally, such uncertainties in the power system networks are addressed by scheduling additional generation capacity as operating reserve, which is usually set by some deterministic rules such as a fixed percentage of load and/or the MW size of the largest contingency in

the system. This chapter investigates an efficient reserve scheduling, along with wind power forecasts. Full mathematical description with nomenclature for this chapter can be found in appendix B.1.

5.1.2 Introduction

There is a growing interest in wind power as a clean and renewable source of energy for power systems throughout the world. Due to its dependency on the weather, wind power supply is uncertain and volatile compared to conventional thermal units production. The uncertainty and variability of wind power demand different measures to ensure the reliability of power system networks.

One of the important computations significantly challenged by these additional uncertainties within market management systems is that of security-constrained unit commitment (SCUC) [95], [96]. SCUC determines which set of generators will be committed, and typically is decided ("clears") in the day-ahead market. Physical and operational constraints include energy balance, power flows, generator capacity and lines' thermal limit. A traditional method to address uncertainty in the power system is to schedule additional generation capacity as operating reserve, which is usually set by some deterministic rules [97], or in some cases, by stochastic rules [98], [99]. Reserve requirements provide flexibility to help system operators satisfy physical and operational constraints when the system experiences deviations from the forecast.

However, current practices for reserve requirements are largely ad hoc based on deterministic rules and approximations, and hence are not guaranteed to produce market solutions that are physically deliverable. Thus, zones are used to disperse the reserve across the system so that the reserve deliverability is improved. Several works based on zonal reserve requirements are proposed to address deliverability issue [100], [101], [102], [103]. The work in [101] focuses on reserve requirements to relieve intra-zonal congestion. Contingency-based zonal reserve requirements are proposed in [100], [103] but without considering renewable resources.

It is important to note that renewable resources such as wind and solar add another dimension of uncertainty, adding greater challenges to maintain system reliability with reserve

requirements at least cost [104]. In most current approaches, higher levels of renewables not only increase the reserve level but also increase the difficulty of predicting network flows and transmission congestion. Some research efforts address methodologies to estimate the sufficient amounts of operating reserves with wind power forecasts [105], [106], [107]. The work [105] is among the first to determine the operating reserve requirement with wind power uncertainty. In [106], the reserve requirement is estimated based on the system generation margin with risk indices, which allows a system operator evaluate reserve needs with the risk level for a given time horizon. The dynamic reserve zones [102] are proposed to improve the deliverability of reserves with wind power forecasts. In this work, optimization problem is solved for each scenario of wind power forecast, which is similar to scenario-based stochastic programming.

An alternative approach to determine sufficient reserves in power system operations uses scheduling models based on stochastic programming. Stochastic programming has been used for traditional sources of uncertainty (generators, transmission lines, and load) [108], [109] and have in recent years received increasing interest as a means to address wind power uncertainty [110], [111], [112] and overcome the shortcomings of deterministic models. It would appear to be far preferable approach since it explicitly represents the events of uncertainties (wind power forecasts) with the network constraints in the model. However, such approach is still computationally difficult, and may not produce a solution within desired time for large-scale SCUC problems.

Therefore, in this work, we propose a new tool to dynamically schedule zonal reserve to enhance the deliverability of energy for the deterministic SCUC problem with wind power forecasts. More specifically, we extend the concept of the system generation margin [106] to develop probability distributions of line flow between zones using the concept of Injection Shift Factor (ISF) [113]. After estimating line flows, a post zonal reserve requirement is developed to help the system operators effectively and efficiently allocate reserves to zones, which mitigate possible congestion caused by wind power forecast uncertainty. In this work, we assume that there is no intra-zonal congestion that interrupts the deliverability of reserves [114]. Moreover, contingencies are not addressed since existing SCUC includes transmission contingency

constraints as reserve requirement.

The organization of this chapter is as follow. Section 5.2 reviews the importance of reserve requirement with wind power forecast and the system generation margin. Section 5.3 describes the probabilistic model that develops the post zonal reserve requirement. Section 5.4 details SCUC formulation with the post zonal reserve requirement. The proposed method is demonstrated through an illustrative example in Section 5.5. Conclusion and future work are in Section 5.6.

5.2 Background

5.2.1 Reserve Requirement

Reserve is defined as backup generation capacity used to provide flexibility to maintain energy balance and mitigate uncertainty [115]. The N-1 reliability requirement, set by the North American Electric Reliability Corporation (NERC), is to ensure that the system withstands the loss of any single bulk element without involuntary load shedding. Obtaining a solution with the consideration of all N-1 events explicitly within SCUC is a challenge for large-scale power systems. The study [116] states that the Midcontinent Independent System Operator (MISO) manages a system with about 45,000 buses and confronts constant performance challenges in solving Day-Ahead SCUC model within the required time window. Therefore, due to the performance challenges for large-scale power systems, the ISOs in the United States currently rely on heuristics, approximations, and polices rather than solving rigorous stochastic programming problem directly [103]. In [117], a policy is described as a mapping (rule) to determine a decision with given the available information in a particular state. Such a policy requires the total system reserve to be sufficient to cover any single generator contingency. In addition, a power system with large amounts of variable generation such as wind and solar heighten the importance of both upward and downward reserves since wind and solar can increase or decrease output unexpectedly [115]. Thus, the variability and uncertainty on system with N-1 reliability have caused the need to effectively and efficiently allocate reserves across the system

[118].

There are two different approaches to formulating the reserve requirements. As discussed before, the first approach is to pre-define (estimate) system wide and/or zonal reserve requirements based on some deterministic rules as inputs to reserve requirement constraints in the optimization. The shortcoming of this approach is that pre-specified zonal reserves are generally suboptimal and may even be infeasible. In addition, deliverability of reserves is not fully addressed since pre-defined zonal reserves could be very different from actual system operating conditions [119]. The second approach is to treat zonal reserves as decision variables incorporating transmission constraints as post zonal reserve requirements in the optimization process. Report in the literature suggest that MISO started with the first approach, but has since enhanced the co-optimization process such that zonal reserve requirements are solved within the optimization to meet both market wide reserve requirements and deliverability issues [119]. Therefore, this chapter seeks to develop a post zonal reserve requirement based on the second approach.

5.2.2 System Generation Margin Model

The system generation margin [106] is the amount that the available generating capacity exceeds the system load, so, being a function of two random variables (load and generation), it is also a random variable. The probability distribution of load, conventional generation and wind power generation are inputs to compute the system generation margin distribution. An example of this distribution for a specific look-ahead time step is depicted in Fig. 5.1.

The classical measures in reliability can be calculated from the system generation margin distribution such as the loss of load probability (LOLP) which is the area (red in Fig. 5.1) on the left side of the y-axis. Such information can be used to set a value for the operating reserve (including demand curve) [120]. For example, additional capacity as reserve indicates shifting Fig. 5.1 to the right by the amount of the reserve, resulting in the reduction of LOLP.

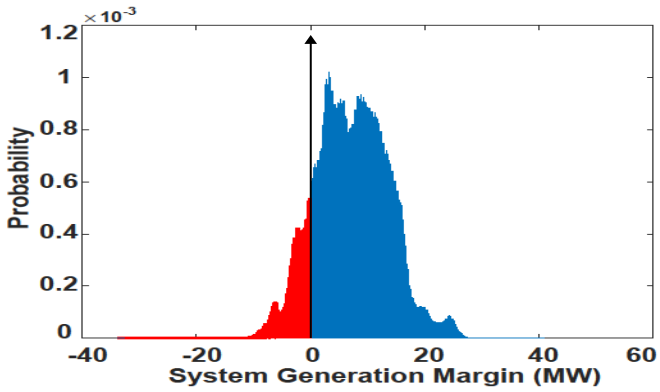

Figure 5.1: An example of system generation margin

5.3 Probabilistic Zonal Reserve Requirement

This section provides the tool to be used to estimate a dynamic zonal reserve requirements to mitigate congestion on critical lines between zones, incorporating wind power forecasts. Approach here is based on the system generation margin [106] and Injection Shift Factor (ISF), which can be easily incorporated with many different standard zonal reserve models (for example, contingency-based zonal reserve model used by ISO New England [121]) and extended to account for N-1 transmission line contingencies. Three sources of uncertainty are considered at each bus to estimate a zonal reserve requirement for this section.

5.3.1 Uncertainty Sources

1) Load Uncertainty (P_D): Load forecast uncertainty is commonly assumed to be a Gaussian distribution with mean zero and a given standard deviations, as in [122], [123].

2) Conventional Generation (P_G): The capacity outage probability (COPT) is usually used to represent the discrete probability distribution of the possible capacity states, to describe the uncertainty of the associated with conventional generation. For this work, we use the outage replacement rate (ORR) [122] instead of the forced outage rate (FOR). The failure rate for the thermal units range from 2% to 5%.

3) Wind Generation Uncertainty (P_W): Two sources of uncertainty pertain in wind power, one coming from the forecast uncertainty and the other from possible wind turbines' unplanned outages. The first source of uncertainty is related with the impossibility of producing perfect

wind power forecast. In this chapter, we only consider this forecast uncertainty, which is estimated from the probabilistic forecasting and represented by a set of quantiles.

Any probabilistic model can be used for the uncertainty of wind power by estimating the probability distribution. In this work, the forecasting model is based on a quantile-copula kernel density estimator (KDE) [124], which produces a probability density function (pdf) of wind power for each look-ahead hour, from which quantiles and scenarios of wind power can be derived. The basic problem, with given a set of explanatory variables X (such as wind speed, direction, etc.) for a given time resolution, is to estimate the conditional density function (5.1) of wind power at time t for each look-ahead time step $t+k$ of a given time horizon. General representation could be expressed as:

$$f_W(w_{t+k} \mid X = x_{t+k|t}) = \frac{f_{W,X}(w_{t+k}, x_{t+k|t})}{f_X(x_{x+k|t})} \tag{5.1}$$

Then, with quantile-copula KDE, the function f_W is estimated on the basis of a given set of historical sample data. Readers may refer to [124], [125] for more detail such as advantages and implementation of the probabilistic wind power forecasting approach. Examples of differing probability distribution for three random variables are illustrated in Fig. 5.2.

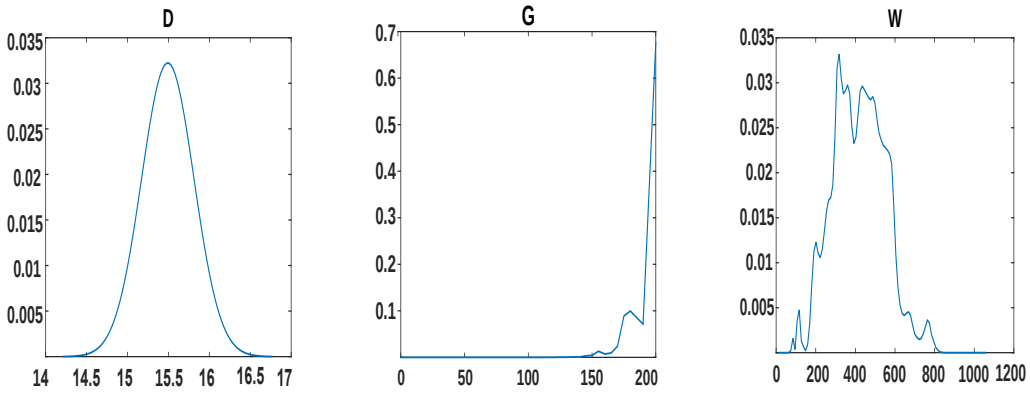

(a) Load (b) Generator (c) Wind

Figure 5.2: An example of three uncertainty sources

5.3.2 Injection Margin

With three random variables given: 1) $P^i_G(G_i = g_i)$, 2) $P^i_W(W_i = w_i)$, and 3) $P^i_D(D_i = d_i)$ at each bus i, the injection margin for bus i ($P^i_M(M = m)$) can be constructed as the sum of conventional generation (G_i), wind (W_i) and negative load (D_i) at bus i, which can be computed by convolution [120]:

$$\begin{aligned} P^i_M(M_i = m_i) &= P^i_M(W_i + G_i + (-D_i)) \\ &= \sum_{d=-\infty}^{\infty} \sum_{g=\infty}^{\infty} P^i_W(W_i = m_i + d_i - g_i) \cdot P^i_G(G_i = g_i) \cdot P^i_D(D_i = d_i) \end{aligned} \tag{5.2}$$

This is similar to the system generation margin approach in terms of the convolution of three probability distribution functions, but differs in that it is calculated for each bus. The preceding convolutions assume independence between conventional generator outage, load and wind power forecast uncertainty at each bus.

5.3.3 Probability of Line Flow

Next step is to estimate the probability distribution for line flows. Recall that F_l, power flow on the line l, can be expressed as a function of injection power $IP_i = W_i + G_i - D_i$ at bus i via the injection shift factor (ISF) [113], yielding:

$$F_l = \sum_i ISF(l,i) \cdot IP_i \tag{5.3}$$

With three random variables (load, generations, wind) contributing, IP_i becomes random variable in a manner analogous to the injection margin $P^i_M(M_i = m_i)$ for bus i, which implies $IP_i = M_i$. This suggests that the probability distribution of line flow can be estimated when the probability distribution of injection margin for each bus is given. Consider the corresponding equation:

$$P(F_l) = P\big(\sum_i ISF(l,i) \cdot M_i\big) \tag{5.4}$$

Since the injection margin $P^i_M(M_i = m_i)$ is discrete distribution, each point in $P^i_M(M_i = m_i)$ can be multiplied by a corresponding value in the ISF without changing probability weight.

Thus, the probability distribution of the line flow can be developed as

$$P(F_l) = P\Big(\sum_i ISF(l,i) \cdot M_i\Big)$$
$$= P\Big(\sum_i M_i^{'}\Big) \tag{5.5}$$

where $M_i^{'}$ is the discrete probability distribution of injection margin after applying the ISF.

The resulting distribution for line flow is then the sum of the injection margin after applying the ISF over all buses. For example, for three bus system, $P(F_l) = P(M_1^{'} + M_2^{'} + M_3^{'})$, which can be again calculated by convolution. Fig. 5.3 illustrates a representative example distribution for the line flow.

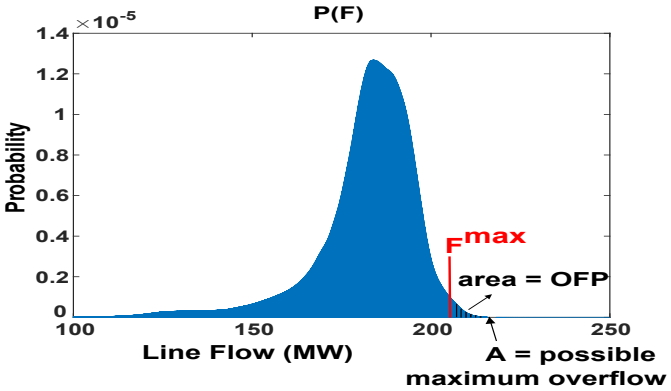

Figure 5.3: Line flow probability distribution function (pdf)

5.3.4 Development of Probabilistic Zonal Reserve Requirement

In this work, we consider only the impact of inter-zonal congestion on zonal reserve requirements, with the assumption of no intra-zonal congestion. Our goal here is to appropriately allocate reserves that can be used to prevent possible congestion on critical lines in the face of wind power forecast uncertainty. With the line flow probability distribution function formulated in (5.5) and illustrated in Fig. 5.3, and given parameter F^{max} (thermal limit of that line), we can obtain the overflow probability (OFP) which is the area of the right of F^{max} in the distribution function. Then, with a given power flow reliability threshold which sets the maximum allowed area right of F^{max}, we can practically obtain a possible maximum overflow (A).

The goal is to reduce the OFP to a specified level (the area of the right of point (A) in the distribution function) by allocating zonal reserves in such a way as to change the distribution function. The difference between (A) and F^{max} describes the amount of power flow change needed to reduce OFP to a preset low level. For line flow adjustment, it is important to recognize that the contribution of zonal reserve to a specific line is influenced by ISF as well. Thus, reserve requirement should be reserves multiplied by ISF, and therefore are not just equal to the amount of power flow change. This is due to the fact that reserves are provided at buses and the amount of injection change at buses will affect line flows via the ISF, which is also reflected in (5.3). This implies that we should have a reserve requirement $\sum_i (ISF(l,i) \cdot Reserve_i)$ where $Reserve_i$ is the reserve variable at bus i for line flow adjustment. Then, the inequalities considering the direction of line flow representing a reserve requirement would be

$$\sum_i (ISF(l,i) \cdot Reserve_i) \leq F_l^{max} - A_l, l \in L^c \tag{5.6a}$$

$$\sum_i (ISF(l,i) \cdot Reserve_i) \geq -F_l^{max} - A_l, l \in L^c \tag{5.6b}$$

where L^c is the set of critical lines. In this work, critical lines are defined as lines having OFP greater than a preset threshold among lines connecting zones; (5.6a) and (5.6b) treat positive and negative (A) respectively.

Equation (5.6) is made appropriate to a zonal reserve requirement just by limiting buses in "FROM ZONE (FZ)" to be those from which the power flow of critical line is coming out. For example, consider the critical line between zone 1 and zone 2. If power flows from zone 1 to zone 2, then FZ^l for this critical line l is zone 1. Buses in zone 1 are only considered for $Reserve_i$. Thus, the probabilistic zonal reserve requirement considering possible transmission network congestion with wind power forecast would be:

$$\sum_{i \in FZ^l} (ISF(l,i) \cdot Reserve_i) \leq F_l^{max} - A_l, l \in L^c \tag{5.7}$$

For the purpose of description, only positive (A) is described in (5.7). A system operator has prior knowledge of the ISF, the line's thermal limit F_l^{max}, and power flow reliability threshold. The zonal reserve requirement (5.7) serves as an additional constraint on system-wide reserve

requirement within the optimization. Thus, the probabilistic post zonal reserve requirement helps a system operator determine $Reserve_i$ in FZ^l, which mitigates possible congestion that might result from errors in the wind power forecast. The development of probabilistic post zonal reserve requirement can be summarized in the following steps:

1) Develop the discretized distribution of wind power, load and power supply from conventional generation unit for a given look-ahead time.

2) Develop the probability distribution of injection margin for each bus based on (5.2).

3) Develop the probability distribution of line flow for lines connecting zones based on (5.5). Then, determine critical lines that have OFP greater than a preset threshold.

4) For each critical line, obtain a possible maximum overflow (A) with power flow reliability threshold.

5) For each critical line l, determine FZ^l from the direction of (A), and construct the post zonal reserve requirement based on (5.7), which then becomes constraints in optimization problem.

5.4 Enhanced Deterministic Unit Commitment With Zonal Reserve for Overflow Protection

5.4.1 Notation and Structure

To allow for the possibility of multiple generators at a bus i, the set G_i denotes all generator at bus i. Reserves $Rup_{g,t}$ and $Rdw_{g,t}$ are general upward and downward reserves, which can be easily extended to account for different reserve types such as spinning and regulation reserves. This chapter uses these general reserves for the purpose of illustrating how probabilistic zonal reserve requirement are formulated and reducing the complexity that is not directly related to the discussion of this chapter.

The overall structure of the simulated problem resembles that of U.S. electricity markets [120], with a day-ahead (DA) market and a real-time (RT) market, which are cleared in sequence. The DA market is cleared by a traditional SCUC and an economic dispatch (ED) optimization model. A DA probabilistic wind power forecast is used for wind power input, and the DA schedule and clearing prices are determined for the next 24 hours. The model co-optimizes the energy and reserves simultaneously, which outputs the hourly DA prices, unit commitment, and generation schedules. After the DA market, the system operator performs a revised commitment procedure focusing on the reliability of the power system. The procedure is termed reliability assessment commitment (RAC). The RAC procedure is performed after the DA market and 1 hour ahead of the real dispatch, and we assume that a 1-hour-ahead wind power forecast is used for this purpose. After the RAC procedure, we consider the ED with the realized availability of wind power generation. Therefore, a fixed forecast wind power is used for the DA schedule and the uncertainty of wind power forecast is introduced in the RT simulations.

5.4.2 Deterministic SCUC Problem with Post Zonal Reserve

The deterministic SCUC with the proposed post zonal reserve is formulated as a mixed integer linear program. The total system operating cost for the objection function includes generator operating costs, startup/shutdown costs, reserve costs and penalty costs for unserved energy/reserves. Based on models [126], [120], [103], the formulation is shown as:

$$\min \sum_{g\in\mathbf{G},t\in\mathbf{T}} \tilde{c}_g\{P_{g,t}\} + SU_g z_{g,t} + SD_g y_{g,t} + RP_g^{\mathrm{UP}}(Rup_{g,t}) + RP_g^{\mathrm{DW}}(Rdw_{g,t})$$
$$+ CR(Rupns_{g,t}) + CR(Rdwns_{g,t}) + \sum_{i\in\mathbf{N},t\in\mathbf{T}} CE(e_{i,t}) \quad \text{subject to}$$

Opertional Requirements:

Unit Commitment Requirements:

Reserve Requirements:

$$\sum_{g} Rup_{g,t} + Rupns_{g,t} \geq SYS_{up}, \forall t \tag{5.8a}$$

$$\sum_{g} Rdw_{g,t} + Rdwns_{g,t} \geq SYS_{dw}, \forall t \tag{5.8b}$$

$$\sum_{g \in G_z} \left(Rup_{g,t}\right) \geq Rup_{z,t}, \sum_{g \in G_z} \left(Rdw_{g,t}\right) \geq Rdw_{z,t}, \forall z, \forall t \tag{5.8c}$$

$$F_{l,t} + \sum_{i} \left(ISF(l,i) \sum_{g \in G_i} (Rup_{g,t})\right) \leq F_l^{\max}, \forall l \in L^c, \forall t \tag{5.8d}$$

$$F_{l,t} - \sum_{i} \left(ISF(l,i) \sum_{g \in G_i} (Rdw_{g,t})\right) \leq F_l^{\max}, \forall l \in L^c, \forall t \tag{5.8e}$$

$$\sum_{i \in FZ^l} \left(ISF(l,i) \sum_{g \in G_i} (Rdw_{g,t})\right) \leq F_l^{\max} - A_{l,t}, \forall l \in L^c, \forall t \tag{5.8f}$$

$$Rup_{g,t} \leq (RRT \times RUR) u_{g,t}, \forall g \in G, \forall t \in T \tag{5.8g}$$

$$Rdw_{g,t} \leq (RRT \times RDR) u_{g,t}, \forall g \in G, \forall t \in T \tag{5.8h}$$

In this formulation, operational requirements include limits on real power flow on each line and energy balance requirements; constraints imposing the limit for transmission line flows and generation output; and the generation ramp rate constraints with reserves. Unit commitment requirements contain binary variable logic, generator minimum up/down equations. System-wide reserve up/down requirements are modeled in (5.8a), and zonal reserve requirements are described in (5.8c). Notice that zonal reserve requirement constraints based on pre-defined requirements from offline study can be enforced at the same time [119]. This work assumes no zonal reserve requirement from offline study. Post reserve requirement transmission constraints are represented in (5.8d), (5.8e). The proposed post zonal reserve requirement is represented in (5.8f) which schedules zonal reserves in FZ^l for critical line l, and constraints (5.8g)/(5.8h) represent the ramp rate (up/down) restriction for reserves. The system reserve requirement, SYS, can be estimated dependent on applicable policies. For example, such policies require that total system reserve is greater than any single generator outage or a fraction of the total demand. In this study, we assume that CE and CR are 1,500/MWh and 500/MWh.

5.5 Simulation and Empirical Results

In this section, case studies are described to evaluate the proposed post zonal reserve requirement with wind power forecasts. The zonal case (ZONE) represents the deterministic SCUC formulation (5.8), whereas the base case (BASE) does not includes the proposed post zonal reserve requirement (5.8f). Two test cases, a 5-bus and a 118-bus system (standard IEEE instances from MATPOWER [23]), are used. Specifically, when developing the zonal reserve requirement, it is assumed that the load is normally distributed with a mean equal to the given deterministic load data and standard deviation equal to 2% of the hourly load. For the dispatch of zonal reserves for critical lines after an event, immediate re-dispatch of generation is not considered. This is in line with current practical practice that MISO does not immediately run a new ED to mitigate transmission congestion [119]. Following an event, MISO deploys available reserves proportionally first. Overall flow of the simulation is illustrated in Fig. 5.4.

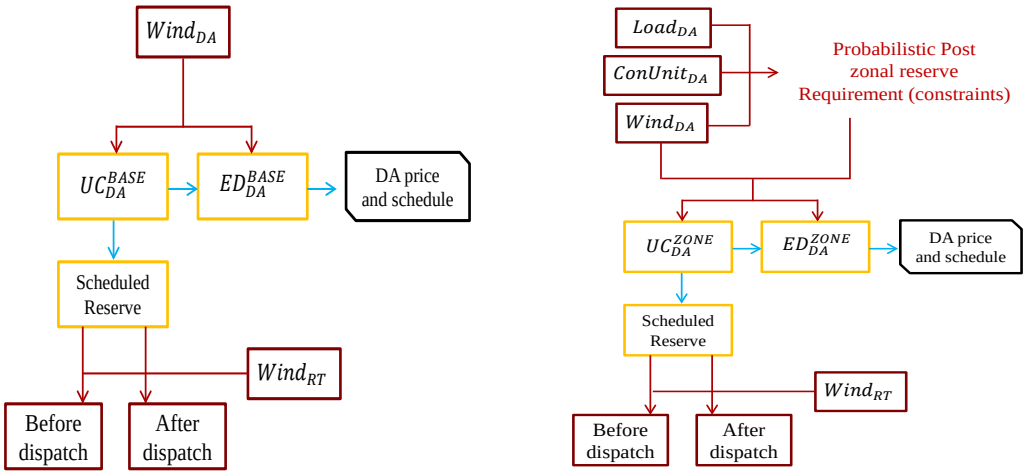

(a) BASE (b) ZONE

Figure 5.4: Overall flow of the simulation

5.5.1 Five-bus test system

This section describes the proposed method by providing an illustrative example with the simple five-bus system depicted in Fig. 5.5, which has two zones. Wind power plants are located

at bus 2 and 4 with forecast power generation 50 MW. The 120 MW of maximum capacity for two transmission lines connecting zones serves as the lines' thermal limit. In this example, values of 100 MW and 20 MW are used for system-wide reserve requirement, SYS_{up} and SYS_{dw} respectively. With the construction of the probability distribution for line flow F_{53} based on (5.5), possible maximum overflow (A) of 135 MW is obtained. Since power flows from zone 2 to zone 1, FZ is zone 2 so $i \in FZ = (4,5)$. With one generator at bus 5 in zone 2, the proposed post zonal reserve requirement can be represented as

$$ISF(53,5)\cdot(Rdw_5) \le F_{53}^{\max} - A_{53}$$
$$\le 120MW - 135MW = -15MW$$

Optimal solutions are given in Fig. 7.7: The first unit at bus 1 produces 0 MW plus 100 MW for energy and reserve, and the second unit at bus 5 produces 225 MW plus -28 MW for energy and reserve; Power flows of the two lines (F_{42}, F_{53}) connecting zones are satisfactory, causing no congestion. Next, suppose that wind power at bus 4 is 70 MW, increased by 20 MW (forecast uncertainty) from 50 MW. This forecast uncertainty brings congestion on F_{53} in excess of 120 MW. Then, we dispatch scheduled reserves, which results in the mitigation of the overflow reducing it from 121 MW to 106 MW. Thus, procured reserves are capable of mitigating the congestion, and are deliverable to correct the critical line F_{53}.

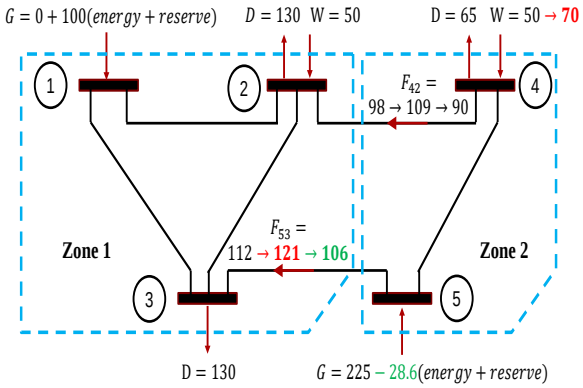

Figure 5.5: Five bus example with and without congestions

5.5.2 IEEE 118-bus test system

This section details the proposed method with 118-bus which has three zones. We assume that three zones are given as an input and each zone has one wind power plant, which indicates the total of three wind power plants. We select two simulation periods that cover high and low levels of load. The first period is from July 1 to July 31, 2006, representing the high load period. The second period is from October 1 to October 31, 2006, representing the low load period. The contingency reserve with the largest unit failure (800 MW) plus 10% of total demand is used for the SYS_{up} and 30 % of SYS_{up} is used for the SYS_{dw}. The value of 0.001 is used for power flow reliability threshold. Simulation contains 24 hours at one-hour intervals.

5.5.2.1 Operating Point

There are 12 lines connecting zones in the test system, and one critical line 54 which has the chance of congestion with wind power forecasts is identified. The line 54 is connected between $from$ bus 30 and to bus 38, and between zone 1 ($from$) and zone 2 (to) with the 300 MW of line's thermal limit. Since it shows possible overflows as the positive direction (flow from zone

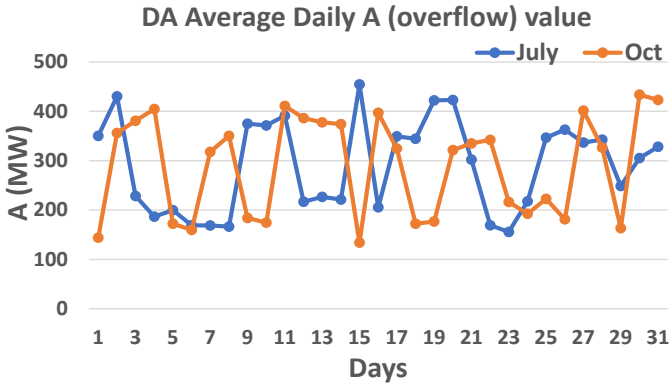

Figure 5.6: Possible maximum overflow (A) on the line 54

1 to zone 2), note that zone 1 is FZ^{54}, which contains 42 buses. Calculated DA average daily possible maximum overflows (A) in July and October are depicted in Fig. 5.6.

While A values greater than 300 MW indicate high probability of congestions with wind power uncertainty, A values less than 300 MW mean small probability of congestions (thus,

no use of post zonal reserve requirement). A values are typically higher in July compared to A values in October due to the high load in July. By solving two cases (BASE and ZONE), average daily scheduled reserves in zone 1 for July and October is shown in Fig. 5.7. For ZONE, UP and DOWN indicate upward and downward reserves respectively. Notice that the ZONE typically allocates more downward reserves than the BASE due to the proposed post zonal reserve requirement which allocates downward reserves considering wind power forecast uncertainty as additional constraints.

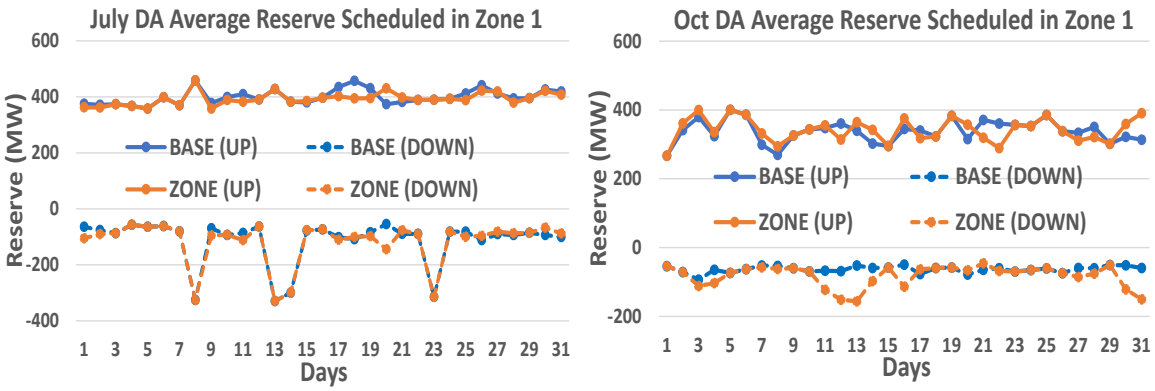

Figure 5.7: Scheduled reserve quantity in zone 1 (FZ^{54}) for July and October

5.5.2.2 Congestion from Wind Power Forecast Errors

In this section, we consider the impact of wind power forecast uncertainty with given DA schedules. Here we assume that forecast uncertainty only occurs in zone 1 where the post zonal reserve requirement is included, and the realized wind power is the same as forecast values for the plants in other two zones (no forecasting uncertainty). The realized wind power generation in the RT economic dispatch is introduced as a source of uncertainty, which can result in underestimated (realized wind is greater than DA forecast) or overestimated (realized wind is less than DA forecast) wind power. We then consider the dispatch of procured reserves by testing resulting DA solutions from the BASE and ZONE shown in Fig. 5.7 with a standard load flow equation. The number of days with congestions before and after the dispatch of scheduled reserves is shown in Table 5.1.

Table 5.1: Number of days with congestions

		Before dispatch		After dispatch	
		BASE	ZONE	BASE	ZONE
Underestimate	July	7	7	5	0
	October	5	5	3	0
Overestimate	July	0	0	0	0
	October	0	0	0	0

For underestimated wind, we only consider downward reserves. It shows that procured reserves of BASE are sometimes not capable of resolving congestions, and thus the number of days with congestion stays nonzero. This is since scheduled downward reserves of the BASE have no guarantee to reduce the amount of line flow. However, all congestions are mitigated with the dispatch of allocated reserves for the ZONE. For overestimated wind, we only consider upward reserves. It shows that procured reserves of BASE and ZONE are all deliverable due to post reserve requirements transmission constraints. These results indicate that the ZONE assigns reserves more effectively and efficiently to mitigate potential congestion with wind power forecasts.

5.5.2.3 Zonal reserve prices and operational cost

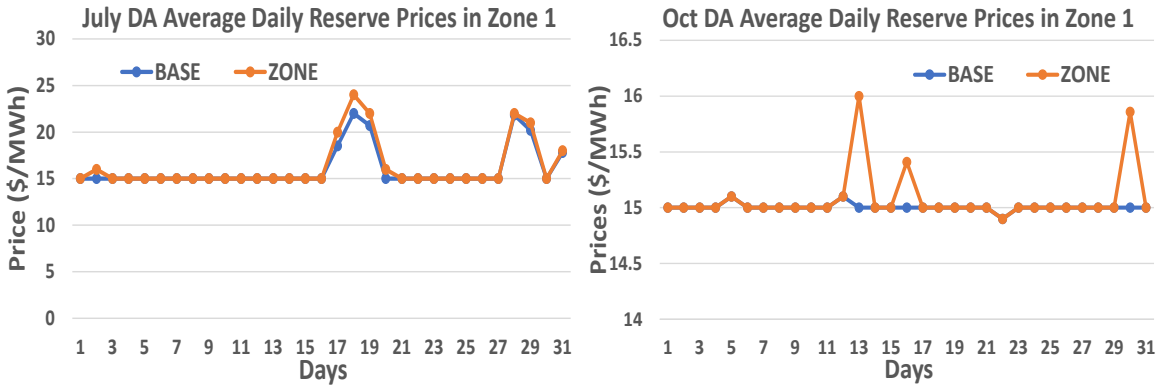

Figure 5.8: DA reserve prices in zone 1 (FZ^{54}) for July and October

Standard marginal pricing concepts indicate that the energy and reserve prices are the dual variables of energy and reserve balance constraints, [119], whose formulation is a linear programming problem since the value of integer variables is fixed in this stage. Fig. 5.8 shows

the zonal market clearing prices (MCPs) in zone 1 for BASE and ZONE. Notice that the ZONE has higher MCP in zone 1 since the post zonal reserve requirement is imposed in zone 1 to mitigate possible congestions with wind power. This implies that resulting MCPs properly reflect the effect of zonal reserve requirement on possible congestions of transmission lines under consideration.

Table 5.2: Average operational cost in July and October

DA-Cost (K$)	July		October	
	BASE	ZONE	BASE	ZONE
Energy/Reserve	4293.9	4294.3	3230.3	3230.4
Unserved energy	506	506	0	0
Unserved reserves	84.3	84.3	0	0
Wind Curtailment	9.4	9.4	20.1	20.1
Total	4893.6	4894	3250.4	3250.5
After wind power uncertainty				
Wind Curtailment	12.5	0	10	0
Total	**4906.1**	**4894**	**3260.4**	**3250.5**

We also consider total average operational cost of energy/reserve, penalty cost for unserved energy/reserve, and wind curtailment, as indicators of operational efficiency. Wind curtailment with associated lost opportunity cost payment of $50/MWh is considered [127]. Table 5.2 shows that operational cost of the ZONE is bit more expensive than the BASE. This can be interpreted as a reliability cost, since it accounts for a wider range of forecast uncertainty. This is based on an optimal trade-off between the expected value of system reliability and the costs of providing reserves. However, the BASE is not able to mitigate a congestion with procured reserves, and hence additional power from wind cannot be used (delivered) for the system. This excess generation with congestions is a fairly serious consideration for renewable generation [128],[129]. Such problems might raise issues of wind power curtailment, disconnection, and storage utilization. To address these, wind curtailment is considered and as a result, final total cost for the BASE is higher than for the ZONE.

5.6 Conclusion and Future work

In this chapter, we have investigated the tool to develop the dynamic scheduling of zonal reserve with wind power in an electricity market where energy and reserves are optimized simultaneously. Specifically, three sources of uncertainty are used to construct the injection margin, and then probability distribution function of line flow by convolution of injection margins after applying ISF. Then, with the goal of reducing OFP to a preset low level, the probabilistic post zonal reserve requirement is developed. The proposed post zonal reserve requirement is tested using the IEEE 118-bus test system, which shows that it efficiently and effectively allocates reserves to mitigate possible congestions with wind power. Our results also show that resulting zonal reserve MCPs properly reflect the effect of zonal reserve requirement on possible congestions of transmission line under consideration as well as the reduced operating cost with the consideration of wind curtailment. Overall, we argue that the proposed tool to develop the post zonal reserve requirement will contribute towards more efficient reserves allocation thorough economic benefits when reserves are dispatched with renewable energy resources. The tool is also compatible with current market designs and should be easy to implement in systems with co-optimization of energy and reserves.

In future work, we plan to extend the zonal reserve requirement to account for line outages. Simply, different ISF' corresponding to line outage can be used to compute probability distribution function of line flow, thereby obtaining a different zonal reserve requirement. Other interesting directions for future research include dynamic reserve zones and storage planning for uncertainty and variability of renewable energy resources, and a comparison of the proposed dynamic scheduling strategy to stochastic UC formulations.

CHAPTER 6

Convex Relaxation for Sparse Tableau Formulation of OPF Problem

6.1 Introduction

There are a wide range of OPF formulations and solution methods, ranging from meta-heuristics [130] to formal deterministic optimization methods [131]. For deterministic methods, many researchers have contributed to improve nonlinear optimization methods adapted to OPF applications, including gradient methods and interior point methods (IPM). MATPOWER [23] is a widely-utilized package based on MATLAB for power flow and optimal power flow problems, publicly available with an implementation of IPM. However, these methods can offer by their nature only local solutions, and may lead to infeasible solutions. Challenges such as these have prevented full ACOPF problems from being solved in real-time operation. Instead, the system operators in the power industry often use DCOPF (an approximate, linearized version of ACOPF) [24].

Recently, convex relaxation approaches have drawn attention of the research community, due to their ability to often obtain a global solution. In particular, second-order cone programming

(SOCP) was first applied to the OPF problem by Jabr [132], and more recently, Lavaei and co-workers [21] applied semidefinite programming (SDP) to the OPF problem. An interesting observation relating to the SDP is that, by solving the dual problem, a test for a zero duality gap can be efficiently computed, in the form of a condition that dual problem produces a solution with a certain semidefinite matrix having a zero eigenvalue of multiplicity two. When satisfied, this condition rigorously confirms that a global solution has been found. It turns out that this condition is satisfied for many of IEEE benchmark systems in the MATPOWER distribution, when a small resistance is added to all transformers that originally possess a zero resistance [21] [133]. This zero duality gap means the relaxation is exact, but unfortunately, the exactness of the SDP relaxations (i.e., rank-1 solution) does not hold for many other realistic power system networks, and the rank of W matrix can be also affected by other constraints such as the value of thermal limits [134]. Even though there exist a limited class of problems for which a rank-1 solution is guaranteed (radial network, load over-satisfaction, absence of generation lower bounds or lossless networks with cyclic graphs), it is hard to retrieve a physically meaningful solution when the SDP relaxation is not exact.

To this end, another attempt to strengthen the SDP relaxation has been made by solving a hierarchy of moment relaxation problems [135]. This approach is used to obtain tighter lower bounds, but usually is restricted to very small systems [136], [137]. Another way to strengthen the SOCP is presented [138]. However, there exist obvious tradeoffs between stronger relaxation solutions and computational efficiency, since one needs more constraints to cut off part of the feasible region for a stronger solution. Another recent relaxation method, the Quadratic Convex (QC) relaxation is studied in [139] [140], and an important conclusion drawn, that QC relaxation is strictly stronger than the SOCP and is comparable to the SDP.

Upon considering existing relaxation techniques, this chapter first considers the prospects of applying two existing recent convex relaxation techniques (SDP and QC) for Sparse Tableau Formulation (STF) of OPF introduced in Chapter 4. In its standard formulation for OPF, the SDP relaxation takes advantage of power network equations (power balance and branch power flow) being quadratic with only voltage phasors as variables to construct the W matrix variable,

as outer product VV^T. However, this approach is hampered in STF because additional variables, such as port currents, must be included when constructing the W matrix. We next examine the QC relaxation which is based on exploiting convex envelopes of quadratic, trigonometric and bilinear terms in the AC power flow equations. The QC relaxation provides greatest benefit when one has a priori information that imposes narrow bounds on bus voltage phase angle differences. Through it focuses on bus voltage angles as key variables the QC relaxation relies heavily on the Y_{bus}-based AC power flow formulations, which suggests that STF also may not be well-suited to use with the QC relaxation.

Therefore, this chapter next derives two alternative approaches to formulate convex relaxations of STF for OPF problems (STF relaxations). Notice that the critical nonlinearity/source of nonconvexity of STF for OPF is the power balance equation with bilinear terms. In addition, only corresponding bus voltage and bus current are present in these bilinear terms, indicating there is no coupling between variables associated with different buses in these equations. Such low-dimensional decoupled nonlinear functions could be advantageous because some empirical results provide the observation that high-dimensional coupled nonlinear functions tend to create more nonconvexity in a feasible region.

With this STF version of the formulation, we apply the McCormick (MC) relaxation [141] to the bilinear constraints, thereby relaxing the original OPF problem. Two approaches, 1) admittance-based and 2) current-based, are proposed, and it is demonstrated that the bounds on variables in the bilinear constraints can be tightened. The MC envelope takes advantage of this bound tightening, and DCOPF-based heuristic method to obtain voltage angle bounds is discussed. Further enhancement with sequential bound tightening (SBT) and reduced spatial branch-and-bound (RSBB) are discussed.

This chapter is organized as follows. Section 6.2 provides the review of SDP and QC relaxations with key observations regarding their use, and then the limitation of the SDP and QC relaxation are discussed in the context of the STF. Section 6.3 proposes two relaxations that are appropriate for use with STF version of OPF. Methods to improve STF relaxations are suggested in Section 6.4 and case studies presented in Section 6.5.

6.2 Consideration of Existing Convex Relaxation Techniques For STF

This section reviews two recent convex relaxation techniques, SDP and QC relaxation [142], and discusses challenges that arise when one seeks to apply them with STF of the OPF problem.

6.2.1 Overview of Semidefinite Programming

In the context of the mathematical description of the standard OPF problem as described in Chapter 1.3, for simplicity this section defines a linear cost objective function associated with each generator

$$\tilde{c}_j(P_{g,j}) = \beta P_{g,j} + \gamma \qquad \forall j \in \mathbf{G} \tag{6.1}$$

This simple cost function is selected to allow focus on the OPF constraint equations, which are key to the SDP formulation. As illustrated in recent literature on semidefinite programming approaches [21] for the standard OPF, we reformulate the OPF problem in a manner that allows it to admit a SDP formulation. The SDP-related admittance matrices in [21] with basis vectors in R^n as $\{e_1, ..., e_n\}$ for every $j \in \mathbf{N}$ and $(ft) \in \mathbf{L}$ can be formulated. First, we define

$$Y_j = e_j e_j^T Y_{bus}$$
$$Y_{ft} = (\overline{y_{ft}} + y_{ft}) e_f e_f^T - y_{ft} e_t e_t^T$$

where $\overline{y_{ft}}$ denotes the value of the shunt element at bus f associated with the line (ft), and y_{ft} denoting the line admittance between buses f and t. Then, related admittance matrices for power injections and line power flows are constructed as

$$H_{j,r} \triangleq \frac{1}{2}\begin{bmatrix} real(Y_j + Y_j^T) & imag(Y_j^T - Y_j) \\ imag(Y_j - Y_j^T) & real(Y_j + Y_j^T) \end{bmatrix}, \quad H_{ft,r} \triangleq \frac{1}{2}\begin{bmatrix} real(Y_{ft} + Y_{ft}^T) & imag(Y_{ft}^T - Y_{ft}) \\ imag(Y_{ft} - Y_{ft}^T) & real(Y_{ft} + Y_{ft}^T) \end{bmatrix}$$
$$H_{j,q} \triangleq \frac{-1}{2}\begin{bmatrix} imag(Y_j + Y_j^T) & real(Y_j - Y_j^T) \\ real(Y_j^T - Y_j) & imag(Y_j + Y_j^T) \end{bmatrix}, \quad H_{ft,r} \triangleq \frac{-1}{2}\begin{bmatrix} imag(Y_{ft} + Y_{ft}^T) & real(Y_{ft}^T - Y_{ft}) \\ real(Y_{ft} - Y_{ft}^T) & imag(Y_{ft} + Y_{ft}^T) \end{bmatrix}$$

$$M_0 \triangleq diag\{e_{(N+slack)}\}$$

$$H_{j,vm} \triangleq \begin{bmatrix} e_j e_j^T & 0 \\ 0 & e_j e_j^T \end{bmatrix}, \quad X \triangleq \begin{bmatrix} real(V) \\ imag(V) \end{bmatrix}$$

where $M_0 \in \{0,1\}^{2N \times 2N}$ such that $M_0(n,n) = 1$ if and only if n corresponds to the index number "$N+slack$." For example, consider the 14 bus system with slack bus $j = 1$, then the index number "$N+slack$" is $15 = 14+1$. Using these defined matrices, the linear relationship for power balance equations and power flow equations can be formed with the outer-product matrix $W \triangleq XX^T$. Here $X = [V_1^d, V_2^d, ..., V_n^d, V_1^q, V_2^q, ..., V_n^q]^T$, and one constructs:

$$P_j = tr(H_{j,r}W) \tag{6.2a}$$

$$Q_j = tr(H_{j,q}W) \tag{6.2b}$$

$$P_{ft} = tr(H_{ft,r}W) \tag{6.2c}$$

$$Q_{ft} = tr(H_{ft,q}W) \tag{6.2d}$$

$$V_j^2 = tr(H_{j,vm}W) \tag{6.2e}$$

where tr indicates the trace operator, consistent with MATLAB notation. Then, the corresponding OPF optimization problem can be written as

$$\textbf{(SDP-OPF)} \quad \min_{W, P_{g,j}, Q_{g,j}} \sum_j \beta_j P_{g,j} + \gamma_j \tag{6.3a}$$

subject to

$$\text{Active. Balance:} \quad tr(H_{j,r}W) = P_{g,j} - P_{d,j} \quad j \in \mathbf{N} \tag{6.3b}$$

$$\text{Reactive. Balance:} \quad tr(H_{j,q}W) = Q_{g,j} - Q_{d,j} \quad j \in \mathbf{N} \tag{6.3c}$$

$$\text{Gen. Limit:} \quad P_j^{min} \le P_{g,j} \le P_j^{max}, \; Q_j^{min} \le Q_{g,j} \le Q_j^{max} \quad j \in \mathbf{G} \tag{6.3d}$$

$$\text{Volt. Limit:} \quad (V_j^{min})^2 \le tr(H_{j,vm}W) \le (V_j^{max})^2 \quad j \in \mathbf{N} \tag{6.3e}$$

$$W \succeq 0, \; rank(W) = 1, \; tr(M_0 W) = 0$$

Thermal limits for lines are omitted from this formulation for the simplicity, but are easily introduced, with more detail in [143]. The constraint $tr(M_0W) = 0$ enforces angle reference

condition (zero angle for the slack bus). The positive semi-definiteness and rank-1 constraints are imposed to ensure that there exists a vector such that $W = XX^T$. Notice that since optimization problem (6.3) has a rank constraint, it is still nonconvex. However, by removing the rank constraint, we obtain a relaxation for semidefinite programming, which leads to the following optimization problem that is convex.

$$\textbf{(SDP-Relaxation)} \quad \min_{W,P_{g,j},Q_{g,j}} \sum_j \beta_j P_{g,j} + \gamma_j \quad j \in \mathbf{G} \tag{6.4a}$$

suject to

$$\text{Active. Balance:} \quad Tr(H_{j,r}W) = P_{g,j} - P_{d,j} \quad j \in \mathbf{N} \tag{6.4b}$$

$$\text{Reactive. Balance:} \quad Tr(H_{j,q}W) = Q_{g,j} - Q_{d,j} \quad j \in \mathbf{N} \tag{6.4c}$$

$$\text{Gen. Limit:} \quad P_j^{min} \le P_{g,j} \le P_j^{max},\ Q_j^{min} \le Q_{g,j} \le Q_j^{max} \quad j \in \mathbf{G} \tag{6.4d}$$

$$\text{Volt. Limit:} \quad (V_j^{min})^2 \le Tr(H_{j,vm}W) \le (V_j^{max})^2 \quad j \in \mathbf{N} \tag{6.4e}$$

$$W \succeq 0,\ tr(M_0 W) = 0$$

This optimization problem (6.4) is a relaxation (SDP relaxation) of the optimization problem (6.3), and may fail to have a rank-1 solution, in which case it provides a solution for W that is no longer physically meaningful.

6.2.2 The limitation of Semidefinite Programming for STF

This section provides an example to demonstrate that the SDP formulation of OPF problem may fail to produce physically meaningful solutions with Sparse Tableau Formulation. A two-bus power system is illustrated in Figure 6.1. The standard SDP produces a rank-1 solution for this system which has only one line as a network element present for the analysis.

The linear element equation for the transmission line is

$$\left[\begin{array}{cc|cc} 1 & -(1+\frac{Z_{12}Y_{12}}{2}) & 0 & Z_{12} \\ 0 & -Y_{12}(1+\frac{Z_{12}Y_{12}}{4}) & 1 & (1+\frac{Z_{12}Y_{12}}{2}) \end{array}\right] \begin{bmatrix} V_1 \\ V_2 \\ i_{12} \\ i_{21} \end{bmatrix} = \begin{bmatrix} 0 \\ 0 \end{bmatrix} \tag{6.5}$$

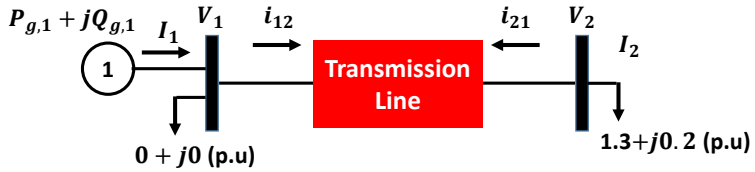

Figure 6.1: Two-Bus Example System

Let us define coefficients as

$$1 + \frac{Z_{12}Y_{12}}{2} = \alpha_{12}^d + \mathbf{j}\alpha_{12}^q$$

$$Z_{12} = \beta_{12}^d + \mathbf{j}\beta_{12}^q$$

$$Y_{12}(1 + \frac{Z_{12}Y_{12}}{4}) = \gamma_{12}^d + \mathbf{j}\gamma_{12}^q$$

Then, we have four linear equality constraints with eight variables as

$$\begin{aligned} g_1(X) &\equiv V_1^d - \alpha_{12}^d V_2^d + \alpha_{12}^q V_2^q + \beta_{12}^d i_{21}^d - \beta_{12}^q i_{21}^q = 0 \\ g_2(X) &\equiv V_1^q - \alpha_{12}^d V_j^q - \alpha_{12}^q V_2^d + \beta_{12}^d i_{21}^q + \beta_{12}^q i_{21}^d = 0 \\ g_3(X) &\equiv i_{12}^d - \gamma_{12}^d V_2^d - \gamma_{12}^q V_2^q + \alpha_{12}^d i_{21}^d - \alpha_{12}^q i_{21}^q = 0 \\ g_4(X) &\equiv i_{12}^q - \gamma_{12}^d V_2^q - \gamma_{12}^q V_2^d + \alpha_{12}^d i_{21}^q + \alpha_{12}^q i_{21}^d = 0 \end{aligned} \tag{6.6}$$

Two nonlinear active power balance equations are given (the point to be made is valid even without inclusion of reactive power balance equations) as:

$$\begin{aligned} P_1 &= V_1^d i_{12}^d + V_1^q i_{12}^q \\ P_2 &= V_2^d i_{21}^d + V_2^q i_{21}^q \end{aligned} \tag{6.7}$$

The optimization vector X for the OPF problem consists of $4n_l \times 1$ vectors of branch current real part i_{ft}^d and branch current imaginary part i_{ft}^q and the $2n_b \times 1$ vectors of bus voltage phasors real part V_j^d and bus voltage phasors imaginary part V_j^q. The dimension of the decision variable X is $(4n_l + 2n_b) \times 1$, and here the resulting vector with the two-bus example is $X = [i_{12}^d, i_{21}^d, i_{12}^q, i_{12}^q, V_1^d, V_2^d, V_1^q, V_2^q]^T$.

For the SDP formulation, key step is to construct the outer product matrix $W = XX^T$ and find corresponding coefficient matrices for the network element equation with transmission

matrix and power balance equation. Unfortunately, linear equations cannot be incorporated directly into the SDP formulation, so we need to introduce a real-valued slack variable c, and this variable must satisfy $c^2 = 1$, indicating c is either -1 or 1. For now assume that $c = 1$. Then, the modified variable is $X = [i_{12}^d, i_{21}^d, i_{12}^q, i_{12}^q, V_1^d, V_2^d, V_1^q, V_2^q, c]^T$. Corresponding $W = XX^T$ matrix and coefficient matrices for $g_1(x), g_2(x), g_3(x), g_4(x)$ would be given as:

$$W = \begin{bmatrix} (i_{12}^d)^2 & i_{12}^d i_{21}^d & \cdots & i_{12}^d V_2^q & i_{12}^d c \\ i_{21}^d i_{12}^d & (i_{21}^d)^2 & & & i_{21}^d c \\ \vdots & & \ddots & & \vdots \\ V_2^d i_{12}^d & & & & \vdots \\ V_2^q i_{12}^d & & & V_2^q & V_2^q c \\ c i_{12}^d & & & & c^2 \end{bmatrix}, SC_{g_1} = \left[\begin{array}{cc} & 0 \\ 0 & \frac{\beta^d}{2} \\ & \vdots \\ & \vdots \\ & \frac{\alpha^d}{2} \\ \hline \text{Last Column}^T & 0 \end{array}\right], \text{similar structure for } g_2, g_3, g_4 \tag{6.8}$$

Thus, we have equations $tr(SC_{g_1} * W) = g_1(X)$, $tr(TSC_{g_2} * W) = g_2(X)$, $tr(SC_{g_3} * W) = g_3(X)$, $tr(SC_{g_4} * W) = g_4(X)$. Notice that coefficient matrices $SC_{g_1}, SC_{g_2}, SC_{g_3}, SC_{g_4}$ have nonzero elements only in the rightmost column and bottom of the matrix. This implies that none of the individual variables in the W matrix not in the rightmost column and bottom are constrained with linear element equations. Now construct the coefficient matrix SC_{P_1} for active power balance equations as

$$SC_{p_1} = \left[\begin{array}{ccc|c} & & & \frac{1}{2} \\ & 0 & & \vdots \\ & & & \frac{1}{2} \\ \hline \frac{1}{2} & \cdots & \frac{1}{2} & 0 \end{array}\right], W = \left[\begin{array}{ccc|c} (i_{12}^d)^2 & & \cdots & i_{12}^d V_1^d \\ & & & i_{12}^q V_1^q \\ & & & \vdots \\ \hline V_1^d i_{12}^d & & & \\ & V_1^q i_{12}^d & & \\ c i_{12}^d & & \cdots & c^2 \end{array}\right], \text{and } tr(SC_{p_1} * W) = P_1 \tag{6.9}$$

The coefficient matrix SC_{P_1} has the structure that most elements are zero, and its corresponding variables in the W matrix are highlighted by being circled in (6.9). These variables are only present in power balance equations and in the objective function. With the objective

function (6.3), we have

$$\min_{W} \beta_1 P_{g,1} + \gamma_1 \tag{6.10}$$

where $P_{g,1} = tr(SC_{p_1} * W) + P_{d,1}$.

RESULT 6.1. (limitation of SDP for STF) Numerical results for Figure 6.1 are given as a counter example to illustrate a simple case in which the SDP approach fails to produce physically meaningful solution for STF. Consider the network data; the voltage magnitudes at all buses are constrained to the range 1.05 to 0.95, and line impedance are specified as $Z = R + \mathbf{j}X = 0.01 + \mathbf{j}0.1$. The active and reactive power output limits of generator are given in Table 6.1.

Generator	P_{min} (p.u)	P_{max} (p.u)	Q_{min} (p.u)	Q_{max} (p.u)
1	0	2	-1	10

Table 6.1: Two-bus generator output limits

The solution matrix W for this particular example is shown:

$$W = \begin{bmatrix} 7.5453 & 0 & 0.0553 & 0 & \boxed{0} & 0 & 0 & 0 & 0 \\ 0 & 8.8418 & 0 & 0 & 0 & -0.65 & 0 & -0.1 & 0 \\ 0.0553 & 0 & 9.9279 & 0 & -1.6799 & 0 & \boxed{0} & 0 & 0 \\ 0 & 0 & 0 & 8.8418 & 0 & 0.1 & 0 & -0.65 & 0 \\ \boxed{0} & 0 & -1.6799 & 0 & 1.0222 & 0 & 0 & 0 & 0 \\ 0 & -0.65 & 0 & 0.1 & 0 & 0.5138 & 0 & 0 & 0 \\ 0 & 0 & \boxed{0} & 0 & 0 & 0 & 0 & 0 & 0 \\ 0 & -0.1 & 0 & -0.65 & 0 & 0 & 0 & 0.5138 & 0 \\ 0 & 0 & 0 & 0 & 0 & 0 & 0 & 0 & 1 \end{bmatrix} \tag{6.11}$$

First of all, notice that this W matrix is a positive semidefinite matrix, but rank is 9 (i.e., it is full rank), which implies the solution is no longer physically meaningful. In terms of problem constraints, all variables in the rightmost column and bottom of the matrix W, related to linear

element equations, are selected to be 0. For power balance equation, observe that $P_{g,1}$ are determined by highlighted variables in the W matrix (6.9).

The optimization problem will seek to minimize $P_{g,1}$ to yield a minimum cost. The solution matrix (6.11) shows that highlighted variables are selected to be 0 implying $V_1^d i_{12}^d = 0$ and $V_1^q i_{12}^q = 0$. Thus, the resulting power balance equation for generator bus 1 with $P_{d,1} = 0$ is $P_{g,1} = tr(SC_{p_1} * W) + P_{d,1} = 0 = P_1^{min}$. For load bus 2, corresponding variables are selected such that $V_2^d i_{21}^d = -0.65$ and $V_2^q i_{21}^q = -0.65$ implying $P_2 = tr(SC_{p_2} * W) \Rightarrow tr(SC_{p_2} * W) + P_{d,2} = 0 \Rightarrow -1.3 + 1.3 = 0$ with $P_{d,2} = 1.3$. In this particular optimization problem, these values are satisfactory since with the increased number of variables in the W matrix, one may view the many off-diagonal variables not involved in any network element constraints as "having the goal of" making W a positive semidefinite matrix.

However, suppose that there exists a global minimizing solution for the problem, for which the generator active power values are P_1^{min}. Therefore, highlighted variables should take values $P_{g,1} = P_1^{min}$ (in this example, $P_{g,1} = 0$) without violating any other constraints in the optimization problem. This proves impossible, because $P_{g,1} = P_1^{min}$ leads to violation of power balance equations, and a rank-1 solution is not guaranteed. Due to the increased size of W matrix and decoupling of linear and nonlinear equations, SDP approach is poorly suited for use with Sparse Tableau Formulation and this motivates us to develop a different approach to have a convex relaxation problem.

6.2.3 The overview of QC relaxation and its Limitation for STF

Consider the line flow equations for a short transmission line representation, with this line connecting (f,t), and b_{ft} and g_{ft} representing the line susceptance and conductance respectively.

$$\begin{aligned} p_{ft} &= g_{ft}(V_f^m)^2 - g_{ft}V_f^m V_t^m cos(\delta_f - \delta_t) - b_{ft}V_f^m V_t^m sin(\delta_f - \delta_t), \quad (ft) \in \mathbf{L} \\ q_{ft} &= -b_{ft}(V_f^m)^2 + b_{ft}V_f^m V_t^m cos(\delta_f - \delta_t) - g_{ft}V_f^m V_t^m sin(\delta_f - \delta_t), \quad (ft) \in \mathbf{L} \end{aligned} \tag{6.12}$$

The QC relaxation seeks a convex relaxation of (6.12) associated with the nonconvex terms; these terms are: $(V_f^m)^2$, $V_f^m V_t^m cos(\delta_f - \delta_t)$ and $V_f^m V_t^m sin(\delta_f - \delta_t)$. To find a convex envelope of

$cos(\delta_f - \delta_t)$ and $sin(\delta_f - \delta_t)$, the important a priori information that the allowable operating range of voltage angle difference $(\delta_f - \delta_t)$ is narrow. For example, if one a priori imposes the bound $|\delta_f - \delta_t| \leq \delta^{max}$ with $\delta^{max} = \frac{\pi}{3}$, then the corresponding quadratic convex relaxation of cos and sin with cs = COV($cos(\delta)$) and ss = COV($sin(\delta)$) can be given by

$$\begin{cases} cs & \leq 1 - \dfrac{1 - cos(\delta^{max})}{(\delta^{max})^2}\delta^2 \\ cs & \geq cos(\delta^{max}), \quad \text{for cosine function} \\ \hline ss & \leq cos\left(\dfrac{\delta^{max}}{2}\right)\left(\delta - \dfrac{\delta^{max}}{2}\right) + sin\left(\dfrac{\delta^{max}}{2}\right) \\ ss & \geq cos\left(\dfrac{\delta^{max}}{2}\right)\left(\delta + \dfrac{\delta^{max}}{2}\right) - sin\left(\dfrac{\delta^{max}}{2}\right), \quad \text{for sine function} \end{cases} \tag{6.13}$$

From here, let us consider how line flow equations of the form (6.12) might be obtained in STF version of the OPF. Let us suppose that the network element k is the line (f,t). Then, network element for the line (f,t) in STF is represented as

$$F_{k,v}\begin{bmatrix} v_{k,a} \\ v_{k,b} \end{bmatrix} + F_{k,i}\begin{bmatrix} i_{k,a} \\ i_{k,b} \end{bmatrix} = 0 \tag{6.14}$$

Here we know that $v_{k,a} = V_f$, $v_{k,b} = V_t$, $i_{k,a} = i_{ft}$ and $i_{k,b} = i_{tf}$. Solving for quantities i gives

$$\begin{bmatrix} i_{ft} \\ i_{ft} \end{bmatrix} = \underbrace{-(F_{k,i})^{-1}F_{k,v}}_{Y_{bus}\ \textbf{matrix for element k}}\begin{bmatrix} V_f \\ V_t \end{bmatrix} \tag{6.15}$$

$$\begin{bmatrix} s_{ft} \\ s_{tf} \end{bmatrix} = \begin{bmatrix} V_f \\ V_t \end{bmatrix} \odot \left(\begin{bmatrix} i_{ft} \\ i_{tf} \end{bmatrix}\right)^* = -\begin{bmatrix} V_f \\ V_t \end{bmatrix} \odot \left((F_{k,i})^{-1}F_{k,v}\begin{bmatrix} V_f \\ V_t \end{bmatrix}\right)^* \tag{6.16}$$

Thus, we have

$$\begin{aligned} p_{ft} &= real(s_{ft}) \\ q_{ft} &= imag(s_{ft}) \end{aligned} \tag{6.17}$$

Observe the (6.12) is equivalent to (6.17), implying that the QC relaxation uses the Y_{bus}-based power flow equations. The Y_{bus}-based power flow equations eliminate the intermediate variables i with the restrictive assumption that $F_{k,i}$ is invertible. The STF avoids this restriction by explicitly retaining the intermediate variables i, but loses the explicit representation of

voltage angle difference terms in the (6.14). Therefore, the QC relaxation that exploits bounds imposing a narrow line angle difference, does not lend itself to application in STF version of the OPF.

6.3 Sparse Tableau Relaxation

This section describes two alternative approaches to construct a convex relaxation problem that is suited to STF for the OPF problem. The relaxation chosen is based on largely engineering insights, rather than a more abstract mathematical reformulation. The approach takes the advantage of STF relation of bus voltage/current variables and element variables by linear equations, thus nonconvexity only appears in power balance at each bus with bilinear terms. Two relaxations are based on the node admittance and node current variables for which appropriate bound can be derived in a fashion that "contains" the originally specified active and reactive power.

6.3.1 Standard Optimal Power Flow Problem

For clarity, here we restate the standard formulation of the OPF problem as

$$\textbf{(S-OPF)} \quad \min_{V,P_g,Q_g} \sum_{j\in\mathbf{G}} \tilde{c}_j(P_{g,j}) \qquad \text{subject to} \tag{6.18a}$$

$$\text{Active. Balance:} \qquad real[V \odot (Y_{bus}V)^*] = P_g - P_d \tag{6.18b}$$

$$\text{Reactive. Balance:} \qquad imag[V \odot (Y_{bus}V)^*] = Q_g - Q_d \tag{6.18c}$$

$$\text{Line Power Flow:} \qquad S_f = V_f \odot (Y_f V)^*, \quad S_t = V_t \odot (Y_t V)^* \tag{6.18d}$$

$$\text{Thermal Limit:} \qquad S_f^2 \le F_{max}^2, \quad S_t^2 \le F_{max}^2 \tag{6.18e}$$

$$\text{Gen. Limit:} \qquad P_j^{min} \le P_{g,j} \le P_j^{max}, \quad Q_{min,j} \le Q_{g,j} \le Q_j^{max}, \quad \forall j \in \mathbf{G} \tag{6.18f}$$

$$\text{Volt. Limit:} \qquad V_j^{min} \le V_j^m \le V_j^{max}, \quad \forall j \in \mathbf{N} \tag{6.18g}$$

We defines $\mathbf{F_S}$ as the feasible region of **S-OPF** problem. This feasible region is typically nonconvex. The following section describes STF of OPF problem, considers its feasible region and constructs the convex relaxation of that problem.

6.3.2 Admittance-Based Convex Relaxation

Consider STF for power system networks, with specified F_v, F_i, A matrices, and variables of port voltage v, port current i, bus voltage V, and bus current I. Then, STF of OPF problem in rectangular coordinates as shown in Chapter 3 can be constructed as

$$\textbf{(STF-OPF)} \quad \min_{v,i,V,I,P_g,Q_g} \sum_{j\in\mathbf{G}} \tilde{c}_j(P_{g,j}) \qquad \text{subject to} \tag{6.19a}$$

$$\text{Linear Element:} \quad real(F_v v + F_i i) = 0 \tag{6.19b}$$

$$imag(F_v v + F_i i) = 0 \tag{6.19c}$$

$$\text{KCL:} \quad real(Ai) = I^d \tag{6.19d}$$

$$imag(Ai) = I^q \tag{6.19e}$$

$$\text{KVL:} \quad v^d = real(A^T V) \tag{6.19f}$$

$$v^q = imag(A^T V) \tag{6.19g}$$

$$\text{Nonlinear Element:} \quad real(V \odot I^*) = -P_d + P_g \tag{6.19h}$$

$$imag(V \odot I^*) = -Q_d + Q_g \tag{6.19i}$$

$$\text{Gen. Limit:} \quad P_j^{min} \le P_{g,j} \le P_j^{max} \quad Q_j^{min} \le Q_{g,j} \le Q_j^{max}, \quad \forall j \in \mathbf{G} \tag{6.19j}$$

$$\text{Volt. Limit:} \quad (V_j^{min})^2 \le (V_j^d)^2 + (V_j^q)^2 \le (V_j^{max})^2, \quad j \in \mathbf{N} \tag{6.19k}$$

$$\text{Curr. Limit:} \quad (i_{k,a/b}^d)^2 + (i_{k,a/b}^q)^2 \le (I_k^{max})^2, \quad k \in \mathbf{L} \tag{6.19l}$$

where k indexes network elements and a/b represent port a and b for any two-port network element k. Let $\mathbf{F_{STF}}$ be the feasible region of **STF-OPF** problem. Notice that critical nonlinear/nonconvex equations appear in (6.19h), (6.19i), (6.19k).

REMARK 6.1. (Equivalent feasible region) $\mathbf{F_S} = \mathbf{F_{STF}}$. Notice that the Y_{bus} can be obtained from STF with the restrictive assumption (see Chapter (3.4)) that bus currents may be related

to bus voltage via $I = \underbrace{-A \cdot (F_i)^{-1} \cdot F_v \cdot A^T}_{\mathbf{Y}_{bus}} V$. This implies that the problem (6.19) can be used to derive problem 6.18 as a special case. Minor differences will of course occur if different choices are made (current magnitude versus apparent power) to impose line thermal limits.

The relaxation is first based on exploiting convex envelopes of bilinear terms in the power balance equations (6.19h), (6.19i). To this end, the approach is first motivated by the fact that at known power flow solution $V_j^0 \neq 0$ at bus j, there always exists a choice of Y_j (admittance) that would produce same P_j^0, Q_j^0 such that

$$P_j^0 + jQ_j^0 = V_j^0 (I_j^0)^* = V_j^0 (Y_j V_j^0)^* = |V_j^0|^2 Y_j^* \tag{6.20a}$$

$$Y_j = \frac{P_j^0 - jQ_j^0}{|V_j^0|^2} \tag{6.20b}$$

With this observation, the key idea is to introduce an intermediate variable Y_j for bus j in **STF-OPF** problem. Figure 6.2 describes this intermediate variable Y for load and generator buses. Note that the sign convention of Y is determined with the power coming out of transmission system networks regardless of the bus type (load bus or generator bus). This implies that the net injected current I_j of bus j can be obtained with $-Y_j V_j = I_j$ by Ohm's law.

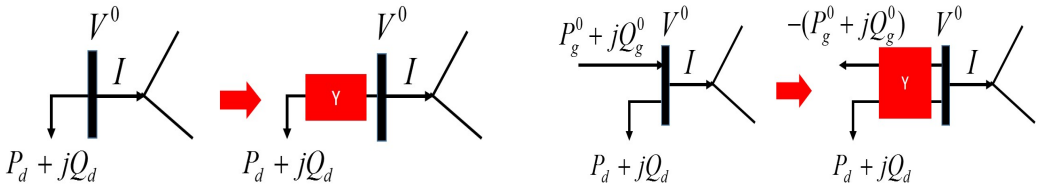

(a) Load Bus (b) Generator Bus

Figure 6.2: Substitution of the admittance variable for load bus and generator bus

6.3.2.1 Introducing intermediate variable Y

As the previous section described, the intermediate admittance variable $Y = [Y_1, ..., Y_n]^T$ with $Y_1 = Y_1^d + jY_1^q$ is introduced in **STF-OPF** and this replaces KCL, Nonlinear Element and voltage magnitude limit, which results in the following optimization problem

$$\textbf{(STFY-OPF)} \quad \min_{v,i,V,I,Y,P_g,Q_g} \sum_{j \in \mathbf{G}} \tilde{c}_j(P_{g,j}) \qquad \text{subject to} \tag{6.21a}$$

$$\text{KCL}: \quad real(Ai) = real(-Y \odot V) = -Y^d \odot V^d + Y^q \odot V^q \tag{6.21b}$$

$$imag(Ai) = imag(-Y \odot V) = -Y^d \odot V^q - Y^q \odot V^d \tag{6.21c}$$

$$\text{Nonlinear Element:} \quad real(V \odot (-Y \odot V)^*) = -Y^d \odot (V^m)^2 = -P_d + P_g \tag{6.21d}$$

$$imag(V \odot (-Y \odot V)^*) = Y^q \odot (V^m)^2 = -Q_d + Q_g \tag{6.21e}$$

$$\text{Volt. Limit:} \quad (V_j^{min})^2 \leq (V_j^m)^2 \leq (V_j^{max})^2, \quad j \in \mathbf{N} \tag{6.21f}$$

$$\text{Volt. Magnitude:} \quad (V_j^d)^2 + (V_j^q)^2 = (V_j^m)^2, \quad j \in \mathbf{N} \tag{6.21g}$$

(6.19b), (6.19c), (6.19f), (6.19g) hold

where V_j^m is voltage magnitude at bus j.

Let the problem and feasible region of (6.21) denote **STFY-OPF** and $\mathbf{F_{STFY}}$ respectively. Compared to **STF-OPF**, additional nonconvex constraints (6.21b), (6.21c) are present in **STFY-OPF**, which are again bilinear constraints. Square of voltage magnitude $(V^m)^2 = [(V_1^m)^2, ..., (V_n^m)^2]^T$ is defined in (6.21g). Power balance equations (6.19h), (6.19i) are reformulated as by

$$P_j = real[V_j(-Y_j V_j)^*] = real[-Y_j^*(V_j V_j^*)] = real[-Y_j^*(V_j^m)^2] = -Y_j^d(V_j^m)^2$$
$$Q_j = imag[V_j(-Y_j V_j)^*] = imag[-Y_j^*(V_j V_j^*)] = imag[-Y_j^*(V_j^m)^2] = Y_j^q(V_j^m)^2$$

We subsequently modify this form with (6.21g) to obtain a bilinear form. Our focus is on the nonconvexity appearing with bilinear terms in (6.21b), (6.21c), (6.21d), (6.21e) and circle equation (6.21g). Possible advantage of this reformulation lies in the fact that nonconvexity only appears at equations associated with individual buses and only corresponding local bus variables are responsible for this nonconvexity. In other words, each nonconvex equation involves small number of variables and are decoupled from one another.

LEMMA 6.1. (Equivalent Feasible Region) $\mathbf{F_S} = \mathbf{F_{STFY}}$.

Proof. ($\Longrightarrow$) Suppose $\overline{x} = (\overline{V}, \overline{S_g})$ is feasible solution for $\mathbf{F_S}$. Then, this solution is also feasible

for $\mathbf{F_{STFY}}$ since feasible $\overline{y} = (\overline{v}, \overline{i}, \overline{I}, \overline{V}, \overline{Y}, \overline{S_g})$ will be determined by

$$\overline{v} = A^T \overline{V} \quad \text{by KVL} \quad (6.19f),(6.19g) \tag{6.23}$$

$$\overline{i} = -(F_i^{-1} F_v) \cdot \overline{v} \quad \text{by linear element eq.} \quad (6.19b),(6.19c) \tag{6.24}$$

$$\overline{I} = A\overline{i} \quad \text{by KCL} \tag{6.25}$$

$$\overline{I} = -\overline{Y} \odot \overline{V} \quad \text{by KCL} \quad (6.21b),(6.21c) \tag{6.26}$$

Similarly, $\overline{Y}$ can be directly determined by $\overline{Y} = \frac{-\overline{S_g} + Sd}{(|\overline{V}|)^2}$, which implies that if $\overline{x} = (\overline{V}, \overline{S_g})$ is feasible for $\mathbf{F_S}$, then it is also feasible for $\mathbf{F_{STFY}}$. So $\mathbf{F_S} \subseteq \mathbf{F_{STFY}}$.

Now consider other direction ($\Longleftarrow$). Let us again suppose that $\overline{y} = (\overline{v}, \overline{i}, \overline{I}, \overline{Y}, \overline{S_g})$ is feasible solution for $\mathbf{F_{STFY}}$. Then, feasible $\overline{x} = (\overline{V}, \overline{S_g})$ can be determined by showing $-\overline{Y} \odot \overline{V} = Y_{bus}\overline{V}$. Consider that

$$-\overline{Y} \odot \overline{V} = A\overline{i} \quad \text{by KCL} \quad (6.21b),(6.21c) \tag{6.27}$$

$$= -A \cdot (F_i^{-1} \cdot F_v) \cdot \overline{v} \quad \text{by linear element eq.} \quad (6.19b),(6.19c) \tag{6.28}$$

$$= -A \cdot (F_i^{-1} \cdot F_v) \cdot A^T \overline{V} \quad \text{by KVL} \quad (6.19f),(6.19g) \tag{6.29}$$

$$= Y_{bus}\overline{V} \tag{6.30}$$

and this leads to having $\overline{V} \odot (-\overline{Y} \odot \overline{V})^* = \overline{V} \odot (Y_{bus}\overline{V})^* = -\overline{S_g} + Sd$. This implies that if $\overline{x} = (\overline{V}, \overline{S_g})$ is feasible for $\mathbf{F_S}$, then it is also feasible for $\mathbf{F_{STFY}}$. So $\mathbf{F_S} \supseteq \mathbf{F_{STFY}}$. Therefore, $\mathbf{F_S} = \mathbf{F_{STFY}}$. ■

The nonconvexity in (6.21) may be attributed to the bilinear expressions of (6.21b), (6.21c), (6.21d), (6.21e). Bilinear terms have been extensively studied in the literature and corresponding convex envelopes are well-developed in the work of McCormick (MC) [22], [141]. The convex envelope of the bilinear term $z = xy$, $(x, y) \in [x_{min}, x_{max}] \times [y_{min}, y_{max}]$ is given by

Lower Envelope:	$z \geq x_{min}y + y_{min}x - x_{min}y_{min}$
Lower Envelope:	$z \geq x_{max}y + y_{max}x - x_{max}y_{max}$
Upper Envelope:	$z \leq x_{min}y + y_{max}x - x_{min}y_{max}$
Upper Envelope:	$z \leq x_{max}y + y_{min}x - x_{max}y_{min}$

Let us denote this convex hull as $MC(xy) = (x, y, z)$. We use this result to construct convex envelopes for bilinear terms (6.21b), (6.21c), (6.21d), (6.21e). In particular, we first define the following new MC variables $z_{1,j} = -Y_j^d V_j^d$, $z_{2,j} = Y_j^q V_j^q$, $z_{3,j} = -Y_j^d V_j^q$, $z_{4,j} = -Y_j^q V_j^d$, $w_{1,j} = -Y_j^d V_{m,j}^2$, $w_{2,j} = Y_j^q V_{m,j}^2$ for each node $j \in \mathbf{N}$. In vector form, MC variables are expressed as $z_1 = -Y^d \odot V^d$, $z_2 = Y^q \odot V^q$, $z_3 = -Y^d \odot V^q$, $z_4 = -Y^q \odot V^d$, $w_1 = -Y^d \odot (V_m)^2$, $w_2 = Y^q \odot (V_m)^2$. Observe that V^d and V^q do not have explicit tight bounds, but instead could have loose bounds as $-V^{max} \leq V^d, V^q \leq V^{max}$. Even though their explicit bounds are loose, V^d, V^q are predominantly constrained by network element equations (6.19b), (6.19c) and voltage limit (6.21f). Convex relaxation of constraints (6.21b), (6.21b), (6.21d), (6.21e) is obtained by the following set of linear constraints.

$$\text{MC-YCOV} = \begin{cases} z_1 \in MC(Y^d \odot V^d), \quad z_2 \in MC(Y^q \odot V^q) \\ z_3 \in MC(Y^d \odot V^q), \quad z_4 \in MC(Y^q \odot V^d) \\ w_1 \in MC(Y^d \odot (V^m)^2) \\ w_2 \in MC(Y^q \odot (V^m)^2) \end{cases} \tag{6.31}$$

The characterizations of the convex hull for remaining nonconvex constraints (6.21g) are more problematic without additional information, but they can be relaxed as follows,

$$\text{Volt. Magnitude:} \qquad (V_j^d)^2 + (V_j^q)^2 \leq (V_j^m)^2, \quad j \in \mathbf{N} \tag{6.32}$$

This relaxation implies that minimum voltage constraints are ignored; in practical applications, this might be unattractive because of voltage stability concerns. However, notice that since higher losses occur at lower voltages, the natural tendency of the optimization will often be toward solutions with higher voltages [37].

6.3.2.2 Finding upper/lower bound for variable Y

Since the quality of the MC relaxation considered in this chapter is strongly dependent on the tightness of variable bounds, it is important to have a tighter bound for the variable Y. An attractive property of introduced variable Y is that we can find a tighter bound for Y from

knowledge of $V^{min}, V^{max}, P^{min}, P^{max}, Q^{min}, Q^{max}$, which contains the original feasible region $\mathbf{F_{STF}}$. Let us consider how such bounds can be identified.

- *Load bus*

Consider the power balance equation at load buses to derive the nonlinear function of Y

$$-(P_d + \mathbf{j}Q_d) = -Y^* \odot (V^m)^2 \tag{6.33a}$$

$$Y = \frac{P_d - \mathbf{j}Q_d}{(V^m)^2} \tag{6.33b}$$

$$Y^d = \frac{P_d}{(V^m)^2}, \quad Y^q = \frac{-Q_d}{(V^m)^2} \tag{6.33c}$$

Thus, we can obtain upper and lower bounds on Y by finding the optima in the following low-dimensional problems:

$$Y^d_{min} = \mathbf{min}\Big(\frac{P_d}{(V^m)^2}\Big), \quad Y^d_{max} = \mathbf{max}\Big(\frac{P_d}{(V^m)^2}\Big) \tag{6.34a}$$

$$Y^q_{min} = \mathbf{min}\Big(\frac{-Q_d}{(V^m)^2}\Big), \quad Y^q_{max} = \mathbf{max}\Big(\frac{-Q_d}{(V^m)^2}\Big) \tag{6.34b}$$

$$\text{all subject to} \quad (6.21f)$$

Each bound is computed by checking end points of $(V^m)^2$ and the unconstrained first-order necessary conditions (FONC). However, equations (6.33c) have no FONC so only $(V^{min})^2$, $(V^{max})^2$ are used to determine bounds for Y^d, Y^q. Then, upper and lower bound on shunt admittances at load buses can be easily obtained by

$$Y^d_{min} = \mathbf{min}\Big(\frac{P_d}{(V^{min})^2}, \frac{P_d}{(V^{max})^2}\Big) \tag{6.35a}$$

$$Y^d_{max} = \mathbf{max}\Big(\frac{P_d}{(V^{min})^2}, \frac{P_d}{(V^{max})^2}\Big) \tag{6.35b}$$

$$Y^q_{min} = \mathbf{min}\Big(\frac{-Q_d}{(V^{min})^2}, \frac{-Q_d}{(V^{max})^2}\Big) \tag{6.35c}$$

$$Y^q_{max} = \mathbf{max}\Big(\frac{-Q_d}{(V^{min})^2}, \frac{-Q_d}{(V^{max})^2}\Big) \tag{6.35d}$$

- *Generator bus*

Similarly, consider the power balance equation at generator buses

$$(P_g + jQ_g) - (P_d + \mathbf{j}Q_d) = -Y^* \odot (V^m)^2 \tag{6.36a}$$

$$Y = \frac{-(P_g - \mathbf{j}Q_g) + (P_d - \mathbf{j}Q_d)}{(V^m)^2} \tag{6.36b}$$

$$Y^d = \frac{-P_g + P_d}{(V^m)^2} \quad Y^q = \frac{Q_g - Q_d}{(V^m)^2} \tag{6.36c}$$

Thus, we can obtain upper and lower bounds on Y by finding the following optima in the following low-dimensional problems:

$$Y^d_{min} = \mathbf{min}\Big(\frac{-P_g + P_d}{(V^m)^2}\Big), \quad Y^d_{max} = \mathbf{max}\Big(\frac{-P_g + P_d}{(V^m)^2}\Big) \tag{6.37a}$$

$$Y^q_{min} = \mathbf{min}\Big(\frac{Q_g - Q_d}{(V^m)^2}\Big), \quad Y^q_{max} = \mathbf{max}\Big(\frac{Q_g - Q_d}{(V^m)^2}\Big) \tag{6.37b}$$

$$\text{all subject to} \quad (6.19\text{j}), (6.21\text{f})$$

Similarly, each bound is computed by checking end points of $(V^m)^2$, P_g, Q_g and the unconstrained first-order necessary conditions (FONC). However, equations (6.36c) have no FONC $\big(Y^d_{Pg} = \frac{-1+P_d}{(V^m)^2} \neq 0$ with P_g, $Y^d_{(Vm)^2} = \frac{P_g - P_d}{(V^m)^4} \neq 0$ with $(V^m)^2\big)$ so only $(V^{min})^2$, $(V^{max})^2$, P^{min}, P^{max}, Q^{min}, Q^{max} are used to determine bounds for Y^d, Y^q. Then, upper and lower bound at generator buses can be easily obtained by

$$Y^d_{min} = \mathbf{min}\Big(\frac{-P^{min} + P_d}{(V^{min})^2}, \frac{-P^{max} + P_d}{(V^{min})^2}, \frac{-P^{min} + P_d}{(V^{max})^2}, \frac{-P^{max} + P_d}{(V^{max})^2}\Big) \tag{6.38a}$$

$$Y^d_{max} = \mathbf{max}\Big(\frac{-P^{min} + P_d}{(V^{min})^2}, \frac{-P^{max} + P_d}{(V^{min})^2}, \frac{-P^{min} + P_d}{(V^{max})^2}, \frac{-P^{max} + P_d}{(V^{max})^2}\Big) \tag{6.38b}$$

$$Y^q_{min} = \mathbf{min}\Big(\frac{Q^{min} - Q_d}{(V^{min})^2}, \frac{Q^{max} - Q_d}{(V^{min})^2}, \frac{Q^{min} - Q_d}{(V^{max})^2}, \frac{Q^{max} - Q_d}{(V^{max})^2}\Big) \tag{6.38c}$$

$$Y^q_{max} = \mathbf{max}\Big(\frac{Q^{min} - Q_d}{(V^{min})^2}, \frac{Q^{max} - Q_d}{(V^{min})^2}, \frac{Q^{min} - Q_d}{(V^{max})^2}, \frac{Q^{max} - Q_d}{(V^{max})^2}\Big) \tag{6.38d}$$

Finally, we have

$$Y^d_{min} \leq Y^d \leq Y^d_{max}, \quad Y^q_{min} \leq Y^q \leq Y^q_{max} \tag{6.39}$$

These bounds are feasible for the original feasible region and are used to construct MC envelopes. Notice that the bound for intermediate variable Y is determined by simple and computationally efficient calculation, with closed-form solutions, and these are added to the

optimization problem (6.21). Let us denote the feasible region of **STFY-OPF** with (6.39) as $\mathbf{F_{STFYB}}$.

LEMMA 6.2. (Equivalent Feasible Region) $\mathbf{F_S} = \mathbf{F_{STFYB}}$.

Proof. From **LEMMA 6.1**, we only need to show $\mathbf{F_S} \subseteq \mathbf{F_{STFYB}}$. Suppose $\overline{x} = (\overline{V}, \overline{S_g})$ is feasible solution for $\mathbf{F_S}$ and $\widetilde{Y} = \{Y \mid Y^d_{min} \le Y_d \le Y^d_{max}, Y^q_{min} \le Y_q \le Y^q_{max}\}$. Then, we want to show that there exists a $\widetilde{Y}$ such that $\widetilde{Y} = \frac{-\overline{S_g}+Sd}{(|\overline{V}|)^2}$. Since $Y^d_{min}, Y^d_{max}, Y^q_{min}, Y^q_{max}$ are calculated as **min**/**max** $\left(\frac{-S_g+Sd}{(|V|)^2}\right)$ with $S^{max}_g, S^{min}_g, V^{min}_j, V^{max}_j$, it is always possible to find a feasible $\overline{Y} = \frac{-\overline{S_g}+Sd}{(|\overline{V}|)^2}$ in the region of $\widetilde{Y}$. ■

6.3.2.3 Convex Relaxation Problem for STFY-OPF

This section formulates the convex relaxation problem for **STFY-OPF**. Let us denote MC variables $z = (z_1, z_2, z_3, z_4)$ and $w = (w_1, w_2)$. Resulting convex relaxation of Sparse Tableau Formulation of OPF with admittance variable Y is constructed as follows:

$$\textbf{(STFY-CONV)} \quad \min_{v,i,V,I,P_g,Q_g,V^m,z,w} \sum_{j \in \mathbf{G}} \tilde{c}_j(P_{g,j}) \qquad \text{subject to} \tag{6.40a}$$

$$\text{Linear Element:} \quad real(F_v v + F_i i) = 0 \tag{6.40b}$$

$$imag(F_v v + F_i i) = 0 \tag{6.40c}$$

$$\text{KCL:} \quad real(Ai) = -z_1 + z_2 \tag{6.40d}$$

$$imag(Ai) = -z_3 - z_4 \tag{6.40e}$$

$$\text{KVL:} \quad v^d = real(A^T V) \tag{6.40f}$$

$$v^q = imag(A^T V) \tag{6.40g}$$

$$\text{Nonlinear Element:} \quad -w_1 = -P_d + P_g \tag{6.40h}$$

$$w_2 = -Q_d + Q_g \tag{6.40i}$$

$$\text{Gen. Limit:} \quad P_j^{min} \le P_{g,j} \le P_j^{max}, \quad Q_{min,j} \le Q_{g,j} \le Q_{max,j}, \quad j \in \mathbf{G} \tag{6.40j}$$

$$\text{Volt. Limit:} \quad (V_j^{min})^2 \le (V_j^m)^2 \le (V_j^{max})^2, \quad j \in \mathbf{N} \tag{6.40k}$$

$$\text{Volt. Magnitude:} \quad (V_j^d)^2 + (V_j^q)^2 \le (V_j^m)^2, \quad j \in \mathbf{N} \tag{6.40l}$$

$$\text{Curr. Limit:} \quad (i_{k/a,b}^d)^2 + (i_{k/a,b}^q)^2 \le (I_k^{max})^2, \quad k \in \mathbf{L} \tag{6.40m}$$

$$\text{MC-constraints:} \quad \text{MC-YCOV} \tag{6.40n}$$

Denote the problem (6.40) as STFY relaxation and the feasible region of this convex relaxation as $\mathbf{F^c_{STFY}}$. This feasible region is equivalent to convex region of the original problem. Notice that since V^d and V^q have loose bounds implying that the variables z have loose MC convex envelopes, this could be a problematic even though they are constrained by other equations (6.40b), (6.40c), (6.40m). Another MC variable w is only constrained by MC-constraints. We will propose a heuristic method to improve the bound on variable z and important parameters, which then influence the quality of the relaxation gap of variable w in the later section.

6.3.3 An Alternate Current-Based Convex Relaxation

This section formulates the convex relaxation problem for STF of OPF in slightly different fashion. Instead of using the variable Y, we directly use net current I injection at each bus. Let this problem and feasible region denote **STFI-OPF** and $\mathbf{F_{STFI}}$ respectively. Advantage of directly finding the bound on variable I is the reduced number of MC variables in the convex relaxation problem.

6.3.3.1 Finding upper/lower limit for variable I

Even though it is not necessary to determine upper/lower limit of variable I to obtain a feasible solution in the problem (6.19), it is important to have a tighter bound for the variable I to apply McCormick envelope, to construct the convex relaxation problem. We will show that one can always find a tighter bound for I from typical given data, which contains the original feasible region $\mathbf{F_{STF}}$. For bounds on V^d, V^q, the (6.41) below is used for this section.

$$-V^{max} \le V^d, V^q \le V^{max} \tag{6.41}$$

- *Load bus*

Consider the power balance equation at load buses to derive the behaviors of injected current I

$$-(P_d + jQ_d) = V \odot (I)^* \tag{6.42a}$$

$$I = \frac{-(P_d + \mathbf{j}Q_d)^*}{V^*} \tag{6.42b}$$

$$I = \frac{-(P_d - \mathbf{j}Q_d)}{V^d - \mathbf{j}V^q} \tag{6.42c}$$

$$I = \frac{-(P_d - \mathbf{j}Q_d)(V^d + \mathbf{j}V^q)}{(V^m)^2} \tag{6.42d}$$

$$I^d = \frac{-P_d V^d - Q_d V^q}{(V^m)^2}, \quad Y^q = \frac{-P_d V^q + Q_d V^d}{(V^m)^2} \tag{6.42e}$$

Thus, we can obtain upper and lower bounds on I by finding the optima in the following low-dimensional problems:

$$I^d_{min} = \mathbf{min}\Big(\frac{-P_d V^d - Q_d V^q}{(V^m)^2}\Big), \quad I^d_{max} = \mathbf{max}\Big(\frac{-P_d V^d - Q_d V^q}{(V^m)^2}\Big) \tag{6.43a}$$

$$I^q_{min} = \mathbf{min}\Big(\frac{-P_d V^q + Q_d V^d}{(V^m)^2}\Big), \quad I^q_{max} = \mathbf{max}\Big(\frac{-P_d V^q + Q_d V^d}{(V^m)^2}\Big) \tag{6.43b}$$

$$\text{all subject to} \quad (6.19k), (6.41)$$

As in the admittance cases, each bound is computed by checking end points of variables and the unconstrained first-order necessary conditions (FONC). However, equations (6.42e) have no FONC $\big(I^d_{V^d} = \frac{-P_d}{(V^m)^2} \neq 0$ with V^d, $I^d_{V^q} = \frac{-Q_d}{(V^m)^2} \neq 0$ with V^q, $I^d_{(V^m)^2} = \frac{P_d V^d + Q_d V^q}{(V^m)^4} \neq 0$ with $(V^m)^2\big)$ so only corner points are used to determine bounds for I^d, I^q. With these, upper and lower bounds at load buses can be easily obtained by

$$aa_{max} = -\mathbf{min}\Big(P_d V^d_{max}, P_d V^d_{min}\Big) - \mathbf{min}\Big(Q_d V^q_{max}, Q_d V^q_{min}\Big)$$

$$aa_{min} = -\mathbf{max}\Big(P_d V^d_{max}, P_d V^d_{min}\Big) - \mathbf{max}\Big(Q_d V^q_{max}, Q_d V^q_{min}\Big)$$

$$bb_{max} = +\mathbf{max}\Big(Q_d V^d_{max}, Q_d V^d_{min}\Big) - \mathbf{min}\Big(P_d V^q_{max}, P_d V^q_{min}\Big)$$

$$bb_{min} = +\mathbf{min}\Big(Q_d V^d_{max}, Q_d V^d_{min}\Big) - \mathbf{max}\Big(P_d V^q_{max}, P_d V^q_{min}\Big)$$

Therefore, its minimum and maximum can be obtained by

$$I^d_{min} = \mathbf{min}\Big(\frac{aa_{max}}{(V^{min})^2}, \frac{aa_{min}}{(V^{min})^2}, \frac{aa_{max}}{(V^{max})^2}, \frac{aa_{min}}{(V^{max})^2}\Big) \tag{6.45a}$$

$$I^d_{max} = \mathbf{max}\Big(\frac{aa_{max}}{(V^{min})^2}, \frac{aa_{min}}{(V^{min})^2}, \frac{aa_{max}}{(V^{max})^2}, \frac{aa_{min}}{(V^{max})^2}\Big) \tag{6.45b}$$

$$I^q_{min} = \mathbf{min}\Big(\frac{bb_{max}}{(V^{min})^2}, \frac{bb_{min}}{(V^{min})^2}, \frac{bb_{max}}{(V^{max})^2}, \frac{bb_{min}}{(V^{max})^2}\Big) \tag{6.45c}$$

$$I^q_{max} = \mathbf{max}\Big(\frac{bb_{max}}{(V^{min})^2}, \frac{bb_{min}}{(V^{min})^2}, \frac{bb_{max}}{(V^{max})^2}, \frac{bb_{min}}{(V^{max})^2}\Big) \tag{6.45d}$$

- *Generator bus*

Similarly, consider the power balance equation at generator buses

$$P_g + jQ_g - (P_d + \mathbf{j}Q_d) = V \odot (I)^* \tag{6.46a}$$

$$I = \frac{(P_g + \mathbf{j}Q_g - P_d - \mathbf{j}Q_d)^*}{V^*} = \frac{(P_g - \mathbf{j}Q_g - P_d + \mathbf{j}Q_d)}{V^d - \mathbf{j}V^q} \tag{6.46b}$$

$$I = \frac{(P_g - \mathbf{j}Q_g - P_d + \mathbf{j}Q_d)(V^d + \mathbf{j}V^q)}{(V^m)^2} \tag{6.46c}$$

$$I^d = \frac{P_g V^d - P_d V^d + Q_g V^q - Q_d V^q}{(V^m)^2}, \quad I^q = \frac{-Q_g V^d + Q_d V^d + P_g V^q - P_d V^q}{(V^m)^2} \tag{6.46d}$$

Thus, we can obtain upper and lower bounds on I by finding the following optima in the following low-dimensional problems:

$$I^d_{min} = \mathbf{min}\Big(\frac{P_g V^d - P_d V^d + Q_g V^q - Q_d V^q}{(V^m)^2}\Big) \tag{6.47a}$$

$$I^d_{max} = \mathbf{max}\Big(\frac{P_g V^d - P_d V^d + Q_g V^q - Q_d V^q}{(V^m)^2}\Big) \tag{6.47b}$$

$$I^q_{min} = \mathbf{min}\Big(\frac{-Q_g V^d + Q_d V^d + P_g V^q - P_d V^q}{(V^m)^2}\Big) \tag{6.47c}$$

$$I^q_{max} = \mathbf{max}\Big(\frac{-Q_g V^d + Q_d V^d + P_g V^q - P_d V^q}{(V^m)^2}\Big) \tag{6.47d}$$

all subject to (6.19j),(6.19k)

Similarly, each bound is computed by checking end points of $(V^m)^2$, P_g, Q_g and the unconstrained first-order necessary conditions (FONC). However, equations (6.46d) have no FONC $\big(I^d_{P_g} = \frac{V^d}{(V^m)^2} \neq 0$ with P_g, $I^d_{Q_g} = \frac{V^q}{(V^m)^2} \neq 0$ with Q_g, $I^d_{V_d} = \frac{-P_d}{(V^m)^2} \neq 0$ with V_d, $I^d_{V_q} = \frac{-Q_d}{(V^m)^2} \neq 0$ with V_q, $I^d_{(V^m)^2} = \frac{P_d V^d + Q_d V^q}{(V^m)^4} \neq 0$ with $(V^m)^2\big)$ so only corner points are used to determine

bounds for I_d, I_q. Then, upper and lower bound at generator buses can be easily obtained by

$$\begin{aligned}
cc_{max} &= \mathbf{max}\Big(P_{max}V^d_{max}, P_{max}V^d_{min}, P_{min}V^d_{max}, P_{min}V^d_{min}\Big) - \mathbf{min}\Big(P_dV^d_{max}, P_dV^d_{min}\Big) \\
&+ \mathbf{max}\Big(Q_{max}V^q_{max}, Q_{max}V^q_{min}, Q_{min}V^q_{max}, Q_{min}V^q_{min}\Big) - \mathbf{min}\Big(Q_dV^q_{max}, Q_dV^q_{min}\Big) \\
cc_{min} &= \mathbf{min}\Big(P_{max}V^d_{max}, P_{max}V^d_{min}, P_{min}V^d_{max}, P_{min}V^d_{min}\Big) - \mathbf{max}\Big(P_dV^d_{max}, P_dV^d_{min}\Big) \\
&+ \mathbf{min}\Big(Q_{max}V^q_{max}, Q_{max}V^q_{min}, Q_{min}V^q_{max}, Q_{min}V^q_{min}\Big) - \mathbf{max}\Big(Q_dV^q_{max}, Q_dV^q_{min}\Big) \\
dd_{min} &= -\mathbf{min}\Big(Q_{max}V^d_{max}, Q_{max}V^d_{min}, Q_{min}V^d_{max}, Q_{min}V^d_{min}\Big) + \mathbf{max}\Big(Q_dV^d_{max}, Q_dV^d_{min}\Big) \\
&+ \mathbf{min}\Big(P_{max}V^q_{max}, P_{max}V^q_{min}, P_{min}V^q_{max}, P_{min}V^q_{min}\Big) - \mathbf{max}\Big(P_dV^q_{max}, P_dV^q_{min}\Big) \\
dd_{min} &= \mathbf{max}\Big(Q_{max}V^d_{max}, Q_{max}V^d_{min}, Q_{min}V^d_{max}, Q_{min}V^d_{min}\Big) + \mathbf{min}\Big(Q_dV^d_{max}, Q_dV^d_{min}\Big) \\
&+ \mathbf{max}\Big(P_{max}V^q_{max}, P_{max}V^q_{min}, P_{min}V^q_{max}, P_{min}V^q_{min}\Big) - \mathbf{min}\Big(P_dV^q_{max}, P_dV^q_{min}\Big)
\end{aligned}$$

$$I^d_{min} = \mathbf{min}\Big(\frac{cc_{max}}{(V^{min})^2}, \frac{cc_{min}}{(V^{min})^2}, \frac{cc_{max}}{(V^{max})^2}, \frac{cc_{min}}{(V^{max})^2}\Big) \tag{6.49a}$$

$$I^d_{max} = \mathbf{max}\Big(\frac{cc_{max}}{(V^{min})^2}, \frac{cc_{min}}{(V^{min})^2}, \frac{cc_{max}}{(V^{max})^2}, \frac{cc_{min}}{(V^{max})^2}\Big) \tag{6.49b}$$

$$I^q_{min} = \mathbf{min}\Big(\frac{dd_{max}}{(V^{min})^2}, \frac{dd_{min}}{(V^{min})^2}, \frac{dd_{max}}{(V^{max})^2}, \frac{dd_{min}}{(V^{max})^2}\Big) \tag{6.49c}$$

$$I^q_{max} = \mathbf{max}\Big(\frac{dd_{max}}{(V^{min})^2}, \frac{dd_{min}}{(V^{min})^2}, \frac{dd_{max}}{(V^{max})^2}, \frac{dd_{min}}{(V^{max})^2}\Big) \tag{6.49d}$$

Finally, we have

$$I^d_{min} \le I^d \le I^d_{max}, \quad I^q_{min} \le I^q \le I^q_{max} \tag{6.50}$$

These bounds are used to construct McCormick envelope. Similarly, we consider MC envelope for bilinear terms in **STFI-OPF**. Let us first define the following MC variables $u_{1,j} = V^d_j I^d_j$, $u_{2,j} = V^q_j I^q_j$, $u_{3,j} = -V^d_j I^q_j$, $u_{4,j} = V^q_j I^d_j$ for each node $j \in \mathbf{N}$. In vector form, MC variables are expressed as $u_1 = V^d \odot I^d$, $u_2 = V^q \odot I^q$, $u_3 = -V^d \odot I^q$, $u_4 = V^q \odot I^d$. Convex relaxation of constraints (6.19h), (6.19i) is obtained by the following set of linear constraints.

$$\text{MC-ICOV} = \begin{cases} u_1 \in MC(V^d \odot I^d), \quad u_2 \in MC(V^q \odot I^q) \\ u_3 \in MC(V^d \odot I^q), \quad u_4 \in MC(V^q \odot I^d) \end{cases} \tag{6.51}$$

Like **STFY-CONV**, voltage magnitude constraints (6.19k) are relaxed as

$$\text{Volt. Magnitude:} \qquad (V_j^d)^2 + (V_j^q)^2 \le (V_j^{max})^2, \quad j \in \mathbf{N} \tag{6.52}$$

6.3.3.2 Convex Relaxation Problem for STFI-OPF

Let $u = (u_1, u_2, u_3, u_4)$ and the convex relaxation of **STFI-OPF** may be constructed below:

$$\textbf{(STFI-CONV)} \quad \min_{v,i,V,I,P_g,Q_g,u} \sum_{j \in \mathbf{G}} \tilde{c}_j(P_{g,j}) \qquad \text{subject to} \tag{6.53a}$$

$$\text{Linear Element:} \qquad real(F_v v + F_i i) = 0 \tag{6.53b}$$

$$imag(F_v v + F_i i) = 0 \tag{6.53c}$$

$$\text{KCL:} \qquad real(Ai) = I^d \tag{6.53d}$$

$$imag(Ai) = I^q \tag{6.53e}$$

$$\text{KVL:} \qquad v^d = real(A^T V) \tag{6.53f}$$

$$v^q = imag(A^T V) \tag{6.53g}$$

$$\text{Nonlinear Element:} \qquad u_1 + u_2 = -P_d + P_g \tag{6.53h}$$

$$-u_3 + u_4 = -Q_d + Q_g \tag{6.53i}$$

$$\text{Gen. Limit:} \qquad P_j^{min} \le P_{g,j} \le P_j^{max}, \quad Q_j^{min} \le Q_{g,j} \le Q_j^{max}, \quad j \in \mathbf{G} \tag{6.53j}$$

$$\text{Volt. Limit:} \qquad (V_j^d)^2 + (V_j^q)^2 \le (V_j^{max})^2, \quad j \in \mathbf{N} \tag{6.53k}$$

$$\text{Curr. Limit:} \qquad (i_{k,a/b}^d)^2 + (i_{k,a/b}^q)^2 \le (I_k^{max})^2, \quad k \in \mathbf{L} \tag{6.53l}$$

$$\text{MC-constraints:} \qquad \text{MC-ICOV} \tag{6.53m}$$

We denote problem (6.53) as STFI relaxation, and the feasible region of this convex relaxation as $\mathbf{F}^{\mathbf{c}}_{\mathbf{STFI}}$. This feasible region is equivalent to convex region of the original problem. Similar to **STFV-CONV**, V^d and V^q have loose bounds implying that the variable u might have loose MC convex envelopes.

6.4 Strengthening STF relaxations

6.4.1 Engineering-based Heuristic for Improvement of V^d and V^q Bounds

The proposed McCormick relaxation of the bilinear constraints are useful when good variable upper and lower bounds are available. From the previous section, we have observed that V^d, V^q have loose bounds, or their bounds are not given. However, we might have a better idea if we have angle constraints; the FERC report [37] discusses a linear representation of the voltage constraints that helps in this regard. This section suggests heuristic method to improve bounds of variable V^d, V^q based on the concepts of [37]. We introduce the following assumption.

ASSUMPTION 6.1. (Voltage angle bound) Suppose that δ^{DC} is bus voltage angle solution from the DCOPF problem. Suppose the feasible solution of bus voltage angle δ for the problem (6.19) stays within $\Delta\delta$ of DCOPF solution δ^{DC}, i.e., suppose each bus voltage angle δ_j can be bounded by

$$\delta_j^{DC} - \Delta\delta \le \delta_j \le \delta_j^{DC} + \Delta\delta, \quad j \in \mathbf{N}$$

where $\Delta\delta$ is specified. This implies $\delta_j^{min} = \delta_j^{DC} - \Delta\delta$, $\delta_j^{max} = \delta_j^{DC} + \Delta\delta$ and graphical interpretation of this assumption is depicted in Figure 6.3 below.

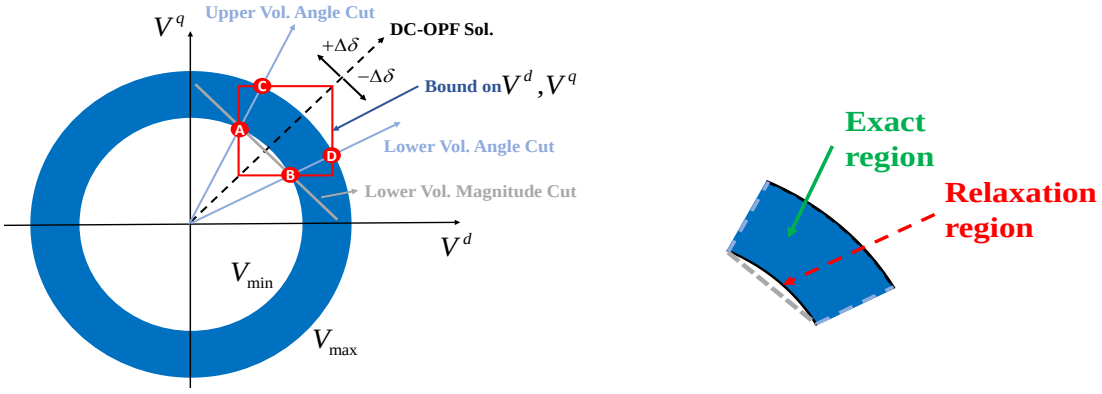

(a) Voltage angle constraints

(b) Feasible Region

Figure 6.3: Voltage angle constraints with DCOPF solution

Figure 6.3a illustrates the DCOPF solution δ^{DC} as the center point, with the feasible range of bus voltage angle δ with $\pm\Delta\delta$ of this center. Figure 6.3b describes each feasible

region in detail with dashed line for relaxation region and solid line for exact nonconvex region. The resulting relaxation region is convex and contains most of the nonconvex constraint set. From the construction in Figure 6.3a, we can find a bound for V_j^d, V_j^q with four points $A_j = (A_j^d, A_j^q), B_j = (B_j^d, B_j^q), C_j = (C_j^d, C_j^q), D_j = (D_j^d, D_j^q)$. These points are calculated as

$$A_j^d = \sqrt{\frac{(V_j^{min})^2}{1+(tan(\delta_j^{max}))^2}}, \quad A_j^q = tan(\delta_j^{max})A_j^d$$

$$B_j^d = \sqrt{\frac{(V_j^{min})^2}{1+(tan(\delta_j^{min}))^2}}, \quad B_j^q = tan(\delta_j^{min})B_j^d$$

$$C_j^d = \sqrt{\frac{(V_j^{max})^2}{1+(tan(\delta_j^{max}))^2}}, \quad C_j^q = tan(\delta_j^{max})C_j^d$$

$$D_j^d = \sqrt{\frac{(V_j^{max})^2}{1+(tan(\delta_j^{min}))^2}}, \quad D_j^q = tan(\delta_j^{min})D_j^d$$

Therefore, $V_{min,j}^d = \mathbf{min}(A_j^d, B_j^d, C_j^d, D_j^d)$, $V_{max,j}^d = \mathbf{max}(A_j^d, B_j^d, C_j^d, D_j^d)$ and $V_{min,j}^q = \mathbf{min}(A_j^q, B_j^q, C_j^q, D_j^q)$, $V_{max,j}^q = \mathbf{max}(A_j^q, B_j^q, C_j^q, D_j^q)$. Additionally, three linear voltage cuts (LIN-VOL), 1) upper voltage angle cut 2) lower voltage angle cut 3) lower voltage magnitude cut for minimum voltage magnitude limit, can be formulated as

$$\text{LIN-VOL} = \begin{cases} V_j^q \le tan(\delta_j^{max})V_j^d & \Longrightarrow \text{Upper voltage angle cut} \\ V_j^q \ge tan(\delta_j^{min})V_j^d & \Longrightarrow \text{Lower voltage angle cut} \\ \hline V_j^q - \alpha_j(V_j^d - A_j^d) + A_j^q \ge 0 \quad \text{for}\, \alpha < 0 & \Longrightarrow \text{Lower voltage magnitude cut} \\ -V_j^q + \alpha_j(V_j^d - A_j^d) - A_j^q \ge 0 \quad \text{for}\, \alpha > 0 & \end{cases} \tag{6.54}$$

where $\alpha_j = \frac{A_j^q - B_j^q}{A_j^d - B_j^d}$.

Finally, tighter bounds given with A, B, C, D for V^d, V^q variables are used to construct (6.39), (6.31), (6.50), (6.51) and LIN-VOL equations (6.54) are added to (6.40) and (6.53) to strengthen the convex relaxation. In this thesis, $\Delta\delta = 20^\circ, 25^\circ, 30^\circ$ are used for case studies. An algorithm finding a guaranteed upper bound of $\Delta\delta$ for use would be valuable to improve this section. For example, recent attempt to find error bounds on the DC power flow is studied in [144]. This

work can be easily extended to find a upper bound of $\Delta\delta$, but leave for future work to investigate the impact of upper bound.

6.4.2 Importance of Active Power Injection Bounds

The other important factors for this convex relaxation problem are MC variables $w_1 \in MC(-Y^d \odot (V^m)^2)$, $w_2 \in MC(Y^q \odot (V^m)^2)$. These MC envelopes are strongly dependent on variable bounds for the square of voltage magnitude $(V^m)^2$ and admittance variable Y. Similarly, for STFI relaxation, MC variables u_1, u_2 are strongly dependent on variable bounds of V and I. In this section, we focus on the variable w_1 due to its direct appearance in the objective function of optimization problem; a similar property holds for the other variable u_1. Notice that bounds V_j^{max}, V_j^{min} for voltage magnitude are typically very narrow in OPF specifications, which implies the quality of w_1 is strongly dependent on bounds for real part of admittance variable Y^d. The bound of admittance variables is constructed with the equation (6.39) by checking end points of $(V^m)^2$, P_g and Q_g. Again, since bounds of voltage magnitude are quite narrow, P^{max} and P^{min} would substantially determine the gap between Y^d_{min} and Y^d_{max}. Notice that MC lower/upper envelopes are linear constraints constructed with bounds V^{min},V^{max},P^{min},P^{max}, and the MC envelope for the bilinear term $Y^d(V^m)^2$ is shown in Figure 6.4.

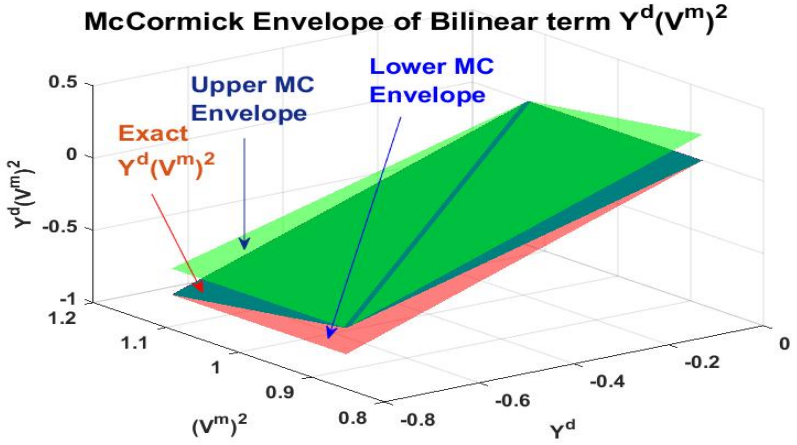

Figure 6.4: McCormick Envelope for the bilinear term $Y^d(V^m)^2$

In terms of convex relaxation, we want to have as small a relaxation gap as possible between

the exact bilinear term and upper/lower MC envelopes. A tighter relaxation gap is obtained when narrow bounds for P_g are given, which indicates the small gap between P^{min} and P^{max}. The diagonal line (2D) from the 3D plane in Figure 6.4 is taken out for a better look and relaxation gap strongly dependent on P^{max} and P^{min} is depicted in Figure 6.5. The first generator from the case14 bus system of MATPOWER [23] is used as a representative example.

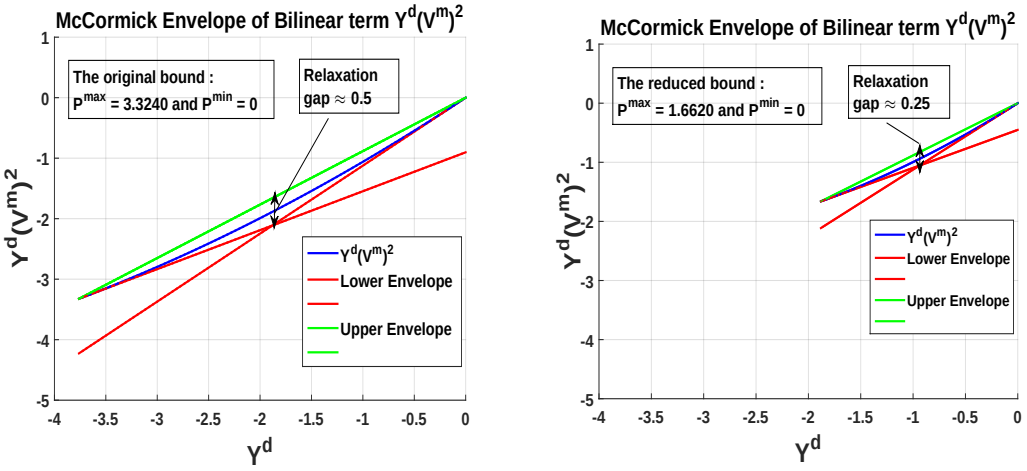

(a) The original bound for P_g

(b) The reduced bound for P_g

Figure 6.5: McCormick envelope of generator 1 for the case14 sytem

Figure 6.5a shows MC envelopes with the original bound for P_g; $P^{max} = 3.3240$ and $P^{min} = 0$ and its relaxation gap defined as the longest distance between lower and upper envelope is approximately equal to 0.5. On the other hand, Figure 6.5b shows MC envelopes with the reduced bound for P_g by 50%; $P^{max} = 0.5P^{max} = 1.6620$ and $P^{min} = 0$. Corresponding relaxation gap is approximately equal to 0.25 reduced by half from the original bound of P_g. This example demonstrates that tighter bounds on P_g are important to have a tighter relaxation solution. We use this important observation to improve STF relaxations with two techniques; 1) sequential bound tightening (SBT) and 2) reduced spatial branch-and-bound (RSBB).

6.4.2.1 Sequential Bound Tightening

The basic idea of bound tightening is to derive tighter valid bounds to improve relaxations before solving (6.40). Based on the importance of active power injection bounds, we are interested

in shrinking the bounds of active/reactive power generation. To this end, approach here is based on sequential bound tightening (SBT) [145]. Let $x_{g,j} = (P_{g,j}, Q_{g,j})$ and we solve slightly modified STFY relaxation, which is shown as (6.55). For each $x_{g,j}$, we first solve (6.55) where we minimize $x_{g,i}$ and then solve (6.55) where we maximize $x_{g,i}$. In both cases, constraint (6.55a) that bounds the original objective function of (6.40) with a best known feasible solution $x^{loc}_{g,j}$ is added, which is shown to be useful. This technique is iteratively applied to tighten the bounds of the variable $x_{g,j}$. Algorithm 1 describes the pseudocode of SBT.

Algorithm 1 Sequential bound tightening on P_g, Q_g vector

Input: $x^{lo}_{g,j} \longleftarrow x^{min}_{g,j}$, $x^{up}_{g,j} \longleftarrow x^{max}_{g,j}$, $x^{min}_{g,j,iter} = x^{max}_{g,j,iter} \longleftarrow 0$, $x^{loc}_{g,j}$, $TOL > 0$.

1: while $|x^{lo}_{g,j} - x^{min}_{g,j,iter}|$ and $|x^{up}_{g,j} - x^{max}_{g,j,iter}| >$ TOL do

2: $x^{min}_{g,j,iter} \longleftarrow x^{lo}_{g,j}, x^{max}_{g,j,iter} \longleftarrow x^{up}_{g,j}$

3: Solve:

$$(x^{min}_{g,j})^* = \mathbf{min}\, x_{g,j}; \quad (x^{max}_{g,j})^* = \mathbf{max}\, x_{g,j}; \quad j \in G$$

$$\text{subject to} \quad \sum_{j \in \mathbf{G}} \tilde{c}_j(P_{g,j}) \leq \sum_{j \in \mathbf{G}} \tilde{c}_j(P^{loc}_{g,j}) \tag{6.55a}$$

$$(6.40), \text{LIN-VOL} \tag{6.55b}$$

$$x^{min}_{g,j,iter} \leq x_{g,j} \leq x^{max}_{g,j,iter} \quad j \in \mathbf{G} \tag{6.55c}$$

4: $x^{lo}_{g,j} \longleftarrow (x^{min}_{g,j})^*$, $x^{up}_{g,j} \longleftarrow (x^{max}_{g,j})^*$

5: end while

6: **return** $x^{lo}_{g,j}, x^{up}_{g,j}$ (tightened bounds)

6.4.2.2 Reduced Spatial Branch-and-Bound

Second technique to improve STF relaxations is spatial branch-and-bound (SBB), a type of branch-and-bound method used for the global optimization of nonlinear programming, which branches in continuous rather than discrete variables [146]. The main idea of SBB is to divide the problem into smaller subproblems by branching the variables, which recursively define partitions of feasible set into two sets, and finding sequences of approximate solutions which converge to the actual solution. Since the bounds of variables is tightened during the branching process, the MC relaxation will become increasingly better. As an example, if the solver branches

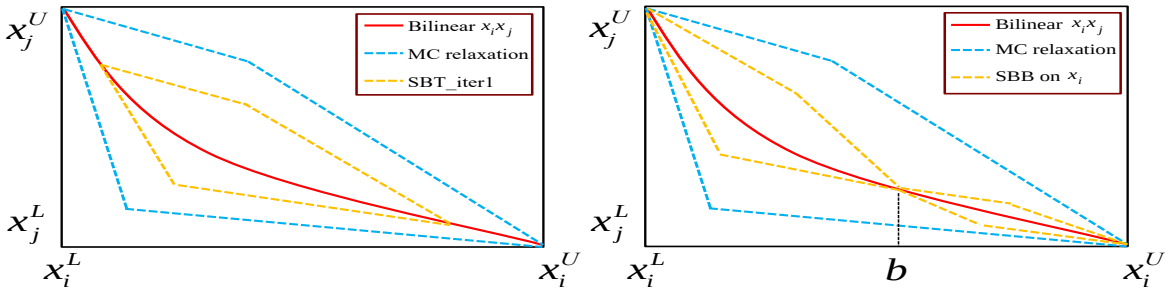

(a) Sequential bound tightening

(b) Spatial branch-and-bound

Figure 6.6: Conceptual feasible regions of bilinear term $x_i x_j$ based on SBT and SBB

on x_i at point b, two new nodes would be created with stronger relaxations. Conceptual feasible regions for bilinear terms based on SBT and SBB are shown in Figure 6.6.

However, explicit enumeration of all solutions is normally impossible due to the exponentially increasing number of potential solutions. Therefore, we propose reduced SBB (RSBB) for finding a near-global solution to improve STF relaxations, rather than finding a global solution. Based on the observation that we obtain a relaxation solution (infeasible solution) which mostly shows up as violations $\left(w_{1,i} \neq Y_i^d (V_i^m)^2 \text{ and } w_{2,i} \neq Y_i^q (V_i^m)^2\right)$ in power flow equations, the goal is to have $w_{1,i} = Y_i^d (V_i^m)^2$ and $w_{2,i} = Y_i^q (V_i^m)^2$ at all bus i as a near-global solution. Algorithm 2 describes the pseudocode of RSBB for finding a near-global solution.

6.5 Case Studies

In this section, we present empirical case studies to evaluate the proposed convex relaxation for Sparse Tableau Formulation of OPF problem. The STFY and STFI relaxation are evaluated on standard IEEE instances available from MATPOWER [23]. Problems are formulated in GAMS and the conic interior point solver MOSEK 8.0 [147] is used to solve STF relaxations (STFY and STFI). Nonlinear solver KNITRO is used to solve typical ACOPF problem. The test cases range from 14 buses to as many as 3000 buses, and included one additional RTS96 test system [90] that does not appear in the MATPOWER distribution.

Notice that we have discussed the importance of active power injection bound and some test cases (typically small test systems) have significantly larger values for the active power

Algorithm 2 Reduced spatial branch-and-bound

1: **Initialization:** Set the convergence tolerance TOL, the upper bound U from the original nonconvex problem (6.19), the lower bound L from the STFY relaxation (6.40) and relaxation solution $w_1^l, w_2^l, Y^{dl}, Y^{ql}, (V^{ml})$. SBT may be performed during this step.
2: **Choice of Region:** Choose a subregion of the problem to be explored. For the initial stage, a subregion is equal to a single region encompassing the set of all variables and their ranges. After the branching, the region with a larger lower bound is chosen. If needed, explore other regions.
3: **Check region:**
If $|w_{1,i}^l - Y_i^{dl}(V_i^{ml})^2|$ and $|w_{2,i}^l - Y_i^{ql}(V_i^{ml})^2| \le TOL$ for all i, then $w_1^l, w_2^l, Y^{dl}, Y^{ql}, (V^{ml})$ is a near-global solution. If not, the algorithm proceeds to the next step.
4: **Branching:** The region is split into two subregions. Bus i is selected as $i^* \leftarrow argmax_i\big(|w_{1,i}^l - Y_i^{dl}(V_i^{ml})^2|, |w_{2,i}^l - Y_i^{ql}(V_i^{ml})^2|\big)$. Then, depending on the location of i^*, active (d) or reactive (q) power flow equation, we branch on the variable $Y_{i^*}^{d/q}$ using $\{Y_{i^*,min}^{d/q} \le Y_{i^*}^{d/q} \le b\}$ and $\{b \le Y_{i^*}^{d/q} \le Y_{i^*,max}^{d/q}\}$ where b is the middle point of $Y_{i^*,min}$ and $Y_{i^*,max}$. Then, for each region, lower/upper bounds for $Y_{i^*}^{d/q}$ are appropriately replaced with b.
5: **Lower Bound and Pruning:** The (6.40) with each region is solved to give a lower bound l with solution $w_1^l, w_2^l, Y^{dl}, Y^{ql}, (V^{ml})$. If the region has $l > U$, it is discarded.
6: **Upper Bound:** The (6.19) with each region is solved to obtain a upper bound u. if $U > u$, set $U = u$ and go to step 2.

generation bound. This may be explained by the fact that some test cases were created for the purpose of only power flow, with the consequence that active power generation bounds are arbitrarily set up. For example, case14 bus system contains 0 value for minimum active power generation bound and this is very unrealistic. Therefore, each test case is conducted with two groups; 1) given bounds (GIVEN) for active power generation and 2) $\mathbf{G^{big}}$, subset of generator buses $\mathbf{G}$, 30% of generators are selected in descending order based on P^{max} with the physical justification that they might represent large-size, base load generators such as nuclear plants which often have narrow bounds. Thus, their active power generation bounds are adjusted to be narrow (NARROW) such that

$$\text{NARROW-1:} \qquad P_j^{AC}(1-0.05) \le P_{g,j} \le P_j^{AC}(1+0.05), \quad j \in \mathbf{G^{big}} \tag{6.56}$$

$$\text{NARROW-2:} \qquad P_j^{AC}(1-\mathbf{rampdown}_j) \le P_{g,j} \le P_j^{AC}(1+\mathbf{rampup}_j), \quad j \in \mathbf{G^{big}} \tag{6.57}$$

where P_j^{AC} is active power generation solution from the original ACOPF problem. NARROW-1 bounds the active power generation to be within 5% of P_j^{AC}. NARROW-2 bounds the active

power generation to be within ramp rates of P_j^{AC}, calculated by [148]. Different values of angle bound $\Delta\delta$ are considered for case studies. For example, case14(20) is case14 bus system with $\Delta\delta = 20$. Comparison is conducted with two separate categories, 1) different values of $\Delta\delta$ with (GIVEN) and 2) fixed $\Delta\delta = 20$ with (GIVEN) and (NARROW).

Relaxation gaps are used to evaluate the quality of various relaxations after a feasible solution from typical ACOPF and a relaxation solution are obtained. Relaxation gaps in this section are given as ratio:

$$\textbf{Gap(\%)} = \frac{local - relaxation}{local} * 100$$

where $local$ refers to the solution obtained by the nonlinear solvers on the ACOPF problem, and $relaxation$ refers to the lower bound produced by the various relaxations. Smaller ratio implies tighter relaxation solution (tighter lower bound for the original problem), and 0% indicates the local solution is actually a global solution.

6.5.1 Evaluation

This section evaluates established STF relaxations. SDP and QC relaxation are not considered due to their reliance on the Y_{bus} for OPF problem. Thus, three formulations are considered: 1) typical ACOPF, 2) STFY relaxation and 3) STFI relaxation. A selected subset of the results are presented in Tables 6.2-6.3. Notice that lines' thermal limits are imposed with apparent power for ACOPF and current magnitude for STF relaxations. A selected subset of the results are presented in Tables 6.2-6.3. For these test systems, it is important to recognize that small test systems (case14 and case300) have significantly larger bounds on active power generation P_g and P^{min} being 0 which is not realistic, while large test systems (case2736sp and case3375wp) including RTS96 have reasonable bounds on P_g.

Table 6.2 illustrates relaxation gap of STF relaxations with different values of $\Delta\delta$. It is easy to see that small $\Delta\delta$ values produce a small relaxation gap as expected from Figure 6.3. Notice that test cases of case14 and case300 exhibit a significant relaxation gap. In contrast to this, the remaining test cases of RTS96, case2736 and case3375 provide a relaxation gap of $<$ 30% and are not strongly dependent on the $\Delta\delta$ value. In particular, RTS96 obtains very strong

	ACOPF		STFY relaxation		STFI relaxation	
	Obj ($/h)	Time (sec)	Gap (%)	Time (sec)	Gap (%)	Time (sec)
case14 ($\Delta\delta$ = 20)	8081.51	0.3	56.14	0.3	67.33	0.3
case14 ($\Delta\delta$ = 25)	8081.51	0.3	61.20	0.3	84.52	0.3
case14 ($\Delta\delta$ = 30)	8081.51	0.3	66.72	0.3	99.76	0.3
RTS96 ($\Delta\delta$ = 20)	240444.08	0.4	2.03	0.4	2.27	0.4
RTS96 ($\Delta\delta$ = 25)	240444.08	0.4	2.03	0.4	2.27	0.4
RTS96 ($\Delta\delta$ = 30)	240444.08	0.4	2.03	0.4	2.27	0.4
case300 ($\Delta\delta$ = 20)	719721.13	0.4	63.91	0.7	79.75	0.6
case300 ($\Delta\delta$ = 25)	719721.13	0.4	70.48	0.7	95.91	0.6
case300 ($\Delta\delta$ = 30)	719721.13	0.4	76.49	0.7	99.8	0.4
case2736sp ($\Delta\delta$ = 20)	1307883.12	2.5	27.67	3.5	27.67	3
case2736sp ($\Delta\delta$ = 25)	1307883.12	2.5	27.67	3.5	27.67	3
case2736sp ($\Delta\delta$ = 30)	1307883.12	2.5	27.67	3.5	27.67	3
case3375wp ($\Delta\delta$ = 20)	7412030.67	11	13.40	12	13.40	18
case3375wp ($\Delta\delta$ = 25)	7412030.67	11	13.40	12	13.40	12
case3375wp ($\Delta\delta$ = 30)	7412030.67	11	13.40	13	13.40	12

Table 6.2: Comparison of STF relaxations with different $\Delta\delta$ values

relaxation solution. Reason is that small test systems (case14 and case300) have significantly larger bounds on active power generation P_g and P^{min} being 0 which is not realistic, while large test systems (case2736 and case3375) including RTS96 have reasonable bounds on P_g. This may be explained by the fact that those test cases (case14 and case300) were created for the purpose of only power flow, with the consequence that active power generation bounds are arbitrarily set up.

Table 6.3 illustrates the impact of bounds of P_g variable. We observe that test cases of RTS96, case2736sp and case3375wp have reasonably tight bounds for the P_g variable. This is especially true for RTS96, which was developed as a test system for assessing reliability. Thus, STF relaxations provide a strong relaxation solution for the RTS96, case2736sp, case3375wp

	ACOPF		STFY		STFI	
	Obj ($/h)	Time (sec)	Gap (%)	Time (sec)	Gap (%)	Time (sec)
case14 (GIVEN)	8081.51	0.3	56.14	0.3	67.33	0.3
case14 (NARROW-1)	8081.51	0.3	23.77	0.3	23.77	0.3
case14 (NARROW-2)	8081.51	0.3	20.26	0.3	23.77	0.3
RTS96 (GIVEN)	240444.08	0.4	2.03	0.4	2.27	0.4
RTS96 (NARROW-1)	234478.97	0.4	0.72	0.4	0.72	0.4
RTS96 (NARROW-2)	238532.98	0.4	0.55	0.4	0.55	0.4
case300 (GIVEN)	719721.13	0.4	63.91	0.7	79.75	0.6
case300 (NARROW-1)	719721.13	0.4	34.51	0.7	34.61	0.6
case300 (NARROW-2)	719721.13	0.4	33.82	0.7	33.91	0.4
case2736sp (GIVEN)	1307883.12	2.5	27.67	3.5	27.67	3
case2736sp (NARROW-1)	1290131.73	2.5	3.74	3.5	3.74	3
case2736sp (NARROW-2)	1304510.67	2.5	1.23	3.5	1.23	3
case3375wp (GIVEN)	7412030.67	11	13.40	12	13.40	18
case3375wp (NARROW-1)	7292990.02	11	3.46	12	3.46	12
case3375wp (NARROW-2)	7356810.91	11	2.20	25	2.20	13

Table 6.3: Comparison of STF relaxations with fixed $\Delta\delta = 20$

test systems. Significant improvement on the optimality gap is achieved with NARROW-1 and NARROW-2 for test cases of case14 and case300, that showed a large optimality gap previously. This is due to the reduced bound on the P_g variable. It is interesting to note that the computational time for STF relaxations is quite attractive, which are as fast as the original problem even in our preliminary, "less than optimized" implementations. STFY relaxation is slightly stronger, but slower than STFI relaxation.

6.5.2 Enhancement

Based on the results of previous section, this section employs SBT and RSBB techniques to enhance relaxation solution for case14 and case300 with unmodified bounds for active power generation, which show significant relaxation gap with basic STF relaxations. For this section,

0.001 of TOL is used for SBT and 0.035 of TOL is used for RSBB (smaller value of TOL could be used with minor improvement). The value of 20 is used for $\Delta\delta$ and resulting relaxation gap is shown in Table 6.4.

	STFY Relaxation Gap	
	Basic	SBT+RSBB
case14	56.14	6.1
case300	63.91	12.69

Table 6.4: STF relaxations with SBT and SBB

For both cases, we obtain stronger relaxation solution as a near global solution satisfying $w_{1,i} = Y_i^d (V_i^m)^2$ and $w_{2,i} = Y_i^q (V_i^m)^2$ for all bus i with minor violations in voltage magnitude limits.

6.5.3 Application

In the previous section, it is demonstrated that STF relaxations show the advantage in computational speed and strength under the condition that active power generation P_g has a narrow bound. This section examines a modification of the OPF problem that is typically very computationally challenging, but which may have features well-suited to STF relaxations.

APPLICATION 6.1. (Corrective SCOPF) The problem that STF relaxations are best suited might be the corrective SOPCF problem, which is expressed as follow:

$$\min_{x^c, u^c} \quad f^0(x^0, u^0) \tag{6.58}$$

subject to

$$g^c(x^c, u^c) = 0, \quad c = 0, 1, 2, ..., cc$$

$$h^c(x^c, u^c) \leq 0, \quad c = 0, 1, 2, ..., cc \tag{6.59}$$

$$|u^0 - u^c| \leq K^c, \quad c = 1, 2, ..., cc \tag{6.60}$$

Here, the amount of corrective control that can be adjusted is limited by an amount K^c and the pre-contingency control setting u^0. K^c is the maximum change for the post-contingency control variables and it could be calculated as a product of an assumed time horizon allowed for

corrective action T^c and assumed maximum rate of change of control variables in response to contingency $\frac{du^c}{dt}_{max}$, thus

$$K^c = T^c \frac{du^c}{dt}_{max} \tag{6.61}$$

For control variable $u^c = P_g$, maximum rate of change could be $\frac{du^c}{dt}_{max} = ramp\ rate$ which can be computed as before and is typically narrow. Thus, if we assume that u^0 is given by a solution from power flow or ACOPF or preventive SCOPF problem and seek to find a control adjustment to satisfy post-contingency constraints, STF relaxations can be used to solve the problem (6.60) and obtain a tight relaxation solution since a bound on P_g is very narrow. Further, lower bound for K^c that the system is secure can be determined by lowering the value of K^c from certain value until the problem becomes infeasible. In fact, if the size of the SCOPF problem becomes large exceeding the computer memory or speed requirement with many contingency constraints, one should use linearized or relaxed SCOPF problem [149].

6.5.4 Discussion

As previously noted, convex relaxation for AC optimal power flow is of great interest because of its ability to (often) obtain a global solution or sufficiently good solution. Many sophisticated and novel approaches for this convex relaxation are proposed and numerous further efforts are suggested to have a stronger relaxation solution for ACOPF problem. A vast majority of these approaches have been developed using the Y_{bus} matrix representation.

It is, however, important to consider other grid representation such as STF which also appears in [150], [151], [152] since grid sees rapid changes in its component technologies, operational objectives and computational tools. This chapter is the first attempt to find a convex envelope of ACOPF problem with more general grid representation using STF. Our test-based observations indicate that STF relaxations show satisfactory results for some test cases, but not for some other test cases. Then, by exploring its bilinear terms, SBT and RSBB are introduced to enhance STF relaxations. Significant improvement is made for small systems, but computational challenges remain for large systems. To this end, parallel computation can

be used for SBT and novel branching rules and the node priority would improve RSBB. Based on the numerical examples, several key points of STF relaxations are made as:

- STF relaxations show advantage in computational time, sometimes considerable and are comparable to original nonconvex problem since it has fewer nonlinear constraints needed to be relaxed. STFI relaxation is bit faster than STFY relaxation.
- STF relaxations shows strength under the condition in which narrow bounds for P_g variable are given. STFY relaxation is bit stronger than STFI relaxation.
- SBT and RSBB can be applied to enhance STF relaxations, but computational challenges remain for large systems.

Obviously, approaches presented here would not be the only way to find a convex envelope of STF for ACOPF. The fact that STF retains a much greater number of intermediate variables, and a much greater number of (but simpler) equations, compared to nodal analysis, suggests that it may offer many other opportunities for useful relaxations.

6.6 Conclusion

In this chapter, we have studied a convex relaxation for OPF that exploits the Sparse Tableau Formulation (STF) of network and component constraints. Two simple engineering-based relaxations of STF based on the node admittance and current are described. Methods to improve the quality of relaxation solution are discussed, exploiting (when available) bounds on bus voltage angles and active power generation. Numerical experiments showed that the computational time for STF relaxations is comparable with original problem due to the fewer nonlinear equations and STF relaxations provide a tight relaxation, displaying objective value within a few percent of local optima of the original problem, under the condition that reasonably tight bounds can be provided on generators' active power. Enhancement as finding a near global solution is described with SBT and RSBB.

There are several natural paths for further exploitation of STF in OPF. 1) Work here represents the first attempt to identify a useful convex relaxation enabled by STF. An alternative

and innovative technique to find a convex envelope of STF for ACOPF would be worthwhile. 2) As an immediate improvement to results here, analytical methods to assign an upper bound on voltage angles $\Delta\delta$ would be very valuable. 3) Tightening McCormick envelope using sequential and dynamic partition [145] would be also great interest since the critical source of nonconvexity for STF of OPF problem is bilinear constraints in terms of power balance equations.

CHAPTER 7

Advanced Modelling of DERs and UPFC devices with Sparse Tableau Formulation for ACOPF

7.1 Introduction

The growing trend towards deployment of distributed and renewable resources in the electric grid clearly impacts decision problems in grid optimization. Historically, the primary decision variables impacting operational cost and reliability were associated with large, central station synchronous generators. Technological trends suggest these variables will need to be expanded to include decisions relating to the distributed energy resources (DERs) [153], [154]. However, the deployment of DERs at the distribution level also suggests that other elements may enter the optimization model, such as the substation configurations at DER interconnection points. Moreover, because many of the distributed resources are wind or solar, their output is often stochastic, following patterns of wind speed or solar isolation. These properties increase the variability and uncertainty of power flows, and change how the electric grids are designed, controlled and protected [155]. For example, with the typical configuration of distribution system networks (high resistance to reactance ratio), voltage magnitudes are sensitive to real

power injections of DERs and high penetration of DERs could cause voltage rise issues [156] that impact the system up to the transmission level. As a result, careful consideration of DERs in optimal operation of the transmission network is required.

In addition, it is often valuable to enhance power flow capability and controllability within transmission network to support more DERs. Flexible AC Transmission System (FACTS) devices offer an attractive mechanism to achieve this [157], [83], while also helping to improve voltage/system stability. The Unified Power Flow Controller (UPFC) provides an example of a particularly versatile FACTS device [158], with its ability to control both the real and reactive power flow through, and the voltage across, a transmission line. As more DERs are deployed, these network control capabilities will likely become more valuable, and motivating this chapter's study of optimization tools to facilitate deployment of DERs with FACTS devices.

For steady-state analysis such as power flow (PF) and optimal power flow (OPF), the majority of existing modeling approaches formulate network equations via the bus admittance matrix Y_{bus}, based on a strict nodal analysis [9]. However, from a circuit standpoint, strict nodal analysis disallows many standard circuit elements such as circuit breakers and branch voltage sources, because it requires that each element current(s) be expressible as a function of its voltage(s). These limitations would impede accurate representation of network elements such as UPFC that can be accurately represented as the series voltage source, together with the real power coupling to the sending-end bus [159], [160], [161]. Moreover, in most existing transmission planning studies, DERs are netted with the distribution system load at the transmission level (DERs are treated as negative load). However, for high penetration of DERs scenarios, netting of DERs with loads at the substation is not recommended [155]; rather, they should be modeled in fashion reflecting their dynamic characteristics and steady-state output. This is a very vast literature, but some research works to formulate OPF with DERs as decision variables include [162], [163], [164]. In particular, [163], [164] formulate OPF as semi-definite programming based on nodal analysis (Y_{bus}). In [154], the author formulates OPF and analyses the impact of DERs on electricity markets with detailed representation of distribution networks.

Detailed representation of substation configurations, as part of accurate modeling for

high penetration of DERs, presents a challenge to simple nodal analysis and Y_{bus} based representations. For example, there is growing recognition of the importance of node-breaker representations [11], [12] to allow representation of circuit breakers in substations. Because nodal analysis is unable to directly represent a circuit breaker as a network branch element, one widely adopted work-around for power flow studies is that of "topology processing." Oversimplifying slightly, topology processing merges or separates buses based on breaker configuration, and constructs a distinct (and possibly differently-dimensioned) Y_{bus} for each case. In many applications, topology processing has been viewed as too cumbersome for incorporation into OPF studies. If one did wish to keep standard Y_{bus} based OPF formulations, this approach would carry with it cumbersome data conversions and verification of each possible breaker configuration of interest. Note that the number of possible configurations grows exponentially with the number of breakers considered. This chapter pursues an alternate modeling philosophy, in which circuit breakers are directly modeled as network elements, with an open or closed position a binary parameter associated with that one individual element. The approach here will not change the network topology for each breaker position change, but rather change only one parameter within one network element.

Using this modeling philosophy, this chapter seeks to develop advanced modeling of power system networks for the accurate representation of substations with high penetration of DERs based on the node-breaker model and UPFC devices to appropriately study their impact. We employ the previously described Sparse Tableau Formulation (STF) from Chapter 3, which provides a very general circuit modeling approach. STF facilitates model construction that is versatile, accurately representing network elements such as circuit breakers (important for representation of substations with DERs) and ideal voltage sources (important for representation of UPFCs). This novel modeling method is applied to solve ACOPF that include DERs and UPFCs, and the impacts of these devices (and the new decision classes of variables they introduce) are analyzed in case studies.

The organization of this chapter is as follow. Section 7.2 reviews STF for standard power system networks. Section 7.3 describes STF for modeling of DERs based on the node-breaker

model and UPFC devices. Then, it is applied to formulate OPF problems. Numerical case studies are presented in Section 7.4, and the conclusions are drawn in Section 7.5.

7.2 Background: Sparse Tableau Formulation

This section briefly reviews the previously introduced STF, and demonstrates the versatility of STF for representing network elements, offering different modeling approaches while being computationally efficient. With variables v, i, V, I (port voltage/current and bus voltage/current), parameters $F_v, F_i, A, \mathbf{I}$ (network element matrices, node-to-element incidence matrix and appropriate dimension of identity matrix), STF for standard power system networks is expressed as

$$\begin{bmatrix} \mathbf{0} & \mathbf{0} & A \\ -A^T & \mathbf{I} & \mathbf{0} \\ \mathbf{0} & F_v & F_i \end{bmatrix} \begin{bmatrix} V \\ v \\ i \end{bmatrix} = \begin{bmatrix} I \\ 0 \\ 0 \end{bmatrix} \tag{7.1}$$

Notice that the equation (7.1) is a general modeling approach for grid element models and network representations. Note also that treatment of power nonlinearity is saved for a subsequent step, because (7.1) treats only linear voltage/current relations. Elements such as circuit breakers and ideal voltage sources can be accurately modeled with STF. To facilitate STF, consider standard power grid elements (transmission line and transformer), whose per phase, positive sequence behavior can be represented as two-port element shown in Figure 7.1.

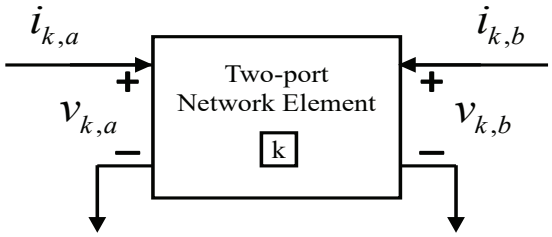

Figure 7.1: Two-port representation for network elements

In this context, port a quantities are typically “sending end” positive sequence voltage and current, and port b quantities are “receiving end.” Then, the linear element equations for each

individual network element k can be expressed as i) linear element equation for transmission line k:

$$\underbrace{\begin{bmatrix} 1 & -(1+\frac{ZY}{2}) \\ 0 & -Y(1+\frac{ZY}{4}) \end{bmatrix}}_{\mathbf{F}_{k,v}} \begin{bmatrix} v_{k,a} \\ v_{k,b} \end{bmatrix} + \underbrace{\begin{bmatrix} 0 & Z \\ 1 & (1+\frac{ZY}{2}) \end{bmatrix}}_{\mathbf{F}_{k,i}} \begin{bmatrix} i_{k,a} \\ i_{k,b} \end{bmatrix} = \begin{bmatrix} 0 \\ 0 \end{bmatrix}$$

where Z, Y are impedance and shunt parameters for line k; or ii) linear element equation for ideal transformer k:

$$\underbrace{\begin{bmatrix} 1 & -n \\ 0 & 0 \end{bmatrix}}_{\mathbf{F}_{k,v}} \begin{bmatrix} v_{k,a} \\ v_{k,b} \end{bmatrix} + \underbrace{\begin{bmatrix} 0 & 0 \\ 1 & \frac{1}{n^*} \end{bmatrix}}_{\mathbf{F}_{k,i}} \begin{bmatrix} i_{k,a} \\ i_{k,b} \end{bmatrix} = \begin{bmatrix} 0 \\ 0 \end{bmatrix}$$

where n is complex turns ratio for transformer k.

Remaining constraints are simple linear expressions imposing KVL and KCL interconnection constraints. Since a node-to-element incident matrix $A \in \mathbb{R}^{nb \times 2nk}$ is formulated to include all network elements and nodes, we need to organize all network element variables (port voltages and port currents) as

$$v \triangleq \begin{bmatrix} v_{1,a} & v_{1,b} & \cdots & v_{nk,a} & v_{nk,b} \end{bmatrix}^T$$
$$i \triangleq \begin{bmatrix} i_{1,a} & i_{1,b} & \cdots & i_{nk,a} & i_{nk,b} \end{bmatrix}^T$$

Notice that $[\cdot]^T$ is the transpose operator; nb is number of buses and nk is number of network elements. Thus, $v, i \in \mathbb{C}^{2nk}$, and goal of KCL is to efficiently assemble the right-hand side of the general current balance equation. The incidence matrix is composed entirely of values of 1 or -1 or 0. In keeping with standard textbook presentations, we define:

$$A(j,r) \triangleq \begin{cases} 1/-1, & \text{if } r\text{th component of } i \text{ corresponds to an} \\ & \text{elements' sending or receiving terminal} \\ & \text{leaving/entering node } j \\ \hline 0, & \text{otherwise} \end{cases} \tag{7.2}$$

Therefore, the current conservation law of KCL is written simply as $Ai = I$ where $I \in \mathbb{C}^{nb}$ is the nodal complex current injection from generators or loads; i is the complex branch current carried away from node by network elements. We can also use A to relate port voltages to bus voltages in a manner that guarantees KVL is automatically satisfied. The linear constraints of KVL are written as $v - A^T V = 0$ where $V \in \mathbb{C}^{nb}$ denotes bus voltages. KVL equation serves to assign the correct bus voltage to any port voltage of a port connected to that bus. Now, to assemble the sparse tableau matrix (7.1), $F_v \in \mathbb{C}^{2nk \times 2nk}$ and $F_i \in \mathbb{C}^{2nk \times 2nk}$ can be constructed in block diagonal form as

$$F_v = \begin{bmatrix} F_{1,v} & 0 & \cdots & 0 \\ 0 & F_{2,v} & 0 & : \\ : & : & \ddots & 0 \\ 0 & \cdots & \cdots & F_{nk,v} \end{bmatrix}, F_i = \begin{bmatrix} F_{1,i} & 0 & \cdots & 0 \\ 0 & F_{2,i} & 0 & : \\ : & : & \ddots & 0 \\ 0 & \cdots & \cdots & F_{nk,i} \end{bmatrix} \tag{7.3}$$

Finally, with matrices F_v, F_i, A and variables v, i, V, I as defined above, we have the STF description of the power network consistent with (7.1).

The remaining step to capture the power flow equations requires specification of the current source elements I. The approach here introduces a special class of nonlinear one-port element to accommodate standard generator and load models as represented in the power flow. The nonlinear element equation for current source I_j for bus j can be defined by

$$f_j(v_j, i_j) = 0 \triangleq i_j = \frac{(S_{g,j} - S_{d,j})^*}{v_j^*} \tag{7.4}$$

For simplicity, the element index j is assumed to be the same as the index of bus to which it connects. With this choice, $S_j = S_{g,j} - S_{d,j}$, $i_j = I_j$, and $v_j = V_j$ implying

$$\Longrightarrow I_j - \frac{S_j^*}{V_j^*} = 0 \tag{7.5}$$

where $S_{g,j}$ and $S_{d,j}$ are specified apparent power generation and load at bus j. Notice that for nonzero v_j equation (7.5) is equivalent to $S_j = V_j (I_j)^*$, which is the typical "power balance equation."

7.3 Advanced Modeling of Power System Networks with STF

This section describes the advanced modeling of power system networks for detailed representation of substations with high penetration of DERs and UPFC devices with STF. Modeling of detailed representation of substations represents distribution network information including circuit breakers based on the node-breaker model. Modeling of UPFC devices will employ ideal complex voltage sources.

7.3.1 Modeling of Distributed Energy Resources

In most existing power system network planning studies, the distribution system load is aggregated at the transmission buses and netted with generation on the distribution system (i.e., DER generation is treated as negative load). However, there is growing recognition of the benefit of modeling DERs to reflect their dynamic characteristics and steady-state output in study cases where a deeper penetration of DERs is expected to influence power flows between the transmission and distribution system [165].

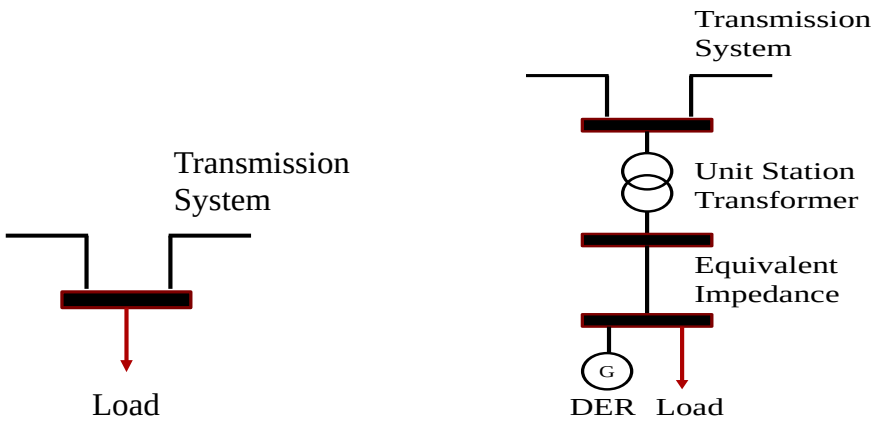

(a) Typical load flow

(b) Recommended load flow

Figure 7.2: Western Electricity Coordinating Council (WECC) recommended power flow model

Figure 7.2 shows the load model for both typical load flow model and recommended load flow model for study of high penetration DERs scenarios from [155]. As is depicted, the recommended load flow model contains distribution network information, which includes equivalent impedance

(EI) for collector systems and the unit station transformer (UST) from the collector system at the interconnection point. This detailed representation of the substation allows accurate analysis of distribution network's impact. However, this recommended model is based on the bus-branch model, which has consolidated circuit breaker information. Since the purpose of detailed representation of substation is to capture its impact with DERs on power system networks, we would assert that consideration of different circuit breaker position in substations is important to accurately analyze its impact with DERs on power system networks. In particular, we are interested in the node-breaker model to represent circuit breaker action that results in bus splits and bus mergers.

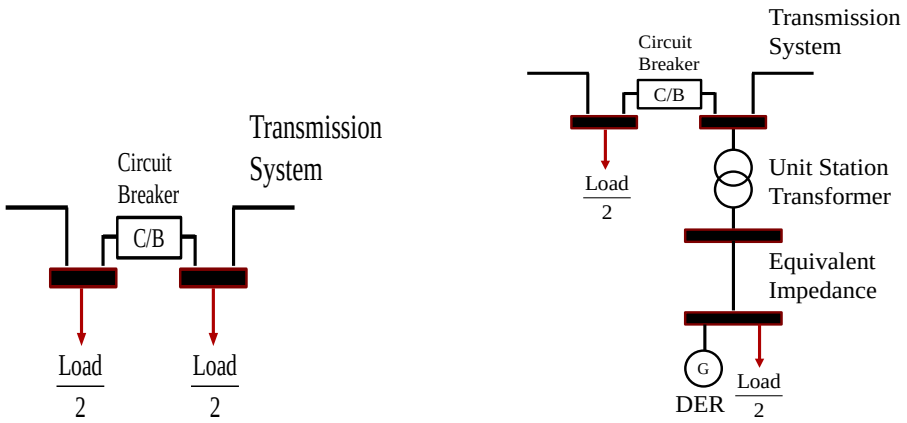

(a) Typical load flow with node-breaker model

(b) Recommended load flow with the node-breaker model

Figure 7.3: WECC Recommended power flow model with the node-breaker model

Consider the load flow model with the node-breaker representation in Figure 7.3. The circuit breaker (C/B) for bus split and bus merger is included at the substation to be expanded to include distribution network information. When C/B is closed (bus merger), the load flow model in Figure 7.2 is equivalent to the model in Figure 7.3. When C/B is open (bus split), they are different and the nodal analysis (Y_{bus}) necessitates topology processing which requires differently dimensioned Y_{bus} to describe the bus split.

7.3.1.1 Modeling of circuit breakers

To model C/Bs with STF, consider the circuit representation of a C/B with binary integer parameter γ indicating switch position.

$$\text{Circuit breaker closed } (\gamma = 1) \Rightarrow v_a - v_b = 0, i_a + i_b = 0$$

$$\Longrightarrow \begin{bmatrix} 1 & -1 \\ 0 & 0 \end{bmatrix} \begin{bmatrix} v_a \\ v_b \end{bmatrix} + \begin{bmatrix} 0 & 0 \\ 1 & 1 \end{bmatrix} \begin{bmatrix} i_a \\ i_b \end{bmatrix} = \begin{bmatrix} 0 \\ 0 \end{bmatrix}$$

$$\text{Circuit breaker open } (\gamma = 0) \Rightarrow i_a = 0, i_b = 0$$

$$\Longrightarrow \begin{bmatrix} 0 & 0 \\ 0 & 0 \end{bmatrix} \begin{bmatrix} v_a \\ v_b \end{bmatrix} + \begin{bmatrix} 1 & 0 \\ 0 & 1 \end{bmatrix} \begin{bmatrix} i_a \\ i_b \end{bmatrix} = \begin{bmatrix} 0 \\ 0 \end{bmatrix}$$

Therefore, linear element equation for network element of C/B k with the binary integer parameter γ is

$$\underbrace{\begin{bmatrix} \gamma & -\gamma \\ 0 & 0 \end{bmatrix}}_{\mathbf{F}_{k,v}} \begin{bmatrix} v_{k,a} \\ v_{k,b} \end{bmatrix} + \underbrace{\begin{bmatrix} (1-\gamma) & 0 \\ \gamma & 1 \end{bmatrix}}_{\mathbf{F}_{k,i}} \begin{bmatrix} i_{k,a} \\ i_{k,b} \end{bmatrix} = \begin{bmatrix} 0 \\ 0 \end{bmatrix} \tag{7.6}$$

with $\gamma = 1$ for C/B closed and $\gamma = 0$ for C/B open.

7.3.1.2 Modeling of unit station transformer and equivalent impedance

UST represents the majority of the impedance between the interconnection point and collector system. Standard data includes transformer terminal voltage, MVA ratings, percent impedance on the transformer's self-cooled MVA base, and X/R ratio. Positive-sequence normalized impedance for these types of transformers is in the range of 7 to 10%, with X/R ratio in the range of 40 to 50 [166]. In this chapter, 200 MVA base is used for the UST, which is twice the 100 MVA of system base.

Collector systems consist of relatively long medium voltage feeders/laterals. In spite of the higher cost, land use agreements usually prefer the use of underground feeders, with equivalent collector system having X/R ratios that are low, and line susceptance high, compared

to typical overhead lines. The equivalent impedance EI for collector system also tends to be small compared to the UST impedance, but is not insignificant. In this work, sample EI parameters of collector system in [166] are used, but a simple method developed by NREL [167] can be used to derive EI and susceptance when more detailed data is available. This chapter focuses on the example of a wind power plant (WPP) as a representative DER, but if desired, suggestions for a photovoltaic plant can be found in [168].

7.3.2 Modeling of UPFC

This section details the modeling of a UPFC via STF based on [159], [160], [161]. A UPFC consists of two switching converters (connected by a common DC link) based on gate-turn off (GTO) valves, which is shown schematically between bus m and n in Figure 7.4. The two converters are connected by a common DC link.

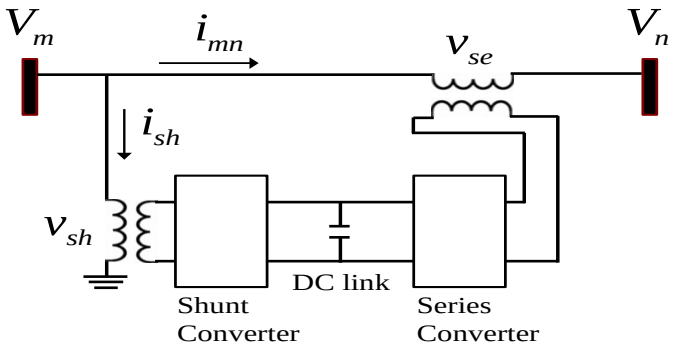

Figure 7.4: UPFC schematic diagram

The series converter is coupled to a transmission line via a series transformer, and its output voltage v_{se} in series with the line acts as a controllable AC voltage source. The series voltage source v_{se} can be used for direct voltage control, series compensation, and phase-shift. The current flowing through the series voltage source v_{se} is transmission line current and generally results in reactive and real power exchange. In order to represent UPFC properly, the v_{se} is stipulated to generate only the reactive power it exchanges with the line. Thus, the real power it exchanges with the line has to be supplied by the shunt converter as if a perfect coupling for real power flow between it and the shunt converter existed.

The shunt converter is connected to the AC power system via a shunt-connected transformer and its primary use is to provide the real power demand of the series converter at the DC link terminal from the AC power system. Since the shunt converter can also generator or absorb reactive power independently of the real power, with proper controls, it can also provide reactive power compensation for the transmission line, in a manner similar to an advanced static VAr compensator. It can thus achieve indirect voltage regulation at the input terminal of UPFC. In this work, it is assumed for clarity that the shunt reactive compensation is not utilized, indicating that the shunt converter of UPFC operates at unity power factor. The real and reactive power exchange between the shunt converter and the AC system voltage are governed by the voltage difference between the shunt converter and the AC system voltage. The voltage difference is determined mostly by the leakage impedance of the shunt-connected transformer with controlled current from the line; this is typically not more than ±15% of the nominal system voltage. Thus, the AC voltage of shunt converter with a maximum/minimum magnitude that is about ±15% of that AC system voltage is used for this work. With these assumptions, the series voltage source, together with the real power coupling to the shunt voltage source representing the voltage of shunt converter as shown in Figure 7.5, is an accurate representation of UPFC.

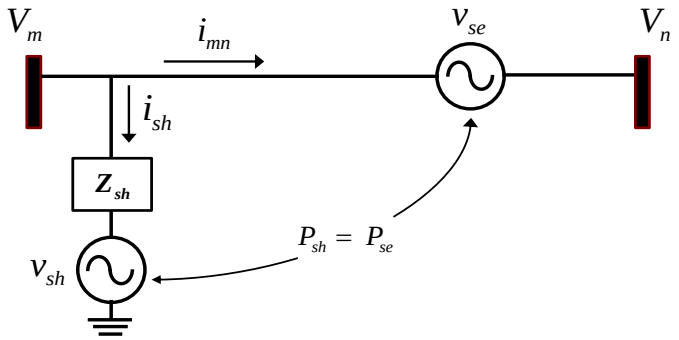

Figure 7.5: UPFC equivalent circuit

In Figure 7.5, the phasors v_{se} and v_{sh} represent the equivalent injected series voltage and shunt voltage sources respectively. Z_{sh} is UPFC shunt coupling transformer impedance which creates the voltage difference between V_m and v_{sh}. The series voltage source v_{se} is controllable voltage with magnitude ($0 \leq |v_{se}| \leq 0.5\, p.u.$) and angle ($0 \leq \delta_{se} \leq 2\pi$), and the shunt

voltage source v_{sh} represents the voltage of shunt converter which contains voltage difference caused by the leakage impedance of the shunt-connected transformer with controllable current i_{sh}. Its typical operational range includes magnitude ($0.85|V_m| \leq |v_{sh}| \leq 1.15|V_m|$) and angle ($0 \leq \delta_{sh} \leq 2\pi$). The real power coupling represents the operational condition that real power exchange P_{se} of the series converter should be equal to the real power exchange P_{sh} of the shunt converter, implying the system needs to be able to generate the power demanded by the series converter.

The majority of existing works model the UPFC through a nodal analysis (Y_{bus}) that is compatible with traditional power flow and optimal power flow studies. To deal with an ideal series voltage source which is not directly representable in nodal analysis, various work-arounds [169],[170],[171] have been proposed: a Voltage Source Model (VSM), a Power Injection Model (PIM), a Shunt Admittance Model (SAM). VSM would be an accurate representation for UPFC, but the symmetric property of Y_{bus} is lost in this approach. PIM and SAM are proposed to eliminate this drawback, but necessitate complex manipulations and disallows direct monitoring of physically meaningful UPFC variables in the modeling and solution approaches. In addition, since Y_{bus} is unable to represent an ideal series voltage source, all three methods require inclusion of the very small leakage impedance of the series-connected transformer. Such very low impedance branches can cause ill-conditioning of Y_{bus} [54], [55].

As an alternative, we employ STF to accurately describe the ideal series voltage source without introducing the negligibly small leakage impedance of the series-connected transformer, nor complicated manipulations to maintain desirable symmetry properties. Consider the two-port representation of a UPFC element u installed on the terminal bus m of transmission line between bus m and bus n, as depicted in Figure 7.6.

Note that se/sh stand for series and shunt voltage source for UPFC respectively. For example, $i_{u,a}^{se/sh}$ is port current for the series/shunt voltage source of UPFC element u at port a. Two additional buses are introduced: $V_{u,se} = V_m + v_{u,se}$ for the series voltage source and $V_{u,sh}$ for the shunt voltage source. The transmission line sees "$V_m + v_{u,se}$" as the effective sending-end voltage. Thus, it is clear that UPFC affects the voltage (both its magnitude and angle) across

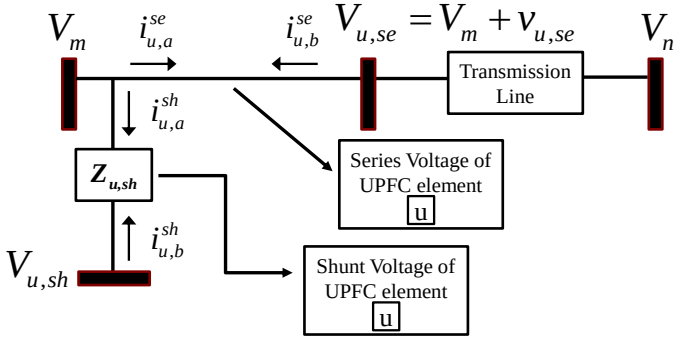

Figure 7.6: Two-port representation of UPFC element u

the transmission line and therefore it is able to control the transmittable real power as well as the reactive power demand of the line. Real and reactive power of the bus $V_{u,sh}$ can be used for real power coupling constraints and shunt reactive compensation. The lossless line with sending-end voltage V_m and receiving-end voltage $V_{u,se}$ is for the series voltage source, and the line having $Z_{u,sh}$ with sending-end voltage V_m and receiving-end voltage $V_{u,sh}$ is for the shunt voltage source. To derive linear element equations for UPFC u, we first consider two algebraic constraints to describe the behavior of ideal series voltage source.

Series voltage source $\Rightarrow v^{se}_{u,b} = v^{se}_{u,a} + v_{u,se}, i^{se}_{u,a} + i^{se}_{u,b} = 0$

$$\underbrace{\begin{bmatrix} -1 & 1 \\ 0 & 0 \end{bmatrix}}_{\mathbf{F}^{se}_{u,v}} \begin{bmatrix} v^{se}_{u,a} \\ v^{se}_{u,b} \end{bmatrix} + \underbrace{\begin{bmatrix} 0 & 0 \\ 1 & 1 \end{bmatrix}}_{\mathbf{F}^{se}_{u,i}} \begin{bmatrix} i^{se}_{u,a} \\ i^{se}_{u,b} \end{bmatrix} = \begin{bmatrix} v_{u,se} \\ 0 \end{bmatrix}$$

where $V_m = v^{se}_{u,a}, V_{u,se} = v^{se}_{u,b}$.

Next, linear element equation for transmission line with only impedance of $Z_{u,sh}$ can be used for the shunt voltage source.

$$\underbrace{\begin{bmatrix} 1 & -1 \\ 0 & 0 \end{bmatrix}}_{\mathbf{F}^{sh}_{u,v}} \begin{bmatrix} v^{sh}_{u,a} \\ v^{sh}_{u,b} \end{bmatrix} + \underbrace{\begin{bmatrix} 0 & Z_{u,sh} \\ 1 & 1 \end{bmatrix}}_{\mathbf{F}^{sh}_{u,i}} \begin{bmatrix} i^{sh}_{u,a} \\ i^{sh}_{u,b} \end{bmatrix} = \begin{bmatrix} 0 \\ 0 \end{bmatrix}$$

where $V_m = v^{sh}_{u,a}, V_{u,sh} = v^{sh}_{u,b}$.

Thus, to facilitate STF for both standard network elements (transmission line, transformer and circuit breaker) and UPFC elements (series/shunt voltage sources), we expand the port

voltage and current variable sets as:

$$v \triangleq \begin{bmatrix} v_{1,a} \\ v_{1,b} \\ \vdots \\ v_{nk,a} \\ v_{nk,b} \\ \hline v^{se}_{1,a} \\ v^{se}_{1,b} \\ v^{sh}_{1,a} \\ v^{sh}_{1,b} \\ \vdots \\ v^{se}_{nu,a} \\ v^{se}_{nu,b} \\ v^{sh}_{nu,a} \\ v^{sh}_{nu,b} \end{bmatrix} \begin{matrix} \left.\begin{matrix} \\ \\ \\ \\ \end{matrix}\right\} v_s \\ \\ \left.\begin{matrix} \\ \\ \\ \\ \\ \\ \\ \\ \\ \end{matrix}\right\} v_u \end{matrix}, \quad i \triangleq \begin{bmatrix} i_{1,a} \\ i_{1,b} \\ \vdots \\ i_{nk,a} \\ i_{nk,b} \\ \hline i^{se}_{1,a} \\ i^{se}_{1,b} \\ i^{sh}_{1,a} \\ i^{sh}_{1,b} \\ \vdots \\ i^{se}_{nu,a} \\ i^{se}_{nu,b} \\ i^{sh}_{nu,a} \\ i^{sh}_{nu,b} \end{bmatrix} \begin{matrix} \left.\begin{matrix} \\ \\ \\ \\ \end{matrix}\right\} i_s \\ \\ \left.\begin{matrix} \\ \\ \\ \\ \\ \\ \\ \\ \\ \end{matrix}\right\} i_u \end{matrix}$$

where nu is number of UPFC elements.

Note that $v_s, i_s \in \mathbb{C}^{2nk}$ contain port variables for standard network elements and $v_u, i_u \in \mathbb{C}^{4nu}$ contain port variables for UPFC elements, resulting in $v, i \in \mathbb{C}^{2nk+4nu}$. Similarly, we can redefine bus voltage and current variable as

$$V \triangleq \begin{bmatrix} V_1 \\ \vdots \\ V_{nb} \\ \hline V_{1,se} \\ V_{1,sh} \\ \vdots \\ V_{nu,se} \\ V_{nu,sh} \end{bmatrix} \begin{matrix} \left.\begin{matrix} \\ \\ \\ \end{matrix}\right\} V_s \\ \\ \left.\begin{matrix} \\ \\ \\ \\ \\ \\ \end{matrix}\right\} V_u \end{matrix}, \quad I \triangleq \begin{bmatrix} I_1 \\ \vdots \\ I_{nb} \\ \hline I_{1,se} \\ I_{1,sh} \\ \vdots \\ I_{nu,se} \\ I_{nu,sh} \end{bmatrix} \begin{matrix} \left.\begin{matrix} \\ \\ \\ \end{matrix}\right\} I_s \\ \\ \left.\begin{matrix} \\ \\ \\ \\ \\ \\ \end{matrix}\right\} I_u \end{matrix}$$

Note that V_s and I_s contain bus variables for original buses of the system and V_u and I_u contain bus variables for additional buses introduced with UPFC elements. The same rule (7.2) for the node-to-element incident matrix A is used to impose KVL and KCL constraints. Then, we redefine linear element matrices $F_v = blkdiag\{F_v^s, F_v^u\} \in \mathbb{C}^{(2nk+4nu)\times(2nk+4nu)}$ and $F_i = blkdiag\{F_i^s, F_i^u\} \in \mathbb{C}^{(2nk+4nu)\times(2nk+4nu)}$ where $blkdiag$ is MATLAB operator creating a block diagonal matrix. Matrices F_v^s, $F_i^s \in \mathbb{C}^{2nk\times 2nk}$ and F_v^u, $F_i^u \in \mathbb{C}^{4nu\times 4nu}$ are again defined as block diagonal matrices that $F_v^s = blkdiag\{F_{1,v}, ..., F_{nk,v}\} \in \mathbb{C}^{2nk\times 2nk}$, $F_i^s = blkdiag\{F_{1,i}, ..., F_{nk,i}\} \in \mathbb{C}^{2nk\times 2nk}$, $F_v^u = blkdiag\{F_{1,v}^{se}, F_{1,v}^{sh}, ..., F_{nu,v}^{se}, F_{nu,v}^{sh}\} \in \mathbb{C}^{4nu\times 4nu}$ and $F_i^u = blkdiag\{F_{1,i}^{se}, F_{1,i}^{sh}, ..., F_{nu,i}^{se}, F_{nu,i}^{sh}\} \in \mathbb{C}^{4nu\times 4nu}$. Finally, we can redefine the right-hand side of linear element equations representing independent source as $0_{is} = [0_s, 0_u]^T \in \mathbb{C}^{2nk+4nu}$ with 0_s and 0_u, defined as

$$0_s \triangleq \Big[0_1, 0, \quad \cdots \quad, 0_{nk}, 0\Big]^T \in \mathbb{C}^{2nk}$$
$$0_u \triangleq \Big[v_{1,se}, 0, 0, 0, \quad \cdots \quad, v_{nu,se}, 0, 0, 0\Big]^T \in \mathbb{C}^{4nu}$$

With this organization of variables and parameters, we have STF which contains KVL ($v - A^T V = 0$), KCL ($Ai = I$) and linear element equations ($F_v + F_i = 0_{is}$) for both standard network elements and the UPFC elements of the power system network. For power flow and optimal power flow studies, we need to capture power balance equations. For original buses j, nonlinear element equations keep their form of $S_j - V_j(I_j)^*$=0. For additional buses j due to the series voltage source of UPFC u, nonlinear equation $V_j(I_j)^* = 0$ is used since there is no generation nor demand at these buses. For additional buses j due to the shunt voltage source of UPFC u, nonlinear equations $-real(V_j(I_j)^*) = real(v_{u,se}(i_{u,a}^{se})^*)$, $imag(V_j(I_j)^*) = 0$. These impose real power energy coupling constraints and unity power factor of shunt reactive compensation.

7.3.3 ACOPF formulation

For optimal power flow studies, the equivalent WPP should be represented as a standard generator. Based on the guidelines [166], for real power level, it is often reasonable to represent a WPP or group of WPPs either off-line or maximum power output during the time frame of

interest. For reactive power capability, many WPPs are capable of operating over a power factor range of 0.95 lagging (generating reactive power) to 0.95 leading (absorbing reacting power) at full active power output [166], [172]. Real and reactive power outputs of WPPs constrained by real power limits (7.7) that reflect wind curtailment are expected to grow in importance with more DERs [127]. If one also introduces power factors limits (7.8), one has:

$$0 \le P_w \le P_w^{max} \tag{7.7}$$

$$Q_w^2 (PF)^2 \le P_w^2 - P_w^2 (PF)^2 \tag{7.8}$$

where PF is power factor 0.95 for WPP; P_w and Q_w are real power and reactive power output of WPP w respectively.

Then, given a connected power system with $\mathbf{N} = \{1, ..., nb\}$ denoting the set of all original buses, $\mathbf{U} = \{1, ..., nu\}$ set of all UPFC elements, $\mathbf{G}$ the set of all generators, $\mathbf{W}$ the set of all WPP, and $\mathbf{L}$ set of all transmission line, one can define sets $\mathbf{N_{se}} = \{nb+1, nb+3, ..., nb+2nu-3, nb+2nu-1\}$ the set of all additional buses due to the series voltage source of UPFC and $\mathbf{N_{sh}} = \{nb+2, nb+4, ..., nb+2nu-2, nb+2nu\}$ the set of all additional buses due to the shunt voltage source of UPFC. With net complex power injection at each bus j, $S_j = P_j + \mathbf{j}Q_j$ where $P_j = P_{g,j} + P_{w,j} - P_{d,j}$ and $Q_j = Q_{g,j} + Q_{w,j} - Q_{d,j}$, a representative OPF problem with STF including both modeling of DERs and UPFC devices takes the following form:

$$\min_{P,Q,v,i,V,I,v_{se}} \quad \sum_{j \in \mathbf{G}} \tilde{c}_j \left(P_{g,j}\right) \quad \text{subject to}$$

$$F_v v + F_i i = 0_{is}, I - Ai = 0, v - A^T V = 0 \tag{7.9a}$$

$$S_j - V_j (I_j)^* = 0; \quad \forall j \in \mathbf{N} \tag{7.9b}$$

$$V_j (I_j)^* = 0; \quad \forall j \in \mathbf{N_{se}} \tag{7.9c}$$

$$real(V_j (I_j)^*) = -real(v_{u,se} (i_{u,a}^{se})^*),$$
$$imag(V_j (I_j)^*) = 0; \quad \forall j \in \mathbf{N_{sh}}, u = \frac{j - nb}{2} \tag{7.9d}$$

$$P_g^{min} \le P_g \le P_g^{max}, Q_g^{min} \le Q_g \le Q_g^{max}; \quad \forall g \in \mathbf{G} \tag{7.9e}$$

$$P_w^{min} \le P_w \le P_w^{max}$$

$$Q_w^2(PF)^2 \leq P_w^2 - P_w^2(PF)^2; \quad \forall w \in \mathbf{W} \tag{7.9f}$$

$$V_j^{min} \leq |V_j| \leq V_j^{max}; \quad \forall j \in \mathbf{N} \tag{7.9g}$$

$$0 \leq |v_{u,se}| \leq 0.5; \quad \forall u \in \mathbf{U} \tag{7.9h}$$

$$0.85|V_m^j| \leq |V_{j,sh}| \leq 1.15|V_m^j|; \quad \forall j \in \mathbf{N_{sh}}, \forall m \in \mathbf{N} \tag{7.9i}$$

$$|i_{k,a/b}| \leq i_k^{max}; \quad \forall k \in \mathbf{L} \tag{7.9j}$$

where $|V_m^j|$ is the voltage magnitude of bus m connected to additional bus j; and $\tilde{c}_j(\cdot)$ is typical individual quadratic generator cost function. This chapter assumes zero incremental cost of WPP power output based on power purchase agreements [173], which typically represent only long-term fixed prices (i.e., feed-in tariff).

7.4 Case studies

Two test systems (5-bus and 118-bus) from the MATPOWER distribution [23] are extended to include the impact of modeling of DERs with detailed representation of substations and UPFC in power system networks. The optimization problem (7.9) is formulated in a general purpose optimization tool [47], using the KNITRO solver. We assume that one scenario, forecasted wind power, is used for maximum power output of WPP (P_w^{max}).

7.4.1 The modified IEEE 5-bus system

The modified 5-bus test system depicted in Figure 7.7 is used for this section. It is assumed

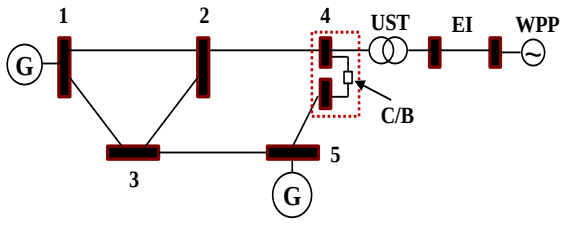

Figure 7.7: Modified 5-bus system with detailed representation of substation 4

that substation 4 contains high penetration of WPP, thus it has distribution network information with UST, C/B and EI. For convenience, this small test system is used in this section to consider

a different combination of scenarios. In particular, two wind power forecast scenarios (0.5 p.u and 1 p.u) for P_w^{max} are considered with on/off status of C/B position. Resulting solutions are summarized in Table 7.1, 7.2. Value of 1.05 is used for V^{max} at all buses. In all cases, WPP consumes reactive power with over a power factor of 0.95, and when C/B is open, voltage magnitude at substation 4 hits the upper limit.

Table 7.1: Result of the modeling of DERs with $P_w^{max} = 0.5$ p.u

	$P_w^{max} = 0.5$ p.u			
	Obj ($/hr)	P_w (p.u)	Q_w (p.u)	$\|V_4\|$ (p.u)
C/B close	880	0.5	-0.104	1.013
C/B open	1034	0.28	-0.092	1.05

For P_w^{max} = 0.5, when C/B is closed, total cost is 880$/hr with maximum real power output of 0.5 p.u and reactive power consumption of -0.104 p.u. However, when C/B is open, total cost increases significantly to 1034$/hr with real power output of 0.28 p.u and reactive power consumption of -0.092 p.u. In this case, available forecast (maximum) real power from wind generation is not fully used due to power factor limit and upper voltage magnitude limit, thus it reduces (curtails) real power output of WPP to 0.28 p.u. Modeling of UST and EI also affects reactive power capability of WPP. This might explain the typical situation that there are restrictions on reactive power capability of WPP [166], [172], which is often dealt with some form of shunt compensation: capacitors, STATCOMs, etc.

Table 7.2: Result of the modeling of DERs with $P_w^{max} = 1$ p.u

	$P_w^{max} = 1$ p.u			
	Obj ($/hr)	P_w (p.u)	Q_w (p.u)	$\|V_4\|$ (p.u)
C/B close	821	1	-0.128	1.037
C/B open	819	1	-0.271	1.05

For P_w^{max} = 1, when C/B is closed, total cost is 821$/hr with maximum real power output of 1 p.u and reactive power consumption of -0.128 p.u. When C/B is open, one obtains the interesting result that total cost is decreased to 819$/hr, and different reactive power consumption is observed at the WPP. These two results demonstrate that detailed representation of substations

with breakers can have non-trivial impact on OPF solutions for high penetration of DERs.

7.4.2 The modified IEEE 118-bus system

The modified 118-bus test system is used to describe the impact of UPFC in power system networks for this section. The shunt transformer impedances $Z_{sh} = 0 + \mathbf{j}0.1$ p.u is used as in [169]. It is assumed that the total real power supplied from WPPs is 20% of the total load and three substations (bus 13, bus 41 and bus 88) are selected to contain high penetration of WPP, thereby contain distribution network information (UST, C/B and EI). 50% of wind power is located at bus 41 and remaining of 50% is located at bus 13 and 88 with 25% each.

7.4.2.1 Effect of UPFC in power system networks

In this section, one UPFC is installed on the terminal bus 23 of transmission line (congested line) between bus 23 and bus 25. Table 7.3 shows the effects of UPFC in terms of total cost and loss in power system network with different status of C/B. Controlled series voltage source of UPFC with real and reactive power exchange with the line is shown in Table 7.4.

Table 7.3: Effect of UPFC in power system networks

	Without UPFC		With UPFC	
	Obj ($/hr)	Loss (p.u)	Obj ($/hr)	Loss (p.u)
All C/B close	195975.97	0.980	195954.00	0.979
1 C/B open	196104.12	1.006	196081.08	1.006
2 C/B open	196313.62	1.039	196290.76	1.039
All C/B open	196304.29	1.050	196281.48	1.050

Table 7.4: Controlled variable of UPFC

	Controlled series voltage source of UPFC			
	$\lvert v_{se}\rvert$ (p.u)	$\angle v_{se}$ (rad)	P_{se} (p.u)	Q_{se} (p.u)
All cases	0.07	1.90	0.031	-0.09

As more C/B open, total cost typically rises with increased loss. Conversely, the UPFC typically helps the system decrease total cost through reduced losses.

7.4.2.2 Number of UPFC and location of UPFC

In this section, we consider different numbers and locations of UPFCs in the power networks, with the setting of all C/B closed. For the analysis of different number of UPFC elements, the first UPFC is located at the same place as above. For additional UPFC elements, two cases are considered 1) UPFCs located randomly and 2) UPFCs located on congested lines.

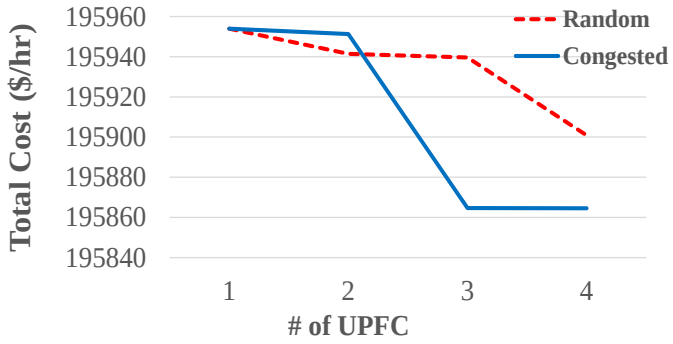

Figure 7.8: Multiple UPFC elements

Random location of UPFC are shown in red dashed line, and blue line for UPFC location on congested line are illustrated in Figure 7.8. As expected, the more UPFCs installed, the more total cost reduction is achieved. Location of UPFCs also matters in terms of amount of total cost reduction. In this specific case, congested lines for UPFC installation are preferable location than random lines.

7.4.2.3 Shunt reactive compensation of UPFC

In this section, we consider the shunt reactive compensation (SRC) function of UPFC with the setting of all C/B closed. To this end, unity power factor constraint $\left(imag(V_j(I_j)^*) = 0; \forall j \in \mathbf{N_{sh}}, u = \frac{j-nb}{2}\right)$ in (7.9d) is removed so that the shunt converter (shunt voltage source) can provide reactive power to the system. With SRC, the shunt voltage source is able to provide the reactive power of 0.0336 p.u to the system, achieving further total cost reduction shown in Table 7.5.

Table 7.5: Shunt reactive compensation of UPFC

	Without SRC		With SRC	
	Obj ($/hr)	Q_{sh} (p.u)	Obj ($/hr)	Q_{sh} (p.u)
All C/B close	195954.00	0	195953.55	0.036

7.5 Conclusion

This chapter has detailed the advanced modeling of power system networks for the accurate representation of substations with high penetration of DERs based on the node-breaker model, and UPFC devices, to appropriately study their impact within transmission network by employing STF. The proposed ACOPF model with STF determines optimal operation of the transmission network with new decision variables associated with DERs and UPFCs. In addition, with its versatility for representation of network elements, it is shown that STF avoids cumbersome topology processing for the modeling of circuit breaker reconfiguration, and avoids complex manipulation and introduction of low impedance branch to represent ideal branch voltage sources for UPFCs. Numerical case studies show that the proposed model can have accurate analysis on their impacts (DERs and UPFCs) by allowing close monitoring of decision variables associated with DERs and UPFCs.

STF allows users to formulate and implement the problem in a manner that is well-suited for the analysis of DER integration into transmission network with FACTS devices. Taking the advantage of STF to accurately represent network elements along with its computational efficiency [174], [175], we believe that STF presents a suitable tool for formulating and implementing optimal operation strategies of practical transmission network systems with high penetration of DERs. An important future research direction related to this work is to consider other DERs such as solar energy, storage, electric vehicles and demand response. Another interesting research direction would be to consider the incorporation of stochastic programming and detailed operational constraints (e.g., capability of active and reactive power output) of renewable energy resources.

CHAPTER 8

Conclusion and Future Work

This chapter summarizes the contributions of this report and outlines plans for future work in applying STF to problems in power systems engineering.

8.1 Conclusions

With the motivation that recognizes the restriction of standard Y_{bus} modeling in the node-breaker representation, which allows realistic representation of substation reconfiguration via circuit breakers in contingency analysis, this thesis has detailed Sparse Tableau Formulation (STF) for power system networks and its applications. STF employs very simple and straightforward algorithms adequate to be implemented by a computer programming language, and are successfully applied for electronic circuit design.

This thesis first in Chapter 2 investigates standard ACOPF problems by providing the comprehensive and extensive examination of the existing OPF problem with a structured, empirical comparison of three different ACOPF formulation. Numerical case studies to evaluate solution properties of the formulations in terms of computational speed, robustness of convergence and objective solution using three different nonlinear solvers; IPOPTH, KNITRO and CONOPT, are

presented. Chapter 2 next proposes additional enhancements: six choices of initial conditions, and D-curve constraint modeling. Based on results, the Polar-PV and Rectangular-CV show the best performance in terms of computational time. For solution algorithms, IPOPTH and KNITRO proved the most attractive solvers, since these were typically faster and more robust in comparison to CONOPT. Moreover, experience has suggested that D-curve constraints have modest impact, with only small increases in computation time and optimal objective value.

Chapter 3 provides the construction of STF for power system networks. It first reviews the general STF from a standard circuit analysis perspective and then examines the characteristics of the power system application that allow simplification of general STF. An illustrative example with four-bus system is given to describe the process of STF for power system network.

Chapter 3 next discusses the relationship between STF and other modeling approaches (Y_{bus} and Modified Nodal Analysis) in those cases for which both may be applied, and examines atypical network elements, modelling of which STF proves particularly advantageous. Useful by-product of STF applied for power flow problem is discussed in terms of contingency analysis since the Jacobian matrix associated with these equations corresponds to the sensitivity matrix relating injection power and current flow on line. STF is then applied to OPF numerical case studies which demonstrate that STF shows little or no penalty in computational speed compared to classic OPF representations constructed in Chapter 2, and sometimes provides considerable advantage in computational speed.

This report next investigates the security-constrained OPF problem. Chapter 4 begins with the definition of “preventive” SCOPF (PSCOPF) and discusses necessary enhancements for the PSCOPF problem; 1) introducing the speed droop-characteristic for each generator as governor power flow equations in contingency cases to formulate the PSCOPF problem. 2) the node-breaker model that STF can be significantly useful. Then, STF is employed to formulate the PSCOPF problem under the node-breaker model and its advantage is discussed. Chapter 4 continues to conduct a numerical experiment with different level of contingency showing that STF provides comparable computational efficiency.

Chapter 5 then investigate an alternative approach to address the security in the power sys-

tem networks using additional generation capacity as operating reserves. Chapter 5 introduces the importance of effectively and efficiently allocating reserves across the system to improve the deliverability of energy with renewable energy resources. Then, we develop a tool to obtain a probabilistic post zonal reserve requirement with three uncertainty sources (conventional generation, load and wind). The proposed post zonal reserve requirement is tested using the IEEE 118-bus test system, which shows that it efficiently and effectively allocates reserves to mitigate possible congestions with wind power. Our results also show that resulting zonal reserve MCPs properly reflect the effect of zonal reserve requirement on possible congestions of transmission line under consideration as well as the reduced operating cost with the consideration of wind curtailment.

In Chapter 6, we explore convex relaxation technique for STF of OPF problem. The limitation of existing convex relaxation techniques for STF is discussed, and then alternative approaches (STF relaxations) are proposed using the McCormick envelope. Several methods to strengthen the convex relaxation problem are discussed and Chapter 6 concludes with numerical case studies and highlight that STF relaxation shows advantage in computational time and strength under the condition that a tight bound for active power generation variable P_g is given.

Finally, Chapter 7 employs STF to develop advanced modeling of DERs and UPFC devices for ACOPF problem. STF is used to accurately model the detailed representation of substations for high penetration of distributed energy resources (DERs). These substations contain distribution network information such as unit state transformer, distribution feeder and circuit breakers. Then, STF is modified to accurately model UPFC which can be best represented as the ideal branch voltage source, together with the real power coupling to the sending-end generator.

8.2 Future Work

With the progress developed so far, there are several directions of this work for further investigation and questions remain elusive.

- **Future Work:**

The first direction involves extending STF for power system network to a more flexible load model. Currently, most existing OPF problem use constant power load models and constant load models are explicitly formulated in this thesis. Extending STF to constant impedance and constant current would be the first step to include the ZIP (constant impedance, constant current, constant power) load model [46]. Importantly, more advanced load models such as dynamic and nonlinear load might be straightforward since STF explicitly model each network element.

The second research proposal is the extension of preventive SCOPF to corrective SCOPF. As it is shown in Chapter 4, the simulation of large numbers of contingencies which involves bus splits and bus mergers is possible with STF. In addition, topological corrective actions (TCA) with pre-defined binary parameters are considered showing that topological change affects the solution of PSCOPF problem. Therefore, it would be important to develop an efficient method to incorporate discrete variables for TCA via circuit breaker switching. On the computational issue for large-scale systems, we also want to consider a contingency filtering scheme to pre-select critical contingencies, thus reduce the number of contingencies.

The third research proposal is to investigate different power system analysis where STF becomes a useful tool. Such problems include the state estimation analysis including zero-impedance current. Such branches (short circuits) are commonly encountered in substation arrangements for the state-estimation problem. It is important to accurately represent this branch current in state-estimation problem. It can be also applied for distribution networks to represent three-phase unbalanced system. Since STF provides a generic multiphase load-flow formulation, it is capable of handling arbitrary network topologies and can be easily expanded to accommodate various network components including FACTS devices for three-phase unbalanced distribution networks.

The fourth research proposal is to investigate more sophisticated network elements such as power electronics based Flexible AC Transmission System (FACTS) devices and High Voltage Direct Current (HVDC). In power system networks, vast majority of elements will be most naturally modeled as one-port or two-port elements. However, power system is facing significant

challenges in operation and planning as a massive number of distributed energy resources (DER) will be integrated into the system. Therefore, advanced modeling method using STF for future power system technologies including various FACTS devices and HVDC would be extremely valuable.

The fifth research proposal is the construction of appropriate linear approximation for STF. Even though it is true that STF can accurately model power system network without any elimination or reduction on data, it might not be easy to derive a linear representation, similar to the DC power flow, for that. If an appropriate linear representation can be derived, then STF can be also applied for other problems mostly using linear representation such as unit commitment.

The final research proposal is to investigate new control, optimization and big-data techniques with STF to implement autonomous power grids which can self-organize and control themselves to create secure, resilient and affordable optimized energy systems. Such techniques would include model predictive control, optimal control, nonlinear programming and mixed-integer programming.

APPENDIX A

Details of standard ACOPF equations for Chapter 2

A.1 AC models

This section details the AC power flow equations used in Chapter 2. We provide three formulations of the AC power flow model, namely polar power-voltage in Section A.1.1, rectangular power-voltage in A.1.2 and rectangular current-voltage in A.1.3.

A.1.1 Polar Power-Voltage Formulation (P)

The polar power-voltage formulation uses the polar form of complex quantities and explicitly uses sines and cosines in the power flow constraints. Real power flow on lines $ijc \in \mathbf{L}$ is modeled here by (A.1 - A.2), while (A.3 - A.4) computes the line's reactive power flow.

$$\begin{aligned}
\text{s.t.} \quad F^P_{jkc} &= \frac{1}{\tau^2_{jkc}} g^{\mathbf{L}}_{jkc} V_j^2 \\
&\quad - \frac{1}{\tau_{jkc}} V_j V_k \left(g^{\mathbf{L}}_{jkc} \cos(\theta_j - \theta_k - \phi_{jkc}) + b^{\mathbf{L}}_{jkc} \sin(\theta_j - \theta_k - \phi_{jkc}) \right) \qquad \forall jkc \in \mathbf{L} \qquad \text{(A.1)} \\
F^P_{kjc} &= g^{\mathbf{L}}_{jkc} V_k^2 \\
&\quad - \frac{1}{\tau_{jkc}} V_j V_k \left(g^{\mathbf{L}}_{jkc} \cos(\theta_k - \theta_j + \phi_{jkc}) + b^{\mathbf{L}}_{jkc} \sin(\theta_k - \theta_j + \phi_{jkc}) \right) \qquad \forall jkc \in \mathbf{L} \qquad \text{(A.2)}
\end{aligned}$$

$$F^Q_{jkc} = -\frac{1}{\tau^2_{jkc}}\left(b^{\mathbf{L}}_{jkc} + \frac{b^C_{jkc}}{2}\right)V_j^2 - \frac{1}{\tau_{jkc}}V_jV_k\left(g^{\mathbf{L}}_{jkc}\cos(\theta_j - \theta_k - \phi_{jkc}) - b^{\mathbf{L}}_{jkc}\sin(\theta_j - \theta_k - \phi_{jkc})\right) \qquad \forall jkc \in \mathbf{L} \qquad \text{(A.3)}$$

$$F^Q_{kjc} = -\left(b_{jkc} + \frac{b^C_{jkc}}{2}\right)V_k^2 - \frac{1}{\tau_{jkc}}V_jV_k\left(g^{\mathbf{L}}_{jkc}\cos(\theta_k - \theta_j + \phi_{jkc}) - b^{\mathbf{L}}_{jkc}\sin(\theta_k - \theta_j + \phi_{jkc})\right) \qquad \forall jkc \in \mathbf{L} \qquad \text{(A.4)}$$

A.1.2 Rectangular Power-Voltage Formulation (R)

The second AC formulation uses the rectangular form of complex quantities, resulting in quadratic power flow constraints with respect to these quantities.

$$\begin{aligned}
\text{s.t.}\quad F^P_{jkc} &= \frac{1}{\tau^2_{jkc}}g^{\mathbf{L}}_{jkc}\left((V^P_j)^2 + (V^Q_k)^2\right) \\
&\quad - \frac{1}{\tau_{jkc}}\left(g^{\mathbf{L}}_{jkc}\cos(\phi_{jkc}) - b^{\mathbf{L}}_{jkc}\sin(\phi_{jkc})\right)\left(V^P_jV^P_k + V^Q_jV^Q_k\right) \\
&\quad - \frac{1}{\tau_{jkc}}\left(b^{\mathbf{L}}_{jkc}\cos(\phi_{jkc}) + g^{\mathbf{L}}_{jkc}\sin(\phi_{jkc})\right)\left(V^P_kV^Q_j - V^P_jV^Q_k\right) \qquad \forall jkc \in \mathbf{L} \qquad \text{(A.5)} \\
F^P_{kjc} &= g^{\mathbf{L}}_{jkc}\left((V^P_k)^2 + (V^Q_j)^2\right) \\
&\quad - \frac{1}{\tau_{jkc}}\left(g^{\mathbf{L}}_{jkc}\cos(\phi_{jkc}) + b^{\mathbf{L}}_{jkc}\sin(\phi_{jkc})\right)\left(V^P_kV^P_j + V^Q_kV^Q_j\right) \\
&\quad - \frac{1}{\tau_{jkc}}\left(b^{\mathbf{L}}_{jkc}\cos(\phi_{jkc}) - g^{\mathbf{L}}_{jkc}\sin(\phi_{jkc})\right)\left(V^P_jV^Q_k - V^P_kV^Q_j\right) \qquad \forall jkc \in \mathbf{L} \qquad \text{(A.6)} \\
F^Q_{jkc} &= -\frac{1}{\tau^2_{jkc}}\left(b^{\mathbf{L}}_{jkc} + \frac{b^C_{jkc}}{2}\right)\left((V^P_j)^2 + (V^Q_k)^2\right) \\
&\quad - \frac{1}{\tau_{jkc}}\left(g^{\mathbf{L}}_{jkc}\cos(\phi_{jkc}) - b^{\mathbf{L}}_{jkc}\sin(\phi_{jkc})\right)\left(V^P_kV^Q_j - V^P_jV^Q_k\right) \\
&\quad - \frac{1}{\tau_{jkc}}\left(b^{\mathbf{L}}_{jkc}\cos(\phi_{jkc}) + g^{\mathbf{L}}_{jkc}\sin(\phi_{jkc})\right)\left(V^P_jV^P_k + V^Q_jV^Q_k\right) \qquad \forall jkc \in \mathbf{L} \qquad \text{(A.7)} \\
F^Q_{kjc} &= -\left(b^{\mathbf{L}}_{jkc} + \frac{b^C_{jkc}}{2}\right)\left((V^P_j)^2 + (V^Q_k)^2\right) \\
&\quad - \frac{1}{\tau_{jkc}}\left(g^{\mathbf{L}}_{jkc}\cos(\phi_{jkc}) + b^{\mathbf{L}}_{jkc}\sin(\phi_{jkc})\right)\left(V^P_jV^Q_k - V^P_kV^Q_j\right) \\
&\quad - \frac{1}{\tau_{jkc}}\left(b^{\mathbf{L}}_{jkc}\cos(\phi_{jkc}) - g^{\mathbf{L}}_{jkc}\sin(\phi_{jkc})\right)\left(V^P_kV^P_j + V^Q_kV^Q_j\right) \qquad \forall jkc \in \mathbf{L} \qquad \text{(A.8)}
\end{aligned}$$

A.1.3 Rectangular Current-Voltage Formulation (IV)

The third AC model presented here is the rectangular current-voltage formulation which considers the flow of current instead of power on a line. Equations (A.9-A.12) define real and reactive current flow on a line.

$$\begin{aligned}
\text{s.t.} \quad I^P_{jkc} = {} & \frac{1}{\tau^2_{jkc}}\left(g^{\mathbf{L}}_{jkc} V^P_j - \left(b^{\mathbf{L}}_{jkc} + \frac{b^C_{jkc}}{2}\right) V^Q_j\right) \\
& - \frac{1}{\tau_{jkc}}\left(g^{\mathbf{L}}_{jkc} V^P_k - b^{\mathbf{L}}_{jkc} V^Q_k\right)\cos\left(\phi_{jkc}\right) \\
& + \frac{1}{\tau_{jkc}}\left(g^{\mathbf{L}}_{jkc} V^Q_k + b^{\mathbf{L}}_{jkc} V^P_k\right)\sin(\phi_{jkc}) \qquad \forall jkc \in \mathbf{L} \qquad \text{(A.9)} \\
I^P_{kjc} = {} & \left(g^{\mathbf{L}}_{jkc} V^P_k - \left(b^{\mathbf{L}}_{jkc} + \frac{b^C_{jkc}}{2}\right) V^Q_k\right) \\
& - \frac{1}{\tau_{jkc}}\left(g^{\mathbf{L}}_{jkc} V^P_j - b^{\mathbf{L}}_{jkc} V^Q_j\right)\cos(-\phi_{jkc}) \\
& + \frac{1}{\tau_{jkc}}\left(g^{\mathbf{L}}_{jkc} V^Q_j + b^{\mathbf{L}}_{jkc} V^P_j\right)\sin(-\phi_{jkc}) \qquad \forall jkc \in \mathbf{L} \qquad \text{(A.10)} \\
I^Q_{jkc} = {} & \frac{1}{\tau^2_{jkc}}\left(g^{\mathbf{L}}_{jkc} V^Q_j + \left(b^{\mathbf{L}}_{jkc} + \frac{b^C_{jkc}}{2}\right) V^P_j\right) \\
& - \frac{1}{\tau_{jkc}}\left(g^{\mathbf{L}}_{jkc} V^Q_k + b^{\mathbf{L}}_{jkc} V^P_k\right)\cos\left(\phi_{jkc}\right) \\
& - \frac{1}{\tau_{jkc}}\left(g^{\mathbf{L}}_{jkc} V^P_k - b^{\mathbf{L}}_{jkc} V^Q_k\right)\sin\left(\phi_{jkc}\right) \qquad \forall jkc \in \mathbf{L} \qquad \text{(A.11)} \\
I^Q_{kjc} = {} & \frac{1}{\tau^2_{jkc}}\left(g^{\mathbf{L}}_{jkc} V^Q_k + \left(b^{\mathbf{L}}_{jkc} + \frac{b^C_{jkc}}{2}\right) V^P_k\right) \\
& - \frac{1}{\tau_{jkc}}\left(g^{\mathbf{L}}_{jkc} V^Q_j + b^{\mathbf{L}}_{jkc} V^P_j\right)\cos(-\phi_{jkc}) \\
& - \frac{1}{\tau_{jkc}}\left(g^{\mathbf{L}}_{jkc} V^P_j - b^{\mathbf{L}}_{jkc} V^Q_j\right)\sin(-\phi_{jkc}) \qquad \forall jkc \in \mathbf{L} \qquad \text{(A.12)}
\end{aligned}$$

APPENDIX B

Details of deterministic UC formulation for Chapter 5

B.1 UC model formulation

A full mathematical description for the deterministic UC formulation is provided, which includes operational constraints, unit commitment constraints and reserve requirement.

B.1.1 Nomenclature

Set	Description
G	Set of generators.
$G_i \in G$	Subset of generators G at bus i.
$G_z \in G$	Subset of generators G at zone z.
L	Set of lines in the transmission network.
L^c	Set of critical lines.
N	Set of buses.
T	Time period for unit commitment schedule.
W	Set of wind power plants.
W_i	Subset of wind power plants at bus i.
Z	Set of reserve zones.
FZ^l	“From Zone" for critical line $l \in L^c$.

B.1.1.1 For probabilistic post zonal reserve requirement model

Parameters	Description
$A_{l,t}$	Possible maximum overflow in line flow distribution function on critical line l, hour t.
$F_l^{\max}$	Thermal limit of line $l \in L$.
ISF	Injection shift factor.
OFP	Overflow probability.

Variables	Description
$f_w(.)$	Density function of wind power w.
$f_{w,X}$	Joint density function of w and X.
f_X	Marginal density function of X.
IP_i	Injection power (MW) at bus i.
d_i/D_i	Amount of load (MW) at bus i.
g_i/G_i	Amount of conventional unit (MW) at bus i.
m_i/M_i	Amount of injection margin (MW) at bus i.
w_i/W_i	Amount of wind power (MW) at bus i.
$P_D^i(D_i{=}d_i)$	Probability mass functions (PMF) of load at bus i.
$P_G^i(G_i{=}g_i)$	PMF of conventional units at bus i.
$P_W^i(W_i{=}w_i)$	PMF of wind power at bus i.
$P_M^i(M_i{=}m_i)$	PMF of injection margin at bus i.
$P(F_l)$	PMF of line flow on line l.
$Reserve_i$	Amount of reserves (MW) at bus i.
w_{t+k}	Wind power output (MW) at time $t+k$.
$x_{t+k\|t}$	X value for time $t+k$ estimated at time t.

B.1.1.2 For enhanced deterministic SCUC model

Parameters	Description
B_{ij}	Line susceptance for line ij.
γ_{ij}	Phase shifting turns ratio for line ij.
θ_{ij}	Phase shifting angle for line ij.
$\tilde{c}_g\{\cdot\}$	Generation cost function for $g \in G$.
CE/CR	Penalty cost of unserved energy/reserves.
$D_{i,t}$	Power demand for bus i, hour t.
F_{ij}^{max}	Thermal limit of line ij.
g_j^s	Shunt conductance at bus i
ISF	Injection shift factor.
MDT_g	Min down time for generator g.
MUT_g	Min up time for generator g.
P_g^{min}	Generator minimum output for generator g.
P_g^{max}	Generator maximum output for generator g.
RP_g^{UP}	Reserve up/down price for $g \in G$
RP_g^{DW}	Reserve up/down price for $g \in G$.
RD_g	Ramp down limit for generator g.
RU_g	Ramp up limit for generator g.
RSD_g	Ramp shutdown limit for generator g.
RSU_g	Ramp startup limit for generator g.
RUR_g	Reserve ramp up limit in a minute for generator g.
RDR_g	Reserve ramp down limit in a minute for generator g.
RRT_g	Reserve responsive time for generator g.
SU_g/SD_g	Start-up/shutdown cost for $g \in G$.
SYS_{up}	System-wide reserve up requirement.
SYS_{dw}	System-wide reserve down requirement.
$WP_{w,t}$	Available wind generation for wind power plant w, hour t.

Variables	Description
$e_{i,t}$	Non-served energy for $i \in N$, $t \in T$.
$F_{ij,t}$	Line flow on line ij, hour t.
$P_{g,t}$	Active power generation for generator g, hour t.
$Rup_{g,t}$	General upward reserve for for generator g, hour t.
$Rdw_{g,t}$	General downward reserve for generator g, hour t.
$Rup_{z,t}$	Reserve up for $z \in Z$, $t \in T$.
$Rdw_{z,t}$	Reserve down for $z \in Z$, $t \in T$.
$Rupns_{g,t}$	Unserved reserve up for $g \in G$, $t \in T$.
$Rdwns_{g,t}$	Unserved reserve down for $g \in G$, $t \in T$.
$\delta_{i,t}$	Voltage angle for bus i, hour t.
$u_{g,t}$	Commitment variable for generator g, hour t.
$y_{g,t}$	Shut-down variable for generator g, hour t.
$z_{g,t}$	Start-up variable for generator g, hour t.

B.1.2 Set of constraints

Since the objective function is given in the Chapter 5, this section shows set of constraints in detail.

Opertional Requirements:

Line flow:

$$F_{ij,t} = \frac{B_{i,j}}{\gamma_{i,j}}(\delta_{j,t} - \delta_{i,t} + \theta_{i,j,c}), \forall ij \in L, \forall t \in T \tag{B.1}$$

Active power balance:

$$\sum_{k \in G_i} P_{k,t} - \sum_{ij \in L} F_{ij,t} + \sum_{ji \in L} F_{ji,t} + \sum_{k \in W_i} WP_{k,t} - D_{i,t} - g_i^s + e_{i,t} = 0, \forall i \in N, \forall t \in T \tag{B.2}$$

Line thermal limit:

$$-F_{ij}^{max} \leq F_{ij,t} \leq F_{ij}^{max}, \forall ij \in L, \forall t \in T \tag{B.3}$$

Generator output limit:

$$P_{g,t} + Rup_{g,t} \leq P_g^{max} u_{g,t}, \forall g \in G, \forall t \in T \tag{B.4}$$

$$P_g^{min} u_{g,t} \leq P_{g,t} - Rdw_{g,t}, \forall g \in G, \forall t \in T \tag{B.5}$$

Generator ramp constraints:

$$P_{g,t} - P_{g,t-1} + Rup_{g,t} \leq RU_g u_{g,t-1} + RSU_g z_{g,t} \tag{B.6}$$

$$P_{g,t-1} - P_{g,t} - Rdw_{g,t} \leq RD_g u_{g,t} + RSD_g y_{g,t}, \forall g \in G, \forall t \in T$$

Unit Commitment Requirements:

Binary variable logic

$$u_{g,t} - u_{g,t-1} = z_{g,t} - y_{g,t}, \forall g \in G, \forall t \in T \tag{B.7}$$

Generator minimum up/down:

$$\sum_{tt=t-MUT_g+1}^{t} z_{g,tt} \leq u_{g,t}, \forall g \in G, \forall t \in T \tag{B.8}$$

$$\sum_{tt=t-MDT_g+1}^{t} y_{g,tt} \leq 1 - u_{g,t}, \forall g \in G, \forall t \in T \tag{B.9}$$

$$u_{g,t} \in \{0,1\}, \forall g \in G, \forall t \in T \tag{B.10}$$

$$0 \leq z_{g,t}, y_{g,t} \leq 1 \, \forall g \in G, \forall t \in T \tag{B.11}$$

Reserve Requirements:

System-wide requirement:

$$\sum_{g} Rup_{g,t} + Rupns_{g,t} \geq SYS_{up}, \forall t \tag{B.12}$$

$$\sum_{g} Rdw_{g,t} + Rdwns_{g,t} \geq SYS_{dw}, \forall t \tag{B.13}$$

Zonal reserve requirement:

$$\sum_{g \in G_z} \left(Rup_{g,t}\right) \geq Rup_{z,t}, \forall z, \forall t \tag{B.14}$$

$$\sum_{g \in G_z} \left(Rdw_{g,t}\right) \geq Rdw_{z,t}, \forall z, \forall t \tag{B.15}$$

Post reserve requirement transmission constraints:

$$F_{l,t} + \sum_{i} \left(ISF(l,i) \sum_{g \in G_i} (Rup_{g,t})\right) \leq F_l^{\max}, \forall l \in L^c, \forall t \tag{B.16}$$

$$F_{l,t} - \sum_{i} \left(ISF(l,i) \sum_{g \in G_i} (Rdw_{g,t})\right) \leq F_l^{\max}, \forall l \in L^c, \forall t \tag{B.17}$$

Probabilistic Post zonal reserve requirement:

$$\sum_{i \in FZ^l} \left(ISF(l,i) \cdot \sum_{g \in G_i} (Rdw_{g,t})\right) \leq F_l^{max} - A_{l,t}, \forall l \in L^c, \forall t \in T \tag{B.18}$$

Reserve ramp constraints:

$$Rup_{g,t} \leq (RRT_g \times RUR_g) u_{g,t}, \forall g \in G, \forall t \in T \tag{B.19}$$

$$Rdw_{g,t} \leq (RRT_g \times RDR_g) u_{g,t}, \forall g \in G, \forall t \in T \tag{B.20}$$

Bibliography

[1] National Academy of Engineering, "Greatest Engineering Achievements of the 20th Century." [Online]. Available: http://www.greatachievements.org/

[2] MIT Energy Laboratory, "Electric Generation Expansion Analysis System," 1980.

[3] M. Shahidehpour and M. Marwali, *Maintenance Scheduling in Restructured Power Systems*. Springer US, 2000.

[4] N. P. Padhy, "Unit Commitment-A Bibliographical Survey," *IEEE Transactions on Power Systems*, vol. 19, no. 2, May 2004.

[5] Department of Energy, "The Smart Grid: An Introduction," 2009.

[6] A. C. Mary B. Cain, Richard P. O'Neill, "History of Optimal Power Flow and Formulations," *Staff Report, Federal Energy Regulatory Commission*, December 2012.

[7] Edison Electric Institute, "INDUSTRY DATA," EEI, Tech. Rep., 2016.

[8] M. Sadiku and C. Alexander, *Fundamentals of Electric Circuits 5th*. Science Engineering & Math, 2011.

[9] J. J. Grainger and J. William D. Stevenson, *Power System Analysis*. McGraw-Hill, 1994.

[10] L. O. Chua, C. A. Desoer, and E. S. Kuh, *Linear and Nonlinear Circuit*. McGraw-Hill, 1987.

[11] General Electric, Siemens, V&R POM Suite, PowerWorld, DSATools, and eTap, "Node-Breaker Modeling Representation," North American Electric Reliability Corporation (NERC), Tech. Rep., 2016.

[12] B. Thomas, S. Kincic, D. Davies, H. Zhang, and J. Sanchez-Gasca, "A New Framework to Facilitate the Use of Node-Breaker Operations Model for Validation of Planning Dynamic Models in WECC," *Power and Energy Society General Meeting (PESGM)*, 2016.

[13] R. Fischl and W. R. Puntel, “Computer-aided design of electric power transmission networks,” *IEEE PAS Conference Paper*, 1972.

[14] W. R. P. et al., “An automated method for long-range planning of transmission networks,” *Proceedings of the 10th Power Industry Computer Applications Conference (PICA)*, 1973.

[15] G. D. HACHTEL, R. K. BRAYTON, and F. G. GUSTAVSON, “The Sparse Tableau Approach to Network Analysis and Design,” *IEEE Transactions on Circuit Theory*, vol. CT-18, no. 1, 1972.

[16] L. W. Nagel and D. O. Pederson, “Simulation Program with Integrated Circuit Emphasis (SPICE),” *presented at 16th Midwest Symp. on Circuit Theory*, 1973.

[17] IBM Program Product Document SH20-1118-0, “ASTAP – Advanced statistical analysis program,” IBM Data Processing Div, Tech. Rep., 1973.

[18] W. T. WEEKS, A. J. JIMENEZ, G. W. MAHONEY, D. MEHTA, H. QASSEMZADEH, and T. R. SCOTT, “Algorithms for ASTAP-A Network-Analysis Program,” *IEEE Transactions on Circuit Theory*, vol. CT-20, no. 6, Novermber 1973.

[19] S. W. DlRECTOR and R. L. SULLIVAN, “A TABLEAU APPROACH TO POWER SYSTEM ANALYSIS AND DESIGN,” *Circuit Theory and Applications*, vol. 7, 1979.

[20] B. Stott, J. Jardim, and O. Alsac, “DC Power Flow Revisited,” *IEEE Transactions on Power Systems*, vol. 24, no. 3, August 2009.

[21] J. Lavaei and S. H. Low, “Zero Duality Gap in Optimal Power Flow Problem,” *IEEE Transactions on Power Systems*, vol. 27, no. 1, February 2012.

[22] G. P. McCormick, “Computability of global solutions to factorable nonconvex programs: Part i - convex underestimating problems,” *Mathematical Programming 10*, 1976.

[23] R. D. Zimmerman and C. E. Murillo-Sanchez, “Matpower: Steady-state operations, planning and analysis tools for power systems research and education,” *IEEE Transactions on Power Systems*, vol. 26, no. 1, December 2011. [Online]. Available: http://www.pserc.cornell.edu//matpower/

[24] A. R. Bergen and V. Vittal, *Power System Analysis 2nd*. Prentice Hall, 2000.

[25] M. S. S. J. Duncan Glover and T. J. Overbye, *Power System Analysis and Design*, 2012.

[26] B. C. Lesieutre and I. A. Hiskens, “Convexity of the Set of Feasible Injections and Revenue Adequacy in FTR Markets,” *IEEE Transactions on Power Systems*, vol. 20, no. 4, November 2005.

[27] J. Carpentier, "Contribution to the Economic Dispatch Problem," *Bull. Soc. Franc. Elect*, vol. 8, no. 3, pp. 431–447, 1962.

[28] C. K. Alexander and M. N. Sadiku, *Fundamentals of Electric Circuits*. McGraw-Hill, 2009.

[29] D. J. Rose and R. A. W. (Eds), "Sparse Matrices and their Applications," *Plenum Press*, 1972.

[30] I. S. Duff, "A Survey of Sparse Matrix Research," *Proceedings of the IEEE*, 1977.

[31] A. J. Wood and B. F. Wollenberg, *Power Generation, Operation, and Control 2nd*. New York J. Wiley & Sons, 1996.

[32] L. L. Lai, H. T. Zhang, S. Mishra, D. Ramasubramanian, C. S. Lai, and F. Y. Xu, "Lessons learned from July 2012 Indian blackout," *Advances in Power System Control, Operation and Management (APSCOM 2012), 9th IET International Conference*, 2012.

[33] H. Dommel, W. Tinney, and W. Powell, "Further developments in Newton's method for power system applications," *IEEE Winter Power Meeting, Conference Paper No. 70 CP 161-PWR New York*, 1970.

[34] W. F. Tinney, "A Presentation to the Workshop in Engineering Mathematics and Computer Sciences," *EPRI publication EAR/EL -7/07*, 1991.

[35] W. Rosehart and J. A. Aguado, "Alternative Optimal Power Flow Formulation," *14th Power Systems Computation Conference (PSCC'14)*, 2002.

[36] G. L. Torres and V. H. Quintana, "An interior-point method for nonlinear optimal power flow using voltage rectangular coordinates," *IEEE Transactions on Power Systems*, vol. 13, no. 4, 1998.

[37] R. P. O'Neill, A. Castillo, and M. B. Cain, "The IV Formulation and Linear Approximations of the AC Optimal Power Flow Problem," *Staff Report, Federal Energy Regulatory Commission*, 2012.

[38] A. Castillo and R. P. O'Neill, "Computational Performance of Solution Techniques Applied to the ACOPF," *Staff Report, Federal Energy Regulatory Commission*, 2013.

[39] V. M. da Costa and A. L. S. Rosa, "A Comparative Analysis of Different Power Flow Methodologies," *Transmission and Distribution Conference and Exposition: Latin America, IEEE/PES*, 2008.

[40] J. Dragosavac, Z. Janda, J. Milanovic, D. Arnautovic, and B. Radojicic, "On-line Estimation of Available Generator Reactive Power for Network Voltage Support," *Power Generation, Transmission, Distribution and Energy Conversion (MEDPOWER 2012), 8th Mediterranean Conference on*, 2012.

[41] Y. Cong, P. Regulski, P. Wall, M. Osborne, and V.Terzija, "On the use of Dynamic Thermal Line Ratings for Improving Operational Tripping Schemes," *IEEE Transactions on Power Delivery*, 2015.

[42] B. Park and C. L. DeMarco, "Active/Reactive Power Decomposition Approaches To The AC Optimal Power Flow Problem," *North American Power Symposium (NAPS)*, September 2014.

[43] B. Tamimi, C. A. Cañizares, and S. Vaez-Zadeh, "Effect of Reactive Power Limit Modeling on Maximum System Loading and Active and Reactive Power Markets," *IEEE Transactions on Power Systems*, vol. 25, no. 2, May 2010.

[44] Z. S. Machado Jr, G. N. Taranto, and D. M. Falcão, "An Optimal Power Flow Formulation Including Detailed Modeling of Generators," *Power Systems Conference and Exposition*, 2004.

[45] UW-Madison, "Documentation on capability curves," 2015, http://www.neos-guide.org/sites/default/files/capability_curves.pdf.

[46] P. Kundur, N. Balu, and M. Lauby, *Power System Stability and Control*. McGraw-hill, 1994.

[47] GAMS, "General Algebraic Modeling System." [Online]. Available: https://www.gams.com/

[48] A. R. Bergen and V. Vittal, *Power System Analysis 2nd*. Prentice Hall, 2000.

[49] C. Ho, A. E. Ruehli, and P. A. Brennan, "The modified nodal approach to network analysis," *IEEE Transactions on Circuits and Systems*, vol. CAS-22, no. 6, 1975.

[50] J. Mahseredjian, S. Dennetiere, L. Dube, B. Khodabakhchian, and L. Gerin-Lajoie, "On a new approach for the simulation of transients in power systems," *Electric Power Systems Research*, 2007.

[51] I. Kocar and Jean-Sebastien Lacroix and F. Therrien, "General and simplified computation of fault flow and contribution of distributed sources in unbalanced distribution networks," *IEEE PES GM*, 2012.

[52] I. Kocar, J. Mahseredjian, U. Karaagac, G. Soykan, and O. Saad, "Multiphase load-flow solution for large-scale distribution systems using mana," *IEEE Transactions on Power Delivery*, vol. 29, no. 2, 2014.

[53] I. Kocar and J.-S. Lacroix, "Implementation of a modified augmented nodal analysis based transformer model into the backward forward sweep solver," *IEEE Transactions on Power Systems*, vol. 27, no. 2, 2012.

[54] A. Monticelli and A. Garcia, "Modeling zero impedance branches in power system state estimation," *IEEE Transactions on Power Systems*, vol. 6, no. 4, 1991.

[55] F. Therrien, I. Kocar, and J. Jatskevich, "A Unified Distribution System State Estimator Using the Concept of Augmented Matrices," *IEEE Transactions on Power Systems*, vol. 28, no. 3, 2013.

[56] B. M. Weedy, *Electric Power Systems 3rd*. John Wiley & Sons, 1987.

[57] M. Oommen and J. Kohler, "Effect of three-winding transformer models on the analysis and protection of mine power systems," *Industry Applications Society Annual Meeting*, 1993.

[58] K. Shaarbafi, "Transformer Modelling Guide," Alberta Electric System Operator (AESO), Tech. Rep., 2014.

[59] D. Kirschen and G. Strbac, "Why Investments Do Not Prevent Blackouts," *The Electricity Journal*, vol. 17, no. 2, 2004.

[60] J. Zhu and K. Cheung, "Flexible Simultaneous Feasibility Test in Energy Market," *Power and Energy Society General Meeting (PESGM)*, 2010.

[61] J. Guo, Y. Fu, Z. Li, and M. Shahidehpour, "Direct Calculation of Line Outage Distribution Factors," *IEEE Transactions on Power Systems*, vol. 24, no. 3, 2009.

[62] T. Guler, G. Gross, and M. Liu, "Generalized Line Outage Distribution Factors," *IEEE Transactions on Power Systems*, vol. 22, no. 3, 2007.

[63] B. Park, L. Tang, M. Ferris, and C. DeMarco, "Examination of three different ACOPF formulations with generator capability curves," *IEEE Transactions on Power Systems*, 2016.

[64] G. Pillo and A. Murli, Eds., *High Performance Algorithms and Software in Nonlinear Optimization*. Springer, 2003.

[65] C. Meszaros and U. Suhl, “Advanced preprocessing techniques for linear and quadratic programming,” *OR Spectrum*, vol. 24, 2003.

[66] J. Kassakian and R. Schalensee, “The Future of the Electric Grid,” *Massachusetts Institute of Technology, Technical Report*, 2011.

[67] O. Alsac and B. Stott, “OPTIMAL LOAD FLOW WITH STEADY-STATE SECURITY,” *IEEE Transactions on Power Apparatus and Systems*, vol. PAS-93, May 1974.

[68] J. Momoh, R. Koessler, M. S. Bond, B. Stott, D. Sun, A. Papalexopoulo, and P. Ristanovic, “Challenges to Optimal Power Flow,” *IEEE Transactions on Power Systems*, vol. 12, no. 1, 1997.

[69] A. J. Ardakani and F. Bouffard, “Identification of Umbrella Constraints in DC-Based Security-Constrained Optimal Power Flow,” *IEEE Transactions on Power Systems*, vol. 28, no. 4, 2013.

[70] O. Alsac, J. Bright, M. Prais, and B. Stott, “FURTHER DEVELOPMENTS IN LP-BASED OPTIMAL POWER FLOW,” *IEEE Transactions on Power Systems*, vol. 5, no. 3, 1990.

[71] A. J. Ardakani and F. Bouffard, “Acceleration of Umbrella Constraint Discovery in Generation Scheduling Problems,” *IEEE Transactions on Power Systems*, vol. 30, no. 4, 2015.

[72] Q. Zhai, X. Guan, J. Cheng, and H. Wu, “Fast Identification of Inactive Security Constraints in SCUC Problems,” *IEEE Transactions on Power Systems*, vol. 25, no. 4, 2010.

[73] F. Capitanescu, M. Glavic, D. Ernst, and L. Wehenkel, “Contingency Filtering Techniques for Preventive Security-Constrained Optimal Power Flow,” *IEEE Transactions on Power Systems*, vol. 22, no. 4, 2007.

[74] D. E. L. W. F. Capitanescu, M. Glavic, “Applications of Security-Constrained Optimal Power Flows,” *Modern Electric Power Systems Symposium, MEPS06*, 2006.

[75] L. Platbrood, F. Capitanescu, C. Merckx, H. Crisciu, and L. Wehenkel, “A generic approach for solving nonlinear-discrete security-constrained optimal power flow problems in large-scale systems,” *IEEE Trans. Power Syst.*, vol. 29, no. 3, 2014.

[76] GARPUR project, “Generally accepted reliability principle with uncertainty modelling and through probabilistic risk assessment,” KU Leuven, Tech. Rep., 2017. [Online]. Available: https://www.sintef.no/globalassets/project/garpur/deliverables/garpur-d10.3d-garpur-workshops-proceedings-all-rp.pdf

[77] S. Grijalva and A. Roy, "Automated handling of arbitrary switching device topologies in planning contingency analysis: Towards temporal interoperability in network security assessment," *IEEE Trans. Power Syst.*, vol. 28, no. 2, 2013.

[78] R. Ramanathan and B. Tuck, "Contingency Analysis Using Node/Breaker Model for Operation Studies," *Power and Energy Society General Meeting (PES)*, 2013.

[79] M. Kemal Celik, "Mixed Node/Breaker and Bus/Branch Models Using CIM," Nexant, Tech. Rep., 2015.

[80] S. W. Director and R. L. Sullivan, "A tableau approach to power system analysis and design," *Circuit Theory and Applications*, vol. 7, 1979.

[81] P. W. Sauer, I. N. Hajj, M. A. Pai, and T. N. Trick, "COMPUTER METHODS IN ELECTRIC NETWORK ANALYSIS," *IEEE Transactions on Power Apparatus and Systems*, vol. PAS-102, no. 6, 1983.

[82] Y. Kim, H. Song, and B. Lee, "Governor-response power flow (GRPF) based long-term voltage stability simulation," *IEEE Transmission & Distribution Asia*, 2009.

[83] "Chapter 3: Technology Assessments-Transmission and Distribution Components," Department of Energy, Tech. Rep., 2015.

[84] ARPA-E, Grid Optimization Competition Design. [Online]. Available: https://arpa-e-foa.energy.gov/FileContent.aspx?FileID=f468a6a9-ac92-40f0-b771-1669cd83afde

[85] K. Karoui, H. Crisciu, and L. Platbrood, "Modeling the primary reserve allocation in preventive and curative security constrained OPF," *Proceedings of the 2010 PES T&D Conference & Exposition*, 2010.

[86] S. Grijalva, "Topology Processing and Real-Time Applications," PowerWorld, Tech. Rep., 2007.

[87] E. B. Fisher, R. P. O'Neill, and M. C. Ferris, "Optimal Transmission Switching," *IEEE Transactions on Power Systems*, vol. 23, no. 3, 2008.

[88] J. E. Tate and T. J. Overbye, "A Comparison of the Optimal Multiplier in Polar and Rectangular Coordinates," *IEEE Transactions on Power Systems*, vol. 20, no. 4, 2005.

[89] A. Wachter and L. T. Biegler, "On the implementation of a primal-dual interior point filter line search algorithm for large-scale nonlinear programming," *Mathematical Programming*, 2006.

[90] C. H. Grigg and at al., "The IEEE Reliability Test System - 1996," *IEEE Transactions on Power Systems*, vol. 14, no. 3, 1999.

[91] NEOS Server. [Online]. Available: http://neos-dev-web.neos-server.org/guide/?q=node/116

[92] P. Peng, S. Chang, and J. Dyer, "Inclusion of post-contingency actions in security constrained scheduling," *FERC Conference on increasing real-time and day-ahead market efficiency through improved software*, 2013.

[93] R. Madani, J. Lavaei, and R. Baldick, "Constraint screening for security analysis of power networks," *IEEE Trans. Power Syst.*, vol. 32, no. 3, 2017.

[94] A. S. Debs, *Modern Power Systems Control and Operation*. Kluwer Academic Publishers, 1988.

[95] Y. Fu, M. Shahidehpour, and Z. Li, "Security-constrained unit commitment with ac constraints," *IEEE Trans. Power Syst.*, vol. 20, no. 3, August 2005.

[96] H. Pinto, F. Magnago, S. Brignone, O. Alsac, and B. Stott, "Security constrained unit commitment: Network modeling and solution issues," *Power Systems Conference and Exposition*, 2006.

[97] Midwest ISO, Energy and Operating Reserve Markets Business Practices Manual, BPM-002-r9.

[98] D. Chattopadhyay and R. Baldick, "Unit commitment with probabilistic reserve," *IEEE Power Engineering Society Winter Meeting*, 2002.

[99] F. Aminifar, M. Fotuhi-Firuzabad, and M. Shahidehpour, "Unit commitment with probabilistic spinning reserve and interruptible load considerations," *IEEE Trans. Power Syst.*, vol. 24, no. 1, 2009.

[100] J. D. Lyon, M. Zhang, and K. W. Hedman, "Locational reserve disqualification for distinct scenarios," *IEEE Trans. Power Syst.*, vol. 30, no. 1, January 2015.

[101] J. D. Lyon, K. W. Hedman, and M. Zhang, "Reserve requirements to efficiently manage intra-zonal congestion," *IEEE Trans. Power Syst.*, vol. 29, no. 1, January 2014.

[102] F. Wang and K. W. Hedman, "Dynamic reserve zones for day-ahead unit commitment with renewable resources," *IEEE Trans. Power Syst.*, vol. 30, no. 2, March 2015.

[103] N. Li, N. G. Singhal, and K. W. Hedman, "An enhanced security-constrained unit commitment model with reserve response set policies," *50th Hawaii International Conference on System Sciences*, 2017.

[104] H. Holttinen, "Impact of hourly wind power variations on the system operation in the nordic countries," *Wind Energy*, vol. 8, 2005.

[105] L. Soder, "Reserve margin planning in a wind-hydro-thermal power system," *IEEE Trans. Power Syst.*, vol. 8, no. 2, 1993.

[106] M. A. Matos and R. J. Bessa, "Setting the operating reserve using probabilistic wind power forecasts," *IEEE Trans. Power Syst.*, vol. 26, no. 2, May 2011.

[107] H. Holttinen, M. Milligan, B. Kirby, T. Acker, V. Neimane, and T. Molinski, "Using standard deviation as a measure of increased operational reserve requirement for wind power," *Wind Eng.*, vol. 32, no. 4, 2008.

[108] S. Takriti, J. R. Birge, and E. Long, "A stochastic model for the unit commitment problem," *IEEE Trans. Power Syst.*, vol. 11, no. 3, 1996.

[109] L. Wu, M. Shahidehpour, and T. Li, "Stochastic security-constrained unit commitment," *IEEE Trans. Power Syst.*, vol. 22, no. 2, May 2007.

[110] R. Barth, H. Brand, P. Meibom, and C.Weber, "A stochastic unit commitment model for the evaluation of the impacts of the integration of large amounts of wind power," *Proc. 9th Int. Conf. Probabilistic Methods Applied to Power Systems*, 2006.

[111] J. M. Morales, A. J. Conejo, and J. Perez-Ruiz, "Economic valuation of reserves in power systems with high penetration of wind power," *IEEE Trans. Power Syst.*, vol. 24, no. 2, 2009.

[112] A. Papavasiliou, S. S. Oren, and R. P. O°ØNeill, "Reserve requirements for wind power integration: A scenario-based stochastic programming framework," *IEEE Trans. Power Syst.*, vol. 26, no. 4, November 2011.

[113] A. J. Wood, B. F. Wollenberg, and G. B. Sheblé, *Power Generation, Operation and Control*, 3rd ed. Wiley-Interscience, 2013.

[114] CAISO, "Intra-zonal congestion caiso dept. of market monitoring," Tech. Rep., 2007. [Online]. Available: http://www.caiso.com/1bb7/1bb77b241b920.pdf

[115] E. Ela, M. Milligan, and B. Kirby, "Operating reserves and variable generation," NREL, Tech. Rep., 2011.

[116] Y. Chen, A. Casto, F. Wang, Q. Wang, X. Wang, and J. Wan, "Improving large scale day-ahead security constrained unit commitment performance," *IEEE Trans. Power Syst.*, vol. 31, no. 6, 2016.

[117] W. B. Powell and S. Meisel, "Tutorial on stochastic optimization in energy i: Modeling and policies," *IEEE Trans. Power Syst.*, 2016.

[118] E. Ela, B. Kirby, E. Lannoye, M. Milligan, D. Flynn, B. Zavadil, and M. O°ØMalley, "Evolution of operating reserve determination in wind power integration studies," *IEEE PES General Meeting*, 2010.

[119] P. G. Yonghong Chen and J. Gardner, "Incorporating post zonal reserve deployment transmission constraints into energy and ancillary service co-optimization," *IEEE Trans. Power Syst.*, vol. 29, no. 2, 2014.

[120] Z. Zhou and A. Botterud, "Dynamic scheduling of operating reserves in co-optimized electricity markets with wind power," *IEEE Trans. Power Syst.*, vol. 29, no. 1, 2014.

[121] T. Zheng and E. Litvinov, "Contingency-based zonal reserve modeling and pricing in a co-optimized energy and reserve market," *IEEE Trans. Power Syst.*, vol. 23, no. 2, May 2008.

[122] R. N. Allan and R. Billinton, *Reliability Evaluation of Power Systems*. Springer, 1996.

[123] M. A. Ortega-Vazquez and D. S. Kirschen, "Economic impact assessment of load forecast errors considering the cost of interruptions," *IEEE PES General Meeting*, 2006.

[124] Z. Zhou, A. Botterud, J. Wang, R. Bessa, H. Keko, J. Sumaili, and V. Miranda, "Application of probabilistic wind power forecasting in electricity markets," *Wind Energy*, 2012.

[125] R. J. Bessa, V. Miranda, A. Botterud, Z. Zhou, and J. Wang, "Time-adaptive quantile-copula for wind power probabilistic forecasting," *Renew. Energy*, vol. 40, no. 1, 2012.

[126] K. W. Hedman, R. P. ÓNeill, and S. S. Oren, "Analyzing valid inequalities of the generation unit commitment problem," *Power Systems Conference and Exposition*, October 2009.

[127] L. Bird, J. Cochran, and X. Wang, "Wind and Solar Energy Curtailment: Experience and Practices in the United States," *National Renewable Energy Laboratory (NREL)*, 2014.

[128] H. Lund, "Renewable energy strategies for sustainable development," *Energy*, vol. 32, 2007.

[129] American Physical Society (APS), "Integrating renewable electricity on the grid," Tech. Rep., 2010.

[130] S. Frank, I. Steponavice, and S. Rebennack, "Optimal Power Flow: A Bibliographic Survey II - Nondeterministic and hybrid methods," *Energy Syst.*, vol. 3, pp. 259–289, Sep 2013.

[131] ——, "Optimal Power Flow: A Bibliographic Survey I - Formulations and Deterministic Methods," *Energy Syst.*, vol. 3, pp. 221–258, Sep 2012.

[132] R. A. Jabr, "Radial Distribution Load Flow Using Conic Programming," *IEEE Transactions on Power Systems*, vol. 21, no. 3, August 2006.

[133] S. Sojoudi and J. Lavaei, "Network Topologies Guaranteeing Zero Duality Gap for Optimal Power Flow Problem," 2011.

[134] B. C. Lesieutre, D. K. Molzahn, A. R. Borden, and C. L. DeMarco, "Examining the Limits of the Application of Semidefinite Programming to Power Flow Problems," *49th Annual Allerton Conference on Communication, Control, and Computing (Allerton)*, 2011.

[135] J. B. LASSERRE, "Global Optimization with Polynomials and the Problem of Moments," *SIAM Journal on Optimization*, vol. 11, no. 3, pp. 796–817, 2001.

[136] C. Josz, J. Maeght, P. Panciatici, and J. C. Gilbert, "Application of the Moment-SOS Approach to Global Optimization of the OPF Problem," *IEEE Transactions on Power Systems*, vol. 30, no. 1, January 2015.

[137] D. K. Molzahn and I. A. Hiskens, "Sparsity-Exploiting Moment-Based Relaxations of the Optimal Power Flow Problem," *IEEE Transactions on Power Systems*, vol. 30, no. 6, November 2015.

[138] B. Kocuk, S. S. Dey, and X. A. Sun, "Strong SOCP Relaxations for the Optimal Power Flow Problem," November 2016.

[139] C. Coffrin, H. L. Hijazi, and P. V. Hentenryck, "The QC Relaxation: A Theoretical and Computational Study on Optimal Power Flow," *IEEE Transactions on Power Systems*, vol. 31, no. 4, July 2016.

[140] H. Hijazi, C. Coffrin, and P. V. Hentenryck, "Convex Quadratic Relaxations for Mixed-Integer Nonlinear Programs in Power Systems," *P.V. Math. Prog. Comp*, 2017.

[141] P. M. Castro, "Tightening piecewise McCormick relaxations for bilinear problems," *Computers and Chemical Engineering*, 2015.

[142] H. Hijazi, C. Coffrin, and P. V. Hentenryck, "Convex Quadratic Relaxations for Mixed-Integer Nonlinear Programs in Power Systems," *P.V. Math. Prog. Comp*, 2017.

[143] D. K. Molzahn, J. T. Holzer, B. C. Lesieutre, and C. L. DeMarco, "Implementation of a Large-Scale Optimal Power Flow Solver Based on Semidefinite Programming," *IEEE Transactions on Power Systems*, vol. 28, no. 4, November 2013.

[144] K. Dvijotham and D. K. Molzahn, "Error Bounds on the DC Power Flow Approximation: A Convex Relaxation Approach," *2016 IEEE 55th Conference on Decision and Control*, 2016.

[145] H. Nagarajan, M. Lu, E. Yamangil, and R. Bent, "Tightening McCormick Relaxations for Nonlinear Programs via Dynamic Multivariate Partitioning," *International Conference on Principles and Practice of Constraint Programming*, 2016.

[146] P. Belotti, J. Lee, L. Liberti, F. Margot, and A. Wachter, "Branching and bounds tighteningtechniques for non-convex MINLP," *Optimization Methods and Software*, 2009. [Online]. Available: https://optimization.mccormick.northwestern.edu/index.php

[147] MOSEK, "The MOSEK optimization tools version 8. User's manual and reference." [Online]. Available: https://mosek.com/

[148] F. E. R. Commission, "RTO Unit Commitment Test System," Tech. Rep., 2012.

[149] F. Capitanescua, J. M. Ramosb, P. c, D. Kirschend, A. M. Marcolinib, L. Platbroode, and L. Wehenkela, "State-of-the-art, challenges, and future trends in security constrained optimal power flow," *Electric Power Systems Research*, vol. 81, 2011.

[150] D. Issicaba, A. S. Costa, and J. L. Colombo, "Real-Time Monitoring of Points of Common Coupling in Distribution Systems Through State Estimation and Geometric Tests," *IEEE Transactions on Smart Grid*, vol. 7, no. 1, 2016.

[151] D. Gorinevsky, S. Boyd, and S. Poll, "Estimation of Faults in DC Electrical Power System," *American Control Conference*, 2009.

[152] J. Klucznik, "Earth wires currents calculation by tableau analysis," *Electric Power Systems Research*, vol. 151, 2017.

[153] "Distributed energy resources subcommittee," PJM, Tech. Rep., 2017.

[154] M. E. Birk, "Impact of Distributed Energy Resources on Locational Marginal Prices and Electricity Networks," Master's thesis, MASSACHUSETTS INSTITUTE OF TECHNOLOGY, 2016.

[155] North American Electric Reliability Corporation (NERC), "Distributed Energy Resources-Connection Modeling and Reliability Considerations," 2017.

[156] A. Keane, L. Ochoa, E. Vittal, C. Dent, and G. Harrison, "Enhanced utilization of voltage control resources with distributed generation," *IEEE Transactions on Power Systems*, vol. 26, no. 1, 2011.

[157] A. Saberian, P. Farzan, M. F. Nejad, H. Hizam, C. Gomes, M. L. b. Othman, M. A. M. Radzi, and M. Z. A. A. Kadir, "Role of FACTS Devices in Improving Penetration of Renewable Energy," *International Power Engineering and Optimization Conference (PEOCO)*, 2013.

[158] Y. Yang, "Unified Power Flow Controller (UPFC) Technology and Project Application," IEEE Standards Association - webinar, Tech. Rep., 2017.

[159] L. Gyuqyi, C. D. Schauder, S. L. williams, T. R. Rietman, D. R. Torgerson, and A. Edris, "THE UNIFIED POWFBFLOW CONTROLLER: A NEW APPROACH TO POWER TRANSMISSION CONTROL," *IEEE Transactions on Power Delivery*, vol. 10, no. 2, 1995.

[160] L. Gyugyi, "Unified power-flow control concept for flexible AC transmission systems," *IEE Proceedings C - Generation, Transmission and Distribution*, vol. 139, no. 4, 1992.

[161] C. Schauder, L. Gyugyi, M. Lund, D. Hamai, T. Rietman, D. Torgerson, and A. Edris, "Operation of the unified power flow controller (UPFC) under practical constraints," *IEEE Transactions on Power Delivery*, vol. 13, no. 2, 1998.

[162] F. Meng, "A generalized optimal power flow program for distribution system analysis and operation with distributed energy resources and solid state transformers," Ph.D. dissertation, Missouri University of Science and Technology, 2014.

[163] D. Gayme and U. Topcu, "Optimal power flow with distributed energy storage dynamics," *2011 American Control Conference*, 2011.

[164] Y. Liu, J. Li, L. Wu, and T. Ortmeyer, "Chordal Relaxation Based ACOPF for Unbalanced Distribution Systems With DERs and Voltage Regulation Devices," *IEEE Transactions on Power Systems*, vol. 33, no. 1, 2018.

[165] North American Electric Reliability Corporation (NERC), "Transmission System Planning Performance Requirements (NERC TPL-001-4)," 2014.

[166] Western Electricity Coordinating Council (WECC), "WECC Wind Power Plant Power Flow Modeling Guide," WECC Wind Generator Modeling Group, Tech. Rep., 2008.

[167] E. Muljadi, A. Ellis, et al, "Equivalencing the Collector System of a Large Wind Power Plant," *IEEE Power Engineering Society Annual Conference*, 2006.

[168] Western Electricity Coordinating Council (WECC), "WECC Guide for Representation of Photovoltaic Systems In Large-Scale Load Flow Simulations," WECC Renewable Energy Modeling Task Force, Tech. Rep., 2010.

[169] A. L'Abbate, M. Trovato, C. Becker, and E. Handschin, "Advanced Steady-State Models of UPFC for Power System Studies," *Power Engineering Society Summer Meeting*, 2002.

[170] C. R. Foerte-Esquivel, E. Acha, and H. Amhriz-Perez, "A Comprehensive Newton-Raphson UPFC Model for the Quadratic Power Flow Solution of Practical Power Networks," *IEEE Transactions on Power Systems*, vol. 15, no. 1, 2000.

[171] M. Noroozian, L. Angquist, M. Ghandhari, and G. Anderson, "USE OF UPFC FOR OPTIMAL POWER FLOW CONTROL," *IEEE Transactions on Power Delivery*, vol. 12, no. 4, 1997.

[172] D. F. Opila, A. M. Zeynu, and I. A. Hiskens, "Wind Farm Reactive Support and Voltage Control," *IREP Symposium-Bulk Power System Dynamics and Control*, 2010.

[173] M. O'boyle, "WHO SHOULD OWN AND OPERATE DISTRIBUTED ENERGY RESOURCES?" 2017.

[174] B. Park, J. Netha, M. C. Ferris, and C. L. DeMarco, "Sparse Tableau Formulation for Optimal Power Flow Applications," 2017.

[175] B. Park and C. L. DeMarco, "Sparse Tableau Relaxation for the Optimal Power Flow Problem," *55th Annual Allerton Conference*, 2017.